Development of Verification Check-Cases for Six Degree-of-Freedom Flight Vehicle Simulations

E. Bruce Jackson[*]

NASA Langley Research Center, Hampton, VA 23681, USA

Dr. Robert Shelton[†] and Dr. A. A. Jackson[‡]

NASA Johnson Space Center, Houston, TX 77058, USA

Manuel P. Castro[§] and Deleena M. Noble[§]

NASA Dryden Flight Research Center, Edwards, CA 93523, USA

Michael M. Madden[¶], Daniel K. Litton[‖], Richard W. Powell[**], Eric M. Queen[††],
Jeremy D. Schidner[††], William A. Sellers[‡‡], Scott A. Striepe[‡‡] and John Aguirre[§§]

NASA Langley Research Center, Hampton, VA 23681, USA

Curtis J. Zimmerman[¶¶]

NASA Marshall Space Flight Center, Huntsville, AL 35812, USA

Emily K. Lewis[***], Scott E. Reardon[†††], Nghia Vuong[‡‡‡] and Michael J. Weinstein[†††]

NASA Ames Research Center, Mountain View, CA 94035, USA

The continuing growth in both computing power and commercial space activities has resulted in a number of start-up organizations that are designing new aerospace vehicles using a variety of commercial off-the-shelf and in-house-developed simulation and analysis tools, including six-degree-of-freedom flight simulation tools.

Verification of the tools' equations of motion and environment models (atmosphere, gravitation, and geodesy) is necessary to assure credibility of results. However, aside from limited examples in textbooks, very little verification data exists for six-degree-of-freedom flight simulation problems.

This paper describes a set of verification check-cases that cover both atmospheric and exo-atmospheric orbital flight. Each scenario consists of well-defined flight vehicles, initial conditions, and maneuvers. These scenarios were implemented and executed in a variety of NASA analytical and real-time simulation tools. The tool set included flat-earth, round-earth, and rotating oblate spheroidal earth geodesy models as well as independently derived

---

[*]Sr. Aerospace Engineer, Dynamic Systems and Control Branch, MS 308, AIAA Associate Fellow.

[†]Lead, JSC Engineering Orbital Dynamics (JEOD), Engineering Directorate, Mail Code ER7.

[‡]Sr. Engineer, Jacobs Engineering Group, Inc., Engineering Directorate, AIAA Associate Fellow.

[§]Aerospace Engineer, DFRC Simulation Engineering, MS 4840.

[¶]Chief Scientist, Simulation Development and Analysis Branch, MS 125B, AIAA Senior Member.

[‖]Assistant Branch Head, Aeroacoustics Branch, MS 463, AIAA Member.

[**]Aerospace Engineer, Analytical Mechanics & Associates, MS 489, AIAA Associate Fellow.

[††]Aerospace Engineer, Atmospheric Flight & Entry Systems Branch, MS 489, AIAA Member (Queen).

[‡‡]Senior Systems Analyst, Stinger Ghaffarin Technologies, Inc, MS 489, AIAA Member.

[§§]Scientific Programmer, Analytical Mechanics & Associates, MS 489

[¶¶]Aerospace Engineer, Guidance, Navigation and Mission Analysis Branch, MSFC/EV42, AIAA Member.

[***]Sr. Simulation Engineer, Science Applications International Corporation, Aerospace Simulation Research & Development Branch, MS 243-6, AIAA Member (Lewis).

[†††]Flight Simulation Engineer, Aerospace Simulation Research& Development Branch, MS 243-5, AIAA Member.

[‡‡‡]System Software Engineer, Aerospace Simulation Research & Development Branch, MS 243-5, AIAA Member.

American Institute of Aeronautics and Astronautics

equations of motion and propagation techniques. The resulting parameter trajectories were over-plotted to yield a family of solutions.

The models are published in the AIAA/ANSI S-119-2011 Flight Dynamics Model Exchange Standard, making them realizable in a variety of proprietary and non-proprietary implementations. This set of models and the resulting NASA-generated trajectory plots may serve as a preliminary verification aide for organizations and individuals that are developing their own simulation tools and frameworks.

Nomenclature

b	Reference wingspan
C	Aerodynamic coefficient
$\bar{C}_{nm}$	Fully-normalized unit-less gravity coefficient of degree n and order m
$\bar{c}$	Mean aerodynamic chord
F	Force
G	universal gravitational constant
$\mathbf{g}$	unit of acceleration
h	Geometric altitude
I	Moment or product of inertia
J_2	First gravitational harmonic
M	RNP matrix to transform ECI into ECEF coordinates, or mass of the earth
m	Mass or gravitational model order
n	Gravitational model degree
P	Intersection of prime meridian and equator
$\bar{P}_{n,m}$	Fully-normalized associated Legendre function of degree n and order m
p	Roll rate
q	Pitch rate
R	Radius
r	Yaw rate or radius
r_e	Equatorial radius of the earth
r_p	Polar radius of the earth
S	Reference area
$\bar{S}_{nm}$	Fully-normalized unitless gravity coefficient of degree n and order m
T	Torque
U	Potential function
x	Body longitudinal axis, +fwd, or one of three inertial rectangular position coordinates
y	Body lateral axis, +right, or second of three inertial rectangular position coordinates
Z	Geopotential height
z	Body vertical axis, +down, or third of three inertial rectangular position coordinates
δ_{ij}	Kronecker delta
ϕ	Bank angle or geocentric latitude
θ	Pitch attitude
ψ	Heading angle
λ	Longitude
μ	Gravitational parameter (product of GM)
ν	Normal vector to the surface of the earth
$\bar{\nu}$	Projection of ν on the equatorial plane of the earth
ω	Earth's mean rotation rate

Subscript

cm	Center of mass
1	Body 1
2	Body 2
D	Drag component
L	Lift component
l	Rolling component

American Institute of Aeronautics and Astronautics

m	Pitching component
n	Yawing component
s	Surface of the earth
xx	Moment of inertia around the x axis
yy	Moment of inertia around the y axis
Y	Sideforce component
zz	Moment of inertia around the z axis
xy	Cross-product of inertia between the x and y axis
yz	Cross-product of inertia between the y and z axis
zx	Cross-product of inertia between the z and x axis

Acronyms

2D	Two-dimensional
3D	Three-dimensional
6-DOF	Six-degree-of-freedom
CM	Center of Mass
DAVE-ML	Dynamic Aerospace Vehicle Exchange Markup Language
DOF	Degrees-of-freedom
DTH	Dryden Time History tool set
ECEF	Earth-centered, earth-fixed (rotating coordinate frame)
ECI	Earth-centered inertial (non-rotating coordinate frame)
EOM	Equations of Motion
FORTRAN	FORMula TRANslator
GEM-T1	Goddard Earth Model T1
IC	Initial conditions
IERS	International Earth Rotation and Reference System Service
ISS	International Space Station
J2000	Earth-centered inertial frame for epoch 2000
JEOD	JSC Engineering Orbital Dynamics
LaSRS++	Langley Standard Real-time Simulation in C++
LQR	Linear Quadratic Regulator
LVLH	Local Vertical, Local Horizontal frame
MAC	Mean Aerodynamic Chord
MAVERIC	Marshall Aerospace Vehicle Representation in C
MET	Marshall Engineering Thermosphere
N.A.	Not Applicable
NED	North-East-Down
POST	Program to Optimize Simulation Trajectories
n/a	not applicable
RNP	Rotation-Nutation-Precession
S-119	ANSI/AIAA S-119-2011 Flight Dynamic Model Exchange Standard
S.L.	Sea Level
TBD	To Be Determined / Defined
TFrames	Tools to Facilitate the Rapid Assembly of Missile Engagement Simulations
VMSRTE	Vertical Motion Simulator Real-Time Environment
WGS 84	World Geodetic System 1984

American Institute of Aeronautics and Astronautics

I. Introduction

This paper documents the principal methods of implementing rigid-body equations of motion, planetary geodetic, gravitation and atmospheric models for simple vehicles in a variety of endo- and exo-atmospheric subsonic, supersonic, and orbital flights with various NASA engineering simulation tools. This effort is intended to provide an additional means of verification of flight simulations.

This is a report on intermediate results, as not all of the simulation models and scenarios have been implemented and checked on each tool. A final NASA report to fully document results is scheduled later this year. That report will include details for obtaining and implementing the same models in the interested reader's favorite simulation tool.

I.A. Overview

Several NASA simulation tools were exercised with increasingly sophisticated vehicles in various initial conditions. These included both atmospheric and exoatmospheric flight. Each scenario uses simple vehicle aerodynamic and inertial models; maneuvering endo-atmospheric scenarios involve a vehicle propulsion model as well for sustained flight.

The assembled toolset included:

Core Dryden Flight Research Center

JEOD Johnson Space Center

LaSRS++ Langley Research Center

MAVERIC Marshall Space Flight Center

POST-II Langley Research Center

VMSRTE Ames Research Center

Each of these tools is synopsized below.

I.B. Problem description

The different NASA, industry and commercial flight simulation tools that are used for flight prediction sometimes provide substantially different results. Some differences can be traced to errors in the implementation of equations of motion (kinematics) and the geodetic, gravitational, and atmosphere models. Differences can also be caused by values of physical constants and varying interpretations of a scenario. Other sources of differences are from inconsistent or limited-precision unit conversions.

Currently, there are no accepted benchmark check-cases that can be used for verification of these simulation tools, which leads to risk in using these tools for flight prediction and design in support of numerous NASA flight projects. And due to the non-linear nature of most simulation scenarios, an analytical, closed-form solution of a trajectory is rarely available.

I.C. Technical approach

A team was assembled by the Technical Fellow for Flight Mechanics, Mr. Dan Murri, at NASA's Engineering and Safety Center in 2012. This group met at NASA Langley Research Center and mapped out an approach to developing check-cases for comparison and cross-verification purposes.

It was agreed that a set of scenarios involving simple models would be developed and then simulated by each participant in their preferred simulation tool. The basic parameters were agreed to and further discussion led to the set of scenarios described here. Formats for specifying the models, initial conditions, and resulting time-history data were agreed to; and a plan for presenting the data was developed.

Rather than require each tool to match within a certain tolerance, a decision was made to present over-plots of the results of the simulation tools rather than attempt to publish a single reference solution.

A rough schedule of events was agreed to, with the intention of publishing a final NASA report at the end of the project and the posting of salient data on a publicly-available website.

American Institute of Aeronautics and Astronautics

I.D.   Simulated scenarios

A set of atmospheric and orbital flight scenarios, models, and initial conditions was developed (see tables 1 and 2). Most of the simulation tools used by participants were developed for either atmospheric or orbital flights, but some generate check-case data for both scenario sets.

I.D.1.   Atmospheric flight

For atmospheric flight, a series of scenarios with increasingly complex models and initial conditions was agreed upon, as shown in table 1. These models ranged from the obligatory cannonball to winged-flight at subsonic, supersonic and transonic speeds.

Key parameters to match are linear and angular accelerations, velocities, and positions in geodetic and inertial frames and are shown in this paper. Due to space limitations, other important comparisons of local (NED) velocities, body-axis velocities, Mach number, true, equivalent and calibrated airspeeds as well as angle of attack, angle of sideslip, and their rates will be compared in the NASA report.

I.D.2.   Orbital flight

The goal of the orbital simulations is to compare propagation of a 6-DOF vehicle in the orbital environment. These cases idealize the vehicle as a rigid body and compare time histories of position, velocity, attitude and attitude rate. The orbital environment is fundamentally different from the atmospheric domain because orbiting bodies are not subject to the strong damping effects of atmospheric flight. Therefore, even tiny perturbations such as higher order gravity terms and third body effects will produce large differences in vehicle state over time.

The orbital scenarios (shown in table 2) are designed to exercise various options ranging from spherical gravity and no drag to full potential model, third body perturbations and drag. The tests are organized in such a way as to build incrementally so that higher order effects can be seen as they are introduced. These scenarios match those developed for an earlier simulation comparison study.[1]

We also compare key parameters which are commonly needed to support vehicle state propagation. For example, in order to compute non-spherical gravitational accelerations, they must be calculated in the Earth-centered, Earth-fixed (ECEF) frame which is how the model is expressed. These accelerations must then be converted into a non-rotating inertial frame for integration. It is necessary to know the orientation of the ECEF frame with respect to an inertial coordinate system. This transformation reflects earth's rotation, nutation and precession (as well as so-called "polar motion") and is commonly called an *RNP* matrix. The RNP transformation is also needed in order to relate the inertial state of the vehicle to locations on the planet, although comparison plots of these values are not shown due to space limitations. Along the same lines, we need a model of the upper atmosphere in order to model drag. We compare output of RNP and atmosphere models as a means of isolating sources of variation among the various simulations.

The orbital cases can be described according to the following outline:

Drag-Free Translation These are primarily designed to test the numerical integration and gravity models. The complexity varies from pure spherical gravity through higher order gravitational harmonics and third body effects.

Translation with Drag These cases are similar to their drag-free counterparts except that a simple drag model is introduced and exercised with constant and variable atmospheric density. In all orbital cases, the drag is modeled by a simple ballistic coefficient.

Rotational Propagation These cases compare the rotational propagation with various initial attitudes, attitude rates, and torques.

Maneuvers These cases involve application of thrust to change the trajectory in various ways.

II.   Vehicle models

A set of reference vehicles was proposed, based mostly on existing non-proprietary vehicle models. An overview of each model is given below. These will be made available on a NASA public website by the end of the project (pending review).

American Institute of Aeronautics and Astronautics

Table 1. Atmospheric check-case scenarios

Number	Name	Verifies	Gravity	Geodesy	Atmosphere	Winds
1	Dropped sphere with no drag	Gravitation, translational EOM	J_2	WGS 84	none	N.A.
2	Tumbling brick with no damping in vacuum	Rotational EOM	$1/R^2$	Round fixed	none	N.A.
3	Tumbling brick with dynamic damping	Inertial coupling	$1/R^2$	Round fixed	fixed S.L.	none
4	Dropped sphere with constant C_D, no wind	Gravitation, integration	$1/R^2$	Round fixed	US Std 1976	still air
5	Dropped sphere with constant C_D, no wind	Earth rotation	$1/R^2$	Round rotating	US Std 1976	still air
6	Dropped sphere with constant C_D, no wind	Ellipsoidal earth	J_2	WGS 84	US Std 1976	still air
7	Dropped sphere with constant C_D + wind	Wind effects	J_2	WGS 84	US Std 1976	steady wind
8	Dropped sphere with constant C_D + 2D wind shear	2D wind	J_2	WGS 84	US Std 1976	$f(h)$
9	Ballistic flight eastward along equator	Translational EOM	J_2	WGS 84	US Std 1976	still air
10	Ballistic flight northward along prime meridian	Coriolis	J_2	WGS 84	US Std 1976	still air

Table 2. Exo-atmospheric check-case scenarios

Number	Name	Verifies	Gravitation	Atmosphere	3rd body pert.	Body
1	Earth Modeling Parameters	Environmental constants	$1/R^2$	none	none	ISS
2	Keplerian Propagation	Integration, RNP, orientation	$1/R^2$	none	none	ISS
3A	Gravity Modeling: 4x4	4x4 Harmonic gravity model	4x4	none	none	ISS
3B	Gravity Modeling: 8x8	8x8 Harmonic gravity model	8x8	none	none	ISS
4	Planetary Ephemeris	Third body gravitational forces	$1/R^2$	none	sun, moon	ISS
5A	Min. Solar Activity	Free molecular flow	$1/R^2$	MET	none	ISS
5B	Mean Solar Activity	Free molecular flow	$1/R^2$	MET	none	ISS
5C	Max. Solar Activity	Free molecular flow	$1/R^2$	MET	none	ISS
6A	Const Density Drag	Response to constant force	$1/R^2$	const	none	sphere
6B	Aero Drag with Dyn. Atmos.	Response to dynamic drag	$1/R^2$	MET	none	sphere
6C	Plane Change Maneuver	Response to propulsion firing	$1/R^2$	MET	none	cylinder
6D	Earth Departure Maneuver	Response to propulsion firing	$1/R^2$	MET	none	cylinder
7A	4x4 Gravity	Translation response	4x4	none	sun, moon	sphere
7B	8x8 Gravity	Translation response	8x8	none	sun, moon	sphere
7C	All Models with 4x4 Gravity	Translation response	4x4	MET	sun, moon	sphere
7D	All Models with 8x8 Gravity	Translation response	8x8	MET	sun, moon	sphere
8A	Zero Initial Attitude Rate	Integration methods for rotation	$1/R^2$	none	none	ISS
8B	Non-Zero Initial Attitude Rate	Integration methods for rotation	$1/R^2$	none	none	ISS
9A	Zero Initial Rate w/ Torque	Rotational response	$1/R^2$	none	none	ISS
9B	Non-Zero Initial Rate w/ Torque	Rotational response	$1/R^2$	none	none	ISS
9C	Zero Initial Rate w/ $T + F$	Rotational response	$1/R^2$	none	none	ISS
9D	Non-Zero Initial Rate w/ $T + F$	Rotational response	$1/R^2$	none	none	ISS
10A	Zero Initial Attitude Rate	Gravity gradient modeling	$1/R^2$	none	none	cylinder
10B	Non-Zero Initial Rate	Gravity gradient modeling	$1/R^2$	none	none	cylinder
10C	Zero Initial Rate; Elliptical Orbit	Gravity gradient modeling	$1/R^2$	none	none	cylinder
10D	Non-Zero Initial Rate; Ellip. Orbit	Gravity gradient modeling	$1/R^2$	none	none	cylinder
FULL	Integrated 6-DOF Orbital Motion	Combined effects response	8x8	MET	sun, moon	ISS

For the orbital scenarios, we only need consider two characteristics of the orbiting vehicle (typically called a satellite):

Mass Distribution The mass of an orbiting vehicle determines its response to outside forces and torques. The mass properties of a satellite are captured by

- Total mass

$$m = \int_B dm \tag{1}$$

where m is the total mass, B is the body of the vehicle, and dm represents a differential unit of mass.

- Center of mass

$$\begin{pmatrix} \bar{x} \\ \bar{y} \\ \bar{z} \end{pmatrix} = \int_B \begin{pmatrix} x \\ y \\ z \end{pmatrix} dm \tag{2}$$

where dm represents a differential element of mass located at the point $\begin{pmatrix} x \\ y \\ z \end{pmatrix}$ and the integration is performed over the volume of the vehicle.

- Inertia tensor

$$I = \begin{bmatrix} I_{xx} & -I_{xy} & -I_{xz} \\ -I_{xy} & I_{yy} & -I_{yz} \\ -I_{xz} & -I_{yz} & I_{zz} \end{bmatrix} \tag{3}$$

and

$$
\begin{aligned}
I_{xx} &= \int_B (\rho_y^2 + \rho_z^2) dm \\
I_{yy} &= \int_B (\rho_x^2 + \rho_z^2) dm \\
I_{zz} &= \int_B (\rho_x^2 + \rho_y^2) dm \\
I_{xy} &= \int_B \rho_x \rho_y dm \\
I_{xz} &= \int_B \rho_x \rho_z dm \\
I_{yz} &= \int_B \rho_y \rho_z dm
\end{aligned} \tag{4}
$$

where

$$\rho = \begin{pmatrix} \rho_x \\ \rho_y \\ \rho_z \end{pmatrix} = \begin{pmatrix} x - \bar{x} \\ y - \bar{y} \\ z - \bar{z} \end{pmatrix} \tag{5}$$

Drag Characteristics In general, the characterization of forces and moments exerted as the vehicle moves through a medium can be quite complex; however, for the purposes of comparing orbital trajectories, a simple ballistic coefficient model will suffice.

For the atmospheric scenarios, the aerodynamic models are typically non-linear and table-based, and propulsion models (if included) are affected by vehicle airspeed. The same mass property definitions given previously still apply.

II.A.   Spheroid - atmospheric check cases

The simplest model used in generating the aerodynamics reference trajectories was a sphere of fixed size, inertia and a constant drag coefficient, as given in tables 3 and 4. These are somewhat arbitrary values.

American Institute of Aeronautics and Astronautics

Table 3. Atmospheric spheroid mass and inertial characteristics

Parameter	Value
I_{xx}	3.6 slug-ft^2
I_{yy}	3.6 slug-ft^2
I_{zz}	3.6 slug-ft^2
I_{xy}	0.0 slug-ft^2
I_{yz}	0.0 slug-ft^2
I_{zx}	0.0 slug-ft^2
m	1.0 slug
x_{cm}	0.0 ft
y_{cm}	0.0 ft
z_{cm}	0.0 ft

Table 4. Spheroid aerodynamic characteristics

Parameter	Value
S	0.1963495 ft^2
C_L	0.0
C_D	0.1
C_Y	0.0
C_l	0.0
C_m	0.0
C_n	0.0

American Institute of Aeronautics and Astronautics

II.B.   Spheroid - orbital check cases

A different spheroid with metric units was used in generating the orbital reference trajectories, of fixed size and inertia as given in table 5. This was reused from the earlier orbital simulation comparison study[1] and has a radius of $1/\sqrt{\pi}$ m.

Table 5. Orbital spheroid mass and inertial characteristics

Parameter	Value
I_{xx}	$2/5\pi$ kg-m^2
I_{yy}	$2/5\pi$ kg-m^2
I_{zz}	$2/5\pi$ kg-m^2
I_{xy}	0.0 kg-m^2
I_{yz}	0.0 kg-m^2
I_{zx}	0.0 kg-m^2
m	1.0 kg
x_{cm}	0.0 m
y_{cm}	0.0 m
z_{cm}	0.0 m

II.C.   Brick

The next-simplest model evaluated was a brick-shaped object with rotational damping, as given in tables 6 and 7. No attempt was made to ascertain the actual parameters; these inertia properties are estimated assuming homogeneity while the aerodynamic characteristics were completely made up.

The brick was assumed to be standard size: 8 inches by 4 inches by 2.25 inches, corresponding to the x, y and z body axes dimensions as shown in figure 1.
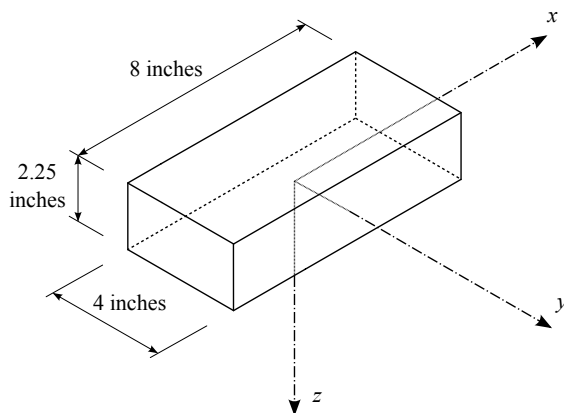
Figure 1. U.S. Standard Face Brick

American Institute of Aeronautics and Astronautics

Table 6. Estimated U.S. standard face brick mass and inertial characteristics

Parameter	Value
I_{xx}	0.00189 slug-ft^2
I_{yy}	0.00621 slug-ft^2
I_{zz}	0.00719 slug-ft^2
I_{xy}	0.0 slug-ft^2
I_{yz}	0.0 slug-ft^2
I_{zx}	0.0 slug-ft^2
m	0.1554 slug
x_{cm}	0.0 ft
y_{cm}	0.0 ft
z_{cm}	0.0 ft

Table 7. Fictitious U.S. face brick aerodynamic characteristics

Parameter	Value
S	0.22222 ft^2
b	0.33333 ft
$\bar{c}$	0.66667 ft
C_L	0.0
C_D	0.01
C_Y	0.0
C_l	0.0
C_m	0.0
C_n	0.0
C_{l_p}	-1.0
C_{l_r}	0.0
C_{m_q}	-1.0
C_{n_p}	0.0
C_{n_r}	-1.0

American Institute of Aeronautics and Astronautics

II.D. Cylinder

A uniform-density cylinder of size 12m x 1m x 1m is used for certain orbital check-cases was reused from the earlier orbital simulation comparison study.[1] Its mass properties are given in table 8. The moments of inertia are about the center of mass.

Table 8. Mass properties for cylinder

Parameter	Value
I_{xx}	500 kg-m^2
I_{yy}	12250 kg-m^2
I_{zz}	12250 kg-m^2
I_{xy}	0.0 kg-m^2
I_{yz}	0.0 kg-m^2
I_{zx}	0.0 kg-m^2
m	1000 kg
x_{cm}	6.0 m
y_{cm}	0.0 m
z_{cm}	0.0 m

II.E. ISS

A shape representative of the International Space Station (ISS), used in certain orbital check-cases, was reused from the earlier orbital simulation comparison study.[1] Its mass properties are given in table 9. The moments and products of inertia are about the center of mass.

Table 9. Mass properties for ISS-like vehicle

Parameter	Value
I_{xx}	1.02×10^8 kg-m^2
I_{yy}	0.91×10^8 kg-m^2
I_{zz}	1.64×10^8 kg-m^2
I_{xy}	6.96×10^6 kg-m^2
I_{yz}	−5.90×10^5 kg-m^2
I_{zx}	5.48×10^6 kg-m^2
m	400,000 kg
x_{cm}	−3.0 m
y_{cm}	−1.5 m
z_{cm}	4.0 m

III. Geodesy models

This section describes the way in which we model the surface of the earth. We describe three simple models which are commonly used in the simulation of atmospheric and orbital vehicles.

There is a connection between models for gravity and those for geodesy. Geodetic models include a reference surface to serve as an idealized sea level. By definition any such surface should also be a level surface for the gravity potential function, i.e. it should be normal to the local gravity vector.

The natural pairing of geodetic and gravitational models considered here is

American Institute of Aeronautics and Astronautics

- Flat Earth – Constant Gravity

- Round Earth – Inverse Square Law

- Ellipsoidal Earth (WGS 84) – Spherical Harmonic

For the round and ellipsoidal models, we locate points using the familiar altitude h, latitude ϕ and longitude λ. The altitude should be measured along the normal vector $\vec{\nu}$ to the surface of the reference shape (sphere or ellipse). The latitude ϕ is defined to be the angle between $\vec{\nu}$ and the equatorial plane $z = 0$. If $\vec{\nu}$ is the projection of $\vec{\nu}$ on the equatorial plane, then the longitude λ is the angle between $0,\vec{P}$ and $\vec{\nu}$ where P is the intersection of the prime meridian and the equator. We adopt the sign convention that east longitude is positive as is latitude north of equator.

III.A.   Flat earth

The simplest way to model the surface of the earth is as a flat plane. The coordinates for such a system are usually given in either runway-aligned coordinates (for terminal maneuvers) or in a three-dimensional framework oriented North, East and Down (sometimes Up). In at least one approximation the position of the vehicle is given as geodetic latitude, longitude and radius from the center of earth, which are spherical coordinates, but the "translational rates" of these spherical positions are integrated as if they were translational rates across a flat plane.

These are valid approximations for the appropriate simulation application but generally lead to errors in line-of-sight calculations and/or high-speed flight.

III.B.   Round earth

The next step on the ladder of complexity is to model the earth as a perfect sphere. To this end, we need only a single number r_e, the radius, to specify the model. The equation of the point s on the surface of a spherical earth is simply

$$x_s{}^2 + y_s{}^2 + z_s{}^2 = r_e^2 \tag{6}$$

The conversion from altitude, latitude and longitude to ECEF Cartesian coordinates is given by

$$\begin{pmatrix} x \\ y \\ z \end{pmatrix} = (h + r_e) \begin{pmatrix} \cos(\phi)\cos(\lambda) \\ \cos(\phi)\sin(\lambda) \\ \sin(\phi) \end{pmatrix} \tag{7}$$

The conversion from earth-centered earth-fixed Cartesian to altitude, latitude, longitude is described by

$$\begin{aligned} h &= \sqrt{x^2 + y^2 + z^2} - r_e \\ \phi &= \sin^{-1}\left(\frac{z}{\sqrt{x^2 + y^2 + z^2}}\right) \\ \lambda &= \operatorname{atan2}(y, x) \end{aligned} \tag{8}$$

where $\operatorname{atan2}(y, x)$ is a 4-quadrant arc-tangent function.

III.C.   WGS 84

The World Geodetic System is a standard for use in cartography, geodesy, and navigation. It comprises a standard coordinate frame for the Earth, a standard spheroidal reference surface (the datum or reference ellipsoid) for raw altitude data, and a gravitational equipotential surface (the geoid) that defines the nominal sea level. The latest revision is WGS 84 (dating from 1984 and last revised in 2004[2]).

Although WGS 84 is based on just four constants, we derive from them an additional parameter – r_p, the polar radius. Due to polar flattening of the earth, r_p is slightly less than r_e. The geodetic ellipsoid is then defined by the equation

$$\frac{x^2 + y^2}{r_e^2} + \frac{z^2}{r_p^2} = 1 \tag{9}$$

American Institute of Aeronautics and Astronautics

The transformations between altitude, latitude, longitude and ECEF Cartesian are significantly more complicated in the elliptical case. Note that all meridians on the reference ellipsoid are congruent ellipses having semi-major axis r_e and semi-minor axis r_p. The eccentricity ϵ of the meridian ellipses is a convenient parameter for expressing these transformations.

$$\epsilon = \sqrt{1 - \left(\frac{r_p}{r_e}\right)^2} \tag{10}$$

Then we can write the transformation from altitude, latitude, longitude to ECEF as

$$\begin{pmatrix} x \\ y \\ z \end{pmatrix} = \begin{pmatrix} \left[h + \frac{r_e}{\sqrt{1-\epsilon^2 \sin^2 \phi}}\right] \cos\phi \cos\lambda \\ \left[h + \frac{r_e}{\sqrt{1-\epsilon^2 \sin^2 \phi}}\right] \cos\phi \sin\lambda \\ \left[h + (1-\epsilon^2)\frac{r_e}{\sqrt{1-\epsilon^2 \sin^2 \phi}}\right] \sin\phi \end{pmatrix} \tag{11}$$

Obtaining a concise transformation from ECEF Cartesian to h, ϕ, λ is a challenging algebra problem which requires use of the quartic formula. For details on this solution, see Borkowski 1987.[3] The author also presents a simple and fast iterative method which is in common use.

IV. Coordinate systems

Coordinate systems are a fundamental consideration in the planning, simulation and execution of space missions. There are often multiple related systems for a single vehicle, and usually at least two for every celestial object. However, most of these systems result from application-specific requirements such as placement of sensors and other devices.

To keep matters as simple and consistent as possible, we specialize to the case of a single vehicle structural system with axes and origin fixed with respect to a rigid vehicle. The mass properties of the vehicle will be defined in terms of this system. Since our orbital cases all involve earth-centric scenarios, we can eliminate all but two planetary systems – Earth-centered inertial (ECI) and ECEF.

The ECI system is not a truly inertial system because its origin is accelerating with the earth as it makes its traversal around the sun. The key "inertial" feature is that the axes of the ECI frame do not rotate. This is critical because propagation of 6DOF dynamics in a rotating frame is extremely complex.

We need the ECEF frame in order to compute gravity and other environmental factors such as atmosphere which are linked to the planet.

There is a key transformation which links these two frames together. This transformation is usually composed of four elements:

- Rotation – the rotation of earth about its polar axis

- Nutation – a "wobble" of the polar axis with respect to some mean value

- Precession – the slow drift of the mean pole around a 23.5 degree cone

- Polar motion – not implemented in these comparisons

The ECI and ECEF systems which we use here are established by the International Earth Rotation and Reference System Service (IERS). The ECI system, known as J2000, is modeled on an equatorial system at the epoch of noon on 1 Jan 2000 in Greenwich, England. It is formally defined with respect to extra-galactic quasar sources.

The IERS publishes code and data to transform J2000 to an earth-fixed system defined by its three coordinate axes $\vec{X}$, $\vec{Y}$ and $\vec{Z}$.

- The $\vec{X}$ axis points from the center of the earth to the intersection of equator and prime meridian.

- the $\vec{Z}$ axis points from the center of the earth to the north pole.

- $\vec{Y} = \vec{Z} \times \vec{X}$

American Institute of Aeronautics and Astronautics

The IERS publishes code and tabular data which can be used to compute $\vec{X}$, $\vec{Y}$ and $\vec{Z}$ in J2000 coordinates. The RNP matrix M which transforms from ECI to ECEF is thus given by

$$M = \begin{pmatrix} \vec{X} \\ \vec{Y} \\ \vec{Z} \end{pmatrix} \tag{12}$$

where $\vec{X}$, $\vec{Y}$ and $\vec{Z}$ comprise the rows of the matrix M.

V.   Gravitation models

We discuss three classes of gravity models commonly used in aircraft and space vehicle simulations.

V.A.   Constant

For the simplest atmospheric model, the well-known English units approximation for acceleration due to gravity, 32.174 ft/s^2, or SI equivalent (9.80665 m/s^2, should be used as a constant where indicated.

V.B.   Inverse Square

The simplest model which could be considered for the propagation of a space vehicle is the model first proposed by Sir Isaac Newton in which the attractive force on each of two masses is given by

$$\vec{F}_1 = \frac{G m_1 m_2 \left(\vec{R}_2 - \vec{R}_1 \right)}{|\vec{R}_2 - \vec{R}_1|^3}$$
$$\vec{F}_2 = \frac{G m_1 m_2 \left(\vec{R}_1 - \vec{R}_2 \right)}{|\vec{R}_2 - \vec{R}_1|^3} \tag{13}$$

where $\vec{R}_1$ and $\vec{R}_2$ are the positions of each of two point masses m_1 and m_2 respectively and G is the universal gravitational constant.

The force is directed so as to represent an equal and opposite attraction between the point masses, and it's magnitude is proportional to the product of the masses divided by the square of the distance, hence the "inverse square" nomenclature.

In a two-mass system, it is possible to solve equation 13 exactly yielding the familiar Keplerian solutions. The differential equations

$$\ddot{\vec{R}}_1 = \frac{G m_2 \left(\vec{R}_2 - \vec{R}_1 \right)}{|\vec{R}_2 - \vec{R}_1|^3}$$
$$\ddot{\vec{R}}_2 = \frac{G m_1 \left(\vec{R}_1 - \vec{R}_2 \right)}{|\vec{R}_2 - \vec{R}_1|^3} \tag{14}$$

can be further simplified to the central force problem described by

$$\ddot{\vec{R}} = -\mu \frac{\vec{R}}{|\vec{R}|^3} \tag{15}$$

where $\vec{R}$ represents the position of m_2 with respect to their common center of mass, and $\mu = G \frac{m_1^3}{(m_1 + m_2)^2}$. For the purposes of simulating a vehicle m_2 in the gravitational well of a planet m_1, the simplification $m_1 >>> m_2$ gives

$$\mu = G m_1 \tag{16}$$

The gravitational acceleration shown in equation 15 can be viewed as the gradient of a potential function, and this approach will also work for higher order gravity models based on spherical harmonics. In general,

American Institute of Aeronautics and Astronautics

we write the equation for the gravitational acceleration $\vec{A}$ as

$$\vec{A} = \nabla \cdot u(\vec{R}) \tag{17}$$

V.C. Spherical Harmonic Gravity Models

The inverse square gravity model relies on the fact that the earth is nearly spherical, and thus its gravitational potential is approximately the same as if the entire mass of the earth were concentrated at its center. The mathematics of spherical harmonic expansions provides a convenient model for the gravitational potential of the earth with its flattening at the poles and other non-spherical irregularities. Gravitational fields are typically developed and expressed in spherical[a], planet-fixed coordinates.
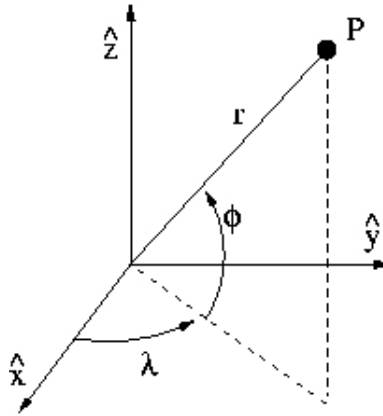
Figure 2. Spherical coordinates.

The coordinate frames in which the fields are developed are typically planet-fixed, that is, fixed with respect to the planetary body and, therefore, are generally non-inertial.

The basic formulation of the spherical harmonic expansion of a potential function is given by [4,5]

$$U(r, \lambda, \phi) = \frac{\mu}{r} \sum_{n=0}^{\infty} \sum_{m=0}^{n} \left(\frac{R}{r}\right)^n \bar{P}_{n,m}(sin\phi)(\bar{C}_{n,m} \cos m\lambda + \bar{S}_{n,m} \sin m\lambda) \tag{18}$$

where (r, λ, ϕ) are the spherical coordinates radius, longitude, and latitude (Figure 2), μ is the gravitational parameter ($\mu = GM$); n and m are model degree and order; R is the mean equatorial radius of the gravitational body; $\bar{P}_{n,m}$ is the fully normalized associated Legendre function of degree n and order m; and $\bar{C}_{nm}$ and $\bar{S}_{nm}$ are fully normalized unit-less gravity coefficients that are related to the mass distribution of the body.[4,6] The overhead bar denotes a coefficient that is fully normalized using the relationship

$$\left\{ \begin{array}{c} \bar{C}_{nm} \\ \bar{S}_{nm} \end{array} \right\} = \sqrt{\frac{(n+m)!}{(2-\delta_{0m})(2n+1)(n-m)!}} \left\{ \begin{array}{c} C_{nm} \\ S_{nm} \end{array} \right\} \tag{19}$$

where $\delta_{0m} = 1$ when $m = 0$, and $\delta_{0m} = 0$ when $m \neq 0$.

The zero-degree term (C_{00}) represents the spherical surface upon which the higher degree terms are imposed. It is unity by definition ($C_{00} = 1$). All $\bar{S}_{nm}$ terms vanish for $m = 0$ because the sine term in equation 18 vanishes when $m = 0$ ($\sin 0 = 0$). It can be shown[4,7] that the location of the center of mass $(\bar{x}, \bar{y}, \bar{z})$ of the gravitational body is related to the un-normalized first degree coefficients by

$$\begin{aligned} \bar{x} &= RC_{11} \\ \bar{y} &= RS_{11} \\ \bar{z} &= RC_{10} \end{aligned} \tag{20}$$

---

[a]Here the term *spherical* means coordinates based on a spherical body as opposed to an oblate elliptical body (i.e., geocentric vs. geodetic coordinates).

American Institute of Aeronautics and Astronautics

The normal practice is to define the spherical coordinate system such that the origin is located at the center of mass. Therefore, the first degree terms C_{10}, C_{11}, and S_{11} all equal zero. With these definitions of the zero-degree and first-degree terms, the spherical harmonic model becomes

$$U(r, \lambda, \phi) = \frac{\mu}{r} \left[1 + \sum_{n=2}^{\infty} \sum_{m=0}^{n} \left(\frac{R}{r} \right)^n \bar{P}_{n,m}(sin\phi)(\bar{C}_{n,m} \cos m\lambda + \bar{S}_{n,m} \sin m\lambda) \right] \tag{21}$$

An important special case of the spherical harmonic gravity model is the μ-J_2 model. The coefficient $\bar{C}_{2,0}$, aka J_2, reflects the oblateness of the earth and dominates the higher order terms. Many simulations only need the accuracy provided by these first two terms of the spherical harmonic expansion, and such implementations are often called μ-J_2 models or just the J_2 gravity model.

V.D.   Gravitational Effects on the Vehicle

The gravitational field is normally the major influence in determining the trajectory of a vehicle orbiting a massive body. There is also a rotational torque applied to the vehicle due to the gravity gradient. To model these effects, it is necessary to compute derivatives of the potential function with respect to inertial Cartesian coordinates as shown in equation 17. This is easy for the inverse square gravity model because we can write u simply in terms of the x, y, and z components of the inertial position $\vec{R}$.

$$u(x, y, z) = \frac{\mu}{\sqrt{x^2 + y^2 + z^2}} \tag{22}$$

Differentiating equation 22 gives

$$\begin{pmatrix} \ddot{x} \\ \ddot{y} \\ \ddot{z} \end{pmatrix} = \frac{-\mu}{(x^2 + y^2 + z^2)^{\frac{3}{2}}} \begin{pmatrix} x \\ y \\ z \end{pmatrix} \tag{23}$$

There is significantly more complexity required to compute the gradient of a potential defined by equation 21. Since the potential is defined in terms of planet fixed coordinates, and the derivatives must be taken with respect to inertial Cartesian coordinates, it is essential to have ready access to the time varying transformation M defined in equation 12. We can write the equation for inertial translational acceleration as

$$\vec{A} = M^T \frac{\partial u}{\partial \vec{R}_{pfixed}} (M\vec{R}_{inertial}) \tag{24}$$

and similarly,

$$H_{inertial} = M^T H_{pfixed} M \tag{25}$$

where $\vec{R}_{pfixed}$ is the Cartesian planet-fixed position, $\vec{R}_{inertial}$ is the inertial Cartesian position, $H_{inertial}$ is the matrix of second derivatives of u with respect to inertial Cartesian coordinates and H_{pfixed} is the matrix of second derivatives of u computed with respect to earth-fixed Cartesian coordinates.

V.D.1.   Gravity Gradient Torque

The other important effect of gravity on orbiting vehicles is the torque exerted by the gravity gradient which can be computed from $H_{inertial}$ as defined in equation 25.

It is convenient to use the inertia tensor I as defined in equations 3 and 4 and a gradient approximation for gravity near the vehicle to provide an accurate estimate of torque due to gravity gradient.

Note that the inertia tensor is commonly expressed in the body-fixed frame, and we often wish to express torque in the body frame. To this end, we transform the gravity gradient matrix from the inertial frame to spacecraft body-fixed coordinates using a similarity transformation

$$G = BH_{inertial}B^T \tag{26}$$

where B is the inertial to body-fixed transformation matrix.

American Institute of Aeronautics and Astronautics

The gravitational torque acting on the spacecraft can then be expressed as

$$\vec{\tau} = \int \vec{\rho} \times G\vec{\rho}dm \tag{27}$$

where the vector $\vec{\rho}$ is defined as in equation 5. The torque can be expressed in terms of I and G as

$$\vec{\tau} = \left(\begin{array}{c} G_{2,3}(I_{zz} - I_{yy}) - G_{1,3}I_{xy} + G_{1,2}I_{xz} - I_{yz}(G_{3,3} - G_{2,2}) \\ G_{1,3}(I_{xx} - I_{zz}) + G_{2,3}I_{xy} - G_{1,2}I_{yz} - I_{xz}(G_{1,1} - G_{3,3}) \\ G_{1,2}(I_{yy} - I_{xx}) - G_{2,3}I_{xz} + G_{1,3}I_{yz} - I_{xy}(G_{2,2} - G_{1,1}) \end{array} \right) \tag{28}$$

VI. Atmosphere models

VI.A. US 1976

The U.S. Standard 1976 Atmosphere model[8] is used for the majority of the atmospheric check-case scenarios (table 1). This model is often implemented as non-linear functions approximated by linear interpolation from a one-dimensional table as a function of either geometric altitude (h) or geopotential height (Z).

VI.B. Marshall Engineering Thermosphere (MET)

The Marshall Engineering Thermosphere Model (MET) is essentially a modified Jacchia 1970 model that includes some spatial and temporal variation patterns of the Jacchia 1971 model. In addition to thermospheric densities and temperatures, the well-documented code provides several often used parameters like gravitational acceleration and specific heat. MET was developed at NASA's Marshall Space Flight Center in Huntsville primarily for engineering applications of low Earth orbiting spacecraft.[9–11]

VII. Data Formats

The use of standard formats significantly speeds up the process of sharing models and comparing results. While quite a bit of manual processing is still required to set up a tool to receive models in an unfamiliar format, and to output data in a compatible binary data packaging format, the ability to accept changes and generate new results is greatly expedited by this investment.

VII.A. Reference models - S-119 format

Most of the models for the atmospheric check-cases were specified using the format specified in a recent AIAA-sponsored flight model exchange format, S-119,[12] which makes use of an XML-based grammar, DAVE-ML.[13] This standard attempts to define the salient flight characteristics of an aerospace vehicle (aerodynamics and inertia, for example) in an unambiguous text file that is human- and machine-readable and easily archived. The most complex model was the single-engine fighter aircraft that included an inertial/mass properties model, a non-linear aerodynamic model, and a set of autopilot models, all defined in DAVE-ML using S-119 variable names.

These models will be made available by NASA prior to publication of the final NASA report.

VII.B. Time-history data

The parameter trajectories from executing the reference models in each check-case scenario were stored in Dryden's flight-test time history format, DTH. This compact format has an efficient storage footprint and is compatible with a set of plotting and analysis tools. Several tools are available on request from Dryden (DFRC-SimHelp@mail.nasa.gov) to work with this type of data.

VII.B.1. DthData

DTH (Dryden Time History) data is a library of functions that can be incorporated into any application for creation of DTH files and is a standalone tool (dthdata) used to process DTH files. The most fundamental capability of the dthdata program is extracting selected signals and time segments from an input file and

American Institute of Aeronautics and Astronautics

writing the selected data to an output file. Other capabilities include converting file formats, merging data from multiple input files, time skewing, interpolating to common output frame times, renaming signals, and generating calculated output signals as functions of the input signals.

DTH data formats can be classified as time history data showing values of various parameters (signals) as functions of time. The parameter values are sampled and recorded at regular time intervals. Various formats are supported to allow interfacing to other tools such as MATLAB or Dryden's Quickplot. Table 10 below describes the supported formats.

Table 10. Time-History Data File Formats supported by DTH tools

Format	File Type	Max. Number Signals	Signal Name Length	Data Precision	Comments	Limits
asc1	text	2000	16	n/a	Readable but inefficient	
asc2	text	2000	13	n/a	Readable but inefficient	
cdf1	text	2000	variable	n/a	Features from rir1 and csv1 formats	lines ≤ 16384 bytes
cmp3	compressed binary	2000	16	3, 4, or 8 bytes	Compressed, machine-independent	
cmp4	compressed binary	2000	16	32- or 64-bit IEEE 754	Compressed, machine-independent	
csv1	text	2000	variable	n/a	Useful with MS Excel	lines ≤ 16384 bytes
rir1	text	9	variable	Double	Radar data file (RIPS)	Fixed delta time (50 msec). No headers.
sif1	binary	2000	10	4 or 8 bytes	Langley format	
unc0	uncompressed binary	800	40	4 bytes	unc3 with longer names	
unc2	uncompressed binary	2000	16	4 bytes	Easy to implement	
unc3	uncompressed binary	2000	16	4 bytes	Easy to implement	

VII.B.2. QuickPlot

QuickPlot is a general-purpose data-plotting tool for engineers and scientists. At Dryden, QuickPlot is primarily used for plotting time-history data obtained during flight-testing or flight simulations. The tool

- Is fast, simple, and powerful

- Uses the X Window environment and is supported on Linux, Solaris and Solaris X86

- Can generate hard-copy in color or black and white Encapsulated PostScript (EPS)

- Can modify and create Signals using algebraic expressions

- Can accept command-line interface and intuitive mouse commands

- Can be driven by prepared command script files

Quickplot presents a flexible data interface so users can read data files in the Dryden Time History (DTH) family of formats and the MATLAB .mat format.

VII.B.3. Dthdiff

Dthdiff is a tool used to compare DTH time history files for validations. The tool is based on DTH data library and supports all of the DTH file formats. The tool supports a number of optional tolerances that provide flexibility in configuring the nature of a comparison. These tolerances are for checking agreement to a number of significant digits, absolute, relative, and percent.

American Institute of Aeronautics and Astronautics

Summary output will indicate the number of samples that failed to meet a specific tolerance test. Optionally the tool will output a QuickPlot script file for those parameters that failed all tolerance tests specified.

VIII.   Simulation Tools Description

A brief description of the represented simulation tools is given in this section.

VIII.A.   JEOD/Trick (JSC)

The JSC Engineering Orbital Dynamics (JEOD) is a suite of models needed to propagate the 6 degree of freedom states of one or more rigid vehicles in the orbital or interplanetary environment. The software models vehicle dynamics, environment, interactions and provides necessary math and software utilities to work with a simulation engine. Trick is a generic simulation tool which provides the infrastructure to define and initialize and run the simulation, and log/display its output. JEOD and Trick leverage a common history which enables an integrated simulation framework for orbital vehicles.

VIII.B.   LaSRS++ (LaRC)

The Langley Standard Real-Time Simulation in C++ (LaSRS++) is an object-oriented framework for construction of aerospace vehicle simulations. LaSRS++ simulations support desktop analysis, hardware-in-the-loop simulations, and high-fidelity, human-in-the-loop simulators. Projects using LaSRS++ have modeled commercial transport aircraft, military fighters, advanced concept aircraft, launch vehicles, planetary landers, crewed spacecraft, planetary aircraft, and unmanned aerial vehicles.

VIII.C.   MAVERIC (MSFC)

MAVERIC is a low to high-fidelity three/six degree-of-freedom (3-DOF/6-DOF) vehicle flight simulation program developed at Marshall Space Flight Center, written primarily in the C and C++ programming languages. MAVERIC was designed to be generic and data-driven and can provide for the rapid development of an end-to-end vehicle flight simulation which starts at launch and ends at "wheel stop" after landing (or splashdown). The vehicle simulation models are layered upon a set of foundational software called TFrames. TFrames is a time-based differential equation solver environment and is public-domain software. TFrames provides an environment for developing a dynamic simulation that insulates the simulation developer from the tedious programming details associated with numerical integration, discrete data sampling, table lookups, etc. High-level routines provide convenient interfaces between the simulation code and the numerical integration engine.

VIII.D.   POST-II (LaRC)

The Program to Optimize Simulated Trajectories II (POST II) is a generalized point mass, discrete parameter targeting and optimization program. POST II provides the capability to target and optimize point mass trajectories for multiple powered or unpowered vehicles near an arbitrary rotating, oblate planet. POST II has been used successfully to solve a wide variety of atmospheric ascent and reentry problems, as well as exo-atmospheric orbital transfer problems. The generality of the program is evidenced by its multiple phase simulation capability which features generalized planet and vehicle models. This flexible simulation capability is augmented by an efficient discrete parameter optimization capability that includes equality and inequality constraints.

POST II increases the trajectory simulation capability of the original POST computer code and provides a state-of-the-art software tool. POST II contains many basic models (such as atmosphere, gravity, propulsion and navigation system models) that are used to simulate a wide variety of launch, orbital, and entry missions. As indicated above, POST II can support multiple vehicles in a single simulation, each with independently defined environments, vehicle and attracting body characteristics. Thus, each vehicle can have its own guidance, navigation, and control system for completely independent, onboard autonomy. Conversely, effects of multi-body and interaction forces that depend on the relationship of one vehicle to another can be included.

Additionally, POST II can support 3DOF and 6DOF trajectories within the same simulation; not only can each vehicle trajectory support different degrees-of-freedom, but also each trajectory segment within

American Institute of Aeronautics and Astronautics

a given simulation can be either 3DOF or 6DOF. The internal structure for variable value storage was adjusted in POST II to permit efficient storage of multiple vehicle/simulation information as well as update coding structure to current standards. This usage of variable structures also increases POST II portability to other platforms. Variable structures (and substructures) also provide code efficiency by allowing the same FORTRAN routines to be used for engineering calculations (e.g., aerothermodynamic heating, aerodynamic forces, propellant flowrates, attitude angles, etc.) of all vehicles by simply exchanging the data of one vehicle for another during the simulation. New input enhancements provide N-dimensional tables, multiple criterion to identify trajectory phase completion, Boolean logic for these multiple criterion, and the ability to use variable (instead of constant) values to trigger events, as well as increase code portability between various computer platforms and operating systems.

Several features related to the multiple vehicle capability of POST II enable trajectory simulations not previously possible in a single POST run. POST II provides the ability to initialize multiple vehicles from the state of another during the simulation. That is, an additional vehicle can be initialized by providing input deltas to another vehicle's state (position, velocity, attitude, and attitude rate) at any event in the simulation. This capability also includes a mechanism for transferring some or all of the parent vehicle's angular momentum to the children vehicles. Also, the ability to activate and/or deactivate any number of vehicles at any event in the simulation is included. The standard POST II input options are available to initialize the state of any vehicle being activated. POST II maintains and increases the user's ability to modify certain subroutines for specific applications. The software is constructed such that user provided code can be included to provide vehicle aerodynamic data, atmosphere model, and even optimization capability. While POST II provides very adequate models for including these data and functions, the user has substantial flexibility to include mission specific models as well as company proprietary representations and functionality. Additionally, support for statistical analysis approaches (such as Monte Carlo dispersion analyses) is also provided.

VIII.E. VMSRTE (ARC)

The Vertical Motion Simulator Real-Time Environment (VMSRTE) provides a flexible environment for man-machine research, capable of rapid prototyping and run-time reconfiguration of vehicle models, simulator hardware, and the surrounding laboratory, combined with efficient operation and data collection. It offers source-level debugging and the ability to alter simulation and facility variables during program execution. A standardized framework streamlines simulation development by providing elements that are common to most simulations. A wide variety of vehicles have been simulated on the VMS including rotorcraft, VSTOL and conventional aircraft, spacecraft, and airships. Research topics have also spanned a wide range, including handling qualities, guidance and display development, flight control design, concept demonstration and evaluation, human-factors, and simulation fidelity requirements.

VIII.F. Core (DFRC)

All current simulations at NASA Dryden are based on a common software framework, called "Core". Core is used for aircraft simulations ranging from gliders to suborbital vehicles and runs on platforms ranging from laptop computers to pilot-in-the-loop / aircraft-in-the-loop simulators. Core is composed of standard models, mathematical routines, a user interface, hardware interfaces, timing routines, data recording and data input subsystems, external application interfaces, and other sharable modules. Core is predominately written in the C++ computer programming language but supports legacy FORTRAN models. Currently the simulators located at NASA Dryden are used for engineering analysis more than for pilot training. Typical simulation tasks include evaluation of new vehicle concepts, control law development and validation, flight safety analysis, mission planning, flight envelope expansion, and post-flight data analysis.

IX.   Results

Several comments should be made regarding the results shown in this paper. As mentioned previously, this paper is basically a snapshot of an on-going project to compare several NASA simulation tools attempting to simulate identical aerospace craft in atmospheric and exoatmospheric flight. While quite a bit of agreement exists (thankfully), some differences are apparent in the results and are discussed in detail for each checkcase.

American Institute of Aeronautics and Astronautics

Some of the differences can be attributed to different initial conditions due to ambiguity in the description of the check-case; these ambiguities will be addressed and corrected for the final report.

One purpose of the check-cases is to assess the extent to which differences in implementation (such as selection of native coordinate systems) can affect results. Initial conditions were provided in a number of coordinate frames so that each simulation can set up the scenario with minimal change in their existing initialization feature. Even so, some ambiguity remained (and the IC sets continued to be refined) which illustrates one of the challenges in communicating simulation models between tools.

In general, the atmospheric results are in English units. This is believed to be common practice in the U.S. even as the orbital community has mostly adopted SI units; this paper reflects that difference between the U.S. aviation and space communities. (Of course there are exceptions in both camps; several of these tools can handle either set of units.)

As these are preliminary results, the identities of the various tools are masked to avoid embarrassment (and to encourage participation) in this voluntary effort. Also, the atmospheric cases use SIM1, SIM2, etc. while the orbital cases use SIM_A, SIM_B, etc. to identify the various simulations; at least one of these simulation tools are represented in both sets of results (atmospheric and orbital) but have different identities. In the final paper, these identities will be harmonized.

Simulation developers were free to pick the time steps and integration methods that they felt gave the most accurate results. There was no requirement to run in real-time (e.g. pilot- or hardware-in-the-loop).

The scales of some of these parameters that are co-plotted may be masking significant differences in the results, but are not shown here due to size limitations. The final report will include plots of residuals between the implementations to assist in exposing small differences.

IX.A. Scenario comparisons – Atmospheric

IX.A.1. Check-case 1 – dropped sphere in vacuo

This section shows cross-plots for five of the selected simulation tools in modeling the dynamics of a spheroid dropped in vacuo, accelerating towards the surface of the earth from 30,000 ft above the equator.

Figures 3 and 4 compare results between NASA simulation tools in geodetic position, Euler angles, local velocities and body rotational rates.

As can be seen, these results match very well. As expected, a slow Eastward movement relative to the ground (positive longitude) results as altitude decreases but inertial velocity, matched to hold geodetic longitude at the original altitude, remains constant.

The only visible discrepancy is a constant pitch angle of $\approx -3.4 \times 10^{-6}$ degrees for SIM3. This variation in pitch could be considered negligible. Nevertheless, the value seems a little large to be driven by machine precision. It also does not appear to be derived from the initial inertial orientation or the initial Earth relative velocity, both of which match the scenario initial condition exactly. The translation of aerodynamic forces into body coordinates in atmospheric check-case 6 below indicates, however, that this is a real difference present within the simulation. Nevertheless, a cause for the difference could not be identified in the data, and this difference is still under investigation.

American Institute of Aeronautics and Astronautics

American Institute of Aeronautics and Astronautics
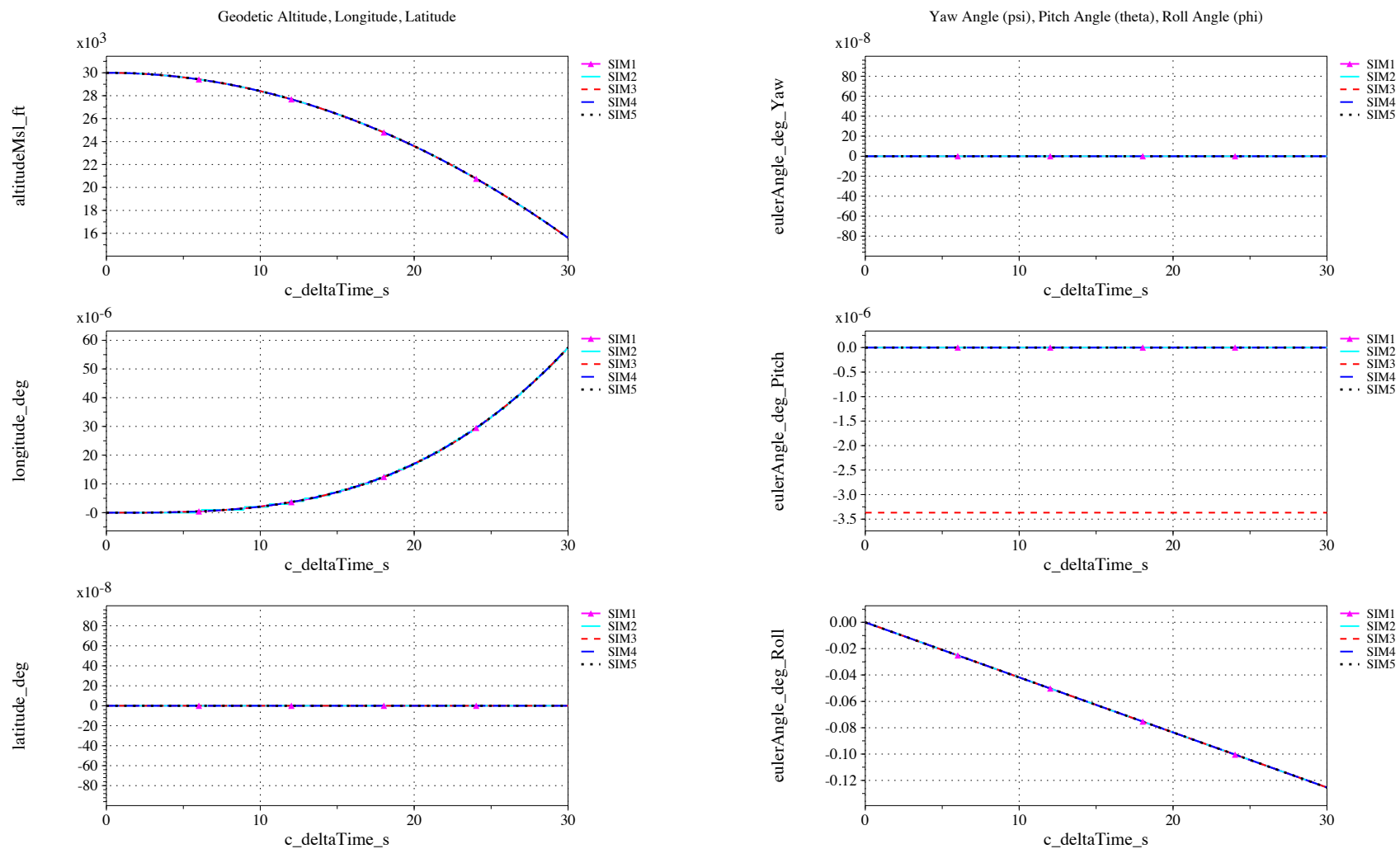
Figure 3. Positions and Rates vs. time (check-case 1: sphere dropped in vacuo)

American Institute of Aeronautics and Astronautics
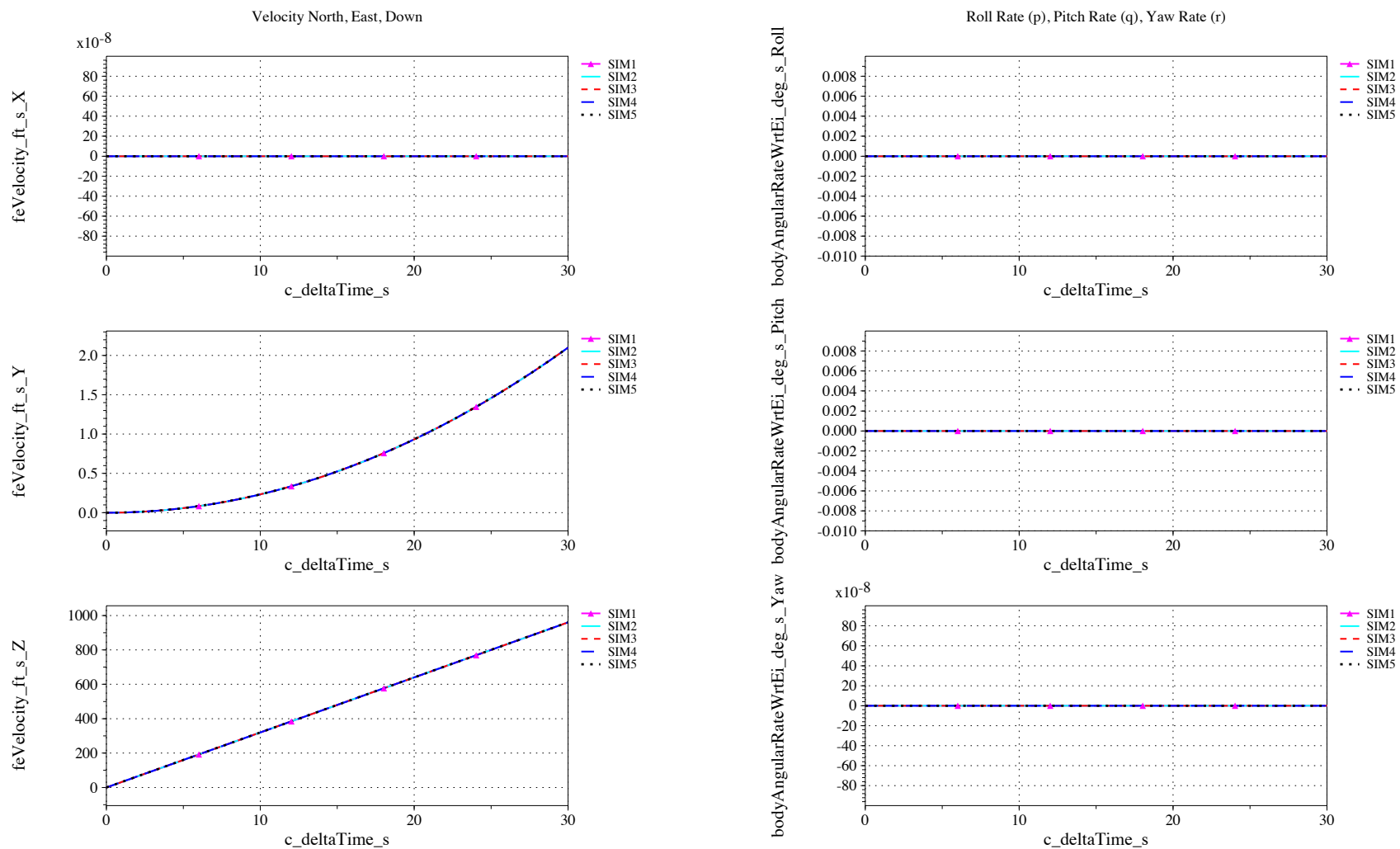
Figure 4. Positions and Rates vs. time (check-case 1: sphere dropped in vacuo)

IX.A.2. Check-case 2 – tumbling brick

This section shows cross-plots for four of the selected simulation tools in modeling the dynamics of a brick tumbling in vacuo with initial body-axis inertial angular rates (10, 20 and 30 deg/s, respectively).

Figures 5 and 6 compare results between NASA simulation tools in geodetic position, Euler angles, local velocities and body rotational rates.

All simulations appear to be in good agreement; however, SIM2 pitch and roll angles slowly depart from the other simulations with time to a maximum of ≈ 3.4 degrees. A cause for the difference could not be found in the data. This divergence is not due to differences in initial angular rates as presented in the recorded data; what differences do exist should produce much smaller divergences in pitch and roll. Also, there is no introduction of moments (aerodynamic moment is zero throughout).

Also apparent are varying definitions and ranges for Euler pitch angle: SIM2 continues to increase pitch angle beyond the range at which other tools wrap around; and those tools disagree on whether pitch angle should range from ±180 or 0 − 360 degrees.

American Institute of Aeronautics and Astronautics

Geodetic Altitude, Longitude, Latitude

Yaw Angle (psi), Pitch Angle (theta), Roll Angle (phi)
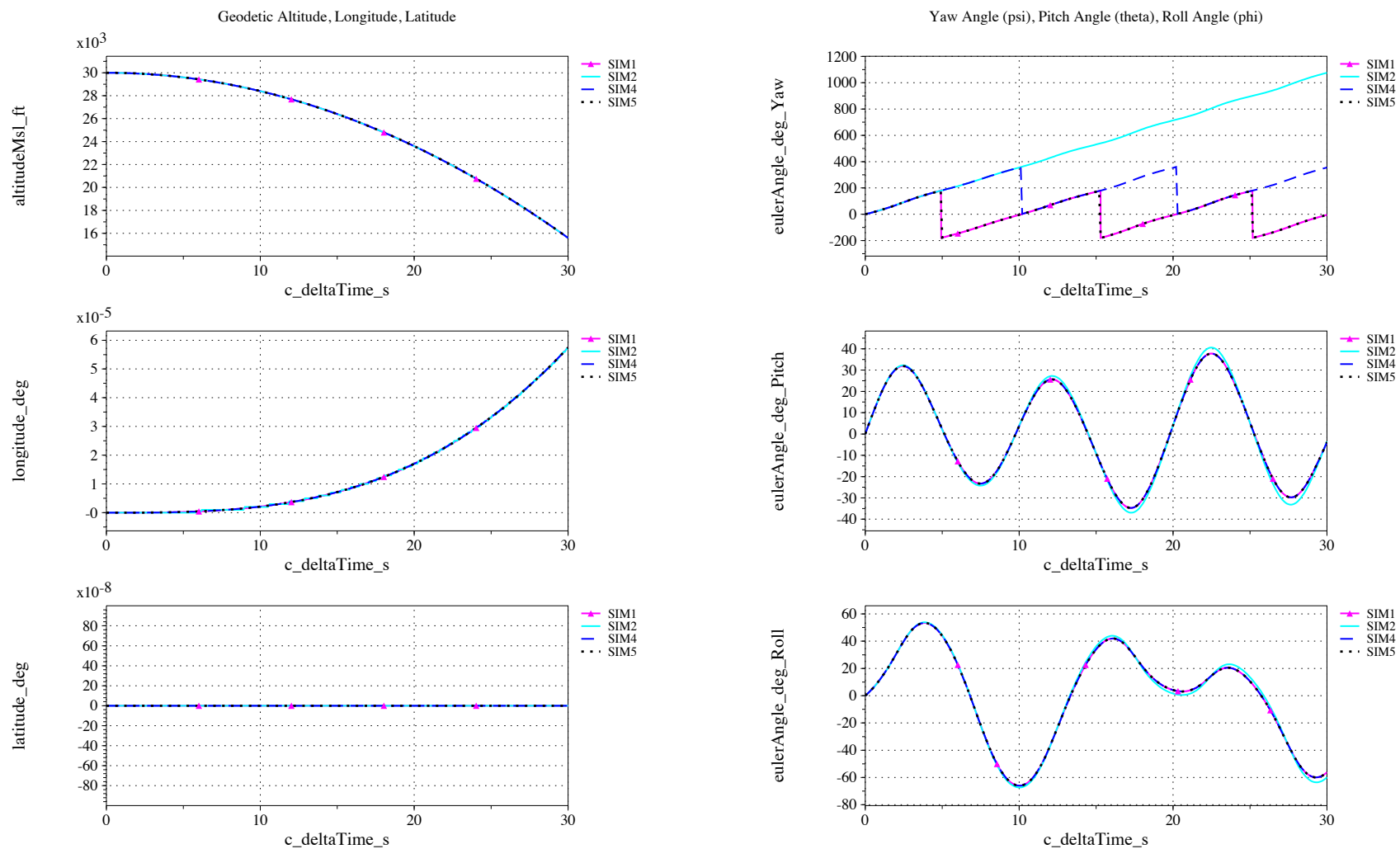
Figure 5. Position and Euler angle vs. time (check-case 2: tumbling brick in vacuo)
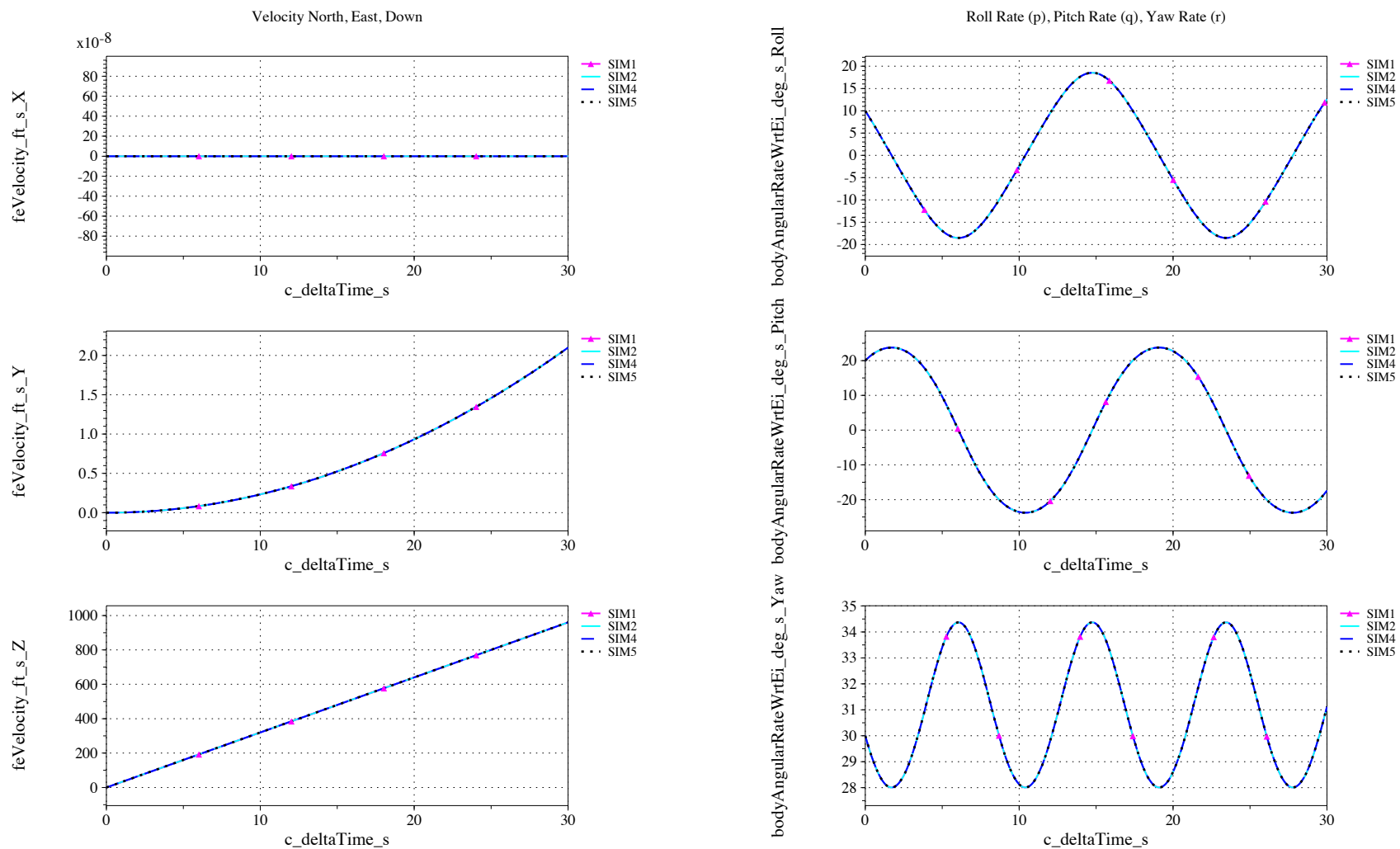
Figure 6. Local velocity and inertial body rates vs. time (check-case 2: tumbling brick in vacuo)

IX.A.3.   *Check-case 3 – tumbling brick with damping*

This section shows cross-plots for four of the selected simulation tools in modeling the dynamics of a brick tumbling as it falls through the atmosphere, after starting with initial body-axis inertial angular rates of 10, 20 and 30 deg/s, respectively.

Figures 7 and 8 compare results between NASA simulation tools in geodetic position, Euler angles, local velocities and body rotational rates.

SIM2 included aerodynamic drag so its position and velocity values in the East and Down directions depart slightly from the other simulations. This also causes the differences in atmospheric properties and gravity values. There was some ambiguity as to whether to include drag; this ambiguity will be eliminated and the cases re-run for the final report, but illustrate the difficulty of precisely nailing down all the parameters of a simulation.

American Institute of Aeronautics and Astronautics

Geodetic Altitude, Longitude, Latitude

Yaw Angle (psi), Pitch Angle (theta), Roll Angle (phi)
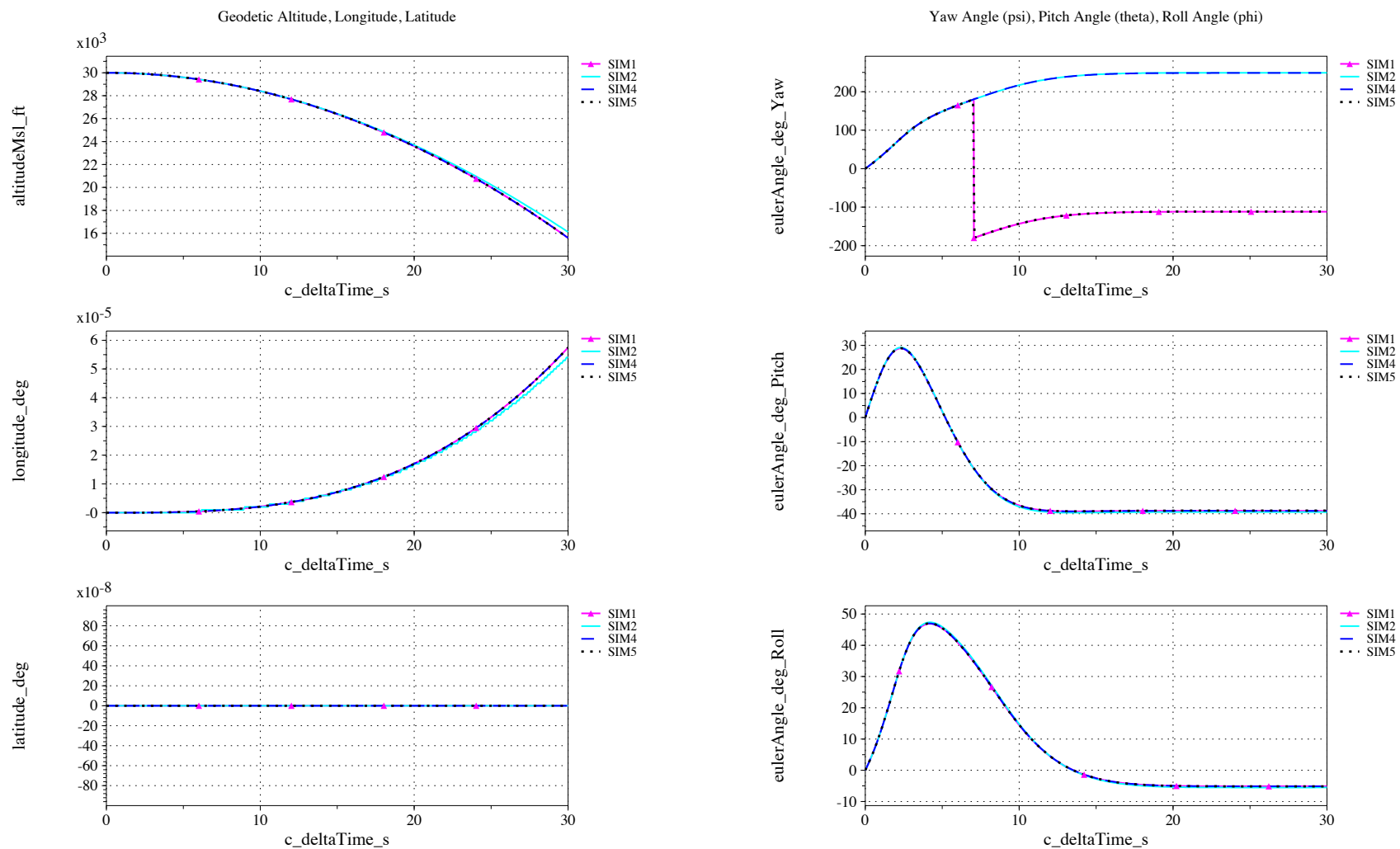
Figure 7. Position and Euler angle vs. time (check-case 3: tumbling brick with damping)
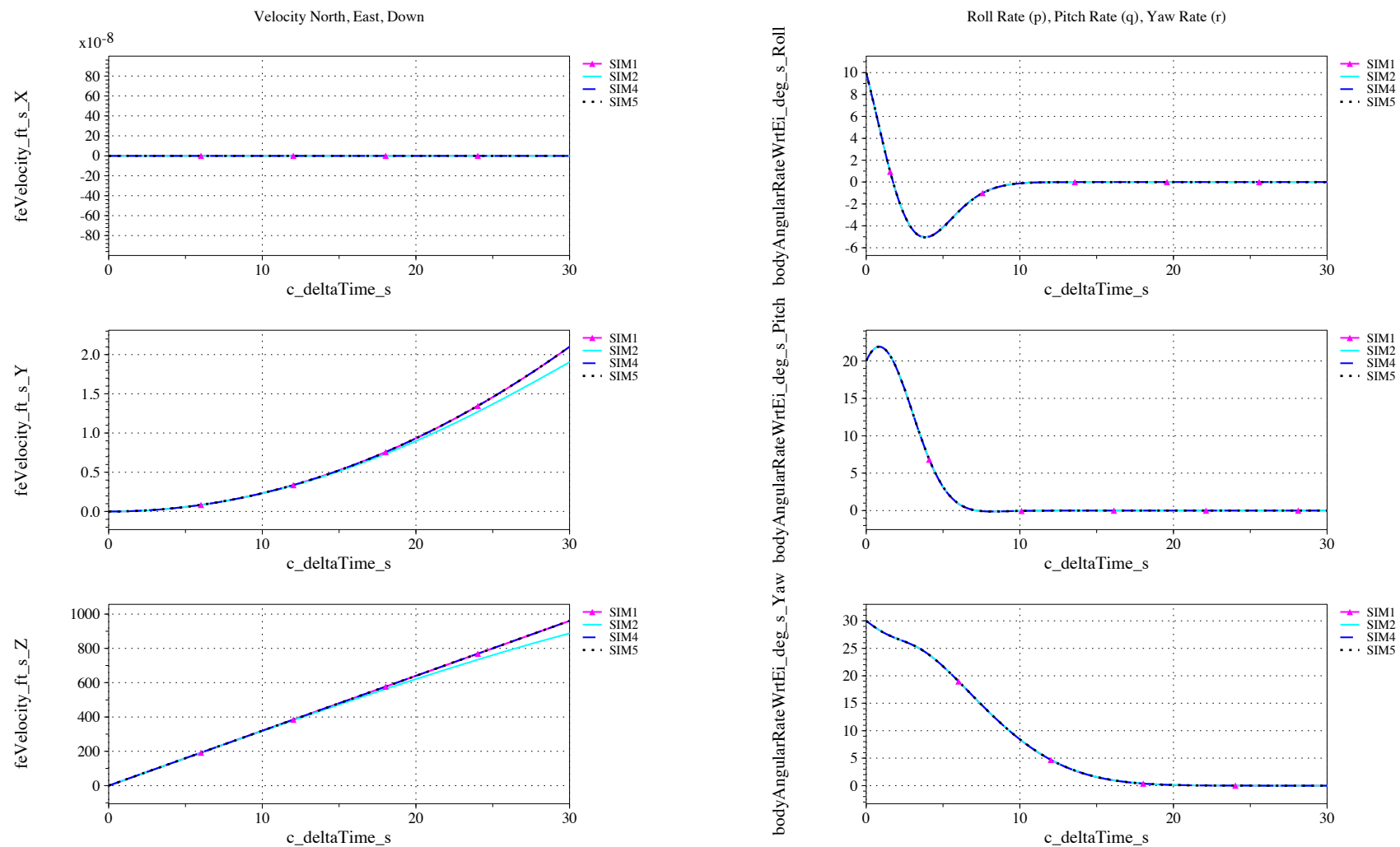
Figure 8. Local velocity and inertial body rates vs. time (check-case 3: tumbling brick with damping)

IX.A.4. Check-case 4 – dropped sphere over round, fixed, Earth

This section shows cross-plots for three of the selected simulation tools in modeling the dynamics of a sphere dropped with a fixed drag coefficient through a still atmosphere in a non-rotating Earth with spherical gravity.

The initial conditions called for initial body-axis rotations of 10, 20 and 30 deg/sec, respectively about the x, y and z axes.

Figures 9 and 10 compare results between NASA simulation tools in geodetic position, Euler angles, local velocities and body rotational rates.

Inertial X positions differ between SIM5 and SIM4 (not shown). SIM5 is using the radius of equal surface area specified for the spherical Earth. SIM4 used the WGS 84 equatorial radius.

All three simulations differ on gravity. SIM2 uses a constant value, g. SIM5 and SIM4 appear to use inverse square. SIM 5 and SIM 4 differ however due to the differences in Earth radius (see above). Gravity differences do not produce position differences large enough to see on the plots.

SIM2 pitch and roll Euler angles are slowly growing in amplitude and heading angle is shifting in phase relative to SIM4 and SIM5. At the end of 30 seconds, the pitch and yaw Euler angles in SIM2 differ from SIM4 and SIM5 by ≈ 5 degrees in pitch and roll and by ≈ 3 degrees in yaw. All three simulations show zero aerodynamic moments and match on angular body rates. Furthermore, none of the simulations travels very far from the starting latitude and longitude (which would change the orientation of the local vertical frame). So, the cause of the Euler angle difference is not apparent from the data posted.

American Institute of Aeronautics and Astronautics

American Institute of Aeronautics and Astronautics
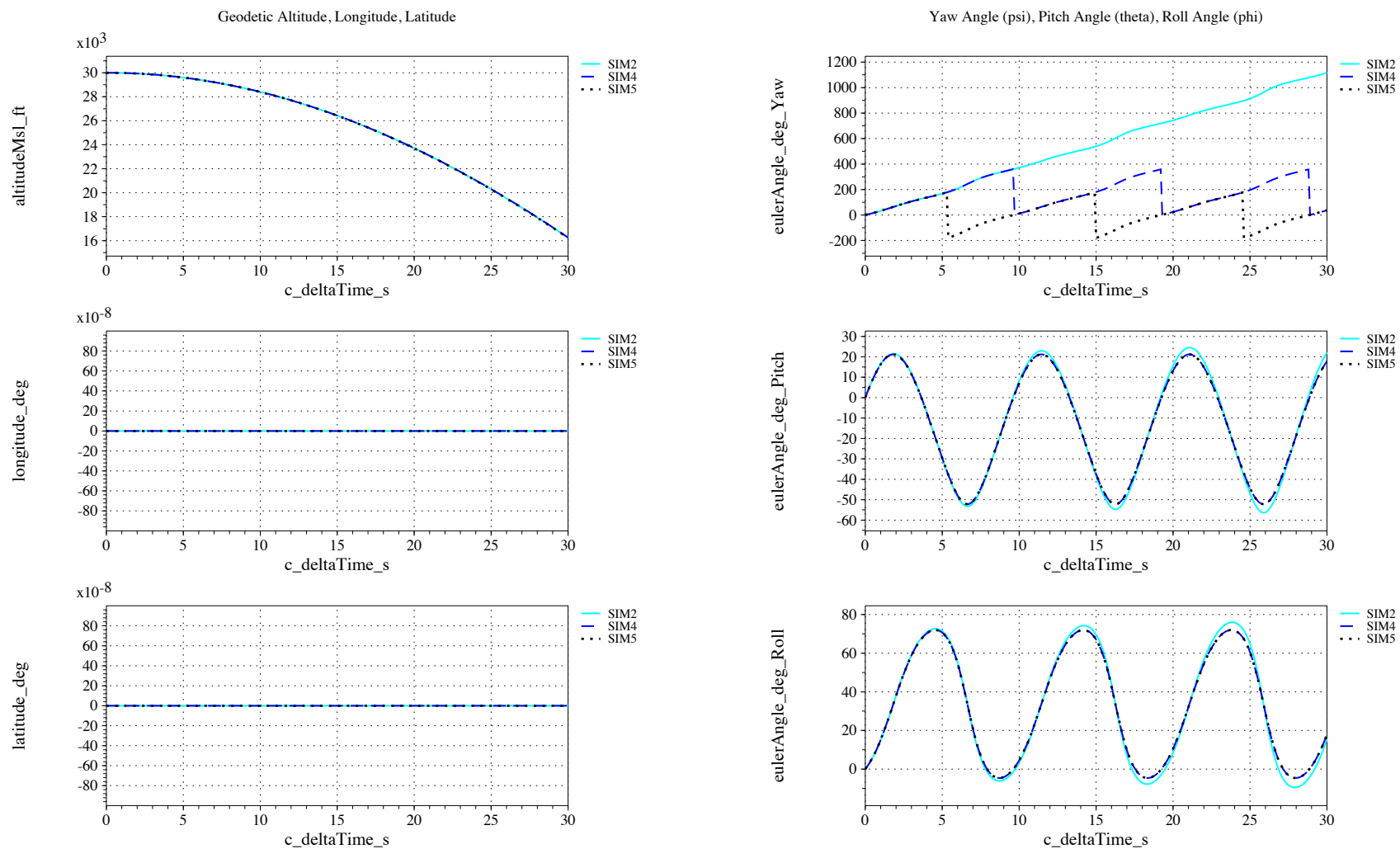
Figure 9. Position and Euler angle vs. time (check-case 4: sphere dropping over non-rotating, spherical earth)
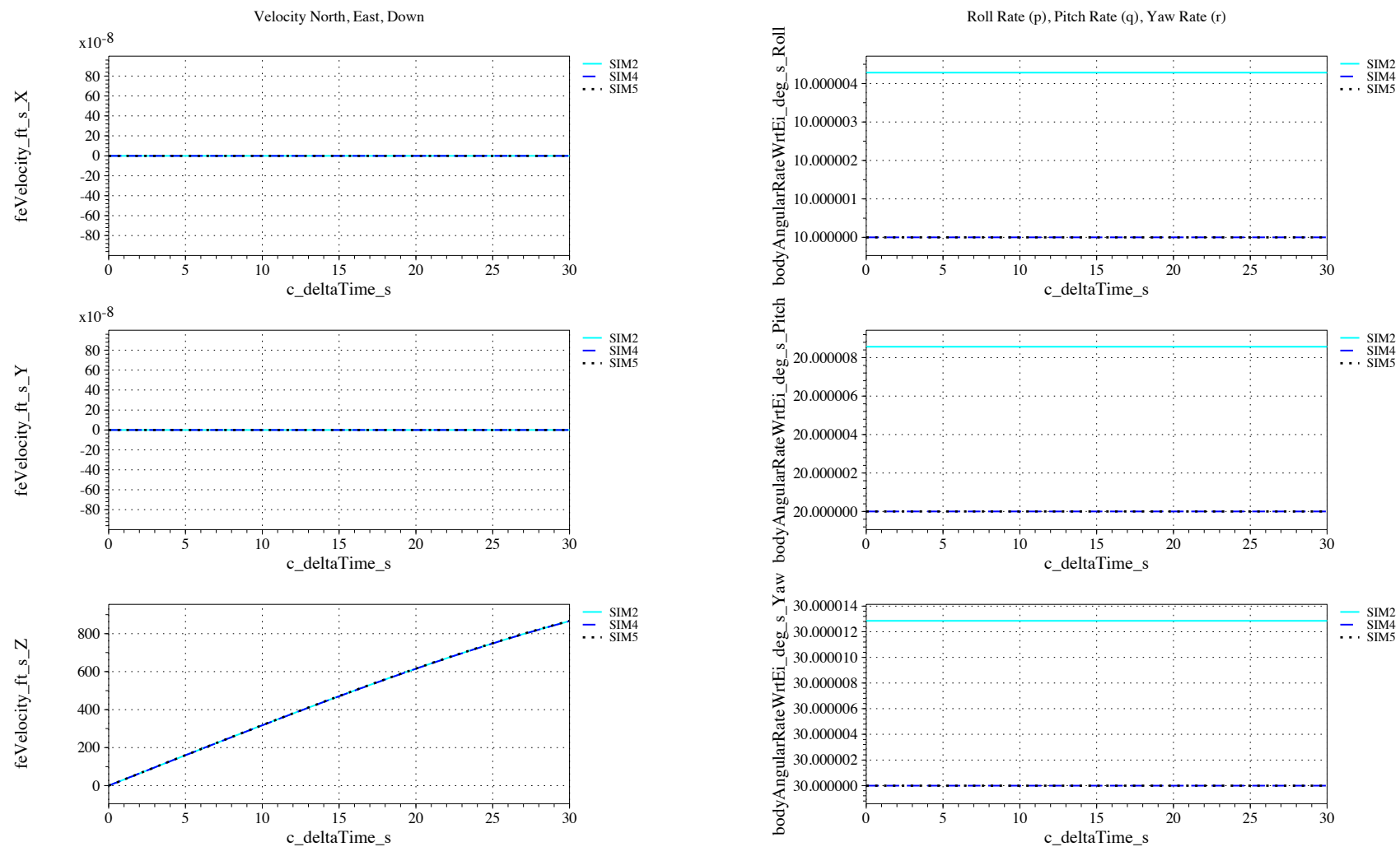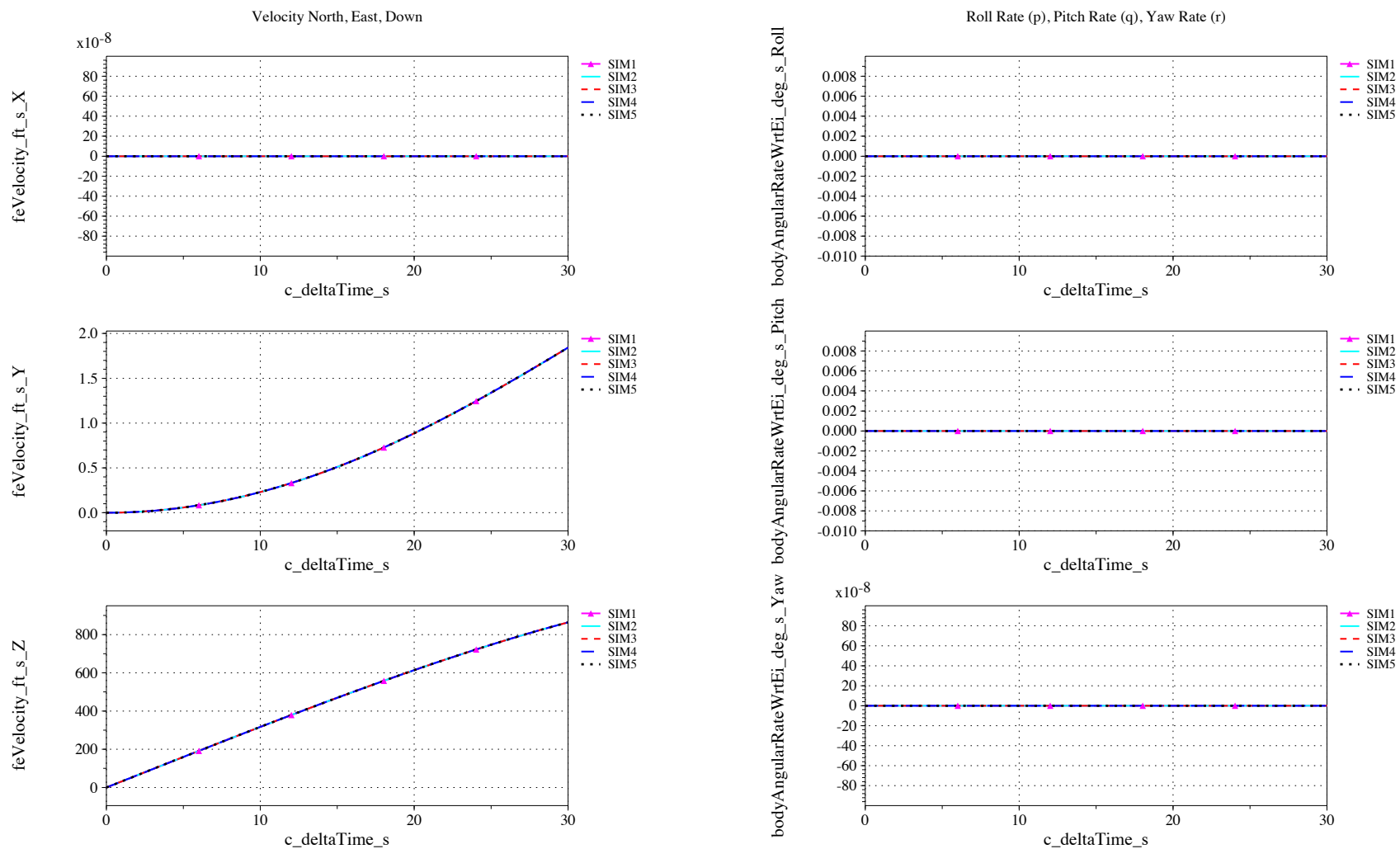
Figure 10. Local velocity and inertial body rates vs. time (check-case 4: sphere dropping over non-rotating, spherical earth)

IX.A.5.   Check-case 5 – dropped sphere over round, rotating, Earth

This section shows cross-plots for three of the selected simulation tools in modeling the dynamics of a sphere dropped with a fixed drag coefficient through a still atmosphere in a round rotating Earth with spherical gravity.

Figures 11 and 12 compare results between NASA simulation tools in geodetic position, Euler angles, local velocities and body rotational rates.

SIM2 appears to have initialized Earth-relative rotation to the specified rate and the other simulations initialized inertial-relative rotation to the specified rate. Therefore, the SIM2 roll rate differs by the rotation of the Earth. Differences in pitch and yaw rates are due to truncated precision of recorded data.

SIM2 Euler angles closely follow the other simulations; nevertheless, its pitch and roll angles are slowly growing in amplitude and its heading angle is shifting in phase relative to SIM4 and SIM5. At the end of 30 seconds, the pitch and yaw Euler angles in SIM2 differ from SIM4 and SIM5 by 5 degrees in pitch and roll and by 3 degrees in yaw. All three simulations show zero aerodynamic moments and nearly match on angular body rates. The difference in body rates does not account for the difference in Euler angles. Furthermore, none of the simulations travels very far from the starting latitude and longitude (which would change the orientation of the local vertical frame). So, the cause of the Euler angle difference is not apparent from the data posted.

Inertial X positions differ between SIM5 and SIM4 (not shown). SIM5 is using the radius of equal surface area specified for the spherical Earth. SIM4 used the WGS 84 equatorial radius.

SIM4 and SIM5 differ on initial inertial velocity towards the East due to differences in Earth radius (see case 4).

All three simulations differ on gravity. SIM2 uses a constant value, g. SIM5 and SIM4 appear to use inverse square. SIM5 and SIM4 differ however due to the differences in Earth radius (see above). Gravity differences do not produce position differences large enough to see on the plots.

American Institute of Aeronautics and Astronautics
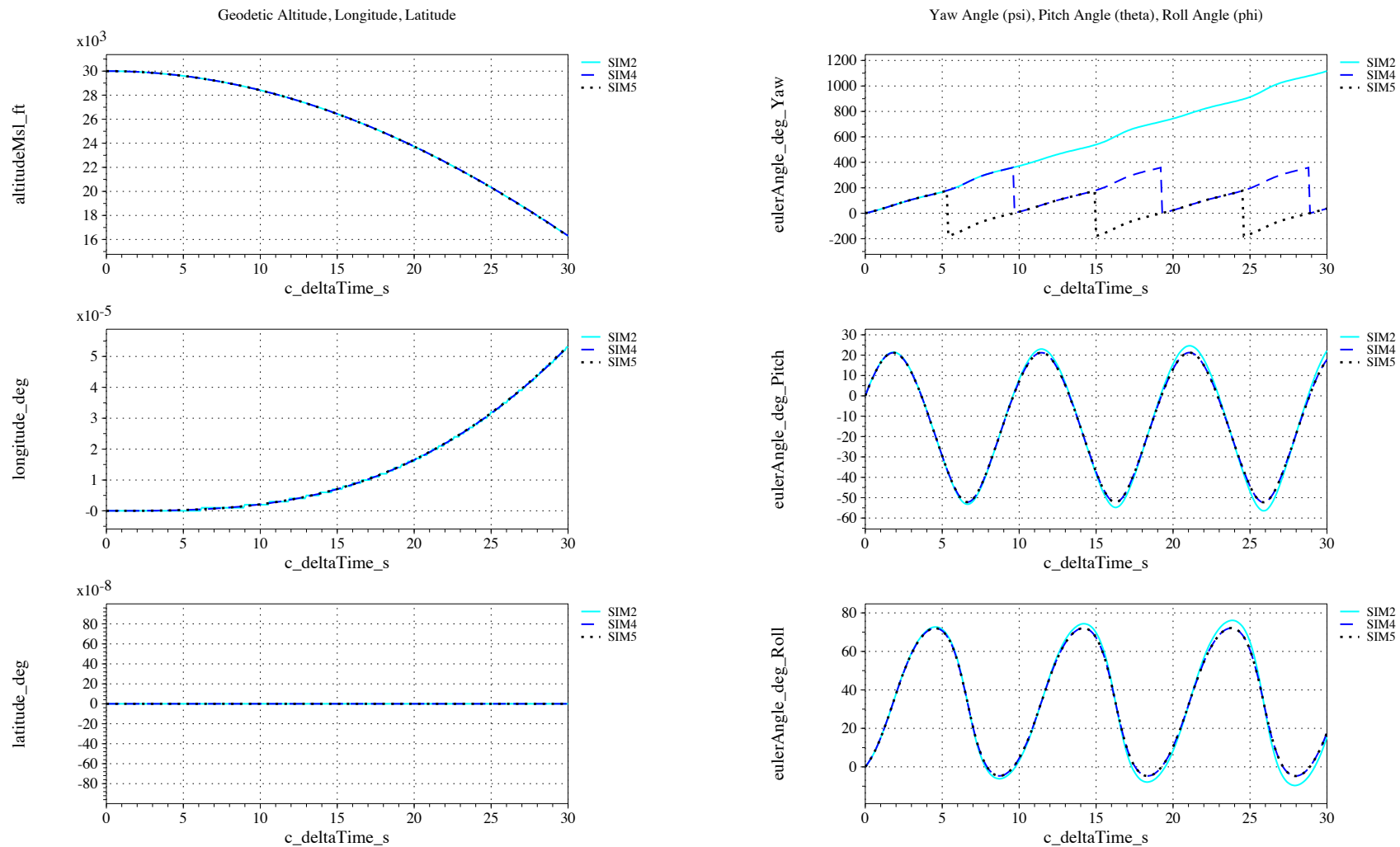
Figure 11. Position and Euler angle vs. time (check-case 5: sphere dropping over rotating, spherical earth)
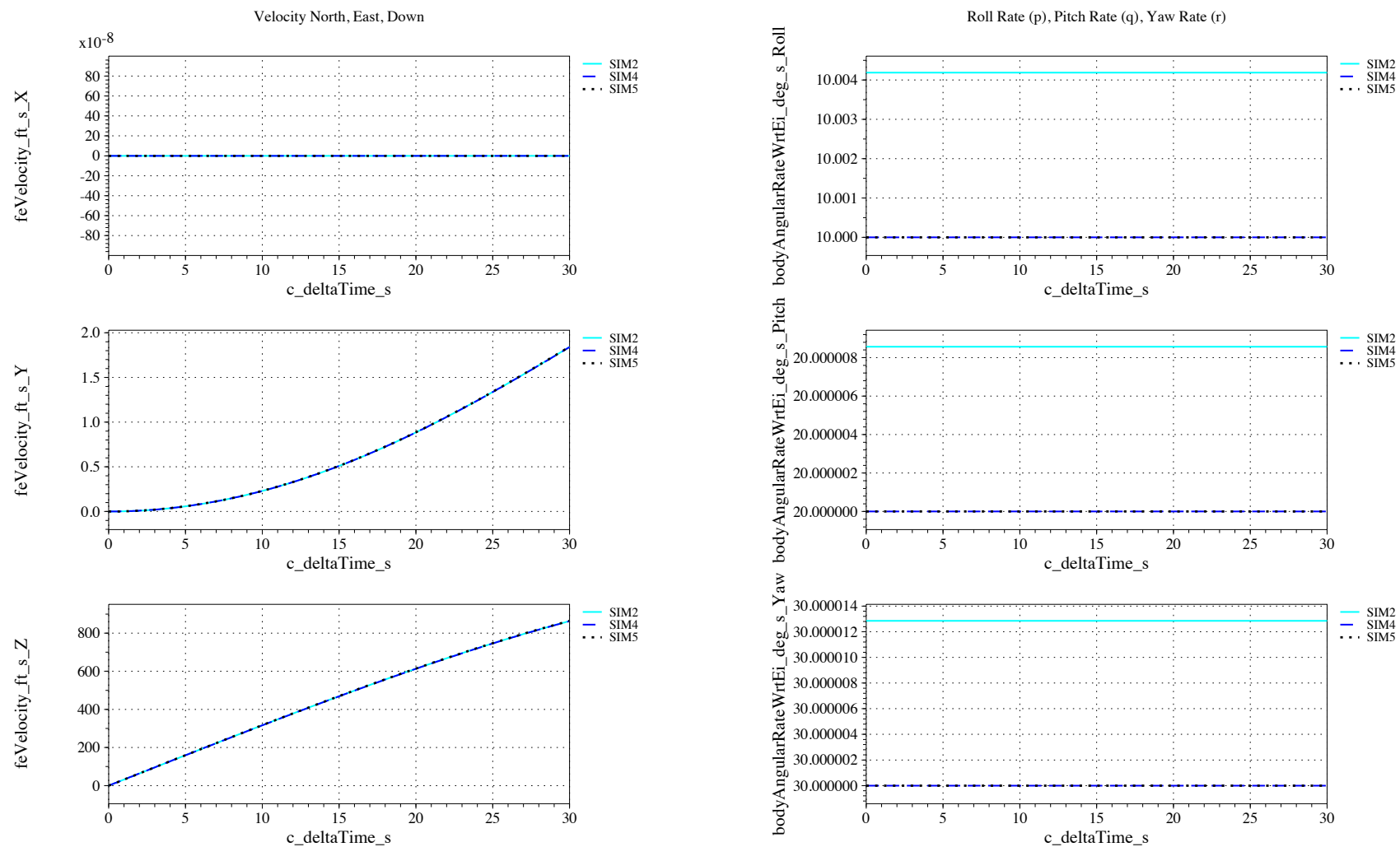
Figure 12. Local velocity and inertial body rates vs. time (check-case 5: sphere dropping over rotating, spherical earth)

IX.A.6.   Check-case 6 – dropped sphere over ellipsoidal, rotating, Earth

This section shows cross-plots for five of the selected simulation tools in modeling the dynamics of a sphere dropped with a fixed drag coefficient through a still atmosphere in a ellipsoidal rotating Earth with J_2 gravitational harmonics.

Figures 13 and 14 compare results between NASA simulation tools in geodetic position, Euler angles, local velocities and body rotational rates.

SIM3 is shown with a -90 degree departure in heading and a -3.5×10^{-6} degree departure in pitch angle. These differences are due to variable selection. The source variables in SIM3 are Euler angles relative to the LVLH frame (which is oriented with respect to the orbit plane). For this case the LVLH frame will be rotated 90 degrees from the geodetic local vertical frame (i.e. North-East-Down). The departure in pitch could be considered negligible. Nevertheless, the value seems a little large to be driven by machine precision. It also does not appear to be derived from the initial inertial orientation or the initial Earth relative velocity, both of which match the scenario initial condition exactly. But, a difference in the recorded X-body aerodynamic force (not shown) appears to indicate that it is a real difference within the simulation. Nevertheless, a cause for the difference could not be identified in the data, and this difference is still under investigation.

American Institute of Aeronautics and Astronautics
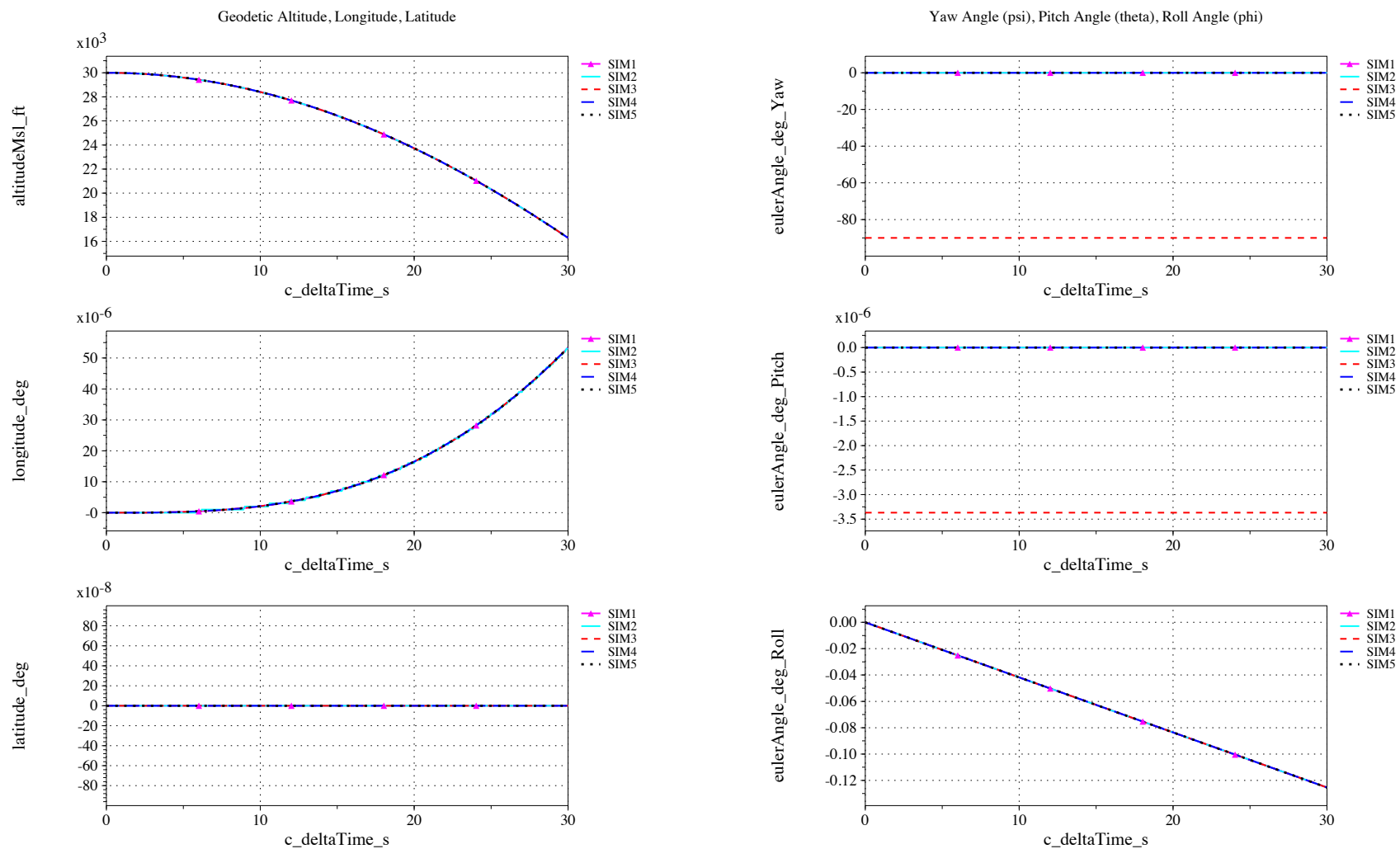
Figure 13. Position and Euler angle vs. time (check-case 6: sphere dropping over rotating, ellipsoidal earth)

American Institute of Aeronautics and Astronautics

American Institute of Aeronautics and Astronautics

Figure 14. Local velocity and inertial body rates vs. time (check-case 6: sphere dropping over rotating, ellipsoidal earth)

IX.A.7.   Check-case 7 – dropped sphere through steady wind field

This section shows cross-plots for five of the selected simulation tools in modeling the dynamics of a sphere having a fixed drag coefficient dropping through a steadily-moving atmosphere of an ellipsoidal rotating Earth with J_2 gravitational harmonics.

Figures 15 and 16 compare results between NASA simulation tools in geodetic position, Euler angles, local velocities and body rotational rates.

SIM2 appears to have initialized Earth-relative rotation to the specified rate and the other simulations initialized inertial-relative rotation to the specified rate. Therefore, the SIM2 roll rate differs by the rotation of the Earth. Differences in pitch and yaw rates are due to truncated precision of recorded data.

The discrepancy in SIM3 Euler angles is the same as previous atmospheric cases. SIM3 is shown with a -90 degree departure in heading and a -3.5×10^{-6} degree departure in pitch angle. These differences are due to variable selection. The source variables in SIM3 are Euler angles relative to the LVLH frame (which is oriented with respect to the orbit plane). For this case the LVLH frame will be rotated 90 degrees from the geodetic local vertical frame (i.e. North-East-Down). The departure in pitch could be considered negligible. Nevertheless, the value seems a little large to be driven by machine precision. It also does not appear to be derived from the initial inertial orientation or the initial Earth relative velocity, both of which match the scenario initial condition exactly.

SIM2 differs in roll angle due to difference in roll rate which causes it to maintain N-E-D orientation while the other simulations maintain inertial orientation (and thus change roll angle at the rotation rate of the Earth).

American Institute of Aeronautics and Astronautics

American Institute of Aeronautics and Astronautics

Figure 15. Position and Euler angle vs. time (check-case 7: sphere dropping through a steady wind field)

American Institute of Aeronautics and Astronautics

42 of 156
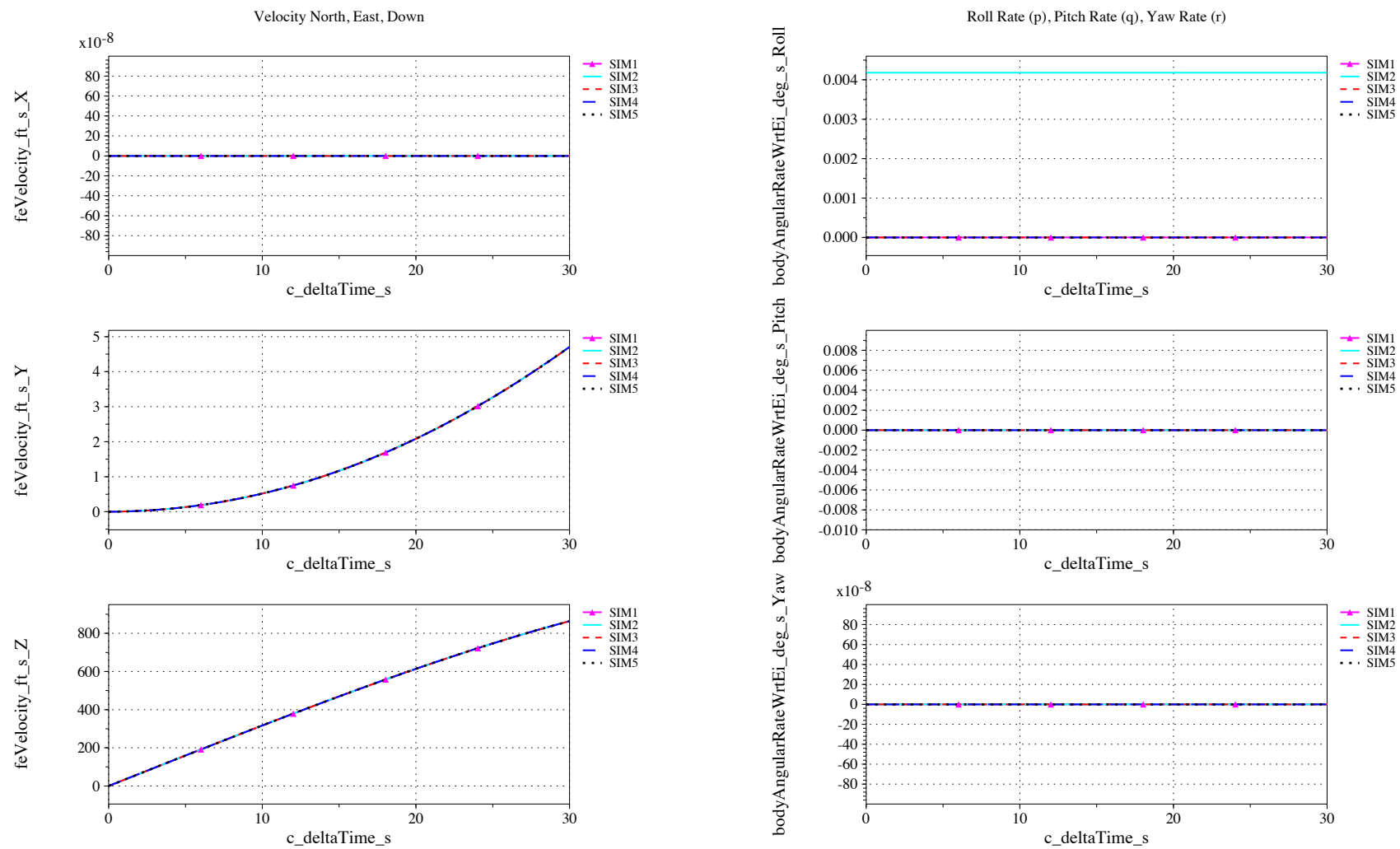
Figure 16. Local velocity and inertial body rates vs. time (check-case 7: sphere dropping through a steady wind field)

IX.A.8.   Check-case 8 – dropped sphere through varying wind field

This section shows cross-plots for five of the selected simulation tools in modeling the dynamics of a sphere dropped with a fixed drag coefficient through an atmosphere with wind velocity as a function of altitude over an ellipsoidal rotating Earth with J_2 gravitational harmonics.

Figures 17 and 18 compare results between NASA simulation tools in geodetic position, Euler angles, local velocities and body rotational rates.

The same comments given in check-case 7 apply to this case:

SIM2 appears to have initialized Earth-relative rotation to the specified rate and the other simulations initialized inertial-relative rotation to the specified rate. Therefore, the SIM2 roll rate differs by the rotation of the Earth. Differences in pitch and yaw rates are due to truncated precision of recorded data.

The discrepancy in SIM3 Euler angles is the same as previous atmospheric cases. SIM3 is shown with a -90 degree departure in heading and a -3.5×10^{-6} degree departure in pitch angle. These differences are due to variable selection. The source variables in SIM3 are Euler angles relative to the LVLH frame (which is oriented with respect to the orbit plane). For this case the LVLH frame will be rotated 90 degrees from the geodetic local vertical frame (i.e. North-East-Down). The departure in pitch could be considered negligible. Nevertheless, the value seems a little large to be driven by machine precision. It also does not appear to be derived from the initial inertial orientation or the initial Earth relative velocity, both of which match the scenario initial condition exactly.

SIM2 differs in roll angle due to difference in roll rate which causes it to maintain N-E-D orientation while the other simulations maintain inertial orientation (and thus change roll angle at the rotation rate of the Earth).

American Institute of Aeronautics and Astronautics

Figure 17. Position and Euler angle vs. time (check-case 8: sphere dropping through a varying wind field)
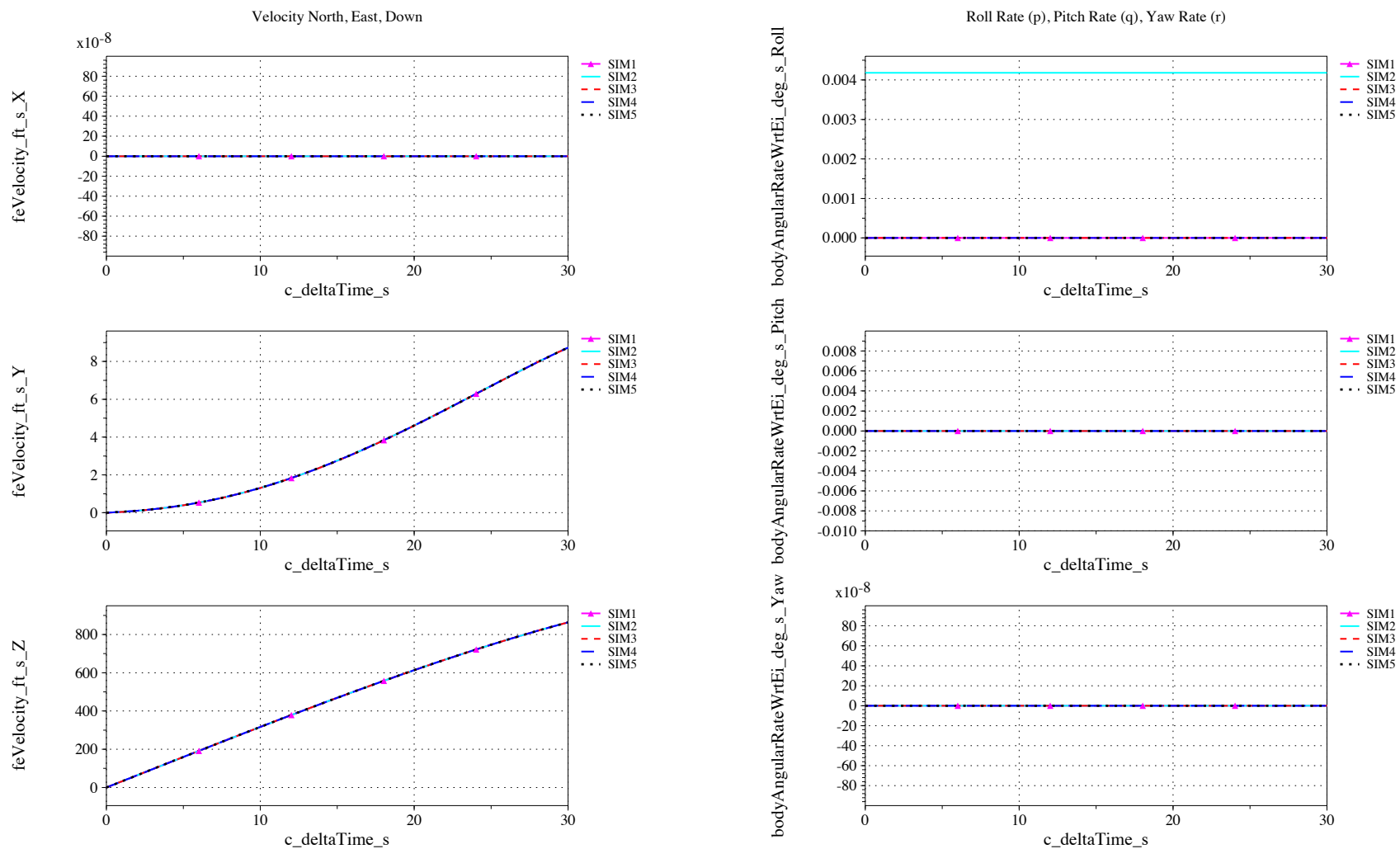
Figure 18. Local velocity and inertial body rates vs. time (check-case 8: sphere dropping through a varying wind field)

IX.A.9. Check-case 9 – eastward ballistic flight of a cannonball

This section shows cross-plots for five of the selected simulation tools in modeling the dynamics of a sphere launched Eastward along the equator of an ellipsoidal rotating Earth with J_2 gravitational harmonics.

Figures 19 and 20 compare results between NASA simulation tools in geodetic position, Euler angles, local velocities and body rotational rates.

Simulations do not agree on initial conditions for inertial pitch and yaw rate. The problem appears to be interpretation of the scenario specification. SIM4 implemented an inertial rate in body coordinates of (0, 0 , ω). This is the inertial rate that appears in the scenario specification except that the rate specified is angular rate in inertial coordinates (not body). SIM3 and SIM5 initialize to zero P, Q, and R as specified for the geodetic-relative rate; this produces an inertial pitch rate opposing the Earth's rotation (i.e. $-\omega$). SIM2 appears to initialize the sphere to a body rate of (0, 0, 0) relative to the local vertical frame, which due to the speed of the vehicle, rotates an additional 0.00274 deg/s in pitch to maintain down orientation when the vehicle travels 1000 fps East. SIM1 shows an inertial rate in body coordinates of [0, 0, 0].

The above rates lead to differences in pitch and roll angles among the simulation tools.

SIM3 differs in heading, again, because its Euler angles are defined relative to LVLH than NED.

The mismatch in this check-case highlight the difficulty of getting separate simulation implementations to match despite making some effort to specify the model and initial conditions exactly.

American Institute of Aeronautics and Astronautics

American Institute of Aeronautics and Astronautics

47 of 156

Geodetic Altitude, Longitude, Latitude

Yaw Angle (psi), Pitch Angle (theta), Roll Angle (phi)
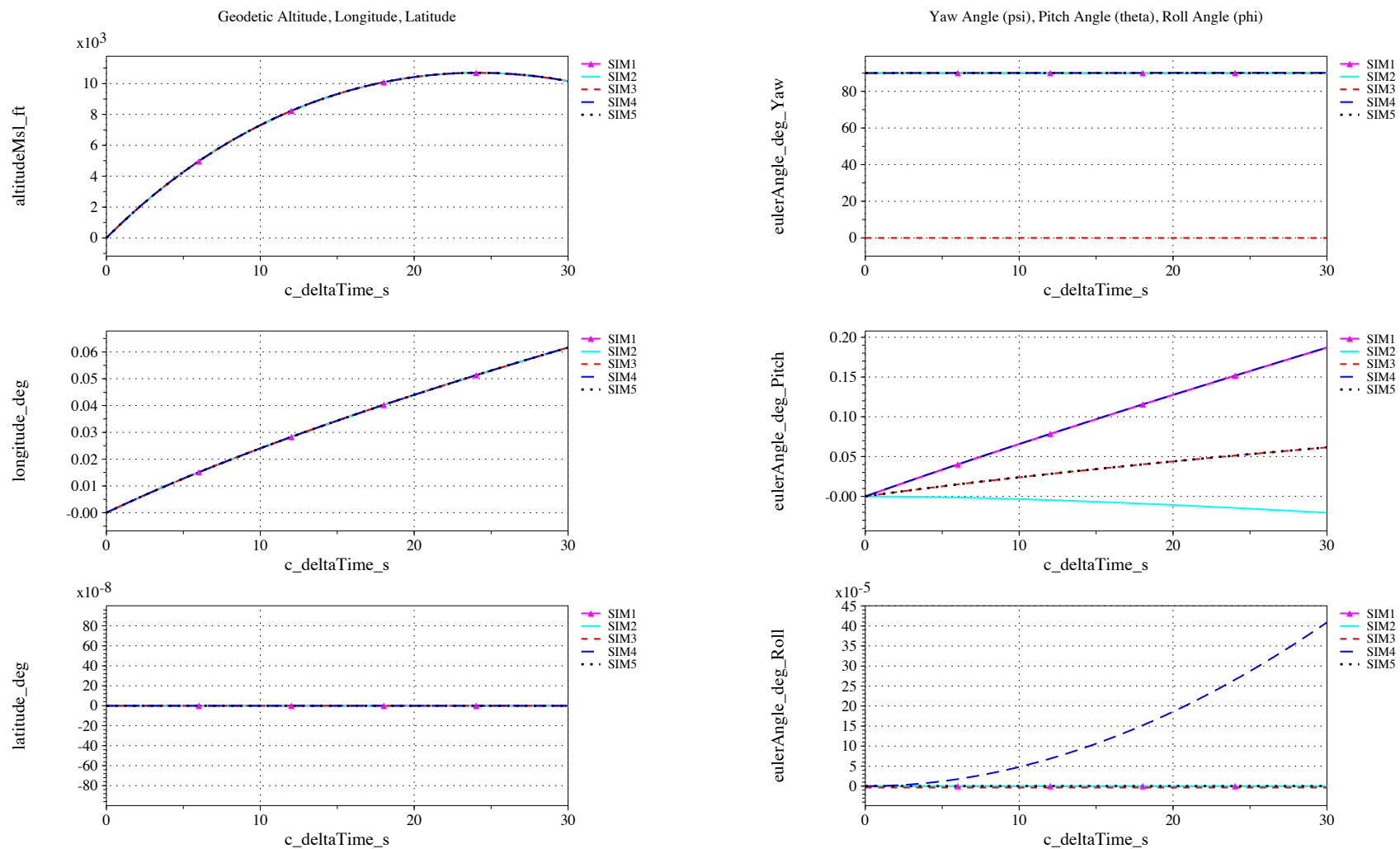
Figure 19. Position and Euler angle vs. time (check-case 9: eastward ballistic flight of a sphere)
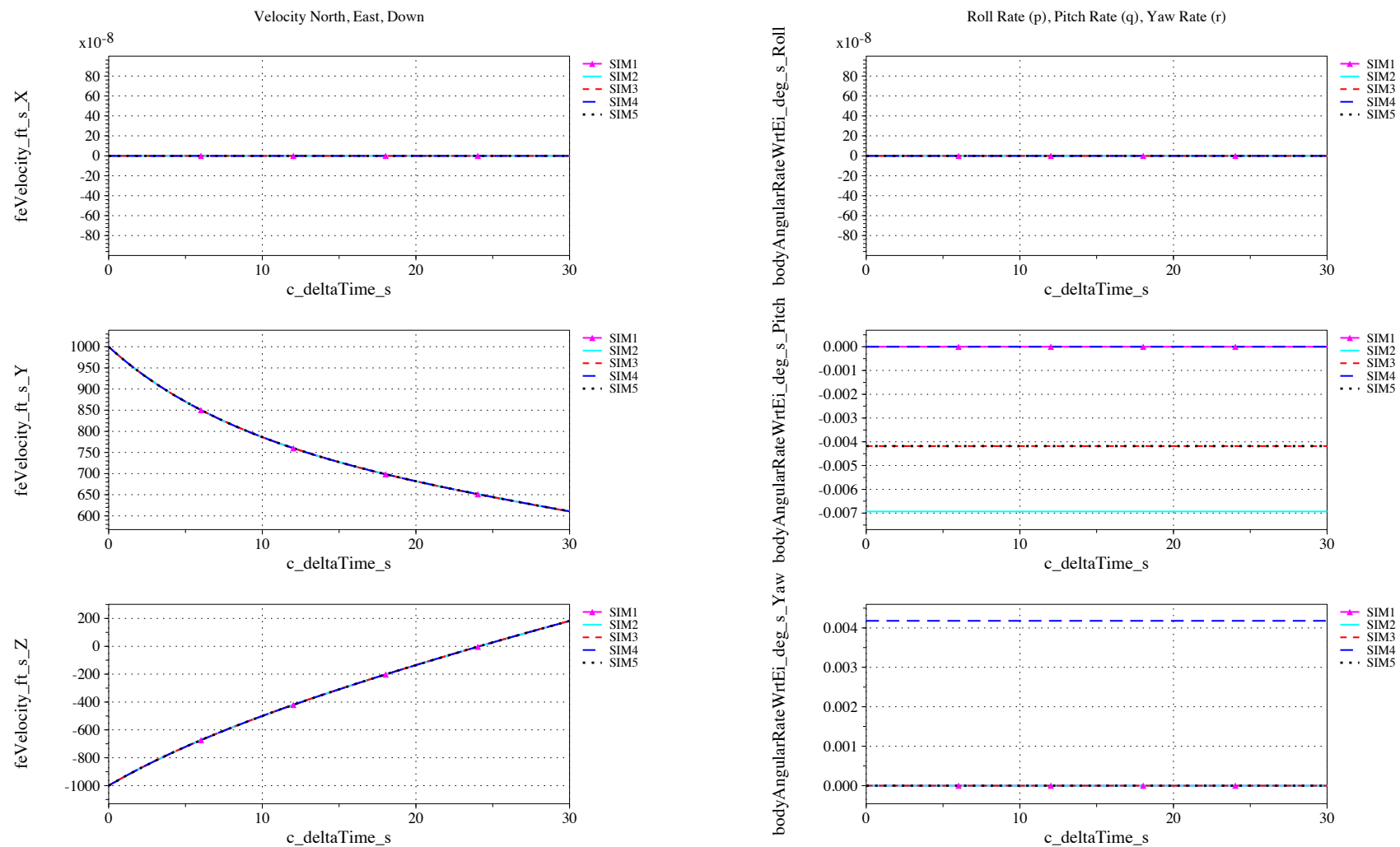
Figure 20. Local velocity and inertial body rates vs. time (check-case 9: eastward ballistic flight of a sphere)

IX.A.10.   Check-case 10 – northward ballistic flight of a cannonball

This section shows cross-plots for five of the selected simulation tools in modeling the dynamics of a sphere launched Northward from the equator of an ellipsoidal rotating Earth with J_2 gravitational harmonics.

Figures 21 and 22 compare results between NASA simulation tools in geodetic position, Euler angles, local velocities and body rotational rates.

Differences in longitude are difficult to discern since SIM4 uses a [0, 360) degree range and drifts just far enough west to generate a value near 360, greatly expanding the scale. Converting the SIM4 data to a range of (-180, 180] and reducing scale is desirable since Coriolis effects will influence longitude.

Difference in SIM3 heading or yaw angle is due to the fact that the plotted values are relative to the LVLH frame. In this case, because the velocity has a northward component, it produces an inertial orbit with an inclination of 33 degrees; therefore, a pure North direction will have a yaw angle of 57 degrees in the LVLH frame. As drag reduces the vehicle velocity, the inclination decreases and the LVLH yaw angle increases.

SIM2 differs in pitch angle due to difference in initial pitch rate.

SIM4 differs in roll angle due to difference in initial roll rate. SIM4 should also differ in yaw angle but this difference is masked by scale of plot (due to SIM3 values).

The simulation tools do not agree on initial conditions for inertial rotation rates. The problem is interpretation of the scenario specification. SIM4 implemented an inertial rate in body coordinates of (0, 0 , ω). This is the inertial rate that appears in the initial condition specification except that the rate specified is angular rate in inertial coordinates (not body). SIM1, SIM3, and SIM5 initialize to zero P, Q, and R as specified for the geodetic-relative rate; this produces an inertial pitch rate opposing the Earth's rotation (i.e. $+\omega$). SIM2 appears to initialize the sphere to a body rate of (0, 0, 0) relative to the local vertical frame, which due to the speed of the vehicle, rotates an additional 0.00274 deg/s in pitch to maintain down orientation when the vehicle travels 1000 fps North.

American Institute of Aeronautics and Astronautics
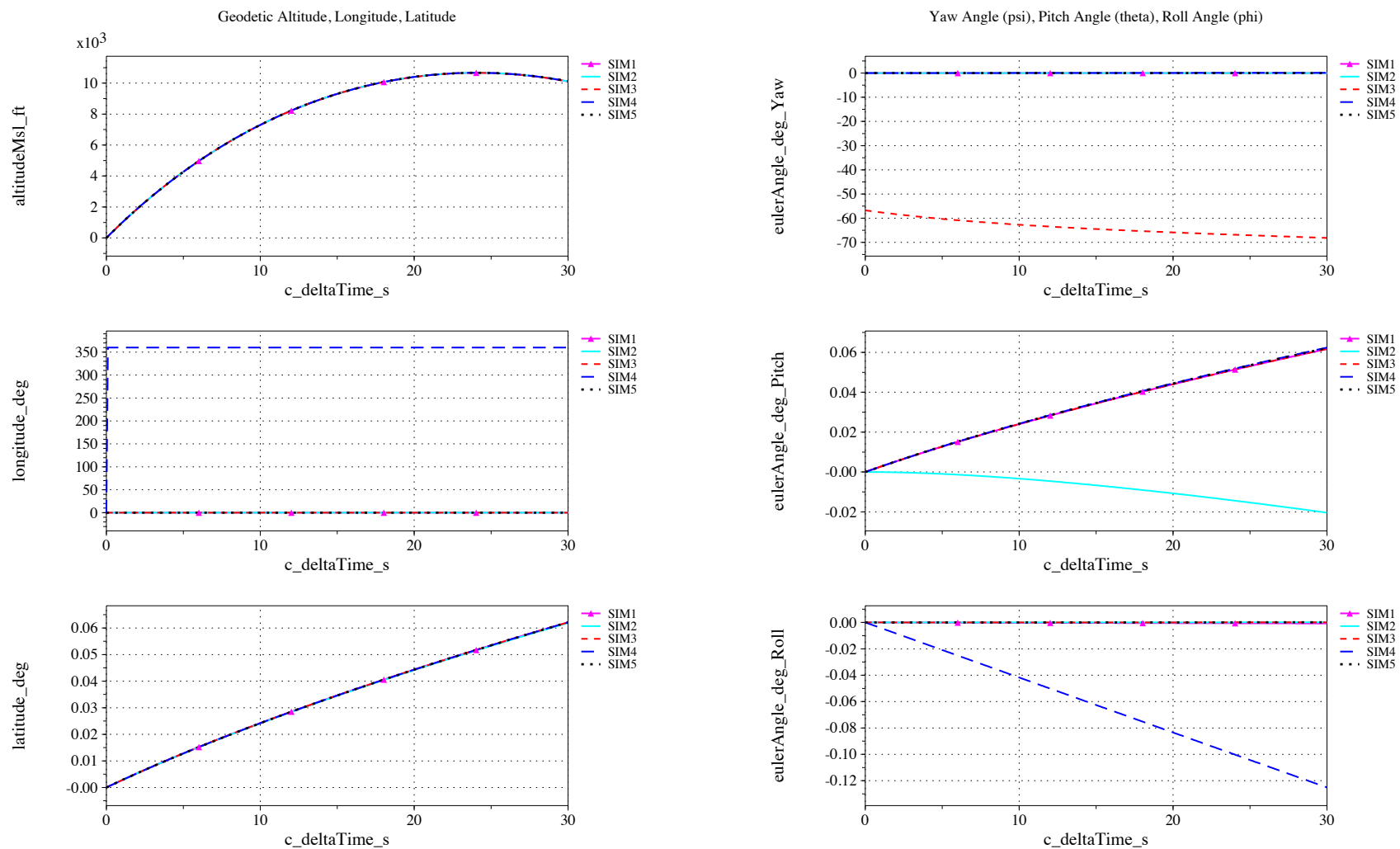
Figure 21. Position and Euler angle vs. time (check-case 10: northward ballistic flight of a sphere)

American Institute of Aeronautics and Astronautics

51 of 156
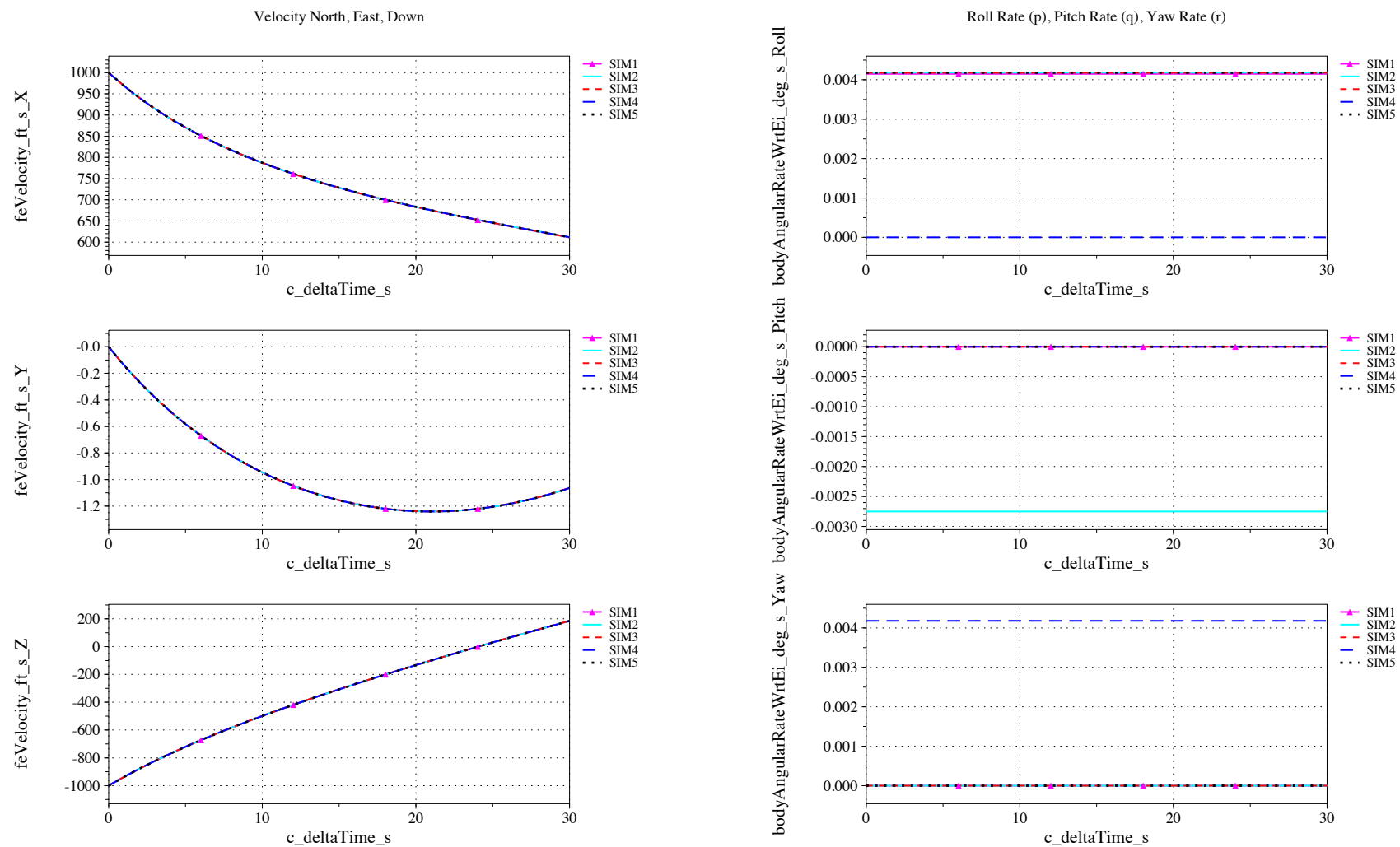
Figure 22. Local velocity and inertial body rates vs. time (check-case 10: northward ballistic flight of a sphere)

IX.B. Scenario comparisons – Orbital

In general the co-plots match well; however, given the scale of the plots, some significant difference may still exist between large quantities. Due to space limitations, however, plots of residual errors between tools are not presented. These are still under investigation.

IX.B.1. Check-case 2 – ISS in spherical gravity

This section shows cross-plots for three of the selected simulation tools in modeling the dynamics of the ISS in orbit, propagating with spherical gravity model and no disturbances.

Figures 23 and 25 compare results between NASA simulation tools in inertial acceleration, atmospheric quantities, rates and velocities and positions and attitudes.

SIM_A shows slightly higher peaks in atmospheric density than SIM_B and SIM_C. There may be a difference in either MET model implementation or interaction (e.g. input values); this difference is being investigated.

American Institute of Aeronautics and Astronautics

American Institute of Aeronautics and Astronautics

53 of 156

X, Y, Z Axis Acceleration in Inertial Frame, includes gravity

Altitude, Density, Temperature

Figure 23. Accelerations and atmospheric quantities vs. time (check-case 02: ISS in spherical gravity)

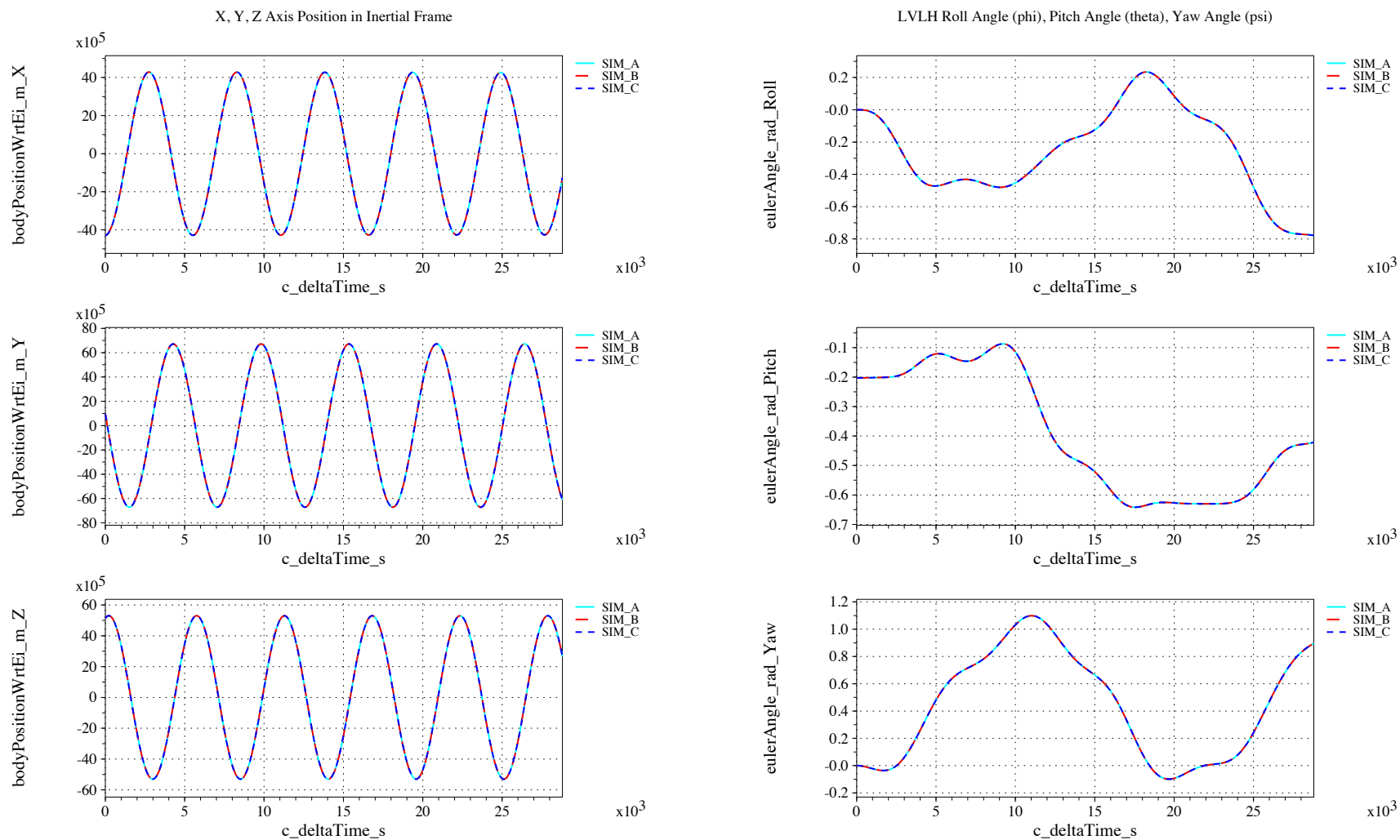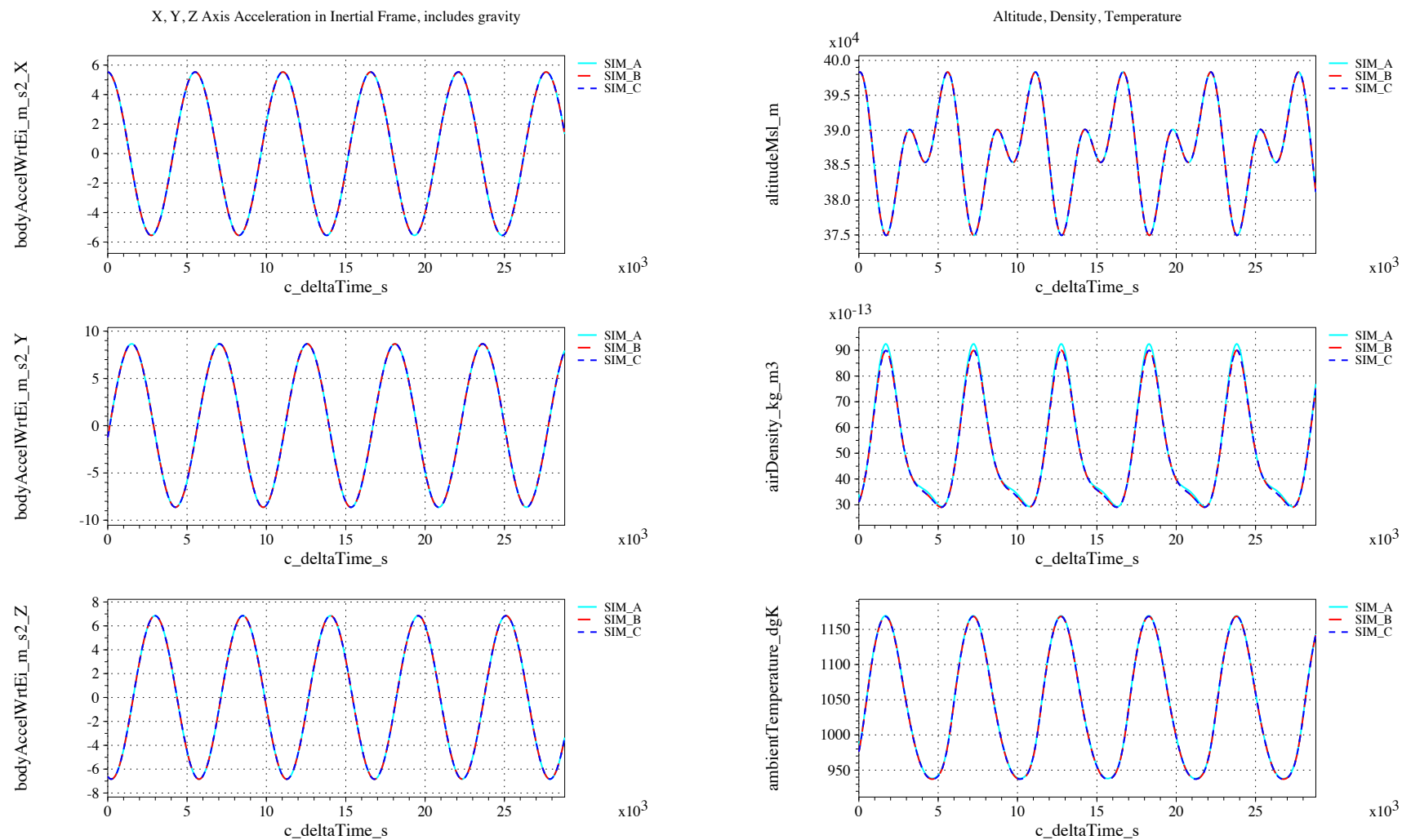**Figure 24. Inertial velocity and body angular rates vs. time (check-case 02: ISS in spherical gravity)**

American Institute of Aeronautics and Astronautics
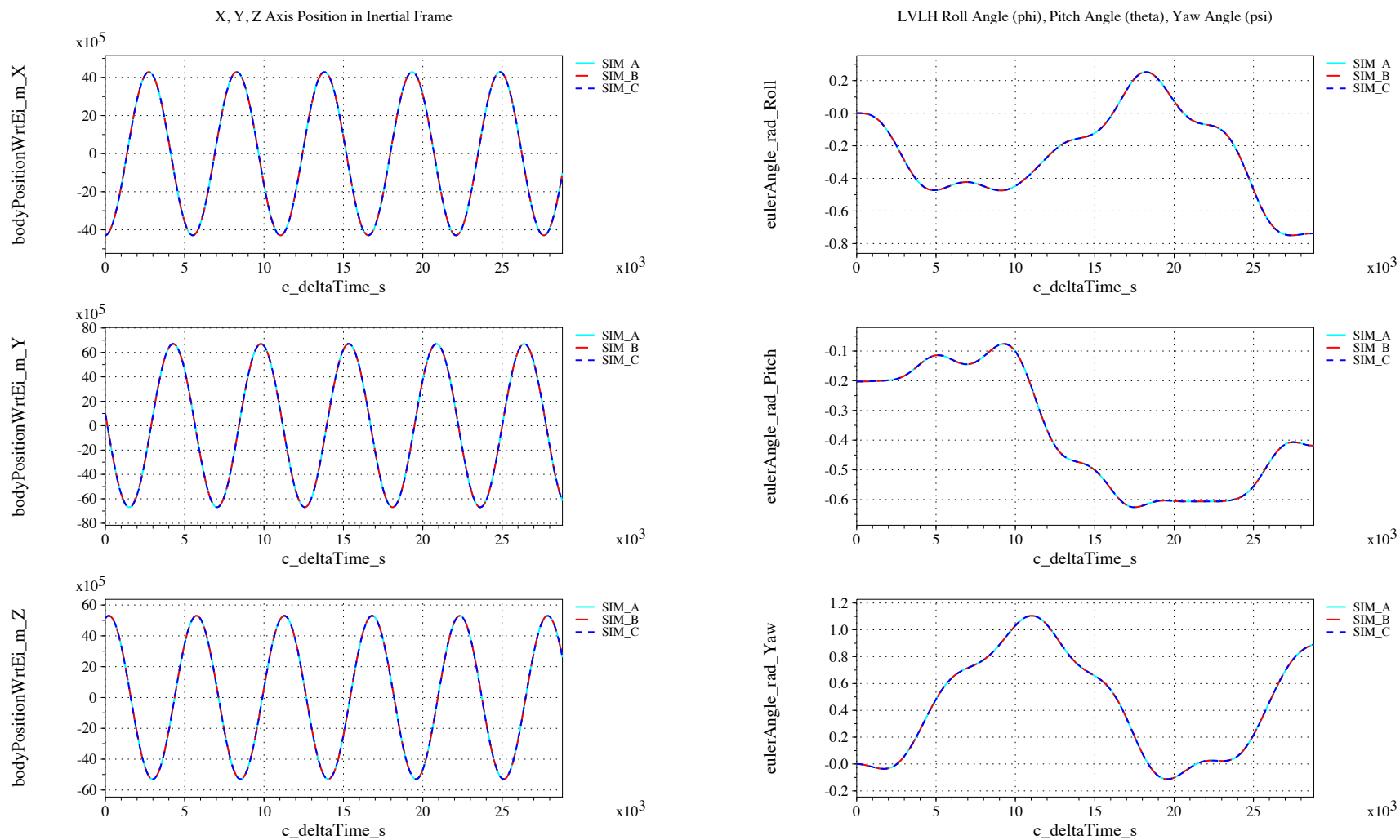
Figure 25. Inertial positions and Euler angles vs. time (check-case 02: ISS in spherical gravity)

IX.B.2. Check-case 3A – ISS in 4x4 harmonic gravity

This section shows cross-plots for three of the selected simulation tools in modeling the dynamics of the ISS in orbit with a 4x4 harmonic gravity model and no disturbances.

Figures 26 and 28 compare results between NASA simulation tools in inertial acceleration, atmospheric quantities, rates and velocities and positions and attitudes.

As in other cases, SIM_A shows slightly higher peaks in atmospheric density than SIM_B and SIM_C. There may be a difference in either MET model implementation or interaction (e.g. input values); this difference is being investigated.

American Institute of Aeronautics and Astronautics

American Institute of Aeronautics and Astronautics

X, Y, Z Axis Acceleration in Inertial Frame, includes gravity

Altitude, Density, Temperature
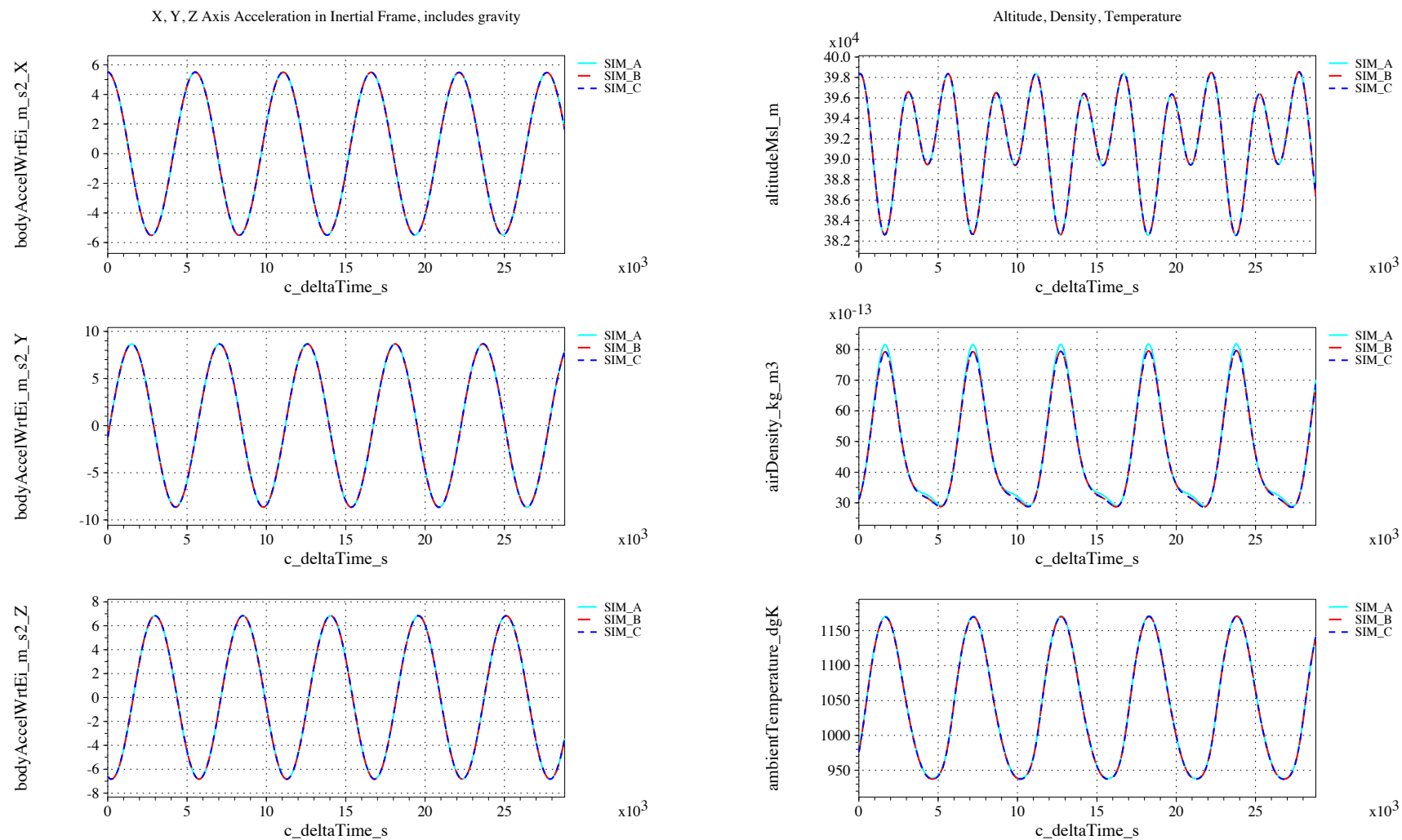
Figure 26. Accelerations and atmospheric quantities vs. time (check-case 03A: ISS in 4x4 harmonic gravity)

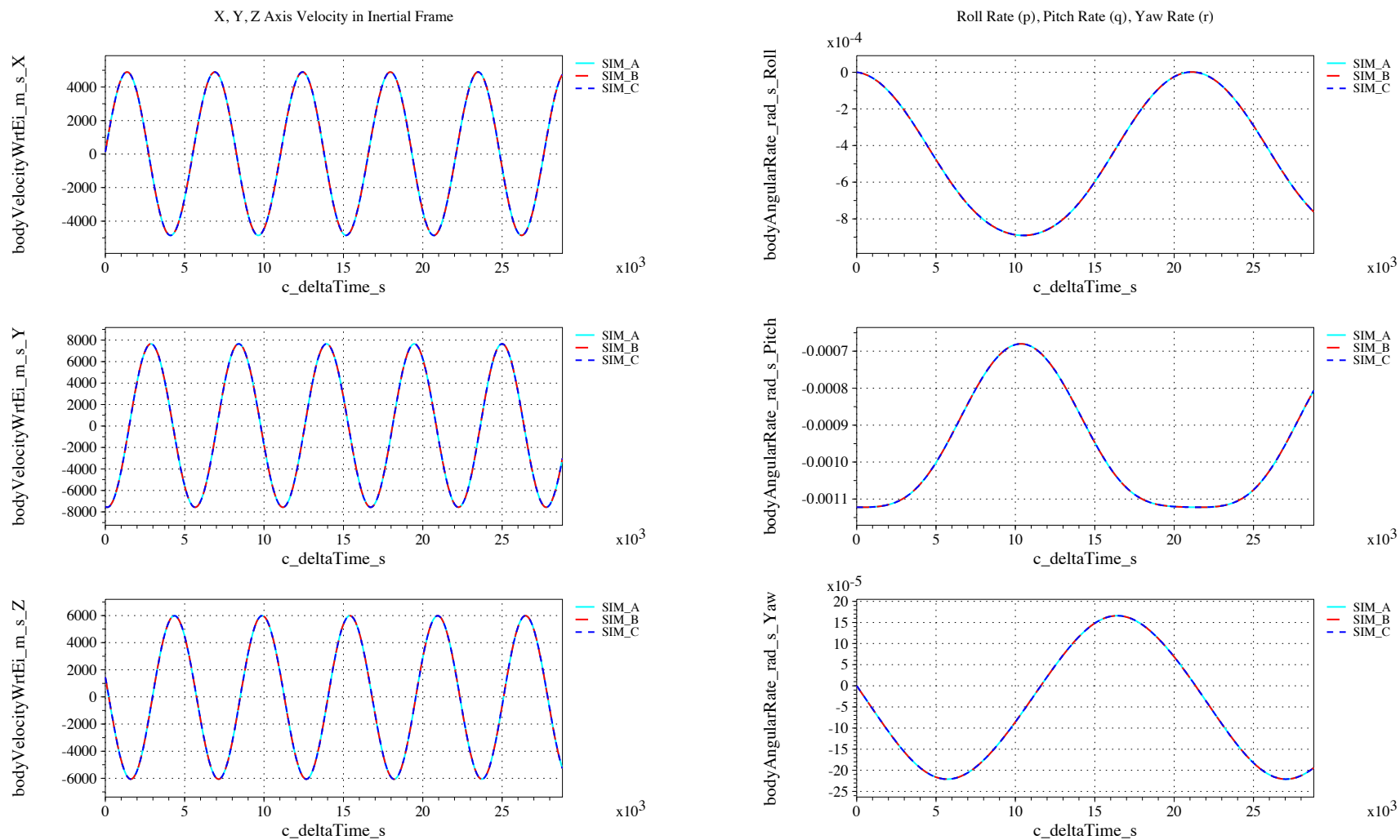American Institute of Aeronautics and Astronautics
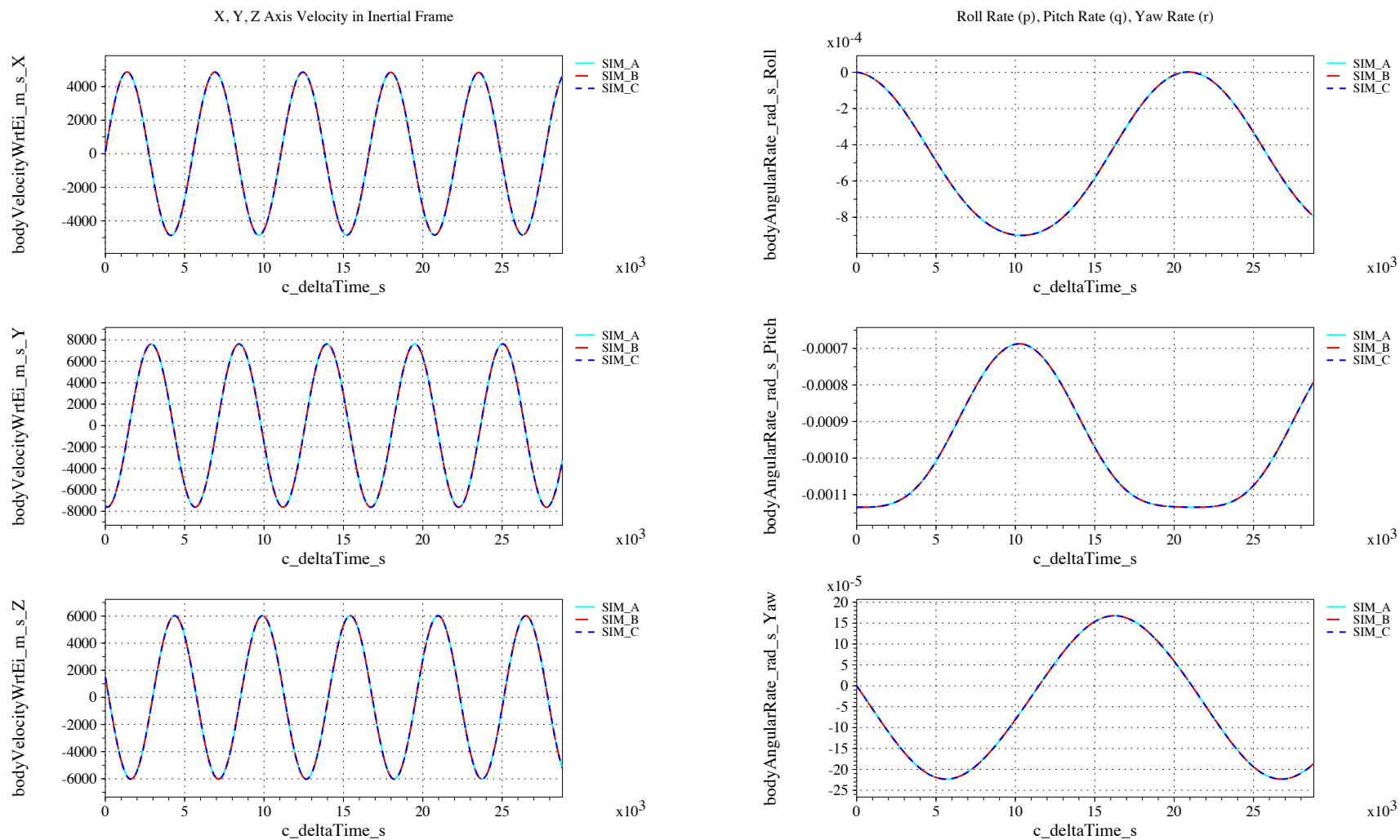
Figure 27. Inertial velocity and body angular rates vs. time (check-case 03A: ISS in 4x4 harmonic gravity)
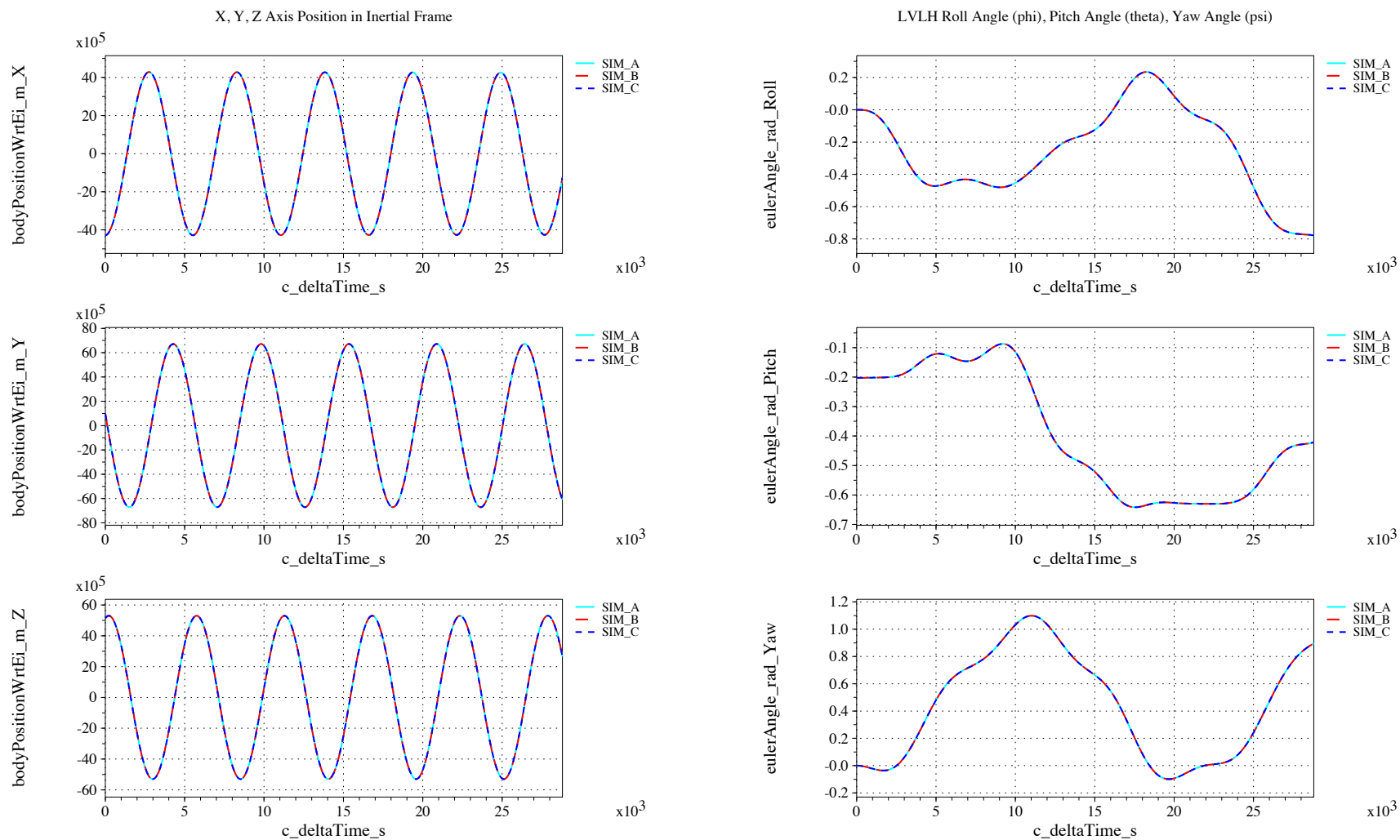
Figure 28. Inertial positions and Euler angles vs. time (check-case 03A: ISS in 4x4 harmonic gravity)

IX.B.3. Check-case 3B – ISS in 8x8 harmonic gravity

This section shows cross-plots for three of the selected simulation tools in modeling the dynamics of the ISS in orbit with a 8x8 harmonic gravity model and no disturbances.

Figures 29 and 31 compare results between NASA simulation tools in inertial acceleration, atmospheric quantities, rates and velocities and positions and attitudes.

As in other cases, SIM_A shows slightly higher peaks in atmospheric density than SIM_B and SIM_C. There may be a difference in either MET model implementation or interaction (e.g. input values); this difference is being investigated.

American Institute of Aeronautics and Astronautics

American Institute of Aeronautics and Astronautics

X, Y, Z Axis Acceleration in Inertial Frame, includes gravity
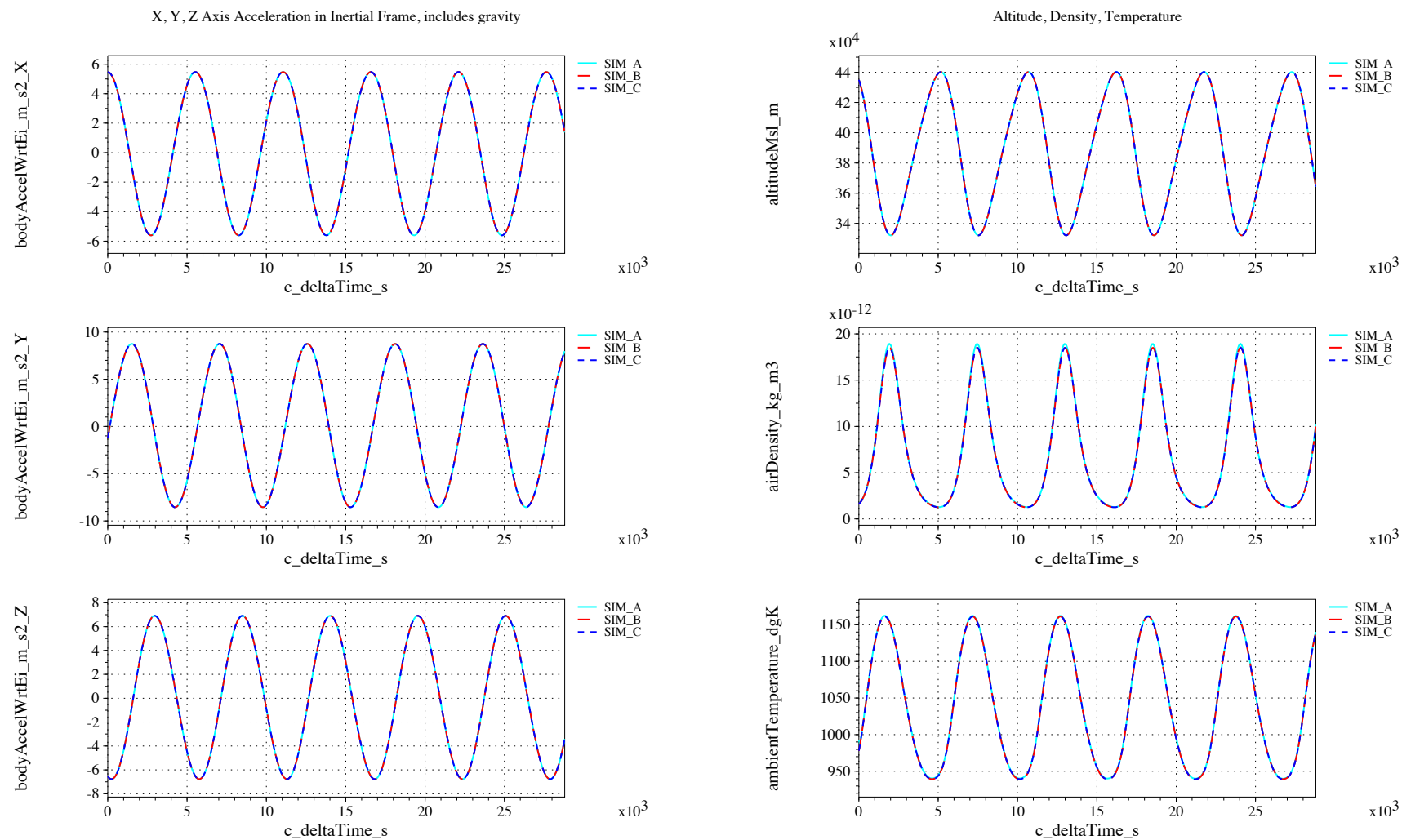
Altitude, Density, Temperature
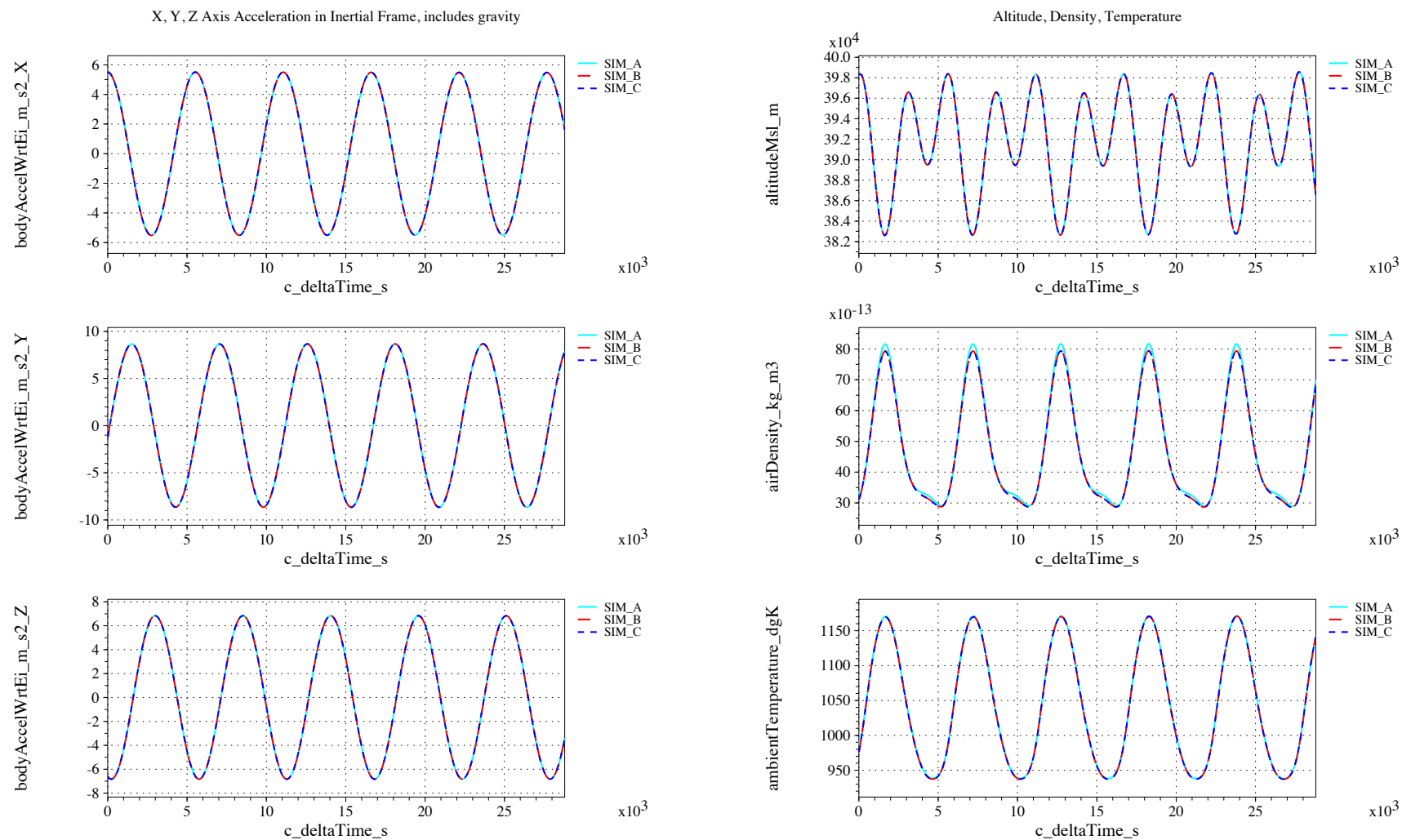
Figure 29. Accelerations and atmospheric quantities vs. time (check-case 03B: ISS in 8x8 harmonic gravity)
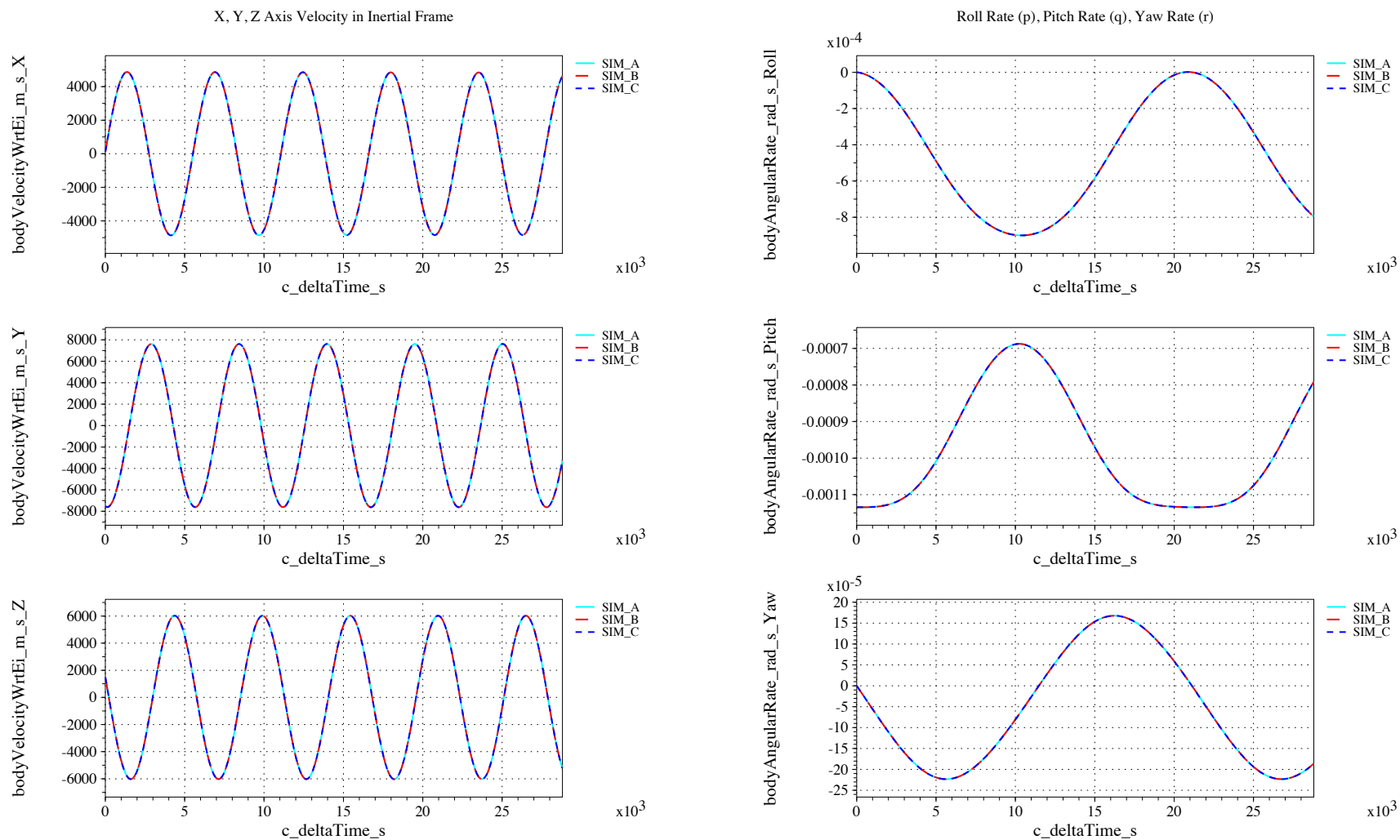
Figure 30. Inertial velocity and body angular rates vs. time (check-case 03B: ISS in 8x8 harmonic gravity)

American Institute of Aeronautics and Astronautics

X, Y, Z Axis Position in Inertial Frame

LVLH Roll Angle (phi), Pitch Angle (theta), Yaw Angle (psi)

Figure 31. Inertial positions and Euler angles vs. time (check-case 03B: ISS in 8x8 harmonic gravity)

IX.B.4.   Check-case 4 – ISS with third-body disturbances

This section shows cross-plots for three of the selected simulation tools in modeling the dynamics of the ISS in orbit with Sun and Moon gravity perturbations.

   Figures 32 and 34 compare results between NASA simulation tools in inertial acceleration, atmospheric quantities, rates and velocities and positions and attitudes.

   As in other cases, SIM_A shows slightly higher peaks in atmospheric density than SIM_B and SIM_C. There may be a difference in either MET model implementation or interaction (e.g. input values); this difference is being investigated.

American Institute of Aeronautics and Astronautics

American Institute of Aeronautics and Astronautics

X, Y, Z Axis Acceleration in Inertial Frame, includes gravity

Altitude, Density, Temperature

Figure 32. Accelerations and atmospheric quantities vs. time (check-case 04: ISS with third-body disturbances)

American Institute of Aeronautics and Astronautics
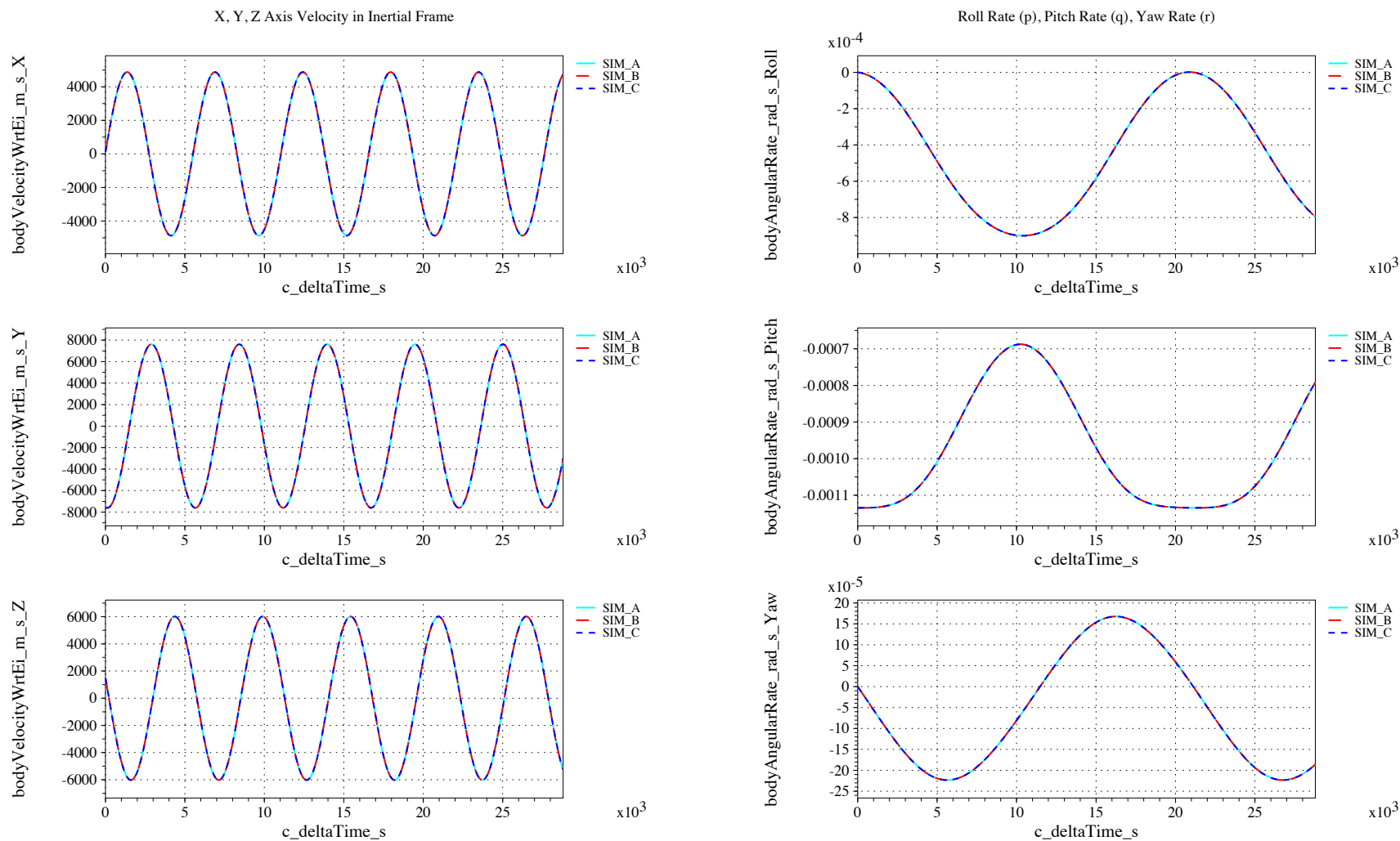
Figure 33. Inertial velocity and body angular rates vs. time (check-case 04: ISS with third-body disturbances)
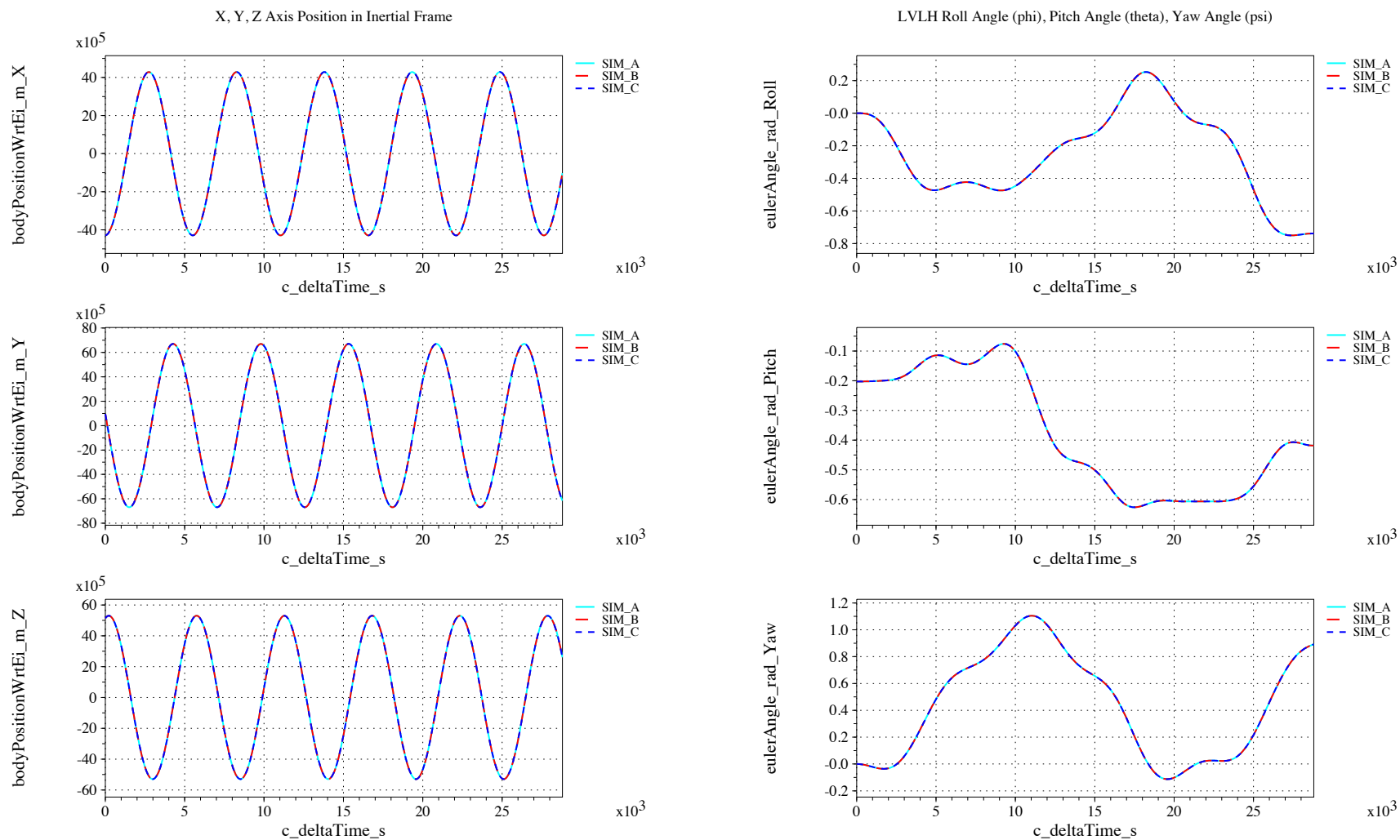
Figure 34. Inertial positions and Euler angles vs. time (check-case 04: ISS with third-body disturbances)

IX.B.5.   Check-case 5A – ISS (minimal solar activity)

This section shows cross-plots for three of the selected simulation tools in modeling the dynamics of the ISS in orbit with minimal solar activity disturbances.

Figures 35 and 37 compare results between NASA simulation tools in inertial acceleration, atmospheric quantities, rates and velocities and positions and attitudes.

It should be noted that inertial angular rates (expressed in body axes) do not match rate-of-change of Euler angles, which measure the position of the body axes relative to LVLH. Not only are these rates and angles measured in different frames, but Euler angles are not orthogonal.

As in other cases, SIM_A shows slightly higher peaks in atmospheric density than SIM_B and SIM_C. There may be a difference in either MET model implementation or interaction (e.g. input values); this difference is being investigated.
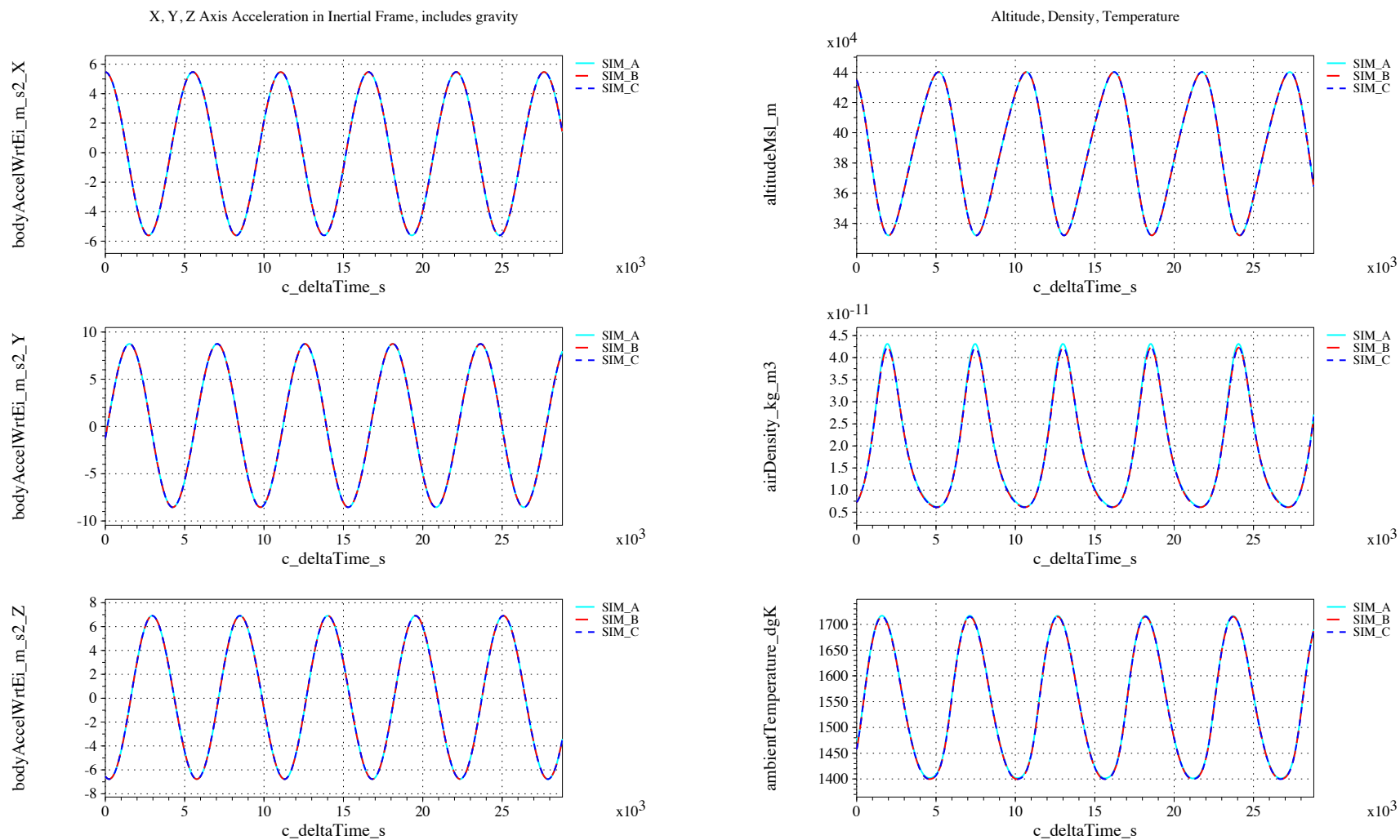
American Institute of Aeronautics and Astronautics

X, Y, Z Axis Acceleration in Inertial Frame, includes gravity

Altitude, Density, Temperature
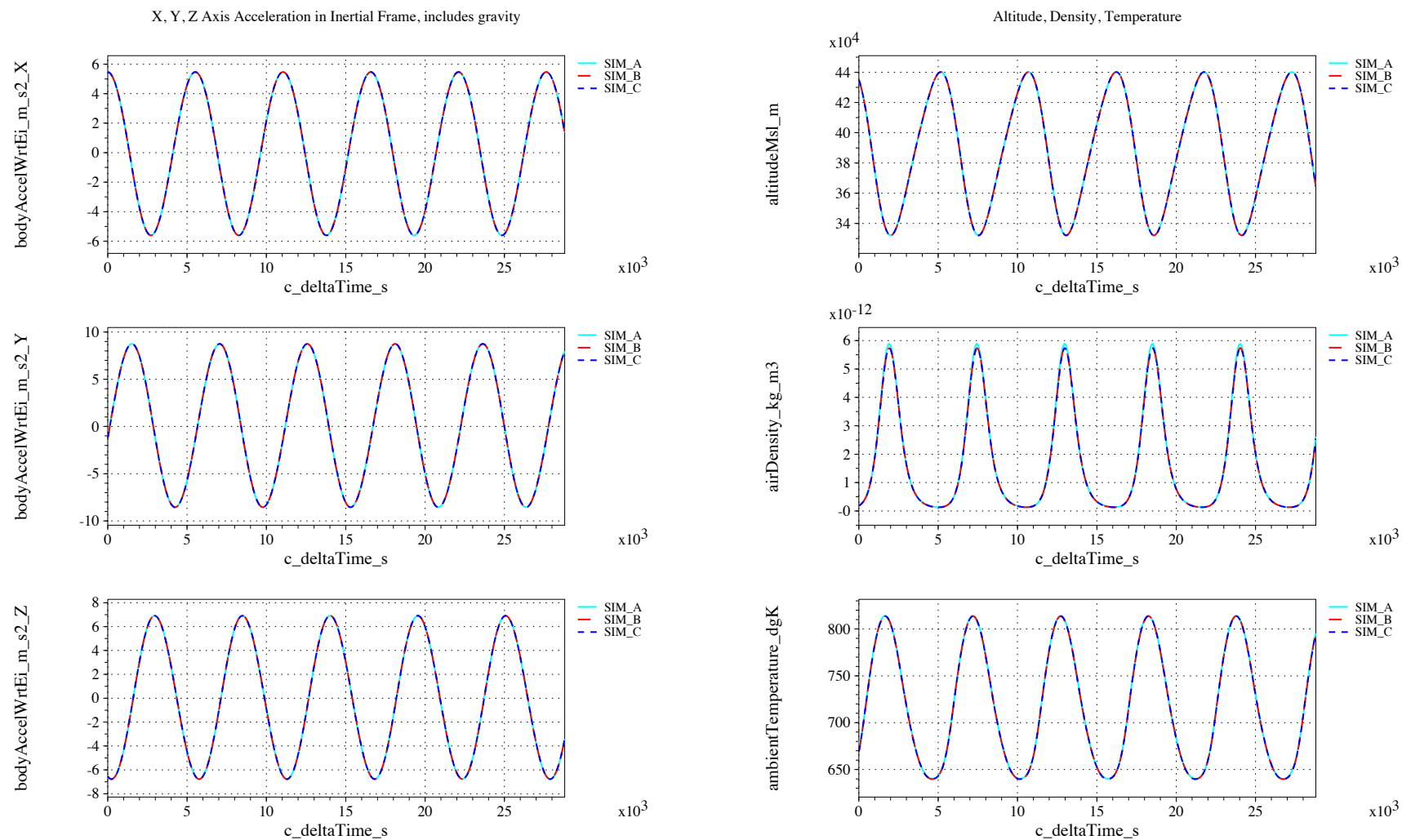
Figure 35. Accelerations and atmospheric quantities vs. time (check-case 05A: ISS (minimal solar activity))
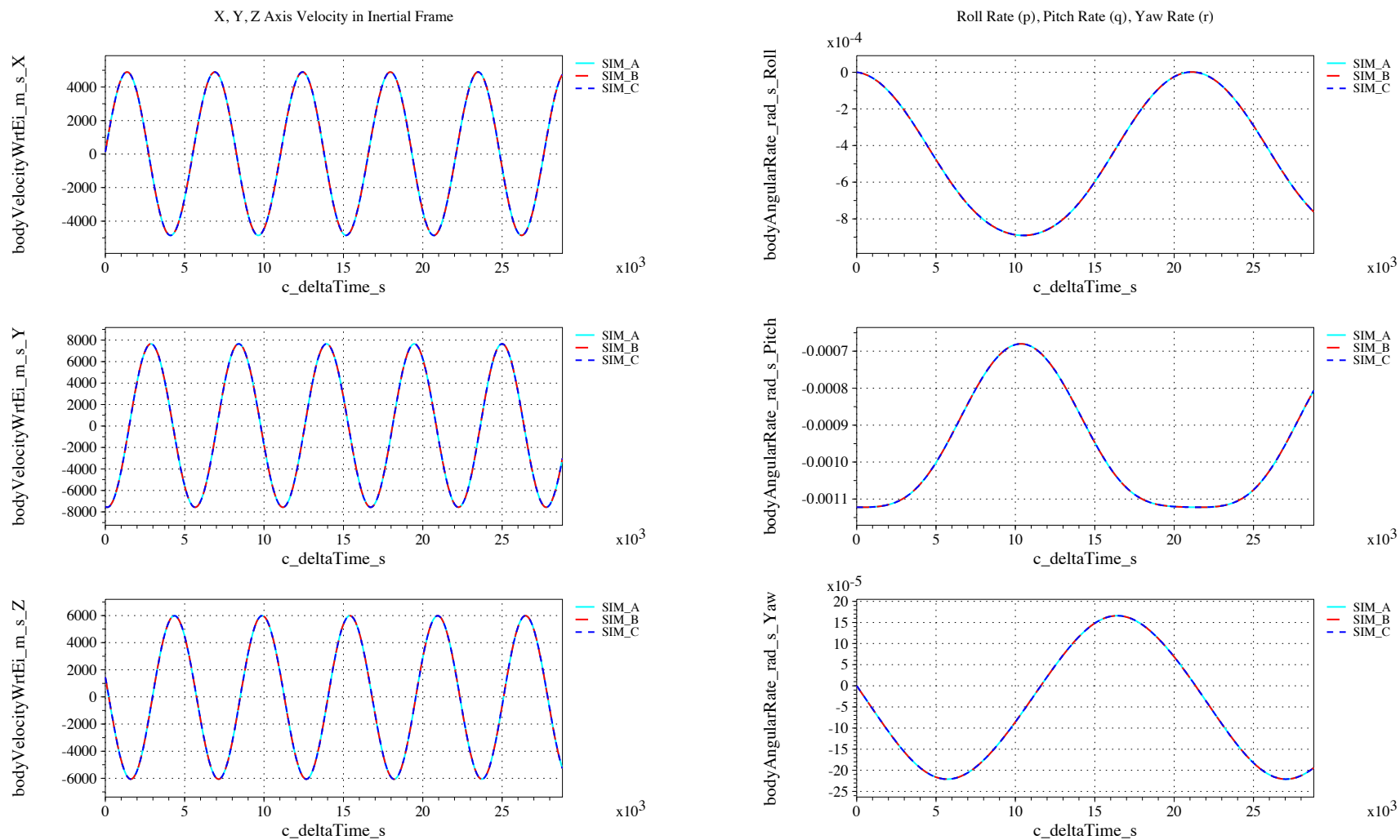
Figure 36. Inertial velocity and body angular rates vs. time (check-case 05A: ISS (minimal solar activity))
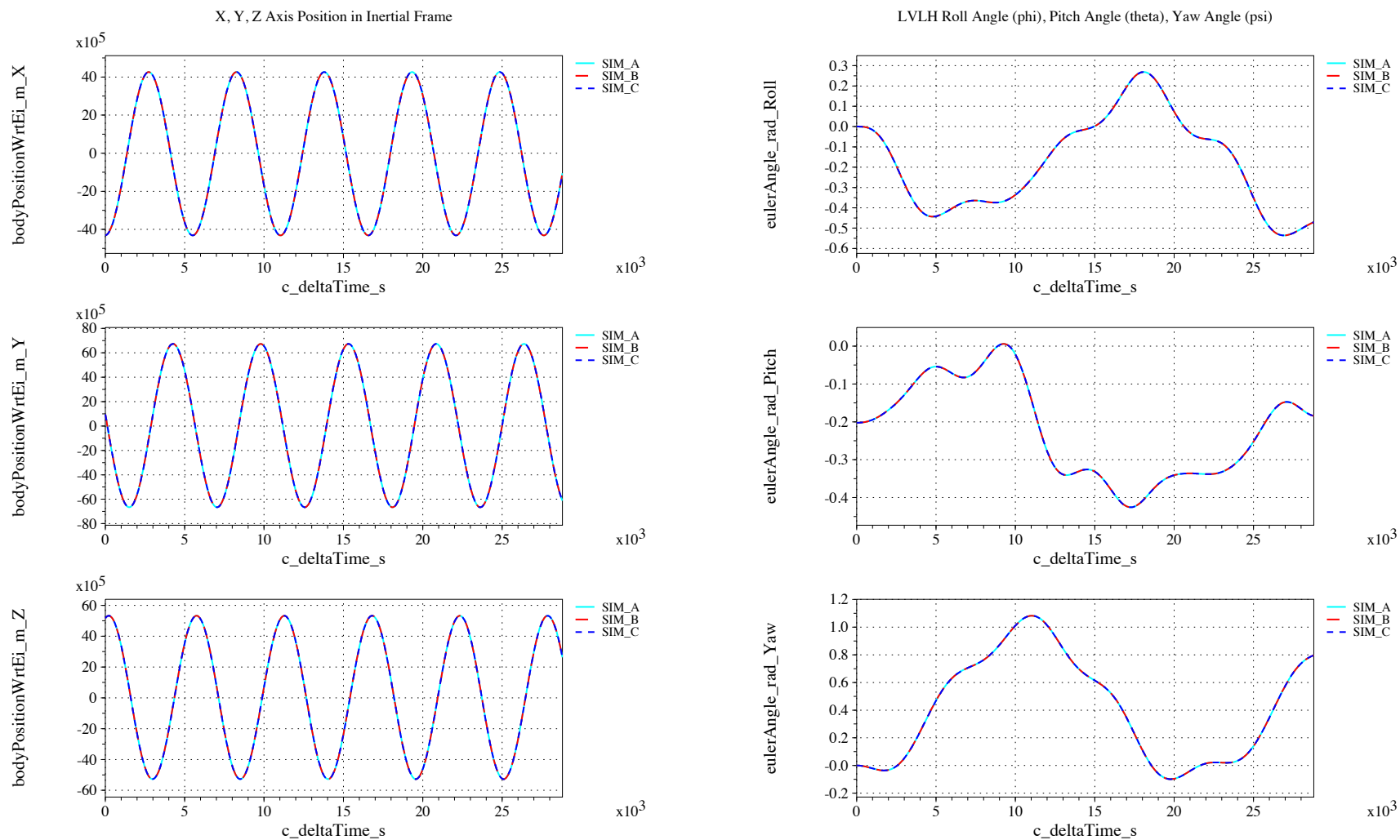
Figure 37. Inertial positions and Euler angles vs. time (check-case 05A: ISS (minimal solar activity))

IX.B.6.   Check-case 5B – ISS (mean solar activity)

This section shows cross-plots for three of the selected simulation tools in modeling the dynamics of the ISS in orbit with mean solar activity disturbances.

Figures 38 and 40 compare results between NASA simulation tools in inertial acceleration, atmospheric quantities, rates and velocities and positions and attitudes.
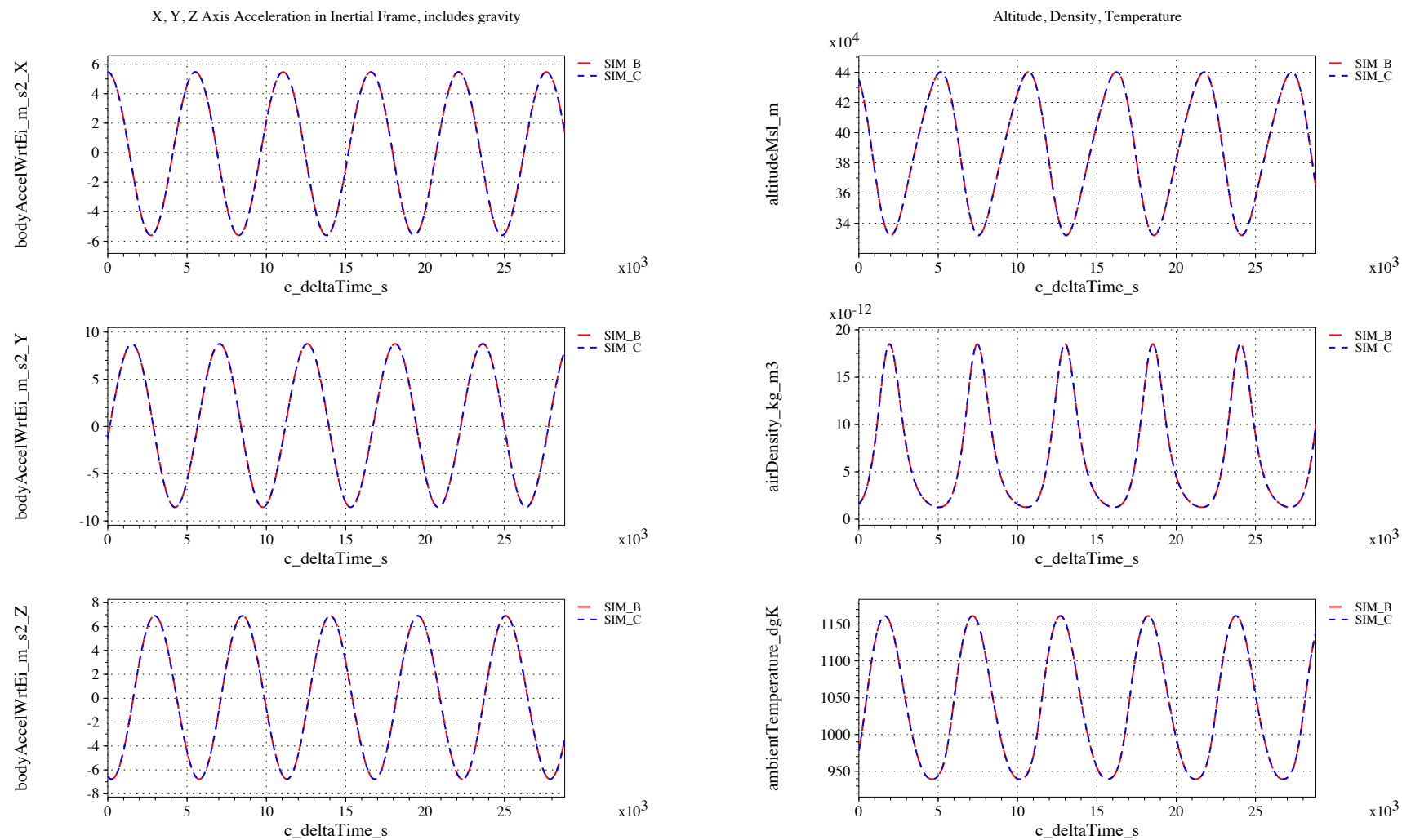
As in other cases, SIM_A shows slightly higher peaks in atmospheric density than SIM_B and SIM_C. There may be a difference in either MET model implementation or interaction (e.g. input values); this difference is being investigated.

American Institute of Aeronautics and Astronautics

Figure 38. Accelerations and atmospheric quantities vs. time (check-case 05B: ISS (mean solar activity))
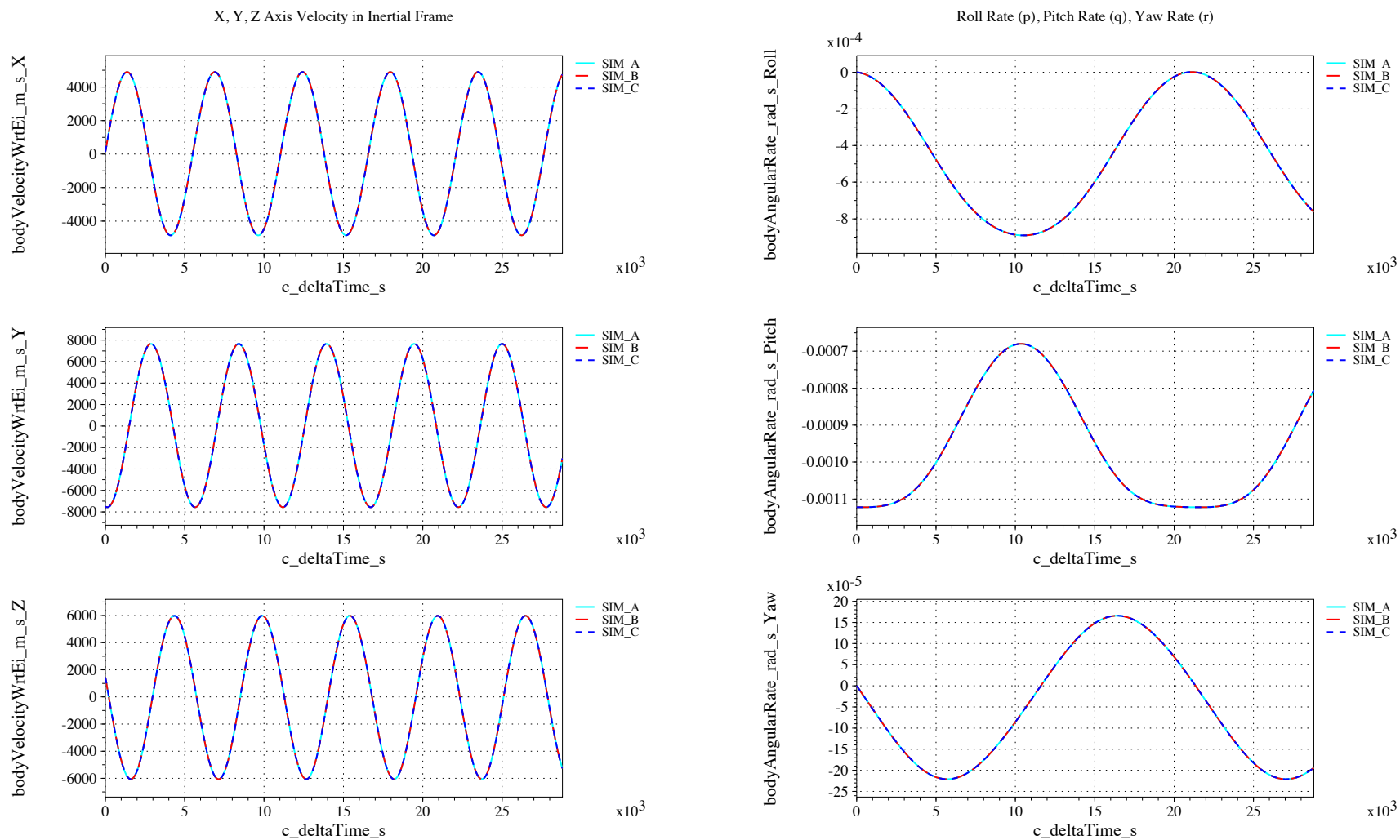
Figure 39. Inertial velocity and body angular rates vs. time (check-case 05B: ISS (mean solar activity))
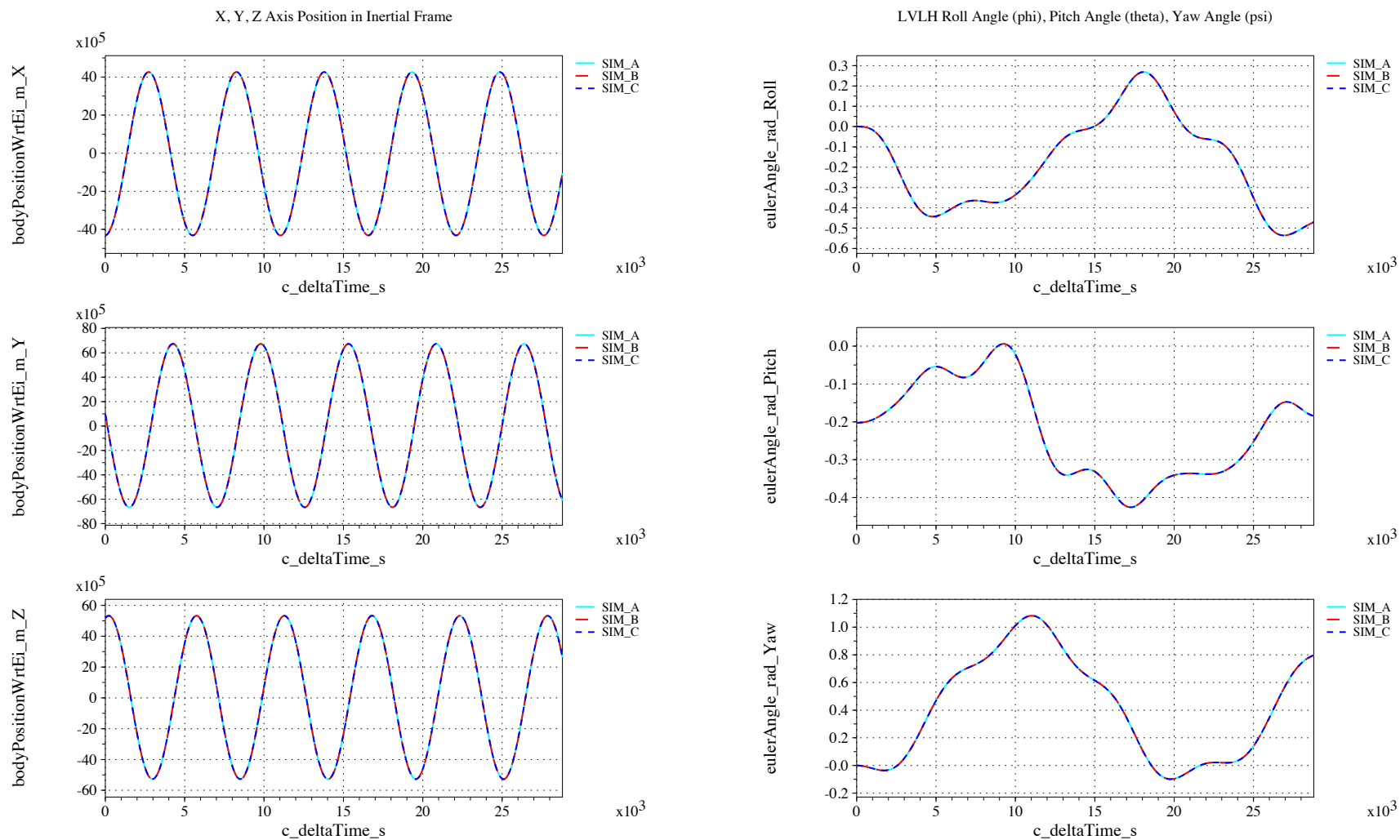
Figure 40. Inertial positions and Euler angles vs. time (check-case 05B: ISS (mean solar activity))

IX.B.7.   Check-case 5C – ISS (maximal solar activity)

This section shows cross-plots for three of the selected simulation tools in modeling the dynamics of the ISS in orbit with maximal solar activity disturbances.

Figures 41 and 43 compare results between NASA simulation tools in inertial acceleration, atmospheric quantities, rates and velocities and positions and attitudes.

As in other cases, SIM_A shows slightly higher peaks in atmospheric density than SIM_B and SIM_C. There may be a difference in either MET model implementation or interaction (e.g. input values); this difference is being investigated.
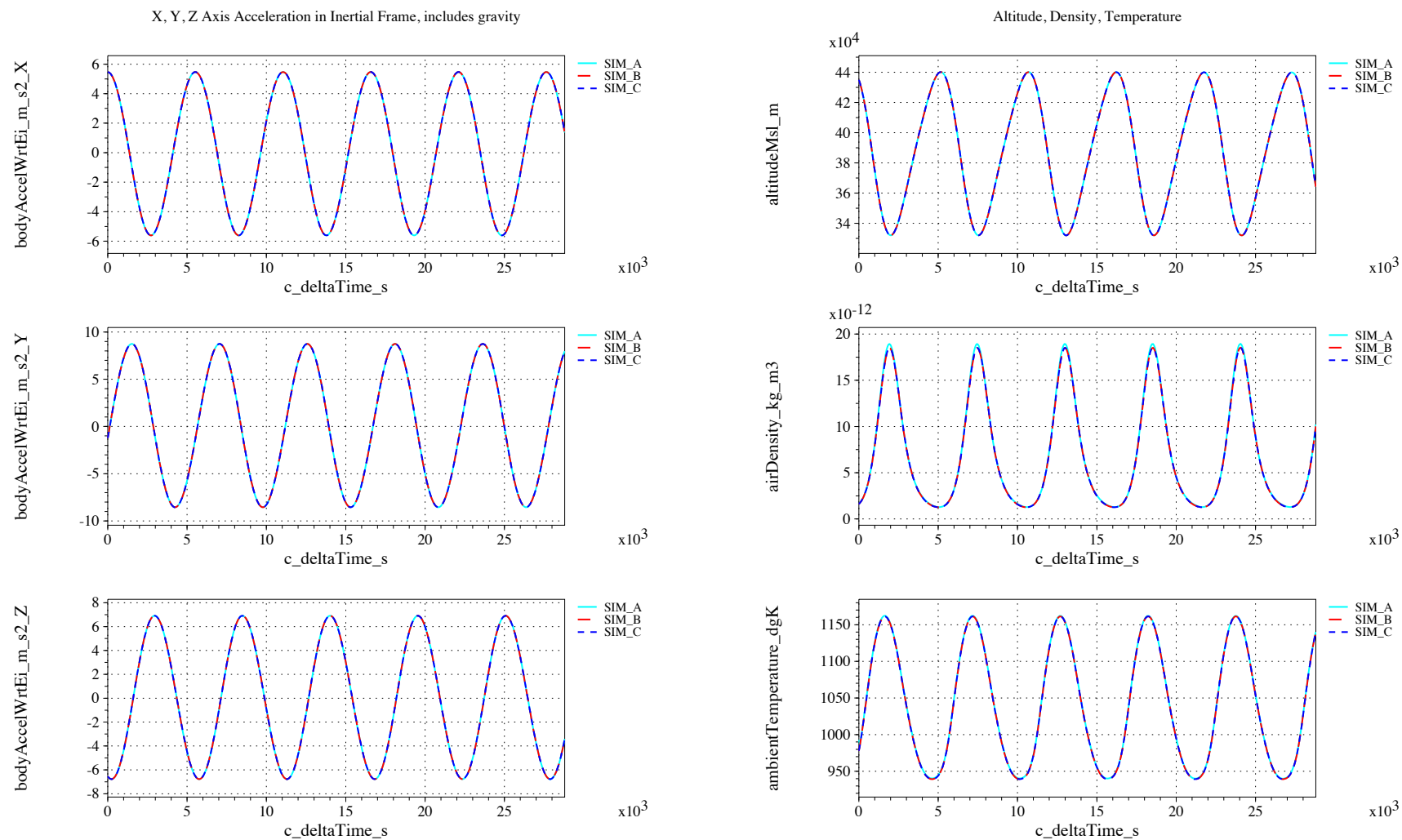
American Institute of Aeronautics and Astronautics

American Institute of Aeronautics and Astronautics

Figure 41. Accelerations and atmospheric quantities vs. time (check-case 05C: ISS (maximal solar activity))

Figure 42. Inertial velocity and body angular rates vs. time (check-case 05C: ISS (maximal solar activity))

Figure 43. Inertial positions and Euler angles vs. time (check-case 05C: ISS (maximal solar activity))

IX.B.8. *Check-case 6A – sphere with fixed drag*

This section shows cross-plots for two of the selected simulation tools in modeling the dynamics of a sphere in orbit with fixed drag (additional simulation results are pending).

Figures 44 and 46 compare results between NASA simulation tools in inertial acceleration, atmospheric quantities, rates and velocities and positions and attitudes.
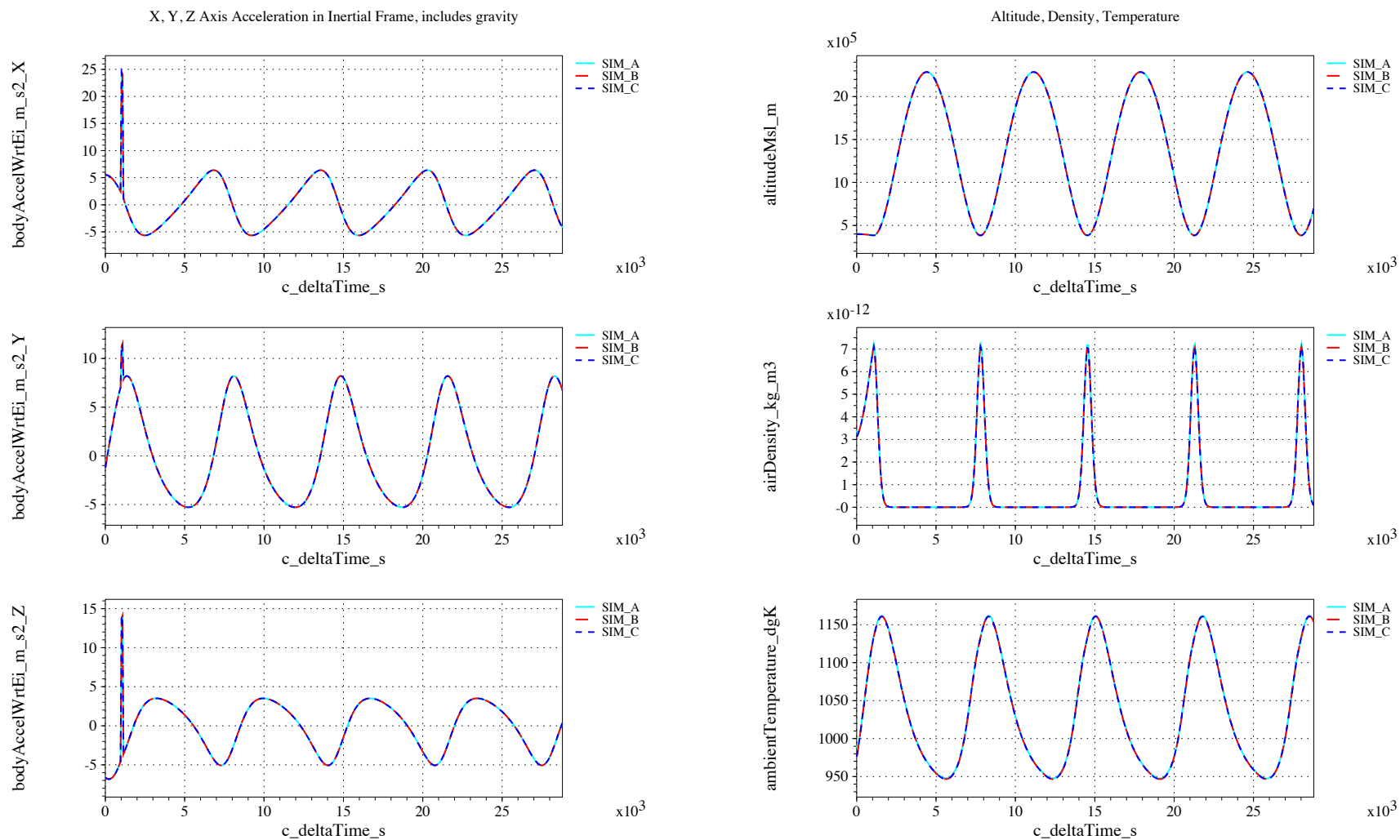
American Institute of Aeronautics and Astronautics

American Institute of Aeronautics and Astronautics

Figure 44. Accelerations and atmospheric quantities vs. time (check-case 06A: sphere with fixed drag)

American Institute of Aeronautics and Astronautics

X, Y, Z Axis Velocity in Inertial Frame

Roll Rate (p), Pitch Rate (q), Yaw Rate (r)
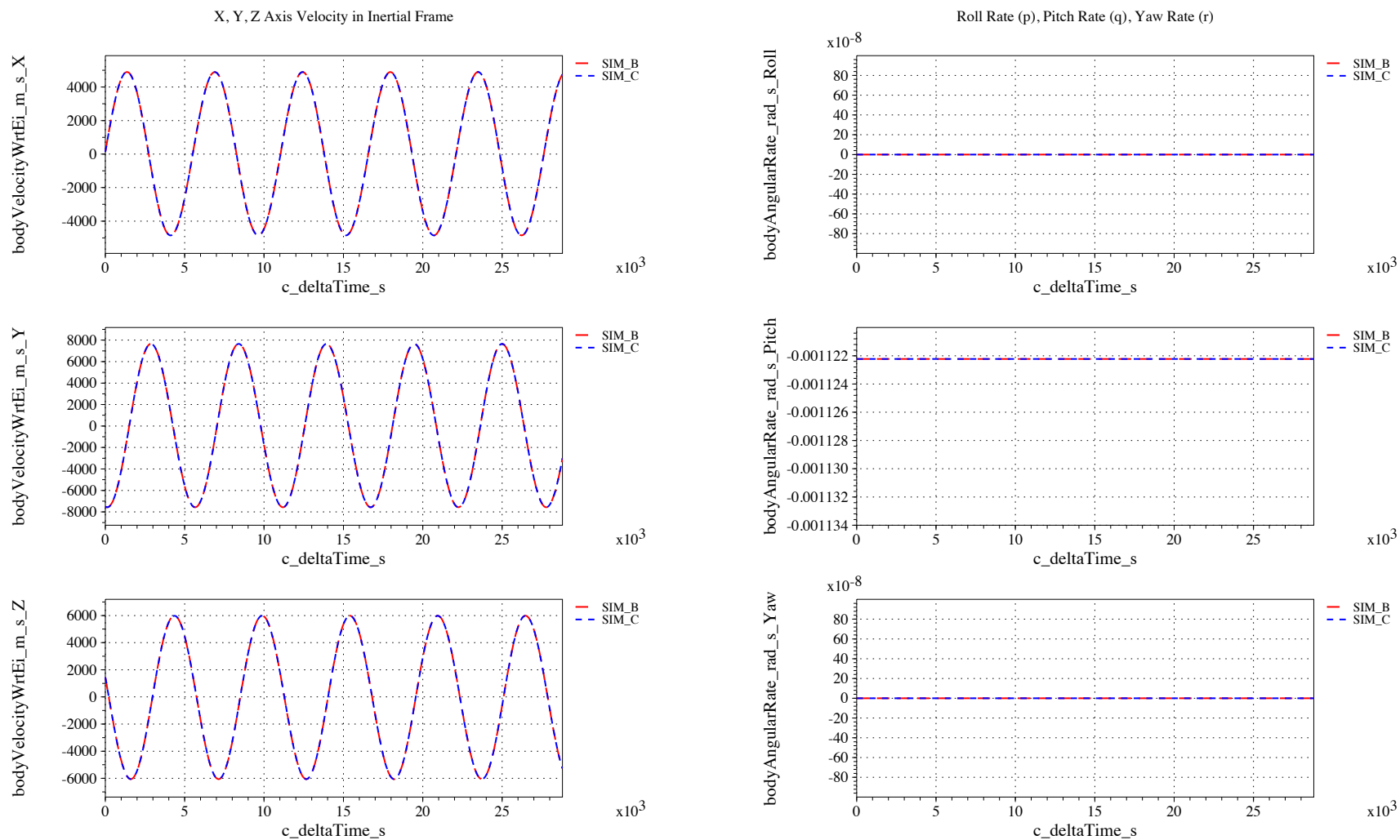
Figure 45. Inertial velocity and body angular rates vs. time (check-case 06A: sphere with fixed drag)
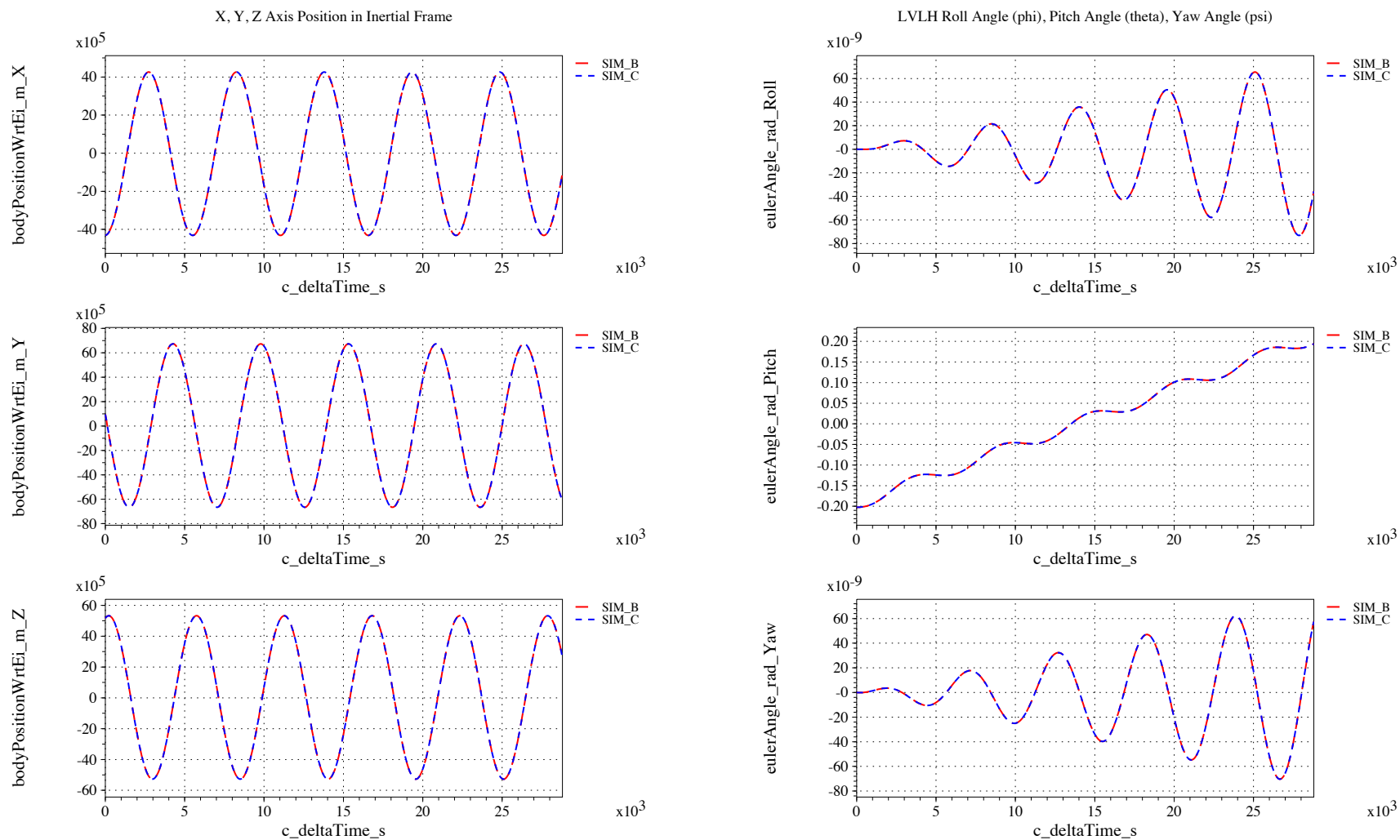
Figure 46. Inertial positions and Euler angles vs. time (check-case 06A: sphere with fixed drag)

IX.B.9.   Check-case 6B – sphere with dynamic drag

This section shows cross-plots for three of the selected simulation tools in modeling the dynamics of a sphere in orbit with dynamically varying drag.

Figures 47 and 49 compare results between NASA simulation tools in inertial acceleration, atmospheric quantities, rates and velocities and positions and attitudes.

SIM_A shows a slight departure in semi-major axis from SIM_B and SIM_C. This may be due to the difference in density which leads to a difference in drag. Unfortunately, SIM_A is not co-plotted in Case 6A which uses a constant density; a match in that case would corroborate this analysis.

SIM_A shows a slight departure in LVLH roll and yaw angles. Again, this could be due to small differences in orbit change due to differences in drag.

As in other cases, SIM_A shows slightly higher peaks in atmospheric density than SIM_B and SIM_C. There may be a difference in either MET model implementation or interaction (e.g. input values); this difference is being investigated.

American Institute of Aeronautics and Astronautics

American Institute of Aeronautics and Astronautics

X, Y, Z Axis Acceleration in Inertial Frame, includes gravity

Altitude, Density, Temperature

Figure 47. Accelerations and atmospheric quantities vs. time (check-case 06B: sphere with dynamic drag)

American Institute of Aeronautics and Astronautics
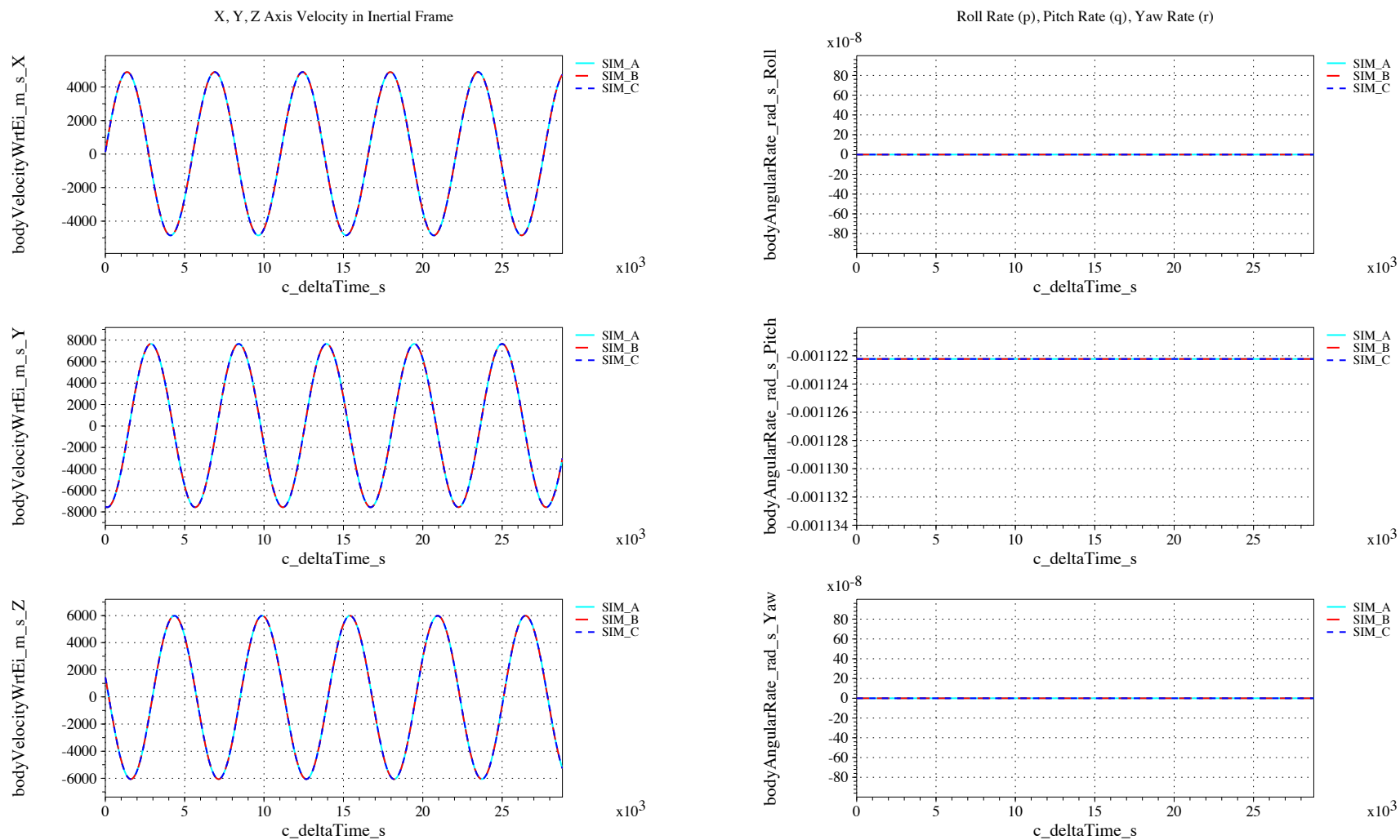
Figure 48. Inertial velocity and body angular rates vs. time (check-case 06B: sphere with dynamic drag)
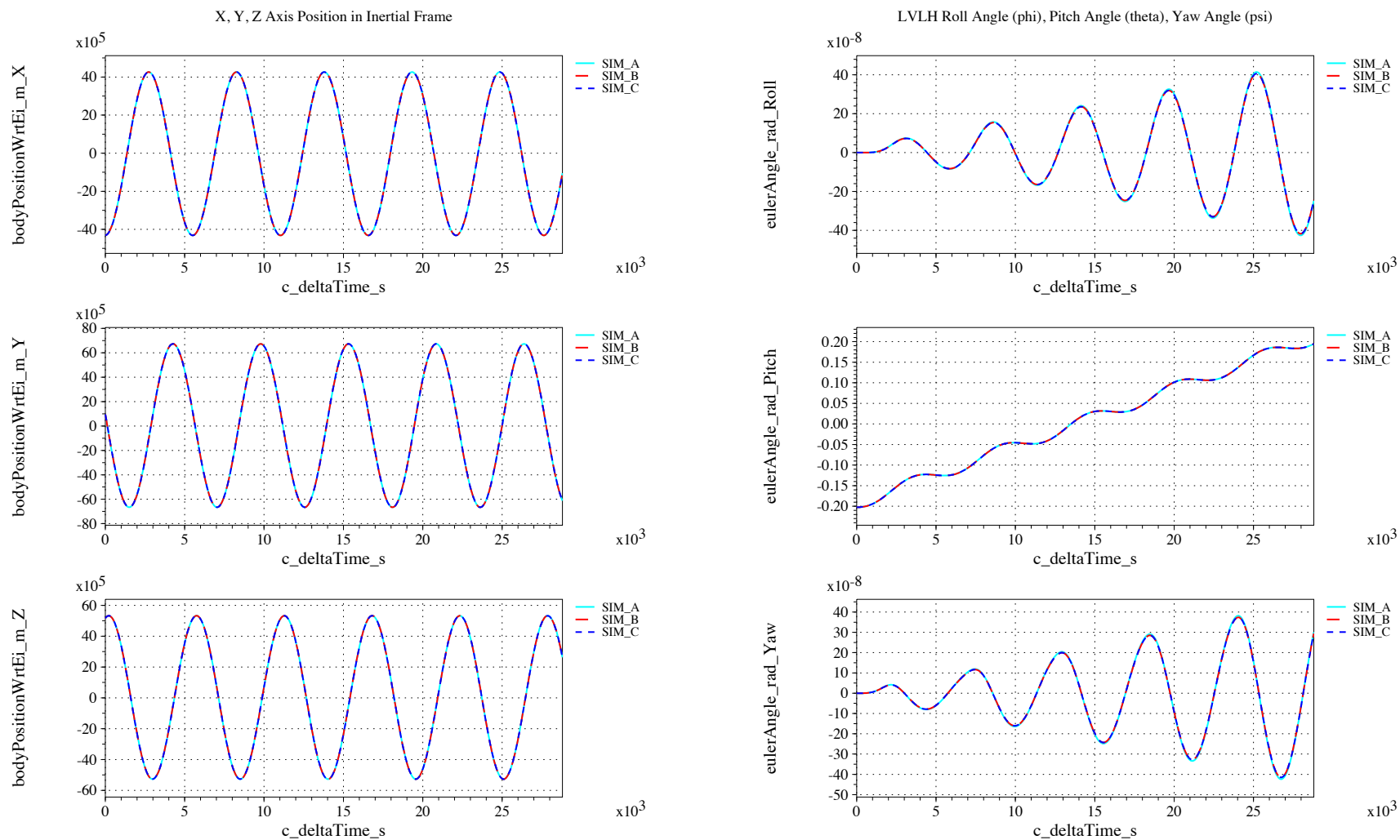
Figure 49. Inertial positions and Euler angles vs. time (check-case 06B: sphere with dynamic drag)

IX.B.10. *Check-case 6C – cylinder undergoing plane change firing*

This section shows cross-plots for three of the selected simulation tools in modeling the dynamics of a cylinder in orbit performing a plane change maneuver with intermittent propulsion.

Figures 50 and 52 compare results between NASA simulation tools in inertial acceleration, atmospheric quantities, rates and velocities and positions and attitudes.

American Institute of Aeronautics and Astronautics

X, Y, Z Axis Acceleration in Inertial Frame, includes gravity

Altitude, Density, Temperature

Figure 50. Accelerations and atmospheric quantities vs. time (check-case 06C: cylinder undergoing plane change firing)

American Institute of Aeronautics and Astronautics
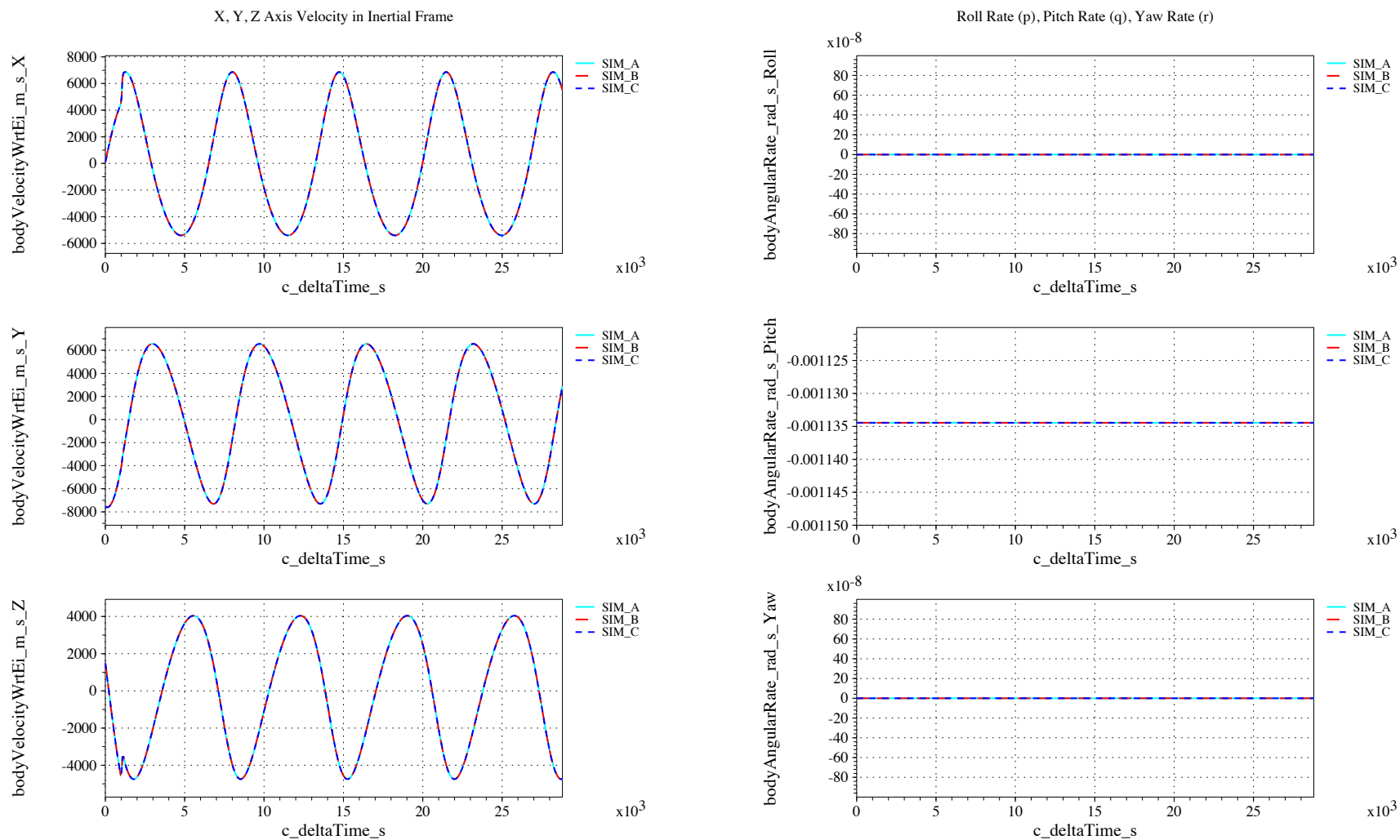
Figure 51. Inertial velocity and body angular rates vs. time (check-case 06C: cylinder undergoing plane change firing)

American Institute of Aeronautics and Astronautics

X, Y, Z Axis Position in Inertial Frame

LVLH Roll Angle (phi), Pitch Angle (theta), Yaw Angle (psi)
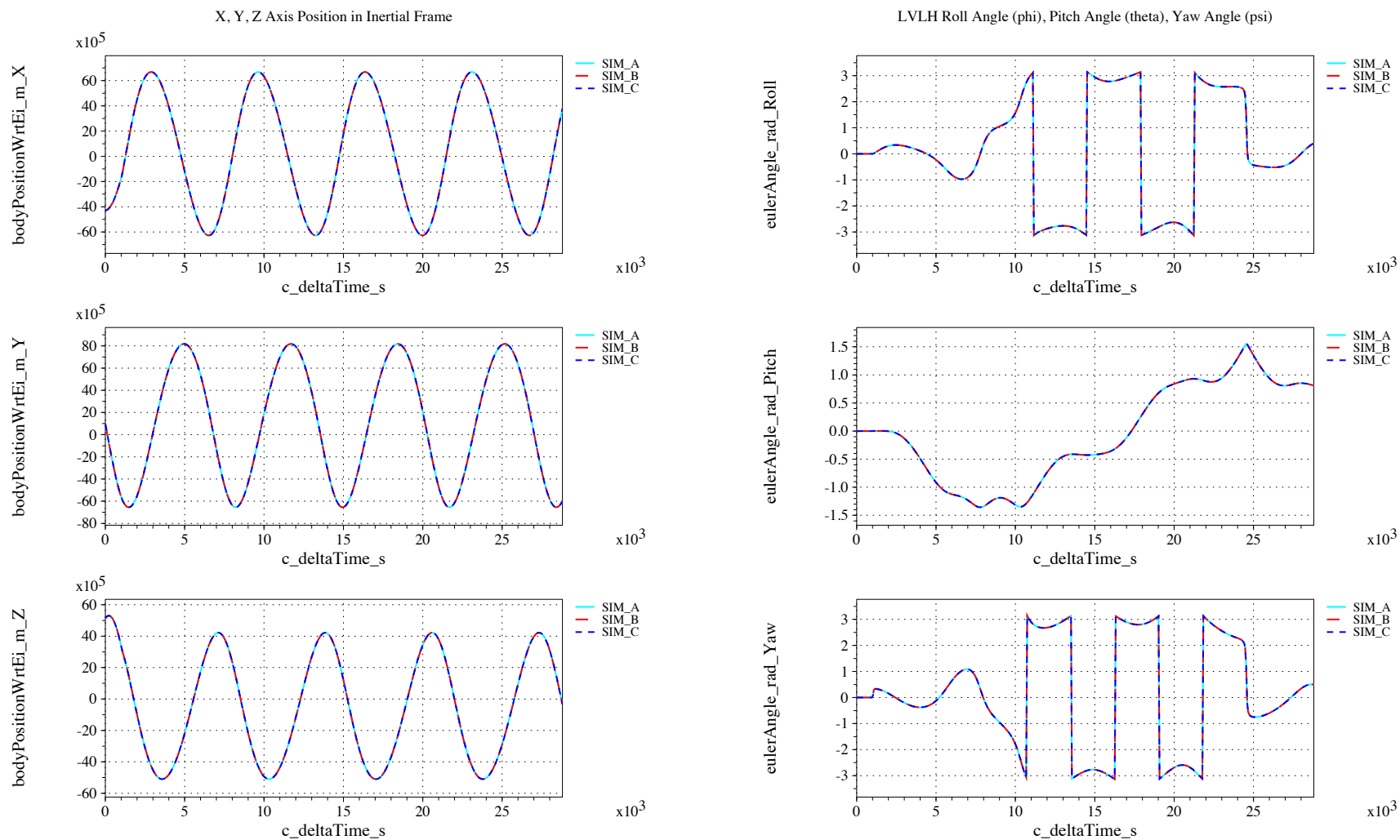
Figure 52. Inertial positions and Euler angles vs. time (check-case 06C: cylinder undergoing plane change firing)

IX.B.11.   Check-case 6D – cylinder undergoing Earth departure firing

This section shows cross-plots for three of the selected simulation tools in modeling the dynamics of a cylinder in orbit performing an Earth departure maneuver with intermittent propulsion.

An initial pitch rate of -0.065 deg/s is due to initial conditions similar to ISS where the vehicle seeks to remain level in the LVLH frame, thus pitching down to match the angular rate relative to the Earth in low Earth orbit.

Figures 53 and 55 compare results between NASA simulation tools in inertial acceleration, atmospheric quantities, rates and velocities and positions and attitudes.

In this scenario, the vehicle is initialized to maintain orientation relative to its initial orbit. The Euler angles presented are relative to the orbit (LVLH frame). However, the Earth escape maneuver changes the orbit to a hyperbolic trajectory. Relative to this trajectory, the vehicle is now seen has having a constant rotation about the LVLH y-axis (which is perpendicular to the plane of the orbital trajectory). Thus, the LVLH pitch angle undergoes linear change from $-\pi$ to $+\pi$ and back with the period of the original orbit. Also, the x-body axis alternates between being on the positive side of the LVLH x-axis to the negative. When the x-body axis lies on the positive side of the LVLH x-axis, LVLH roll and yaw angles are zero. However, when the x-body axis lies on the negative side of the LVLH x-axis, the LVLH roll and yaw angles can have a value of $\pm\pi$. Which value actually gets computed is highly sensitive to the implementation of the Euler angle computation, round-off error, and residual differences between simulations. As seen in figure 55, the simulations do not agree on which side of $\pm\pi$ they lie and the simulations themselves swap between +pi and -pi at different times during each period. Though they appear large, these differences are superficial as they represent equivalent orientations.

American Institute of Aeronautics and Astronautics

American Institute of Aeronautics and Astronautics
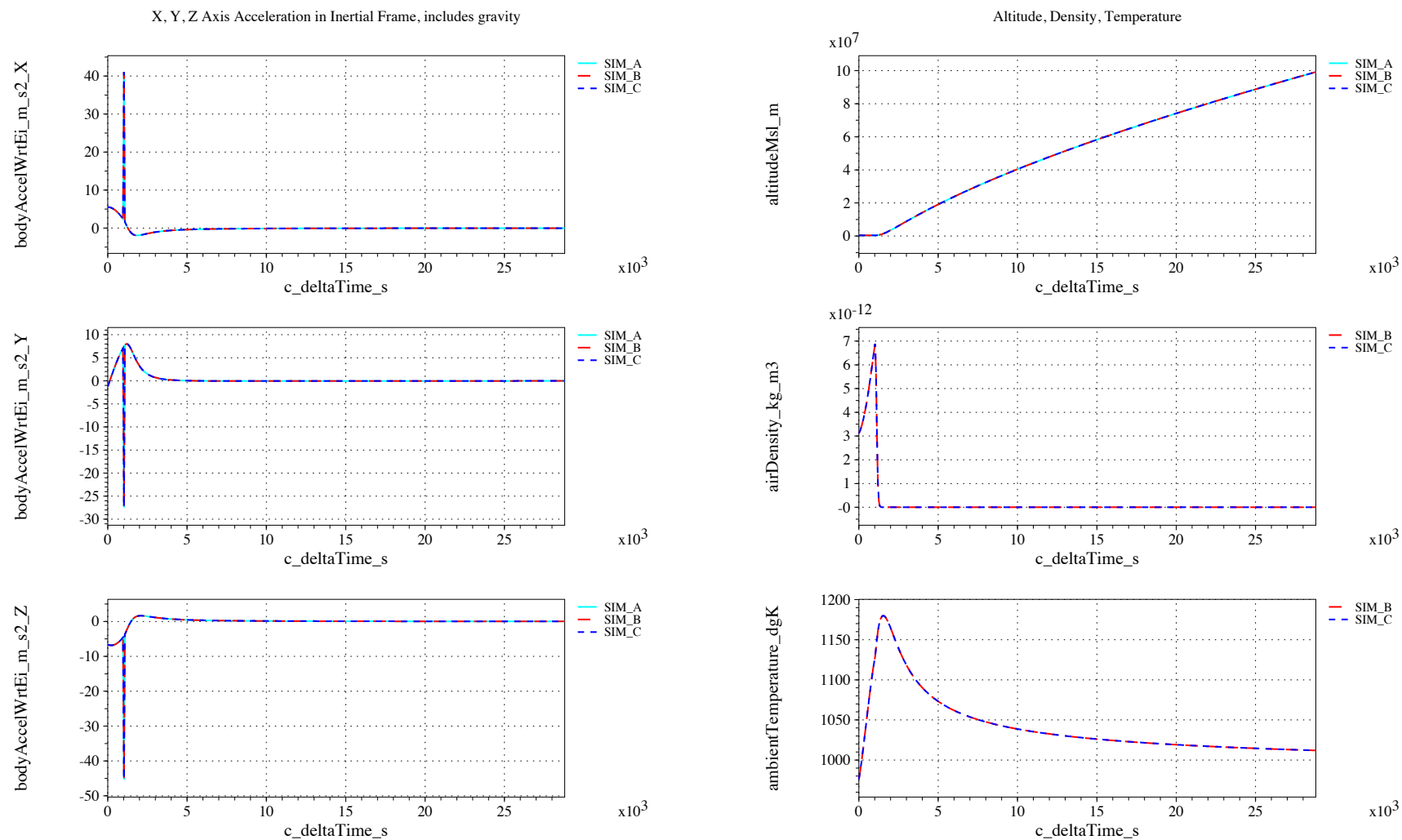
Figure 53. Accelerations and atmospheric quantities vs. time (check-case 06D: cylinder undergoing Earth departure firing)

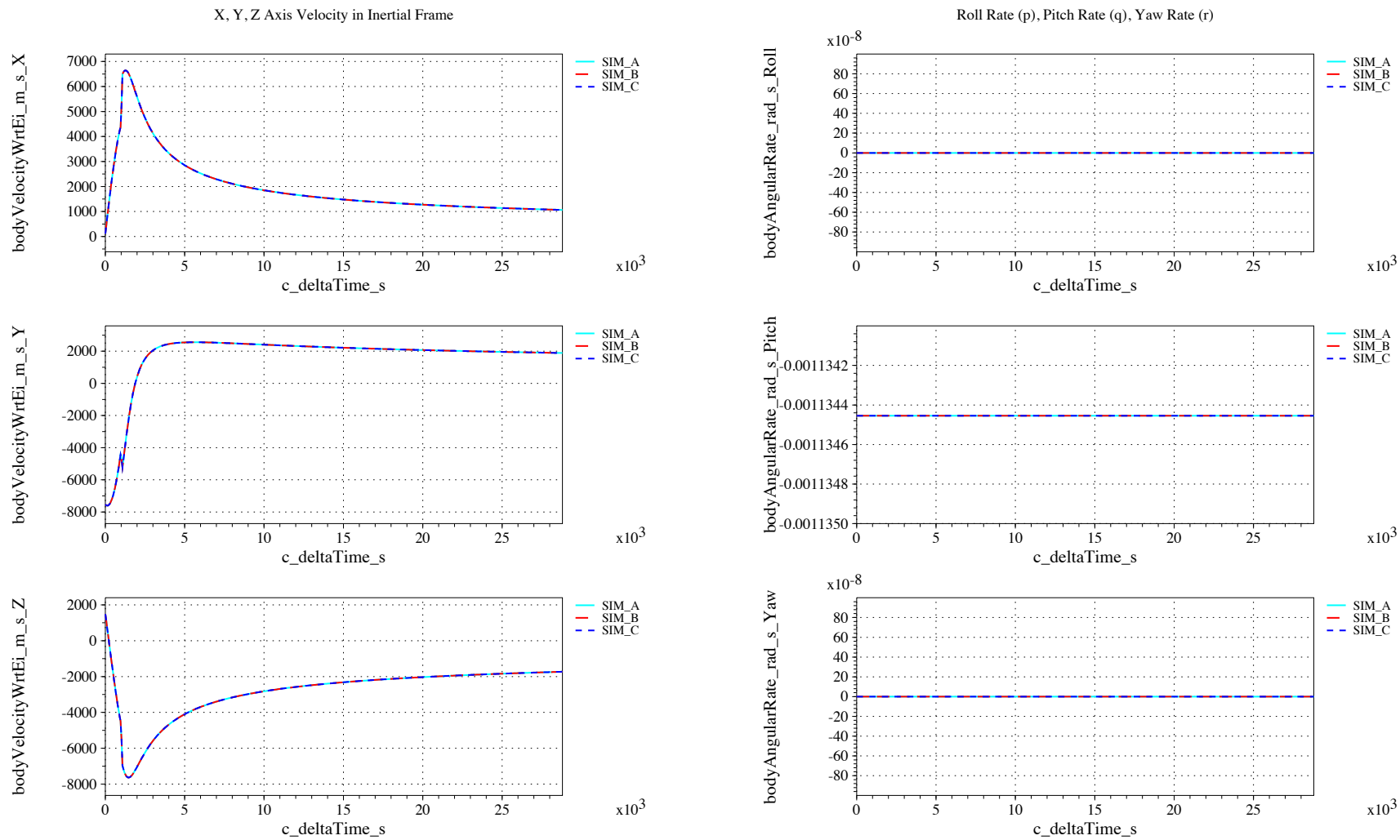American Institute of Aeronautics and Astronautics

Figure 54. Inertial velocity and body angular rates vs. time (check-case 06D: cylinder undergoing Earth departure firing)

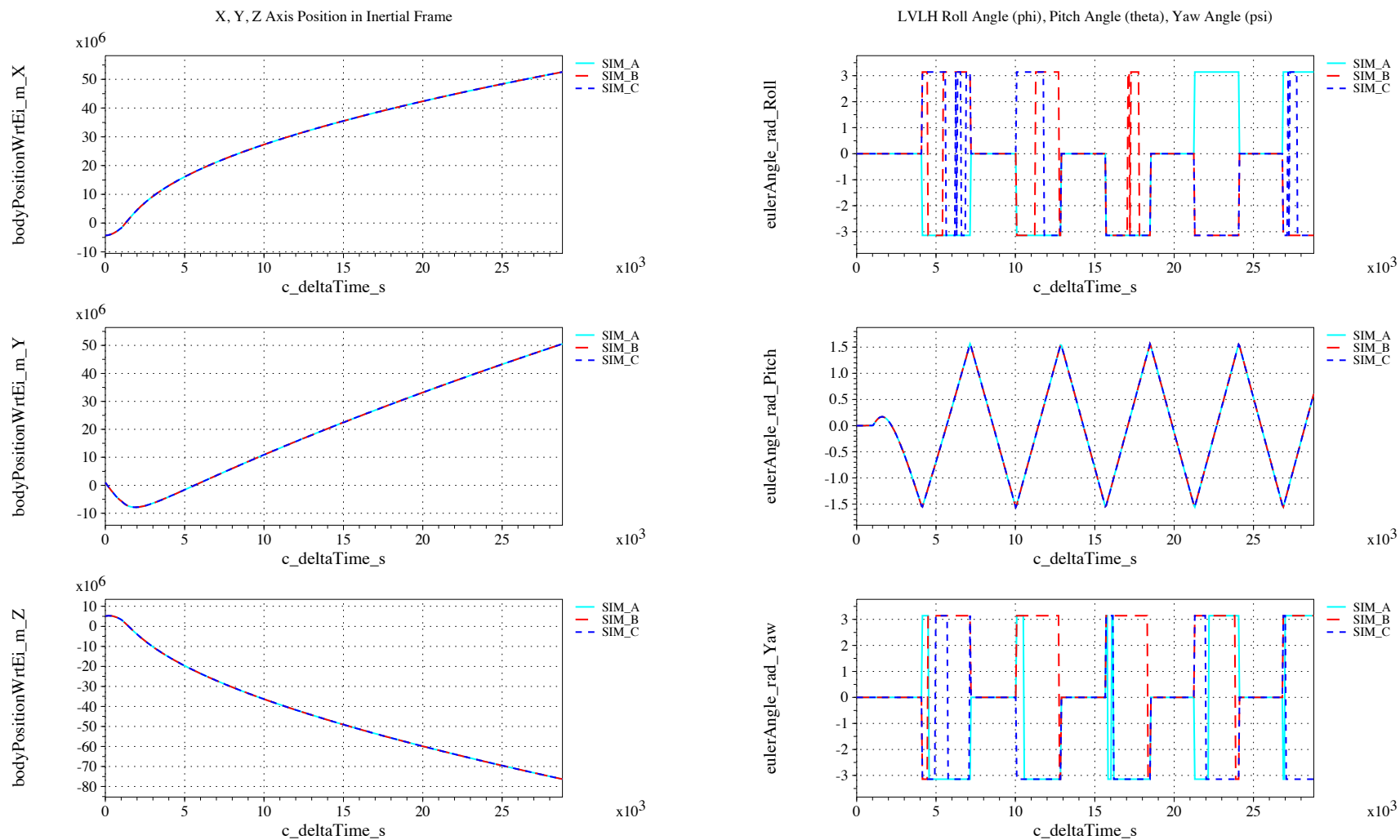American Institute of Aeronautics and Astronautics

95 of 156

X, Y, Z Axis Position in Inertial Frame

LVLH Roll Angle (phi), Pitch Angle (theta), Yaw Angle (psi)

Figure 55. Inertial positions and Euler angles vs. time (check-case 06D: cylinder undergoing Earth departure firing)

IX.B.12.   Check-case 7A – sphere in 4x4 gravity and third-body perturbations

This section shows cross-plots for three of the selected simulation tools in modeling the dynamics of a sphere in orbit responding to a 4x4 gravity model, planetary ephemeris, and third-body perturbations.

Figures 56 and 58 compare results between NASA simulation tools in inertial acceleration, atmospheric quantities, rates and velocities and positions and attitudes.

As in other cases, SIM_A shows slightly higher peaks in atmospheric density than SIM_B and SIM_C. There may be a difference in either MET model implementation or interaction (e.g. input values); this difference is being investigated.
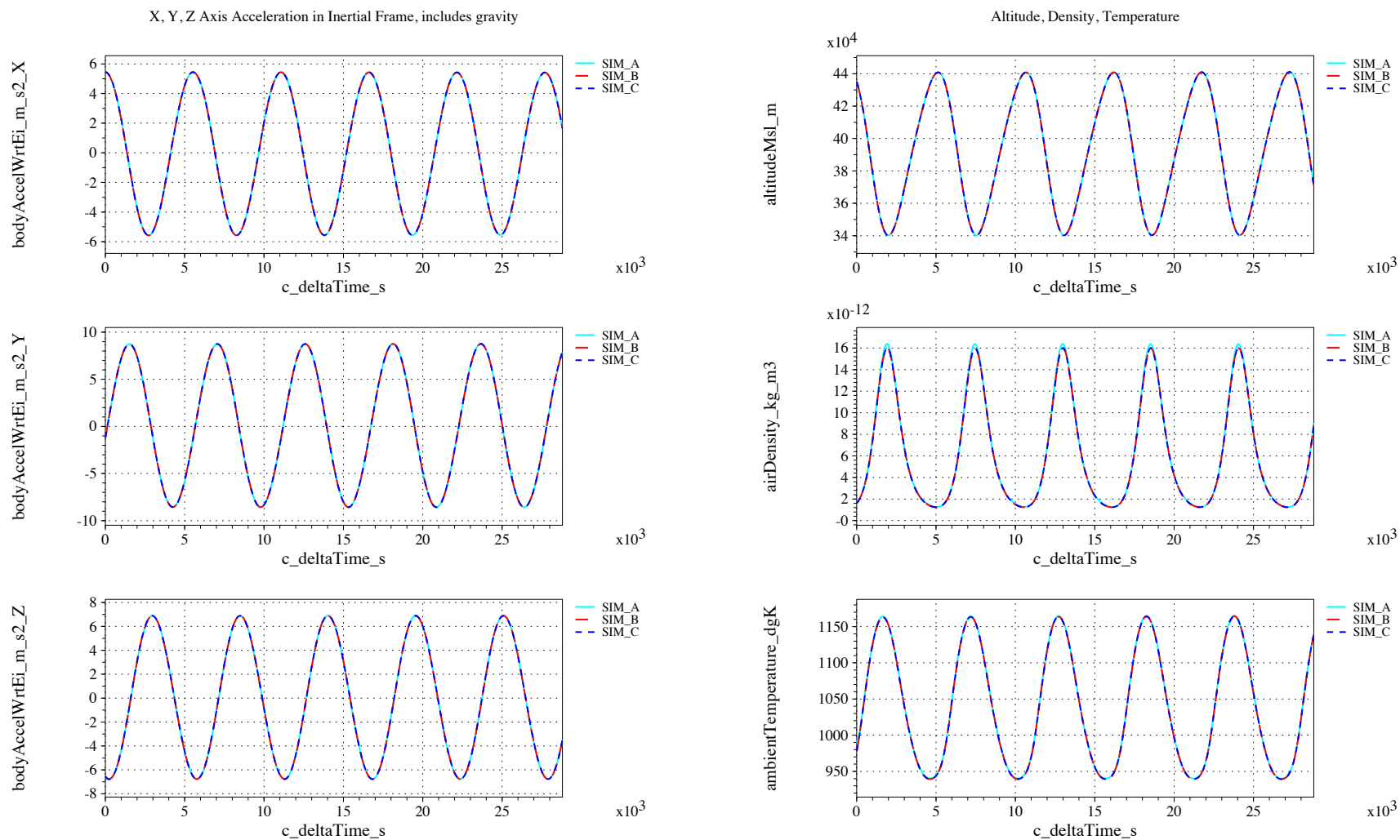
American Institute of Aeronautics and Astronautics
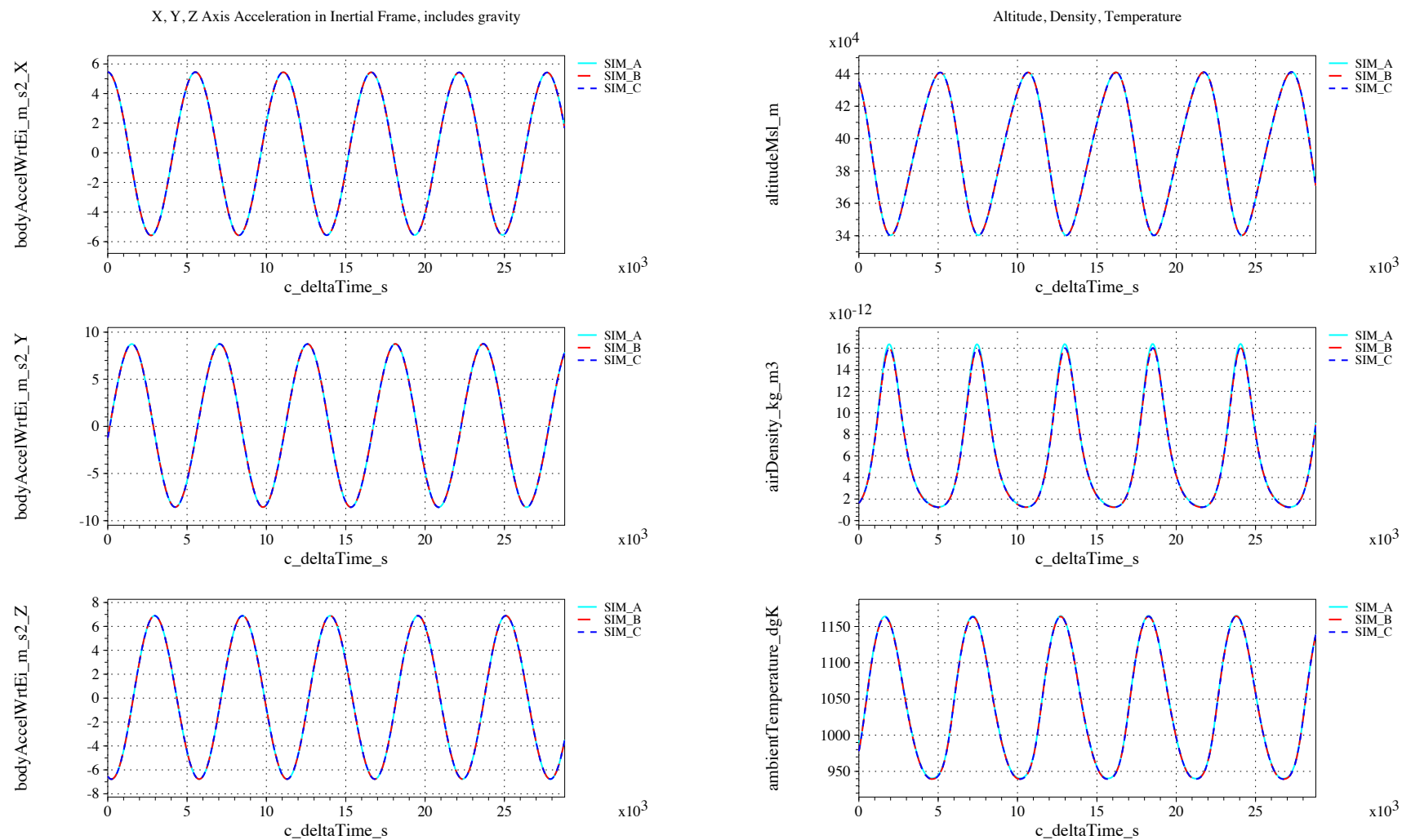
Figure 56. Accelerations and atmospheric quantities vs. time (check-case 07A: sphere in 4x4 gravity and third-body perturbations)

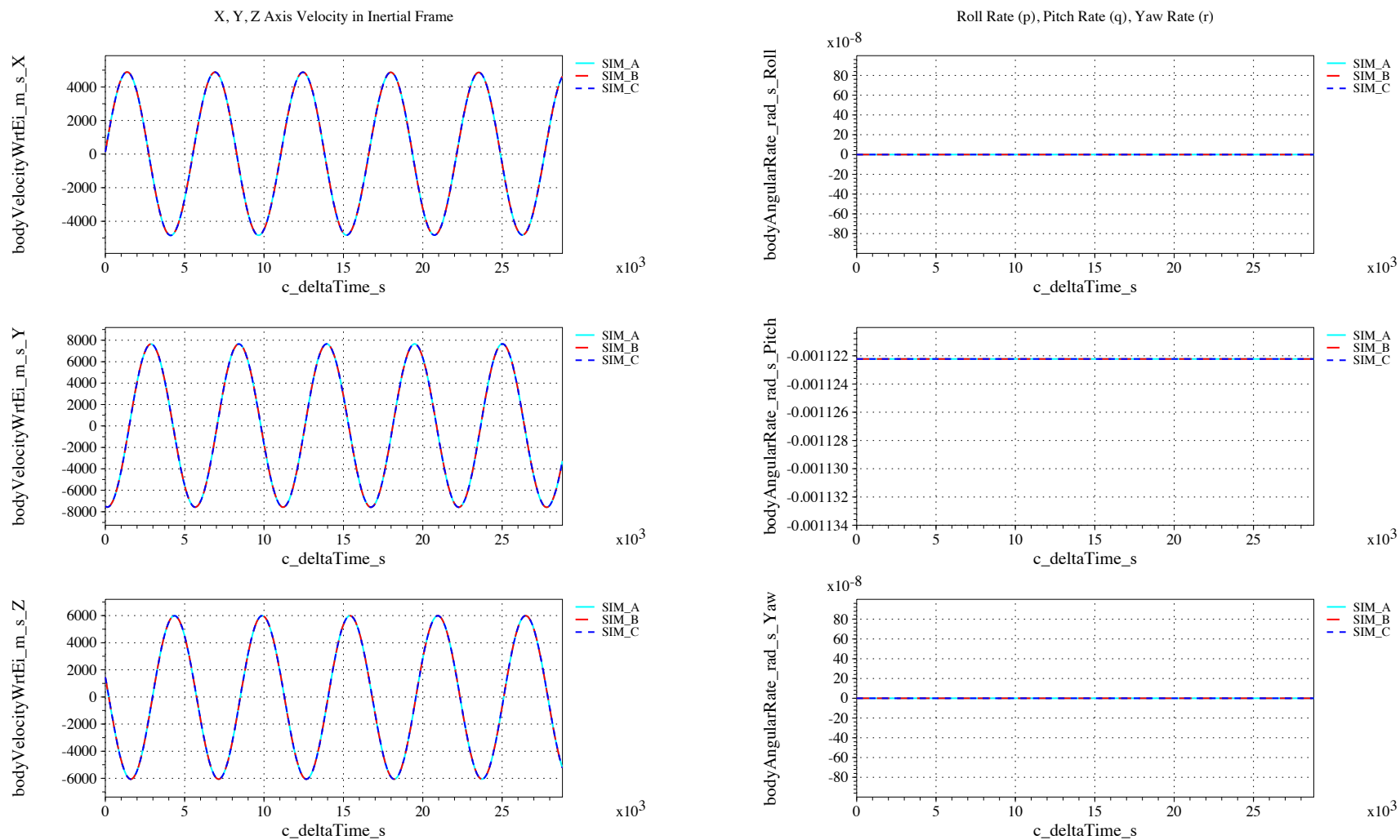American Institute of Aeronautics and Astronautics

X, Y, Z Axis Velocity in Inertial Frame

Roll Rate (p), Pitch Rate (q), Yaw Rate (r)
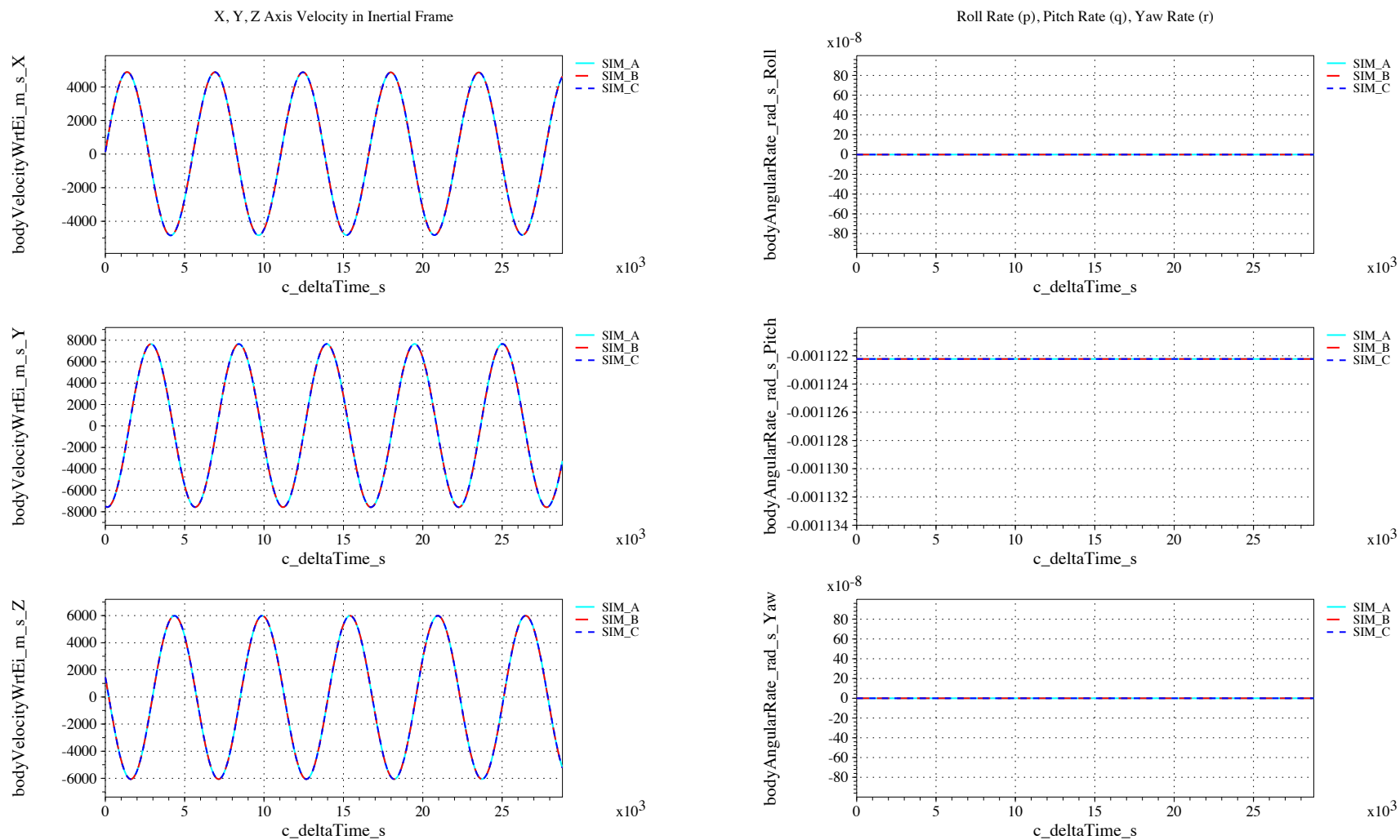
Figure 57. Inertial velocity and body angular rates vs. time (check-case 07A: sphere in 4x4 gravity and third-body perturbations)

American Institute of Aeronautics and Astronautics

X, Y, Z Axis Position in Inertial Frame

LVLH Roll Angle (phi), Pitch Angle (theta), Yaw Angle (psi)
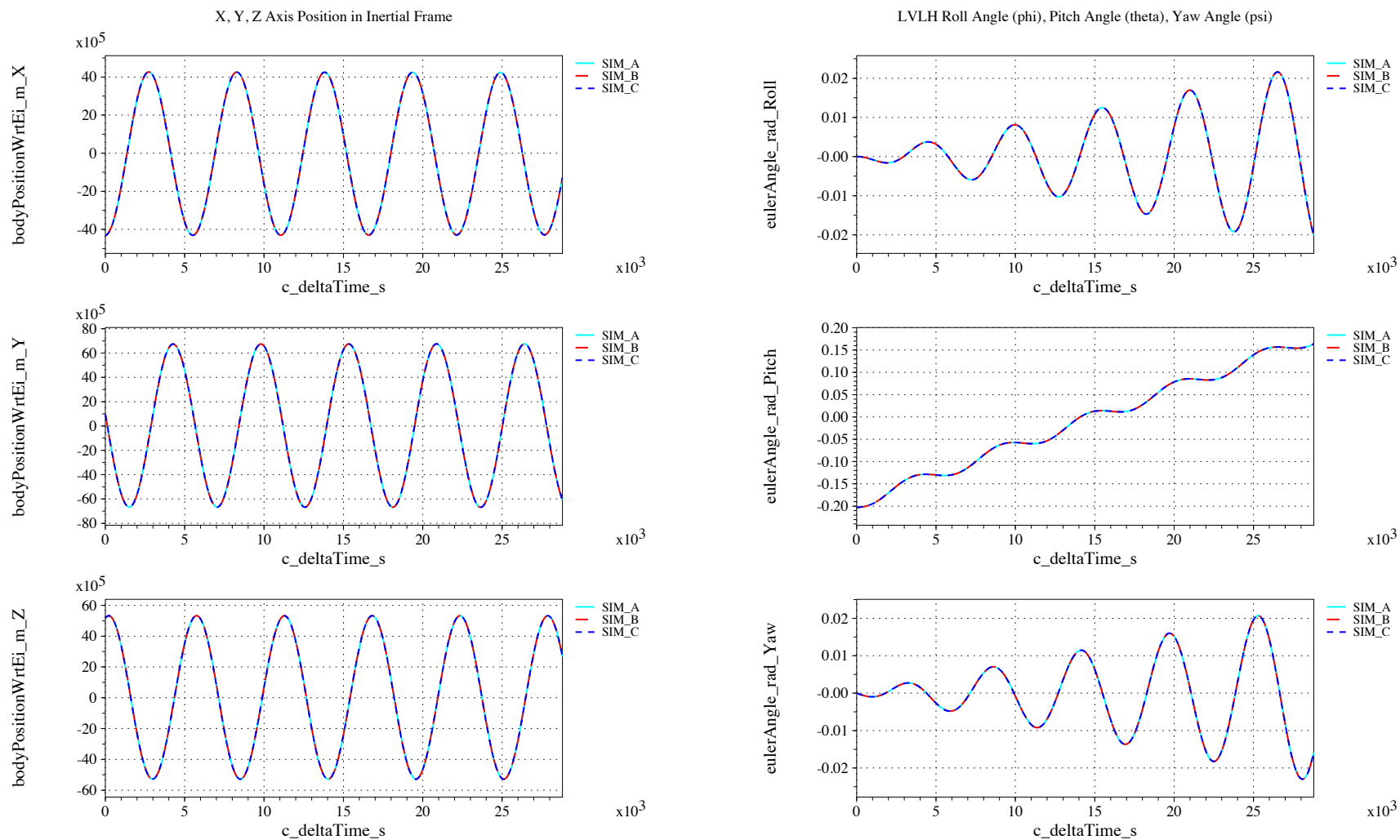
Figure 58. Inertial positions and Euler angles vs. time (check-case 07A: sphere in 4x4 gravity and third-body perturbations)

IX.B.13.   Check-case 7B – sphere in 8x8 gravity and third-body perturbations

This section shows cross-plots for three of the selected simulation tools in modeling the dynamics of a sphere in orbit responding to an 8x8 gravity model, planetary ephemeris, and third-body perturbations.

Figures 59 and 61 compare results between NASA simulation tools in inertial acceleration, atmospheric quantities, rates and velocities and positions and attitudes.

As in other cases, SIM_A shows slightly higher peaks in atmospheric density than SIM_B and SIM_C. There may be a difference in either MET model implementation or interaction (e.g. input values); this difference is being investigated.
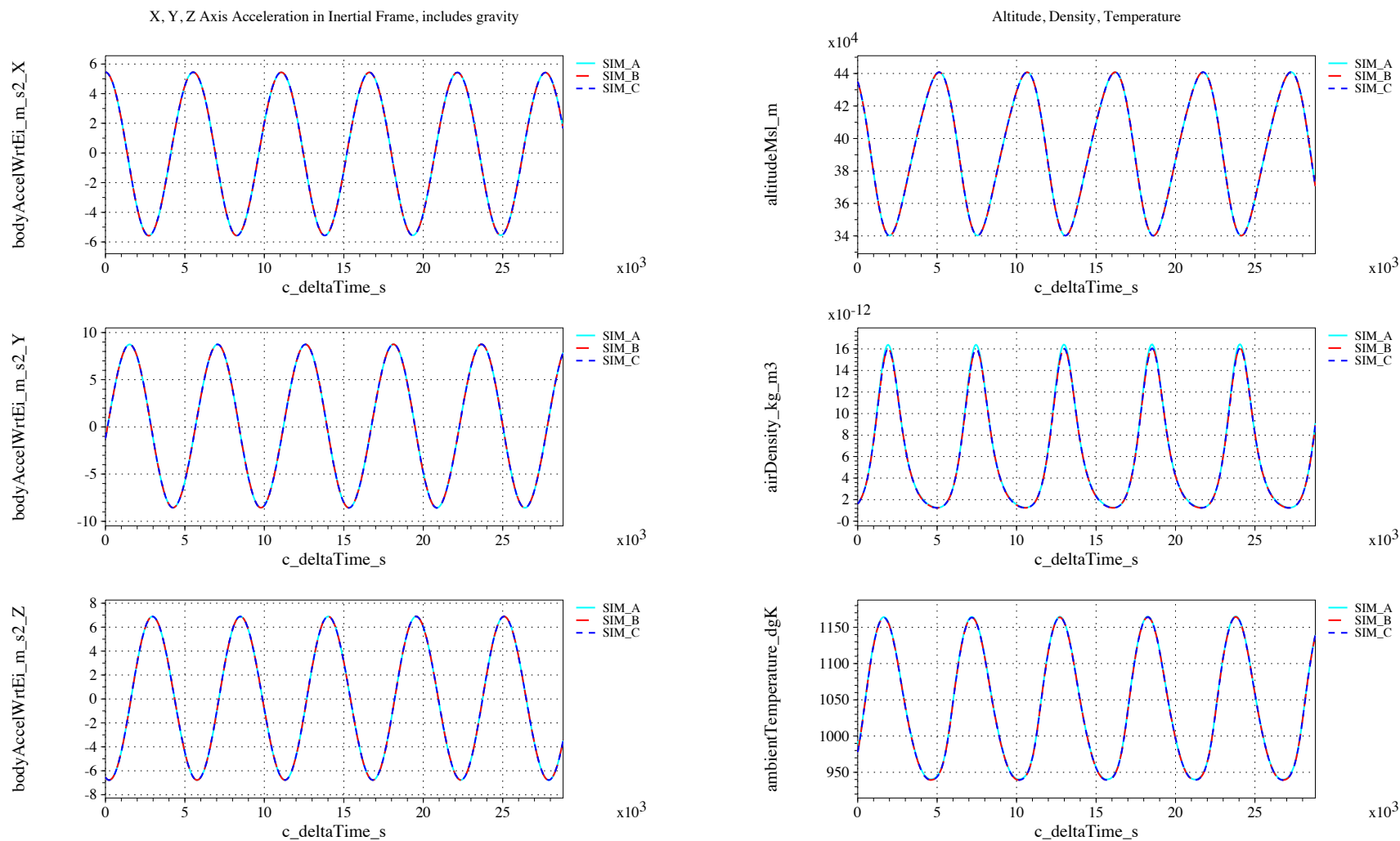
American Institute of Aeronautics and Astronautics

American Institute of Aeronautics and Astronautics

X, Y, Z Axis Acceleration in Inertial Frame, includes gravity

Altitude, Density, Temperature

Figure 59. Accelerations and atmospheric quantities vs. time (check-case 07B: sphere in 8x8 gravity and third-body perturbations)

American Institute of Aeronautics and Astronautics

X, Y, Z Axis Velocity in Inertial Frame

Roll Rate (p), Pitch Rate (q), Yaw Rate (r)

Figure 60. Inertial velocity and body angular rates vs. time (check-case 07B: sphere in 8x8 gravity and third-body perturbations)
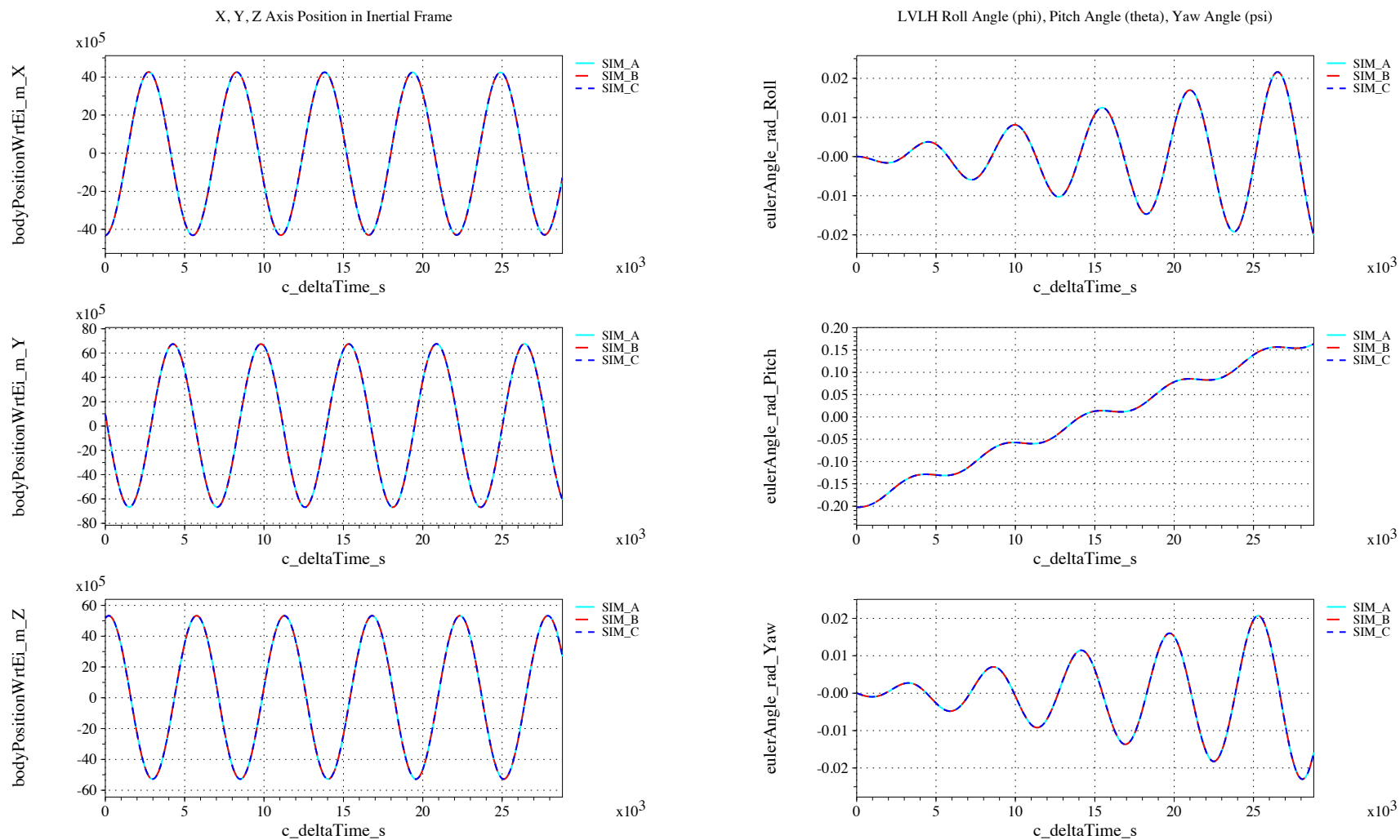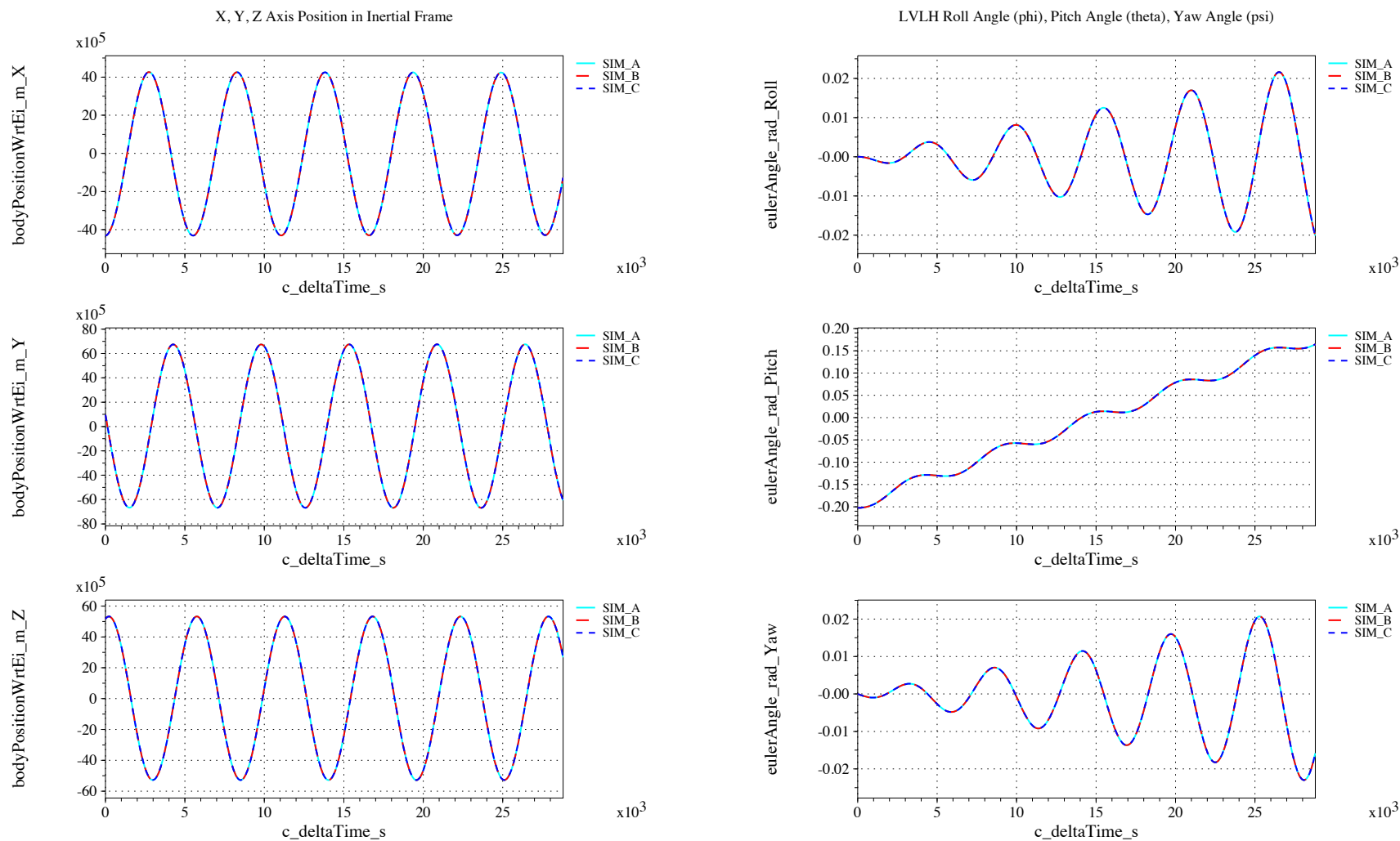
Figure 61. Inertial positions and Euler angles vs. time (check-case 07B: sphere in 8x8 gravity and third-body perturbations)

IX.B.14.   Check-case 7C – sphere in 4x4 gravity with drag and third-body perturbations

This section shows cross-plots for three of the selected simulation tools in modeling the dynamics of a sphere in orbit responding to a 4x4 gravity model, atmospheric drag, planetary ephemeris, and third-body perturbations.

Figures 62 and 64 compare results between NASA simulation tools in inertial acceleration, atmospheric quantities, rates and velocities and positions and attitudes. As in other cases, SIM_A shows slightly higher peaks in atmospheric density than SIM_B and SIM_C. There may be a difference in either MET model implementation or interaction (e.g. input values); this difference is being investigated.
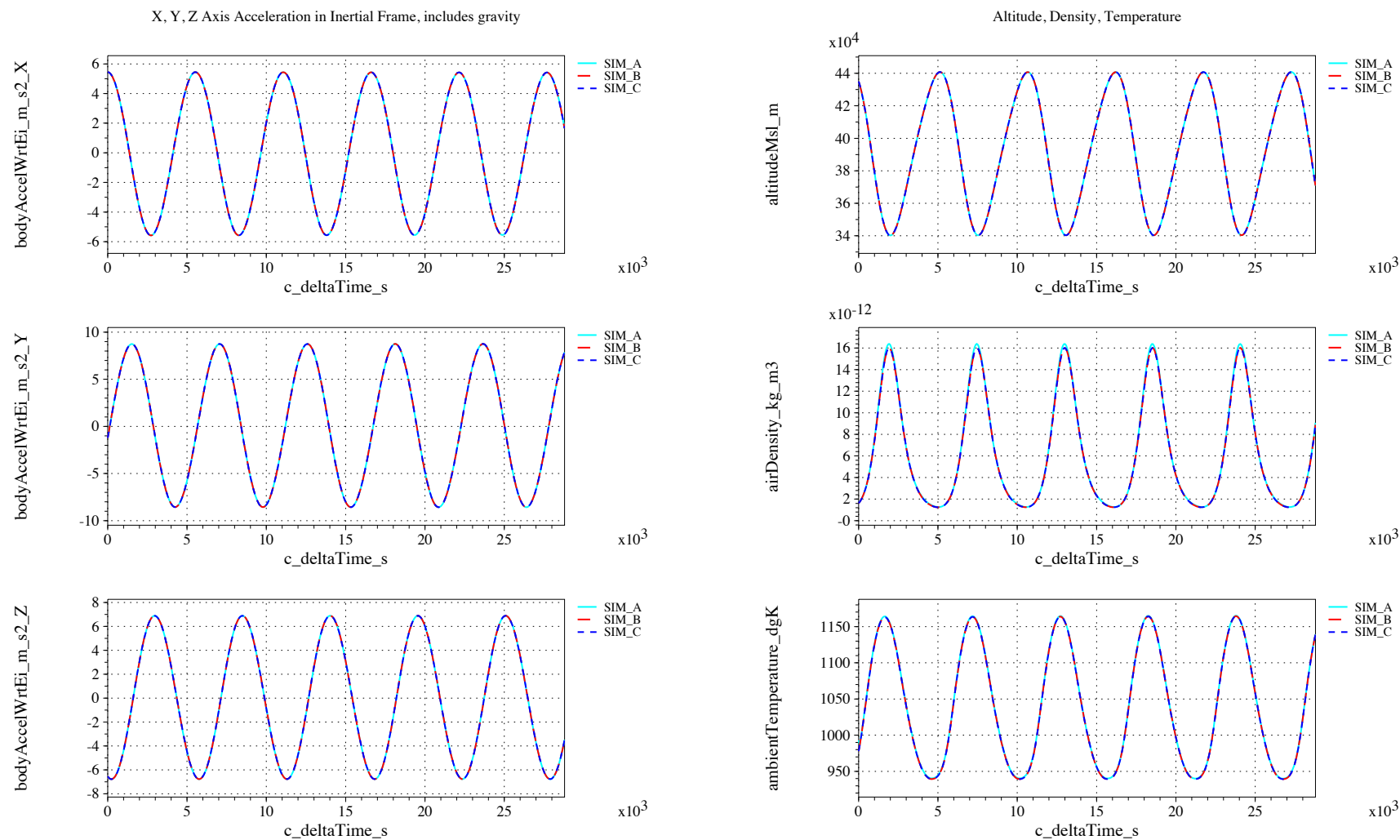
American Institute of Aeronautics and Astronautics

American Institute of Aeronautics and Astronautics

Figure 62. Accelerations and atmospheric quantities vs. time (check-case 07C: sphere in 4x4 gravity with drag and third-body perturbations)

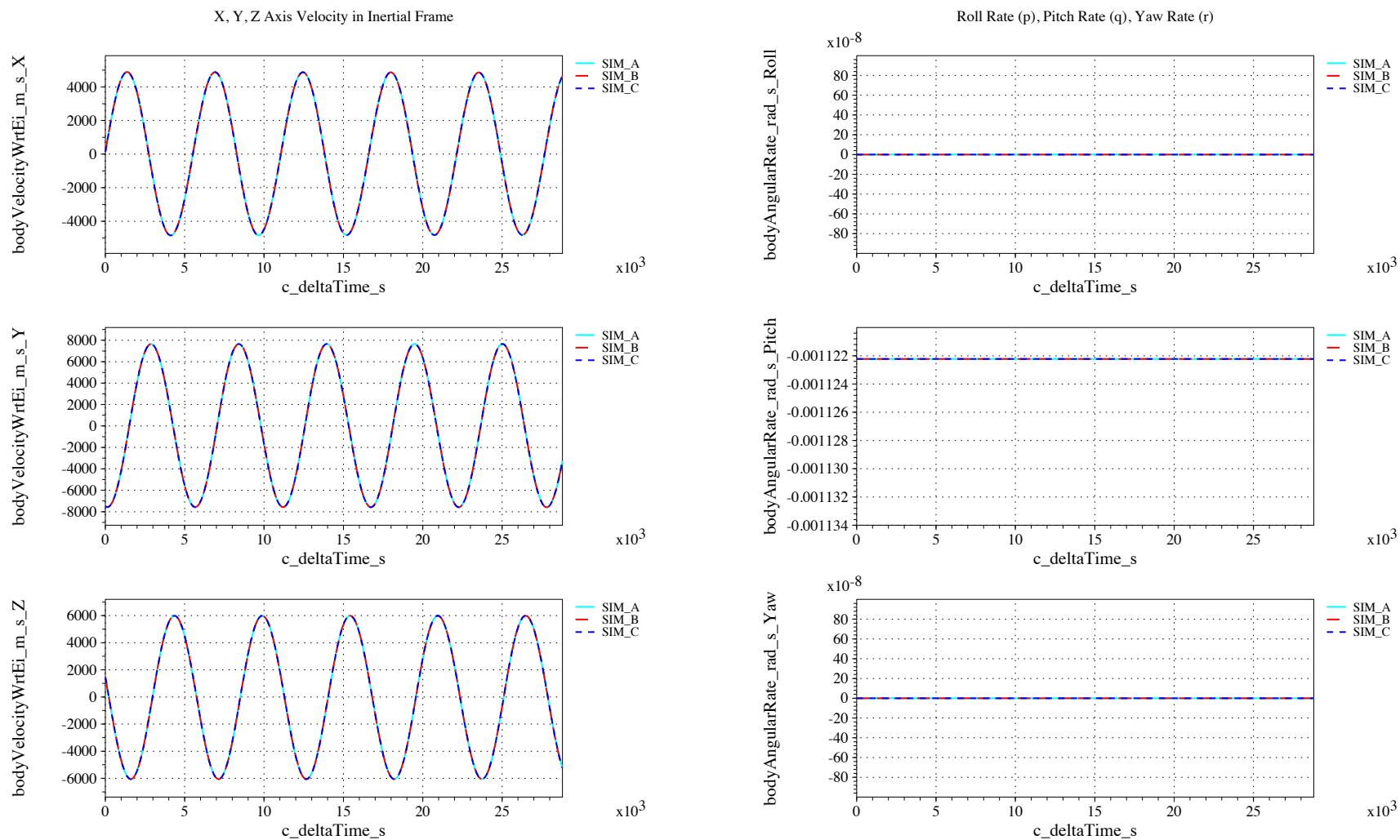American Institute of Aeronautics and Astronautics
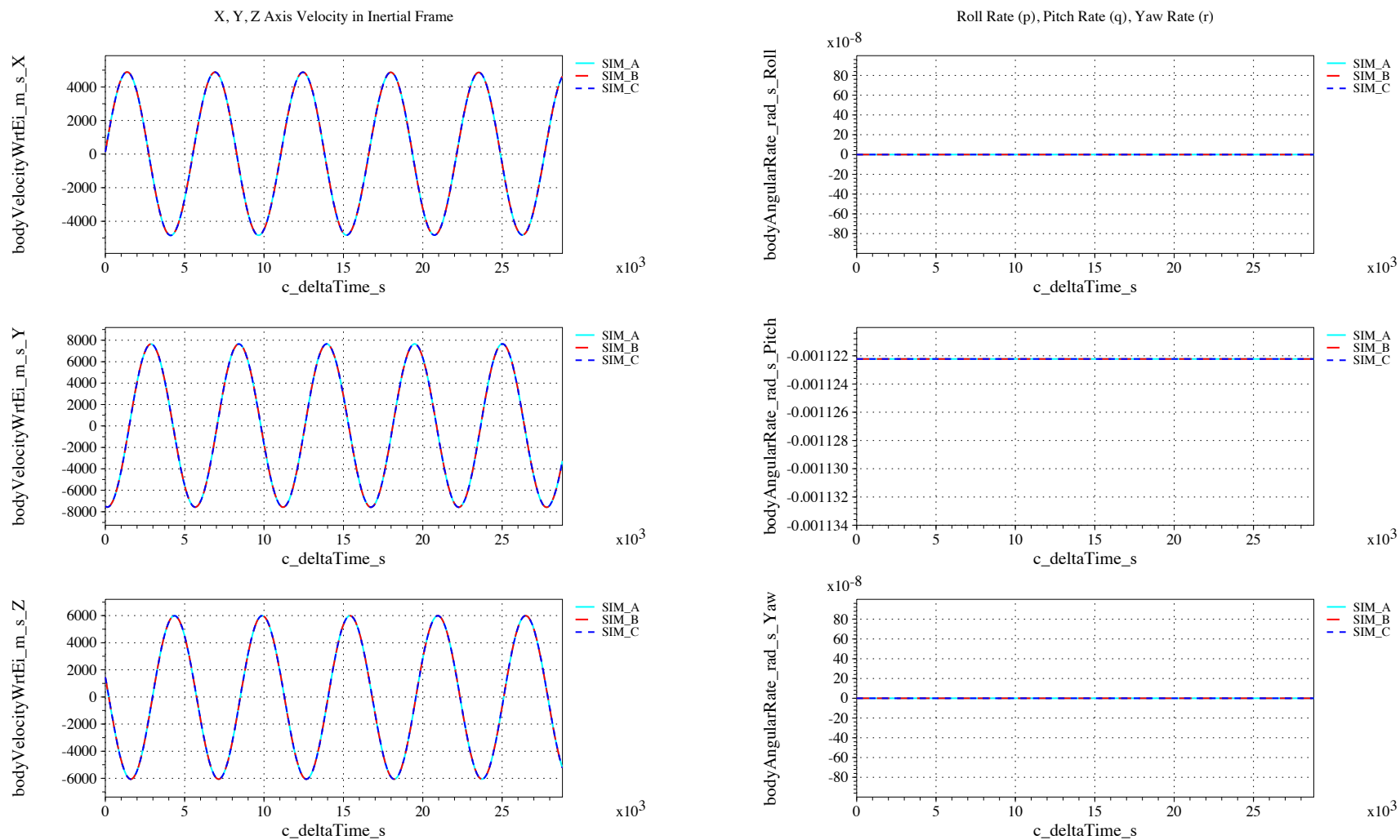
Figure 63. Inertial velocity and body angular rates vs. time (check-case 07C: sphere in 4x4 gravity with drag and third-body perturbations)
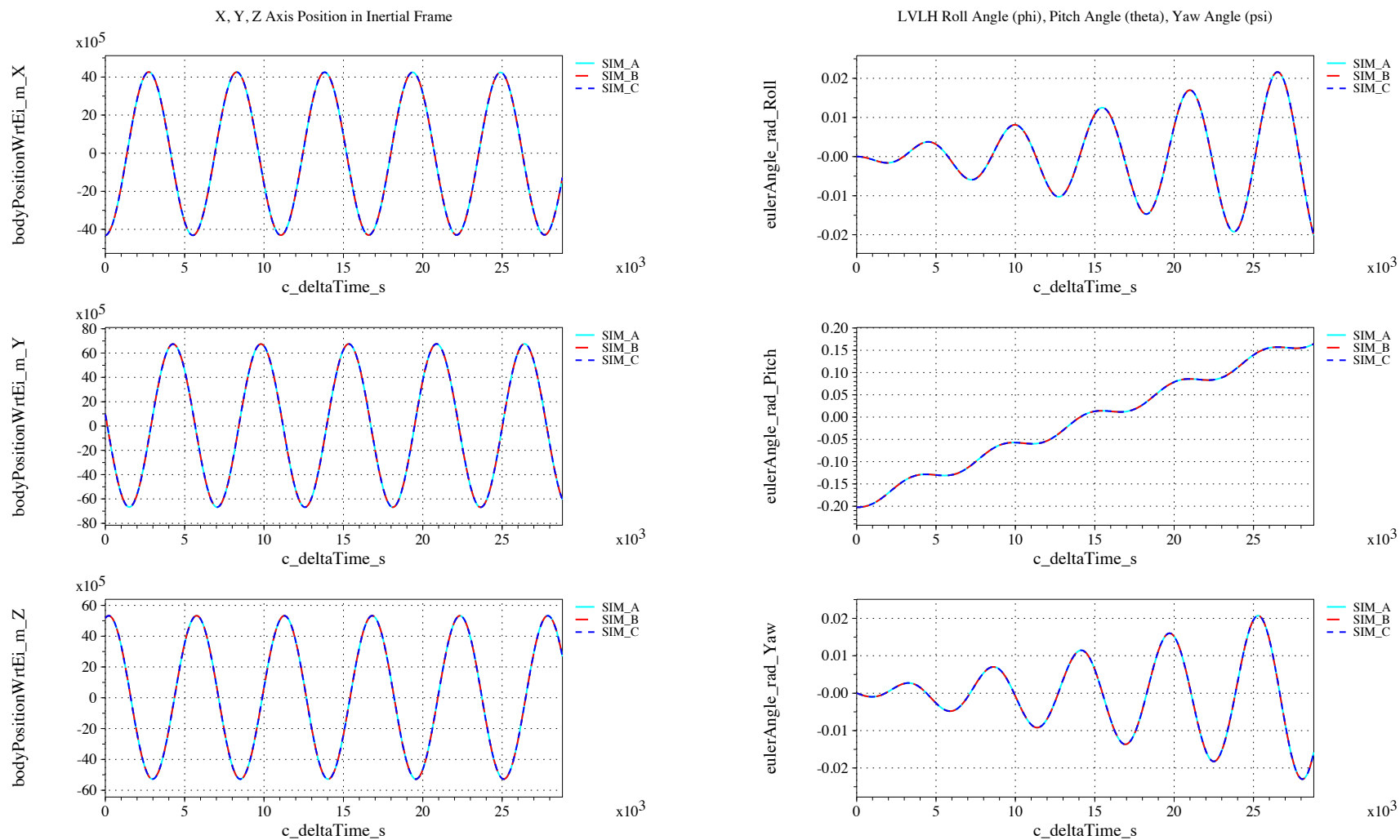
Figure 64. Inertial positions and Euler angles vs. time (check-case 07C: sphere in 4x4 gravity with drag and third-body perturbations)

IX.B.15.   Check-case 7D – sphere in 8x8 gravity with drag and third-body perturbations

This section shows cross-plots for three of the selected simulation tools in modeling the dynamics of a sphere in orbit responding to an 8x8 gravity model, atmospheric drag, planetary ephemeris, and third-body perturbations.

Figures 65 and 67 compare results between NASA simulation tools in inertial acceleration, atmospheric quantities, rates and velocities and positions and attitudes. As in other cases, SIM_A shows slightly higher peaks in atmospheric density than SIM_B and SIM_C. There may be a difference in either MET model implementation or interaction (e.g. input values); this difference is being investigated.

American Institute of Aeronautics and Astronautics

American Institute of Aeronautics and Astronautics

Figure 65. Accelerations and atmospheric quantities vs. time (check-case 07D: sphere in 8x8 gravity with drag and third-body perturbations)

American Institute of Aeronautics and Astronautics

X, Y, Z Axis Velocity in Inertial Frame

Roll Rate (p), Pitch Rate (q), Yaw Rate (r)

Figure 66.   Inertial velocity and body angular rates vs. time (check-case 07D: sphere in 8x8 gravity with drag and third-body perturbations)

American Institute of Aeronautics and Astronautics

Figure 67. Inertial positions and Euler angles vs. time (check-case 07D: sphere in 8x8 gravity with drag and third-body perturbations)

IX.B.16. Check-case 8A – ISS free rotation with zero rates

This section shows cross-plots for three of the selected simulation tools in modeling the dynamics of the ISS in torque-free rotation starting with zero inertial rate.

Figures 68 and 70 compare results between NASA simulation tools in inertial acceleration, atmospheric quantities, rates and velocities and positions and attitudes.

In this scenario, the vehicle is initialized to maintain inertial orientation. The Euler angles, however, are presented are relative to the orbit (LVLH frame). Relative to the orbit, the vehicle is seen has having a constant rotation about the LVLH y-axis (which is perpendicular to the plane of the orbit). Thus, the LVLH pitch angle undergoes linear change from $-\pi$ to $+\pi$ and back with the period of the orbit. Also, the x-body axis alternates between being on the positive side of the LVLH x-axis to the negative. When the x-body axis lies on the positive side of the LVLH x-axis, LVLH roll and yaw angles are zero. However, when the x-body axis lies on the negative side of the LVLH x-axis, the LVLH roll and yaw angles can have a value of $+\pi$ or $-\pi$. Which value actually gets computed is highly sensitive to the implementation of the Euler angle computation, round-off error, and residual differences between simulations. As seen in figure 70, the simulations do not agree on which side of $\pm\pi$ they lie and the simulations themselves swap between +pi and -pi at different times during each period. Though they appear large, these differences are superficial as they represent equivalent orientations.

As in other cases, SIM_A shows slightly higher peaks in atmospheric density than SIM_B and SIM_C. There may be a difference in either MET model implementation or interaction (e.g. input values); this difference is being investigated.
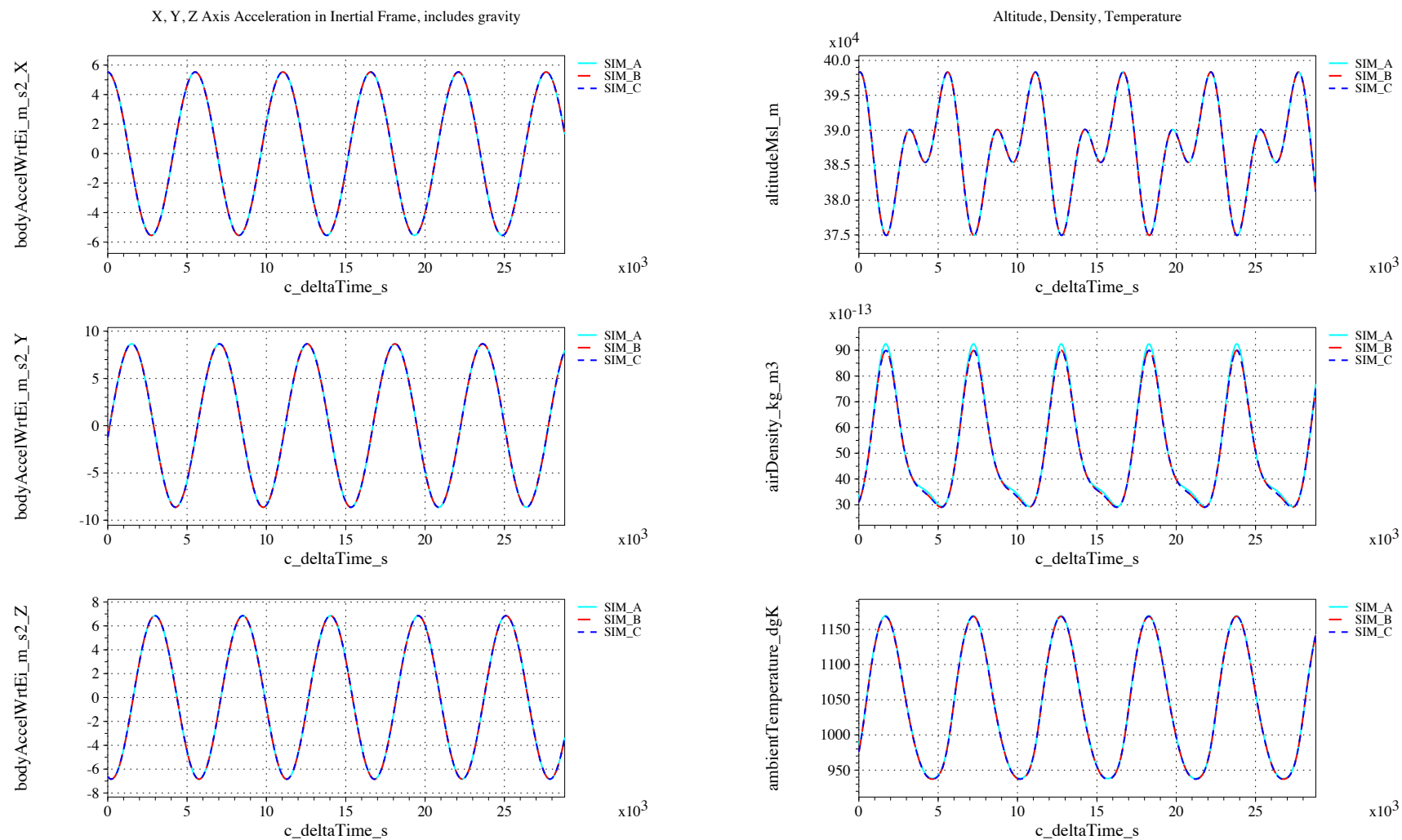
American Institute of Aeronautics and Astronautics

American Institute of Aeronautics and Astronautics

Figure 68. Accelerations and atmospheric quantities vs. time (check-case 08A: ISS free rotation with zero rates)

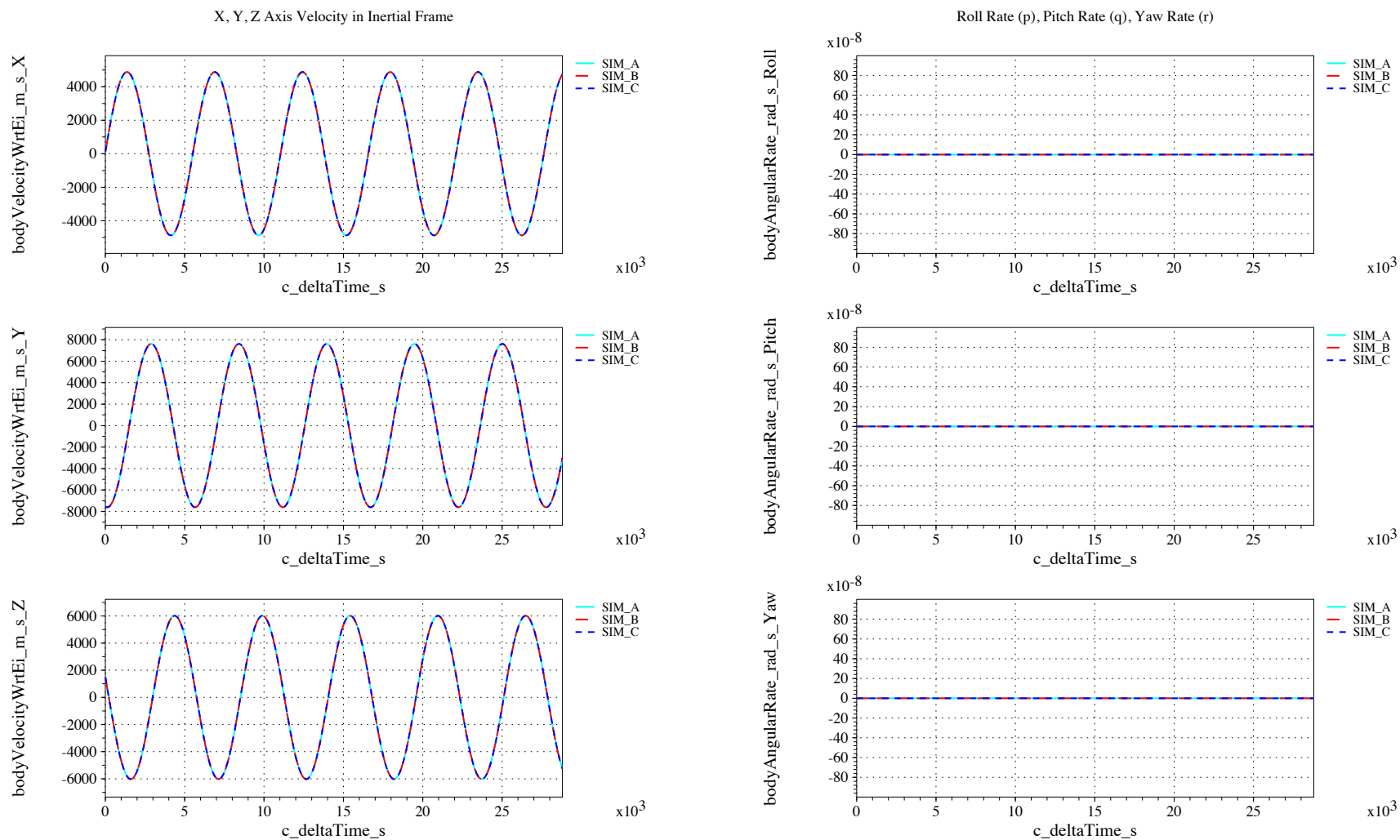American Institute of Aeronautics and Astronautics

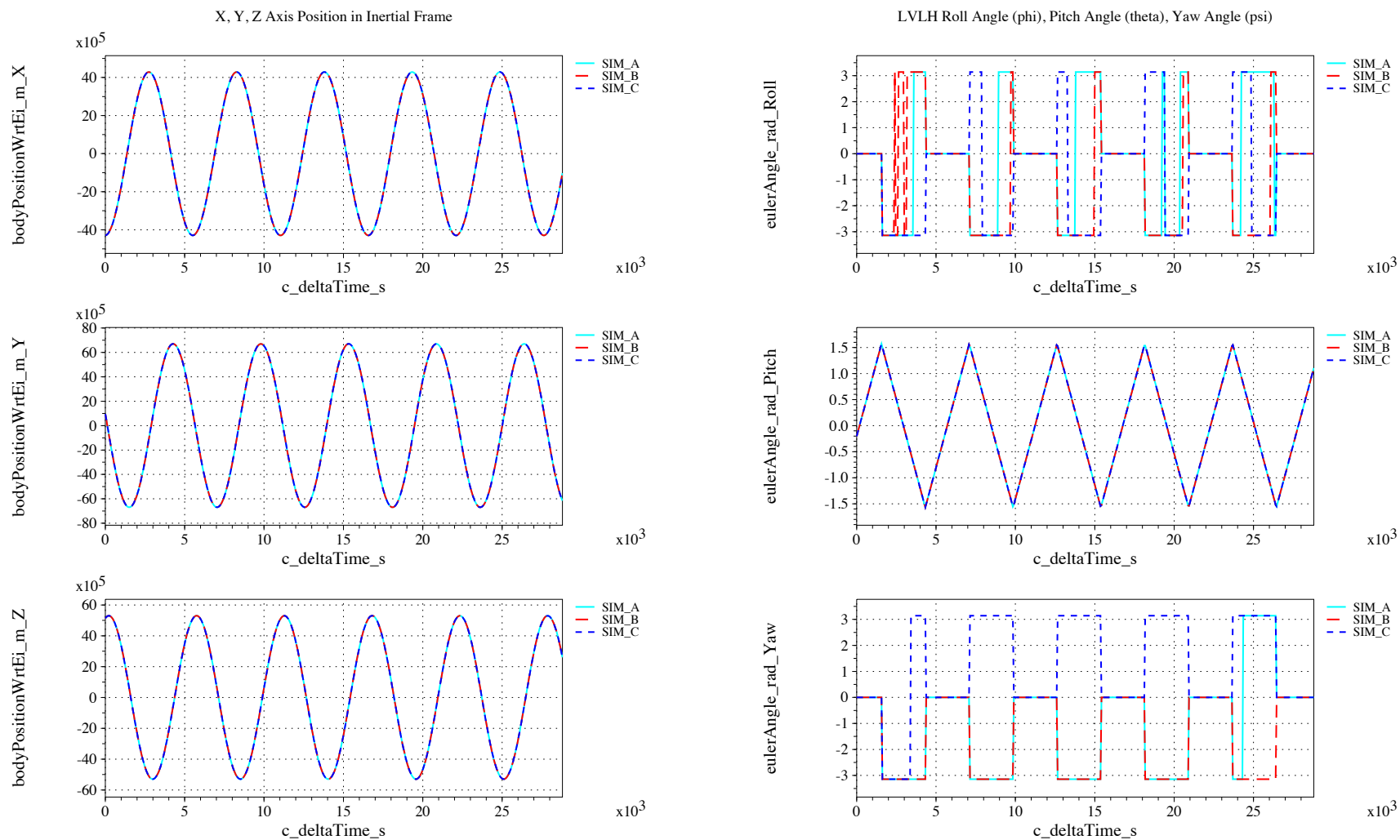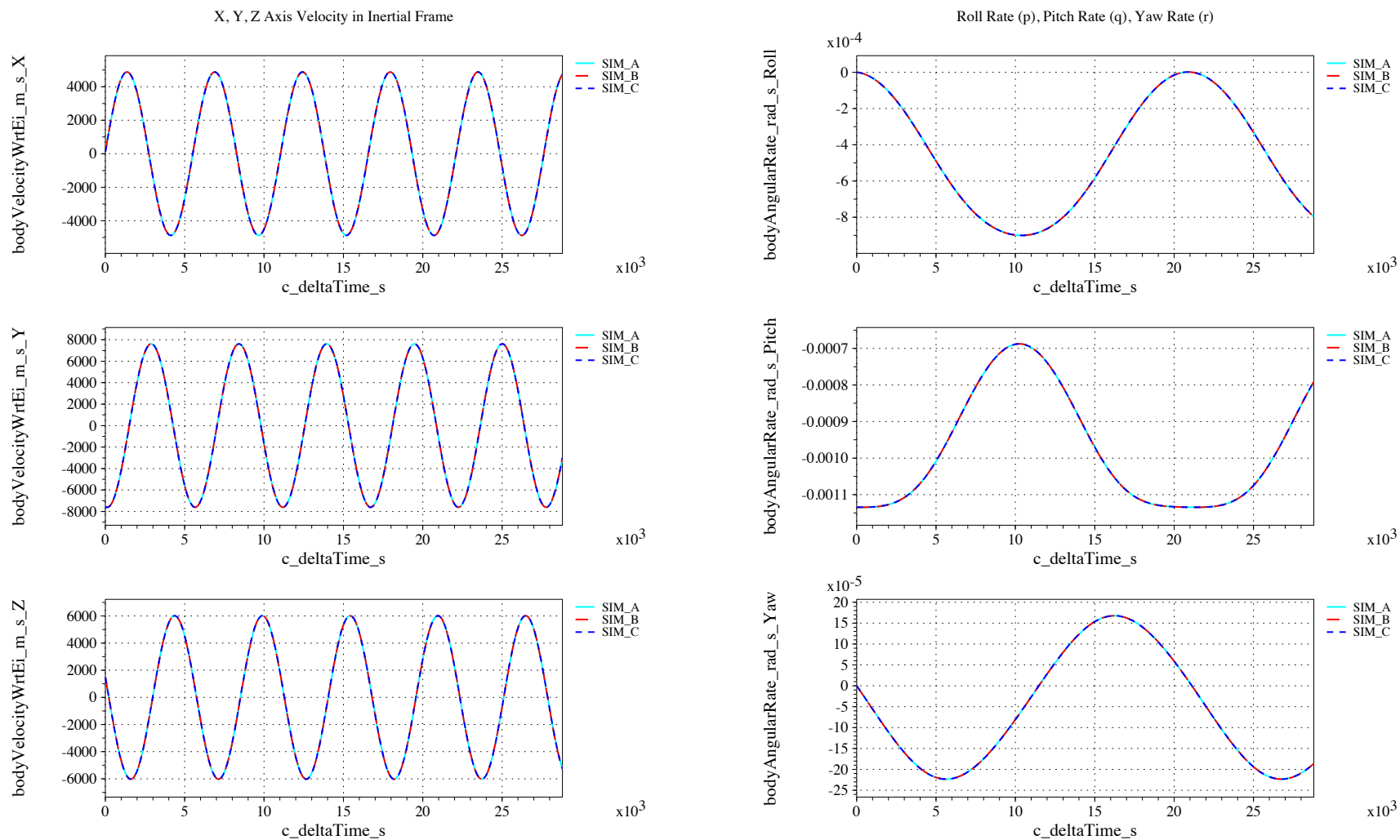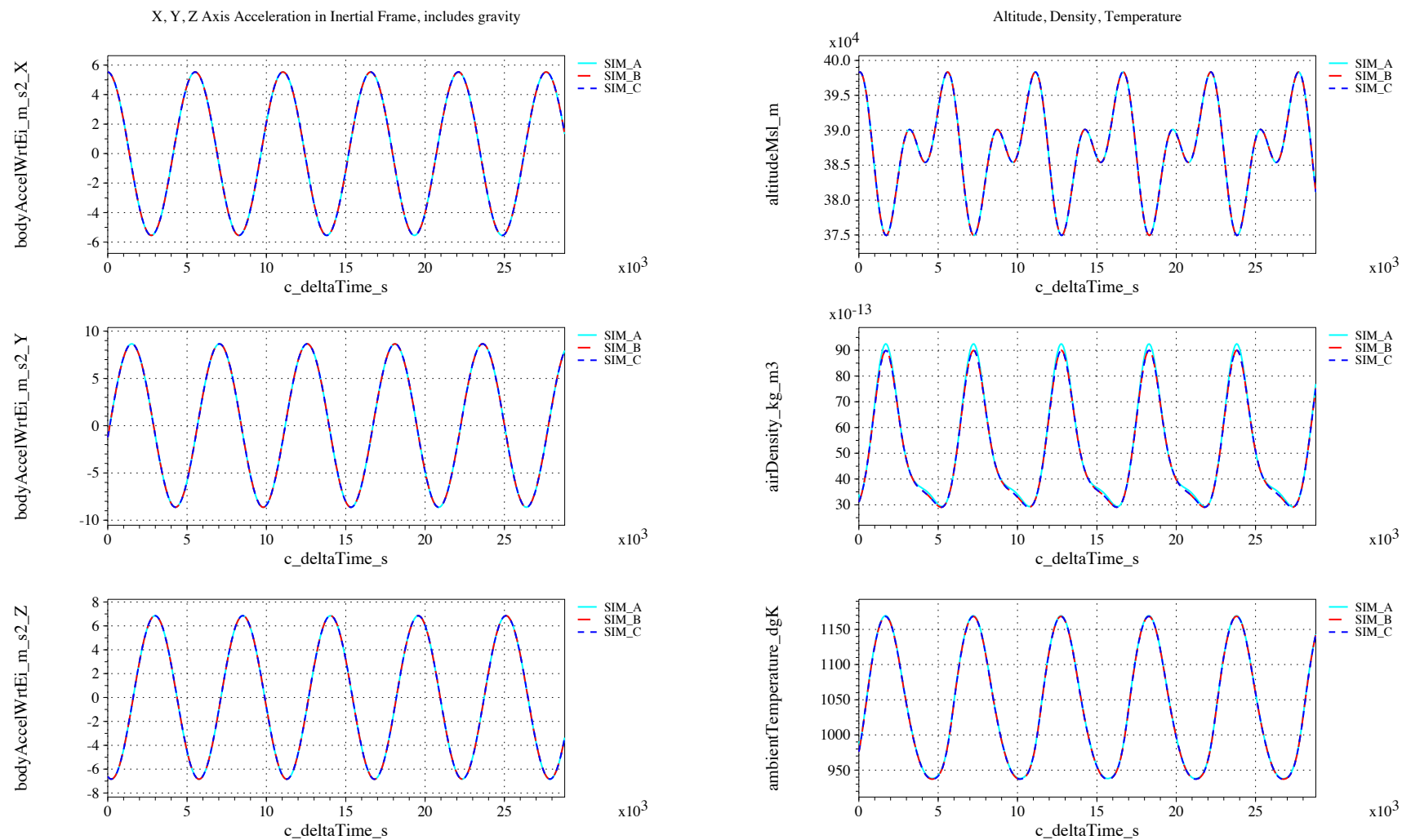**Figure 69. Inertial velocity and body angular rates vs. time (check-case 08A: ISS free rotation with zero rates)**

Figure 70. Inertial positions and Euler angles vs. time (check-case 08A: ISS free rotation with zero rates)

IX.B.17. Check-case 8B – ISS free rotation with non-zero rates

This section shows cross-plots for three of the selected simulation tools in modeling the dynamics of the ISS in torque-free rotation starting with a non-zero inertial rate.

Figures 71 and 73 compare results between NASA simulation tools in inertial acceleration, atmospheric quantities, rates and velocities and positions and attitudes.

As in other cases, SIM_A shows slightly higher peaks in atmospheric density than SIM_B and SIM_C. There may be a difference in either MET model implementation or interaction (e.g. input values); this difference is being investigated.

American Institute of Aeronautics and Astronautics

Figure 71. Accelerations and atmospheric quantities vs. time (check-case 08B: ISS free rotation with non-zero rates)

Figure 72. Inertial velocity and body angular rates vs. time (check-case 08B: ISS free rotation with non-zero rates)
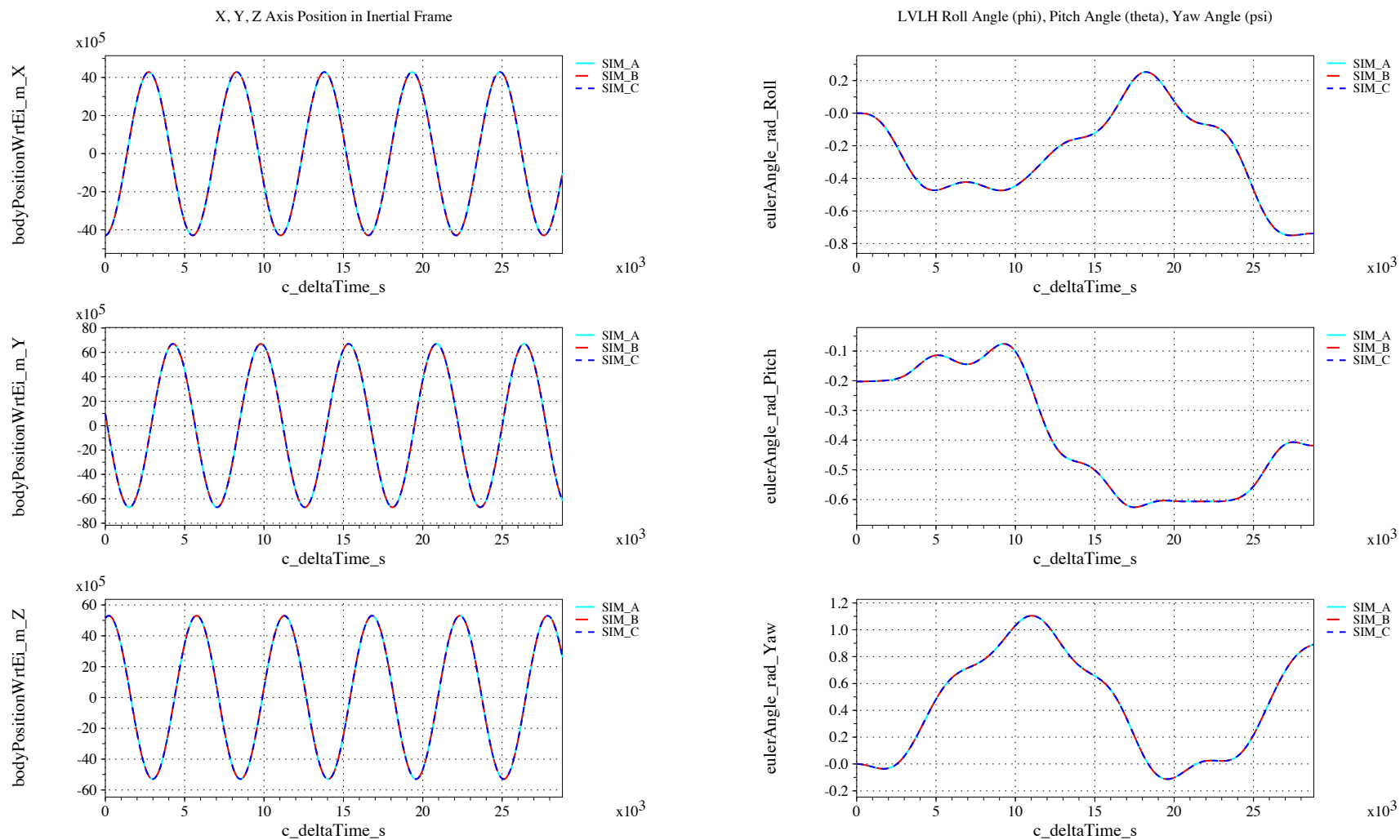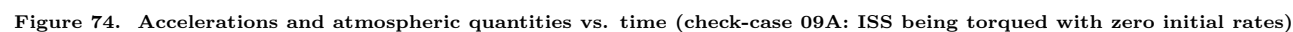
X, Y, Z Axis Position in Inertial Frame

LVLH Roll Angle (phi), Pitch Angle (theta), Yaw Angle (psi)

Figure 73. Inertial positions and Euler angles vs. time (check-case 08B: ISS free rotation with non-zero rates)

IX.B.18.   Check-case 9A – ISS being torqued with zero initial rates

This section shows cross-plots for three of the selected simulation tools in modeling the dynamics of the ISS in responding to an external torque starting with zero inertial rate.

Figures 74 and 76 compare results between NASA simulation tools in inertial acceleration, atmospheric quantities, rates and velocities and positions and attitudes.

As in other cases, SIM_A shows slightly higher peaks in atmospheric density than SIM_B and SIM_C. There may be a difference in either MET model implementation or interaction (e.g. input values); this difference is being investigated.

American Institute of Aeronautics and Astronautics

American Institute of Aeronautics and Astronautics

Figure 74. Accelerations and atmospheric quantities vs. time (check-case 09A: ISS being torqued with zero initial rates)

American Institute of Aeronautics and Astronautics
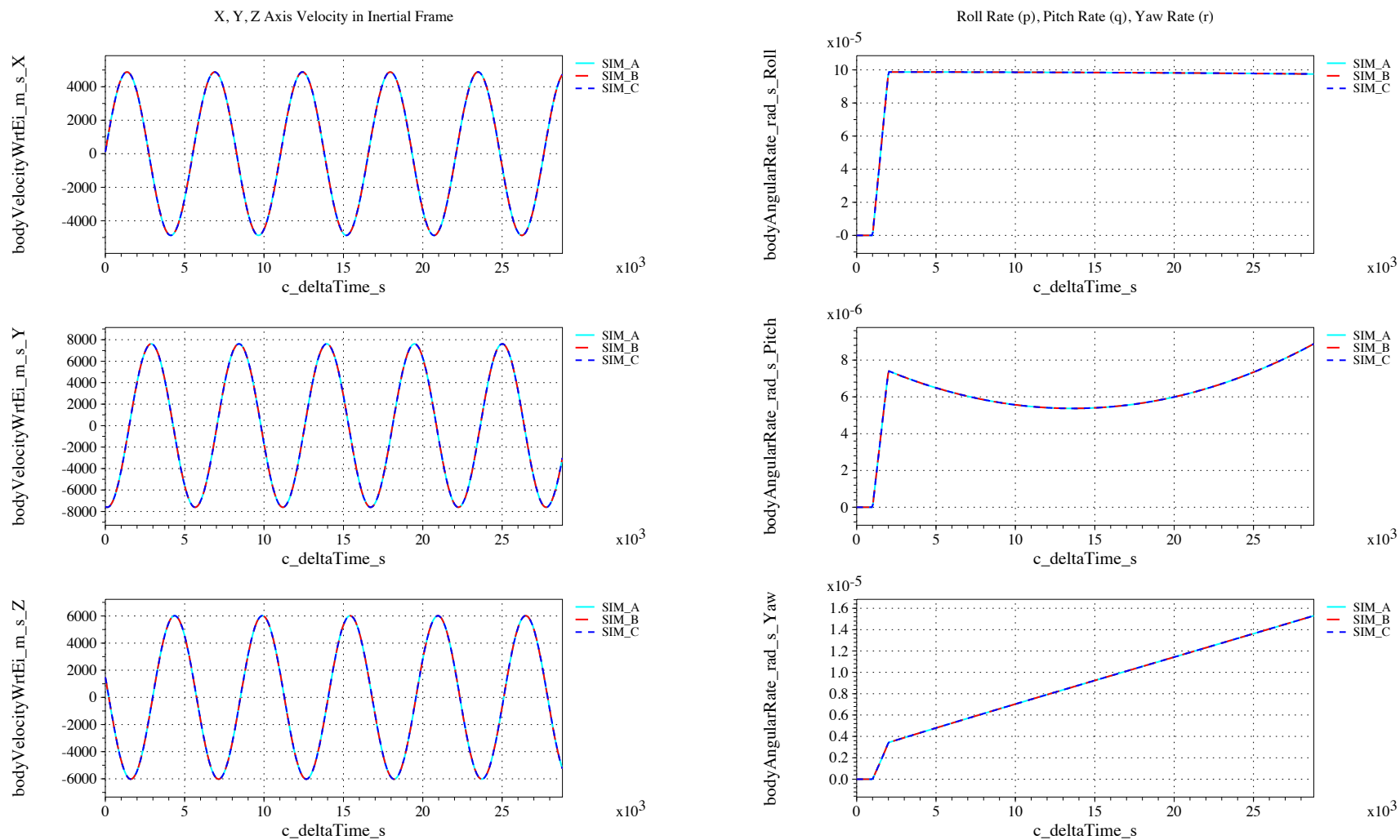
Figure 75. Inertial velocity and body angular rates vs. time (check-case 09A: ISS being torqued with zero initial rates)
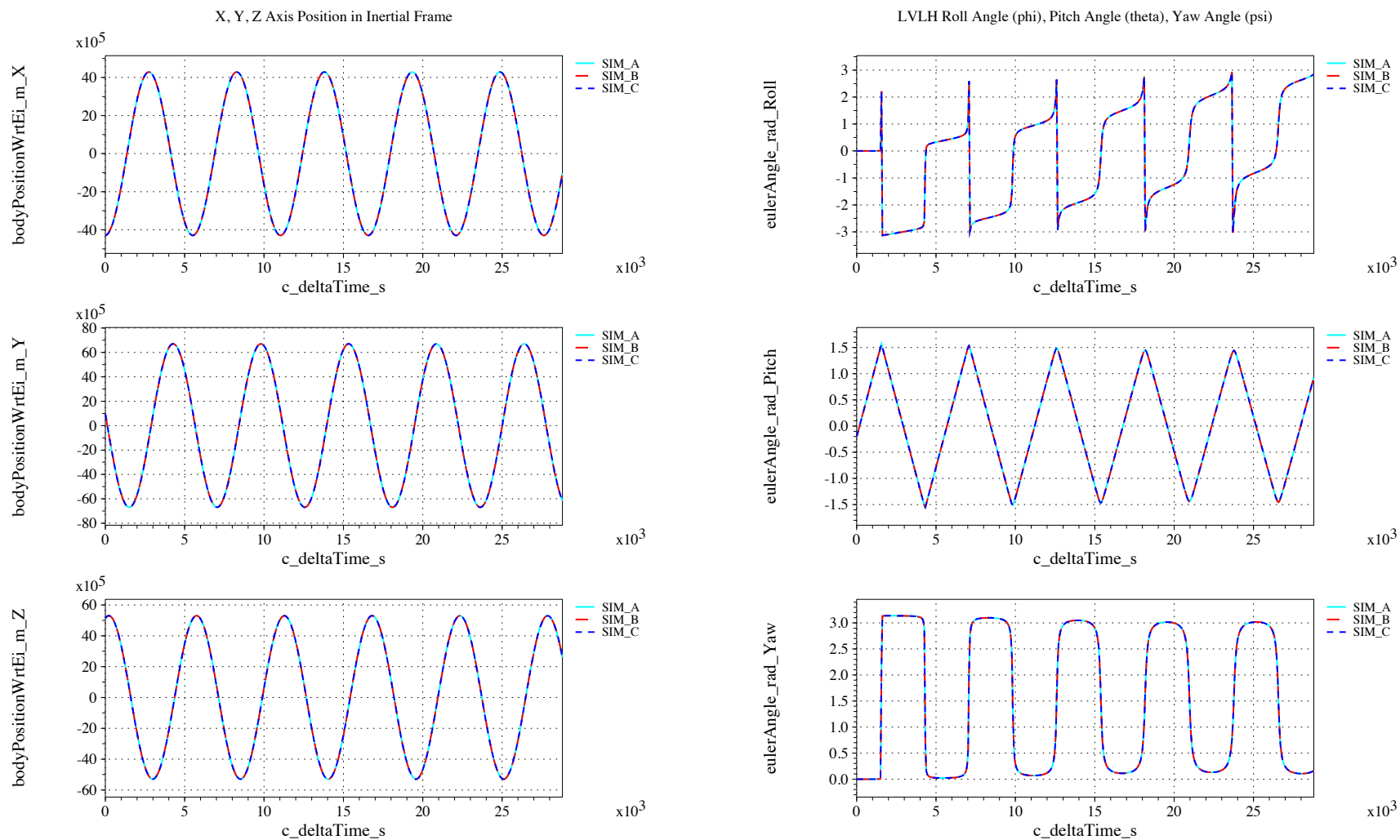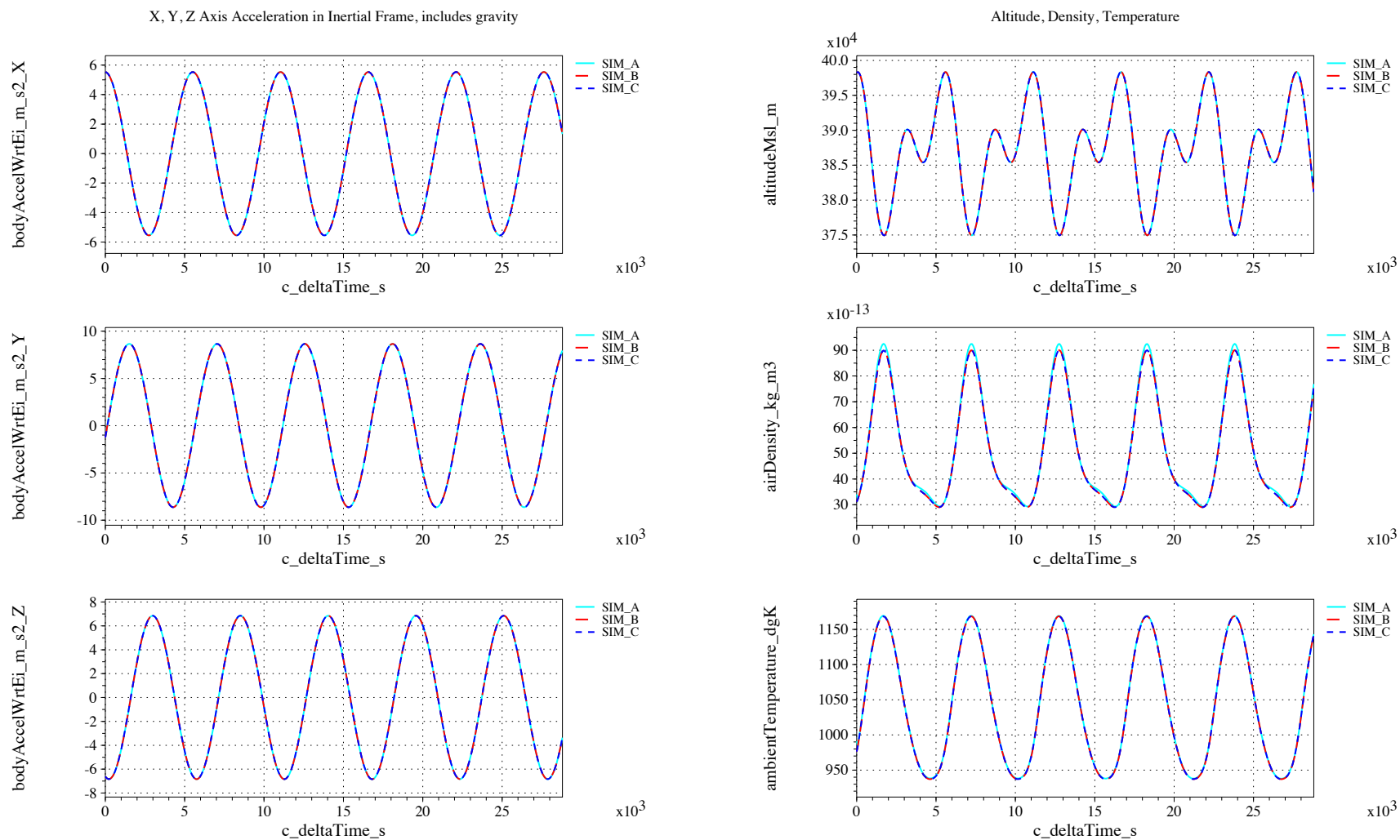
American Institute of Aeronautics and Astronautics

Figure 76. Inertial positions and Euler angles vs. time (check-case 09A: ISS being torqued with zero initial rates)

IX.B.19.   Check-case 9B – ISS being torqued with non-zero initial rates

This section shows cross-plots for three of the selected simulation tools in modeling the dynamics of the ISS in responding to an external torque starting with a non-zero inertial rate.

Figures 77 and 79 compare results between NASA simulation tools in inertial acceleration, atmospheric quantities, rates and velocities and positions and attitudes.

As in other cases, SIM_A shows slightly higher peaks in atmospheric density than SIM_B and SIM_C. There may be a difference in either MET model implementation or interaction (e.g. input values); this difference is being investigated.

American Institute of Aeronautics and Astronautics

X, Y, Z Axis Acceleration in Inertial Frame, includes gravity

Altitude, Density, Temperature

Figure 77. Accelerations and atmospheric quantities vs. time (check-case 09B: ISS being torqued with non-zero initial rates)

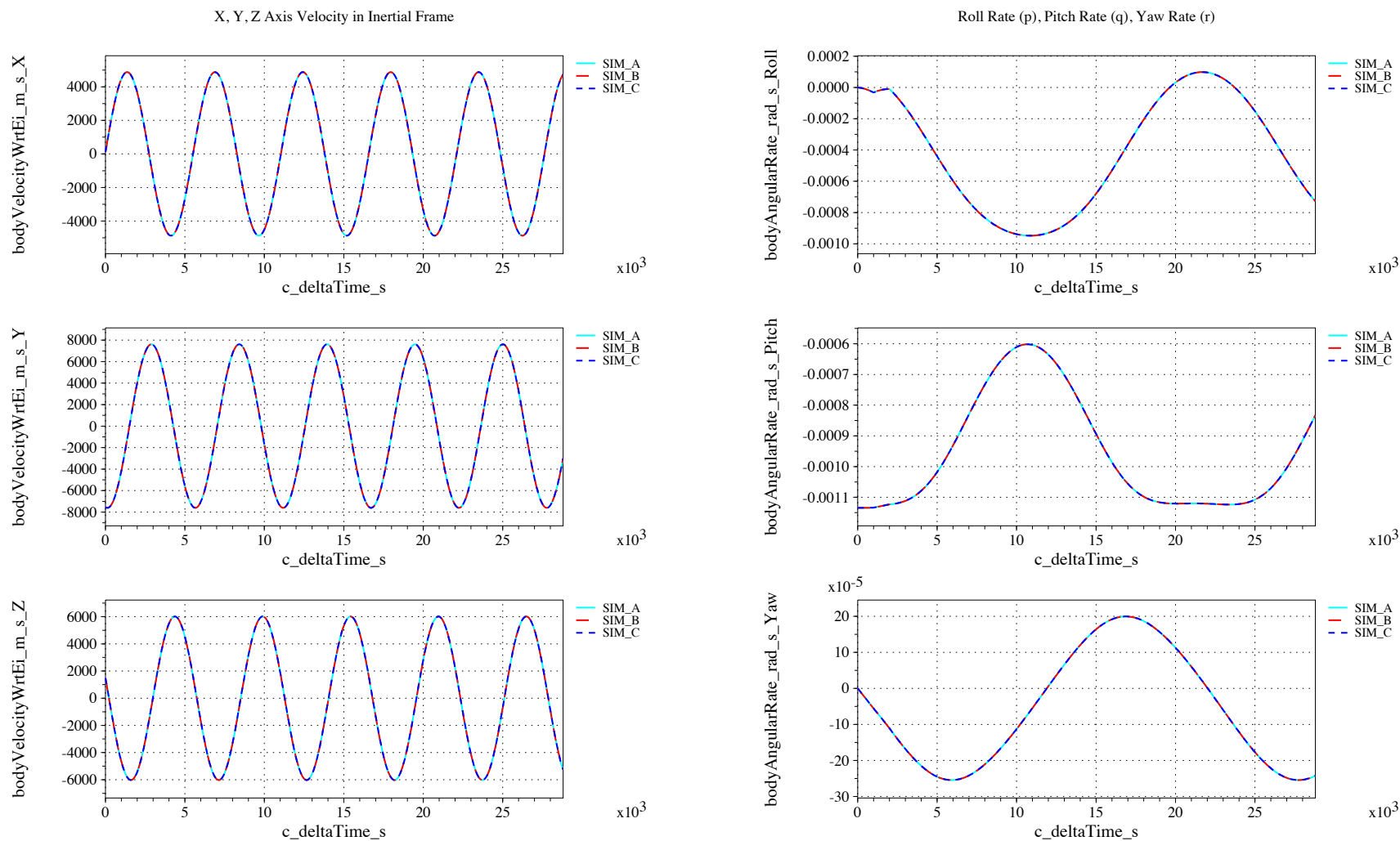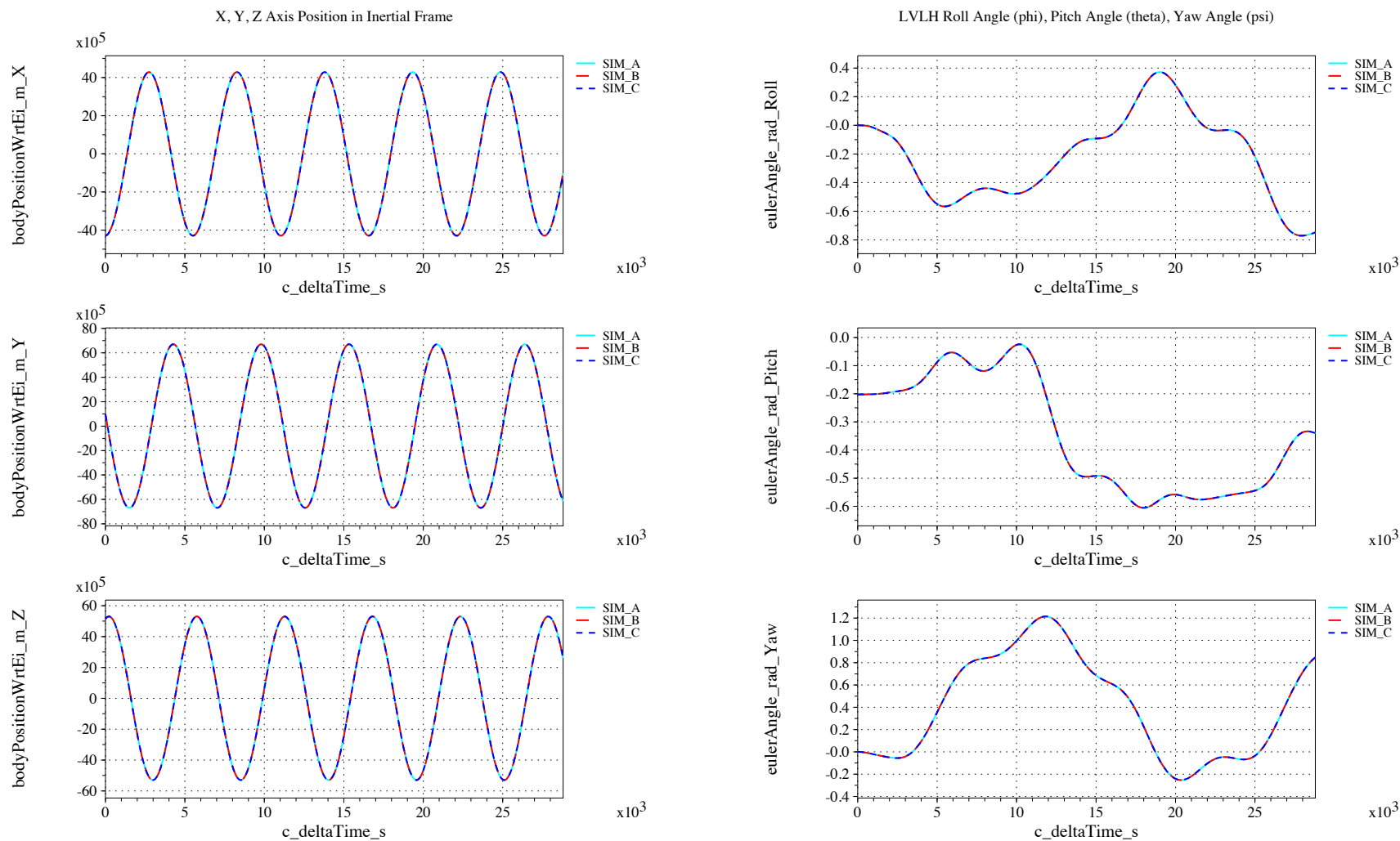American Institute of Aeronautics and Astronautics

Figure 78. Inertial velocity and body angular rates vs. time (check-case 09B: ISS being torqued with non-zero initial rates)

American Institute of Aeronautics and Astronautics

Figure 79. Inertial positions and Euler angles vs. time (check-case 09B: ISS being torqued with non-zero initial rates)

IX.B.20. Check-case 9C – ISS under torque and force with zero initial rates

This section shows cross-plots for three of the selected simulation tools in modeling the dynamics of the ISS in responding to external torque and force starting with zero inertial rate.

Figures 80 and 82 compare results between NASA simulation tools in inertial acceleration, atmospheric quantities, rates and velocities and positions and attitudes.

As in other cases, SIM_A shows slightly higher peaks in atmospheric density than SIM_B and SIM_C. There may be a difference in either MET model implementation or interaction (e.g. input values); this difference is being investigated.
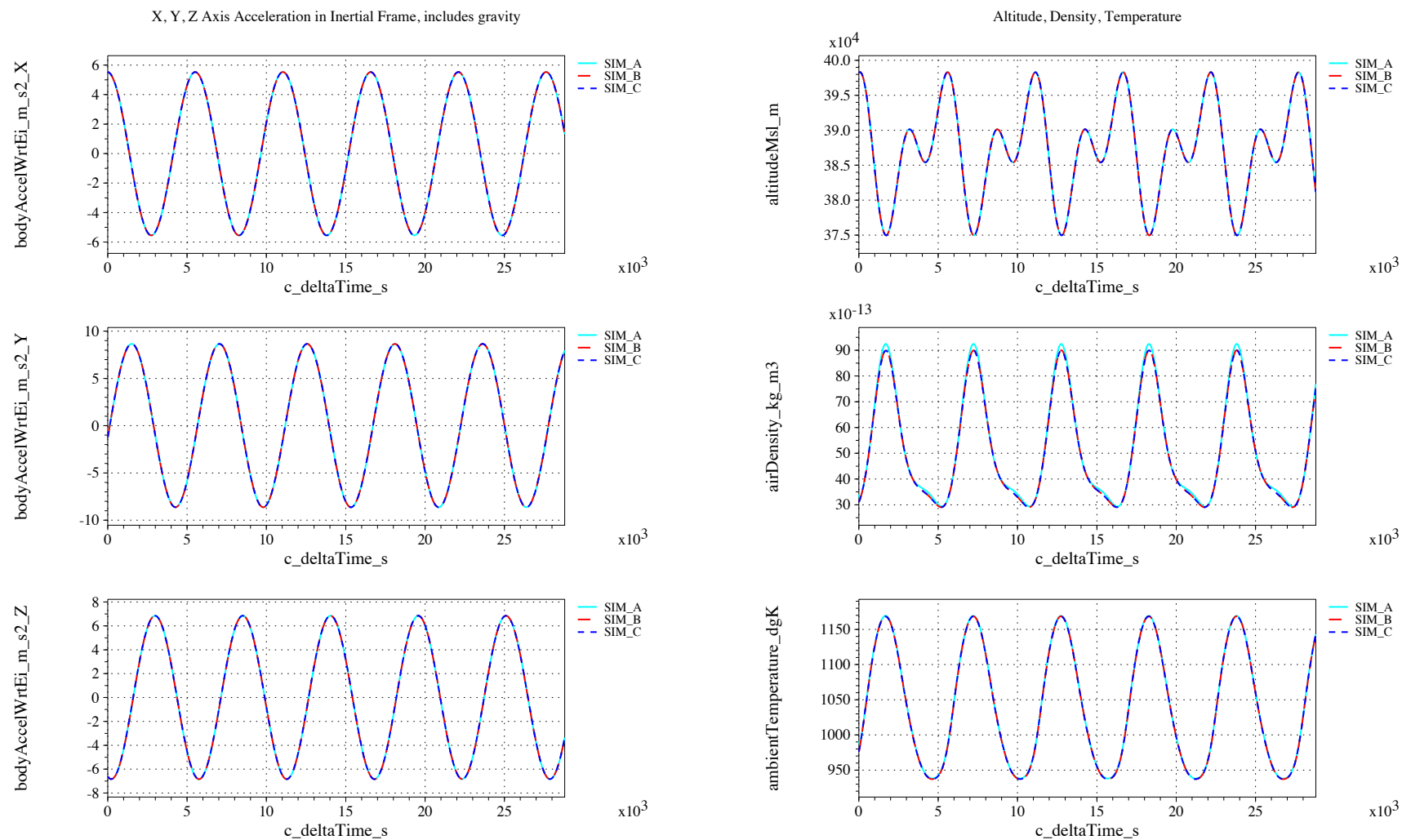
American Institute of Aeronautics and Astronautics

American Institute of Aeronautics and Astronautics

X, Y, Z Axis Acceleration in Inertial Frame, includes gravity

Altitude, Density, Temperature

Figure 80. Accelerations and atmospheric quantities vs. time (check-case 09C: ISS under torque and force with zero initial rates)
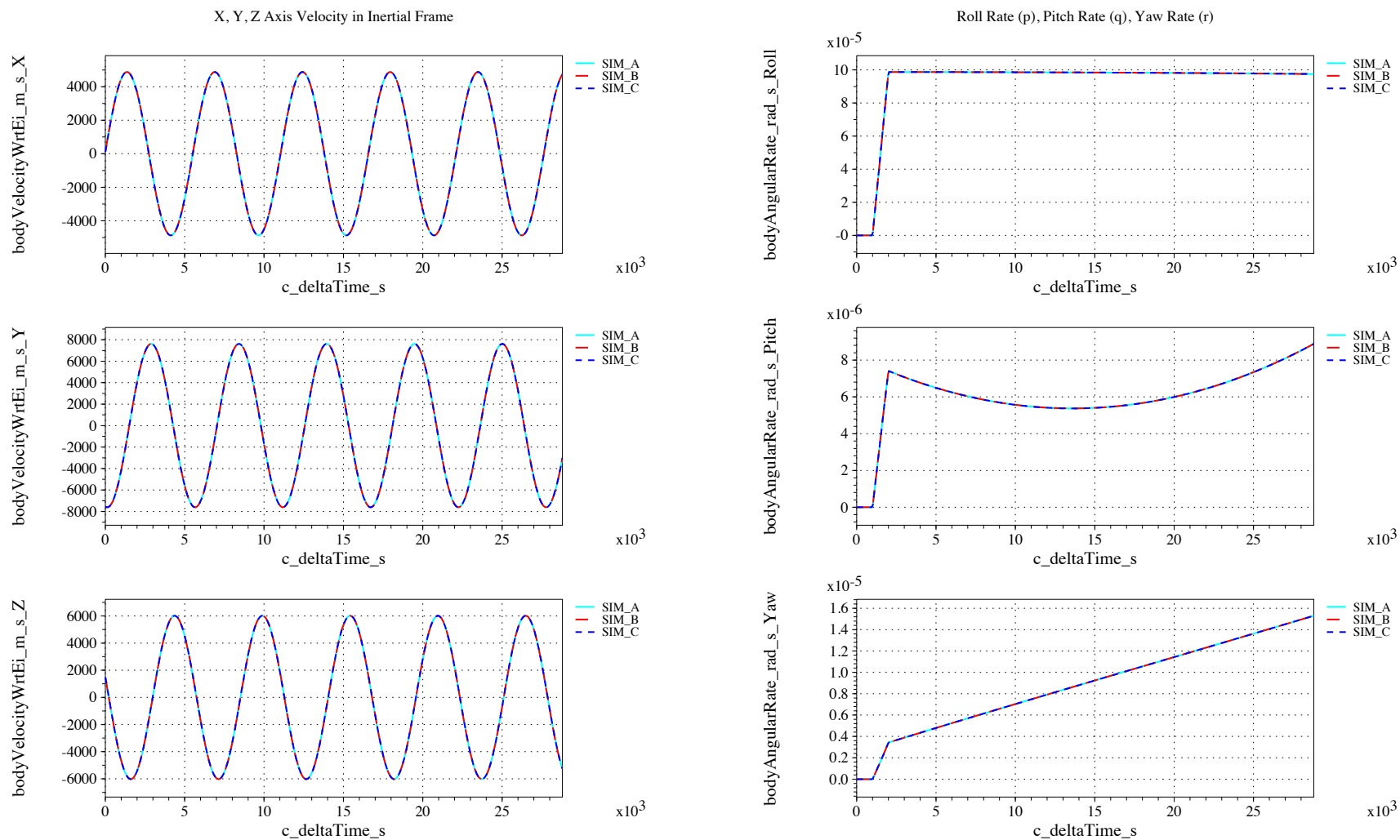
American Institute of Aeronautics and Astronautics

Figure 81. Inertial velocity and body angular rates vs. time (check-case 09C: ISS under torque and force with zero initial rates)
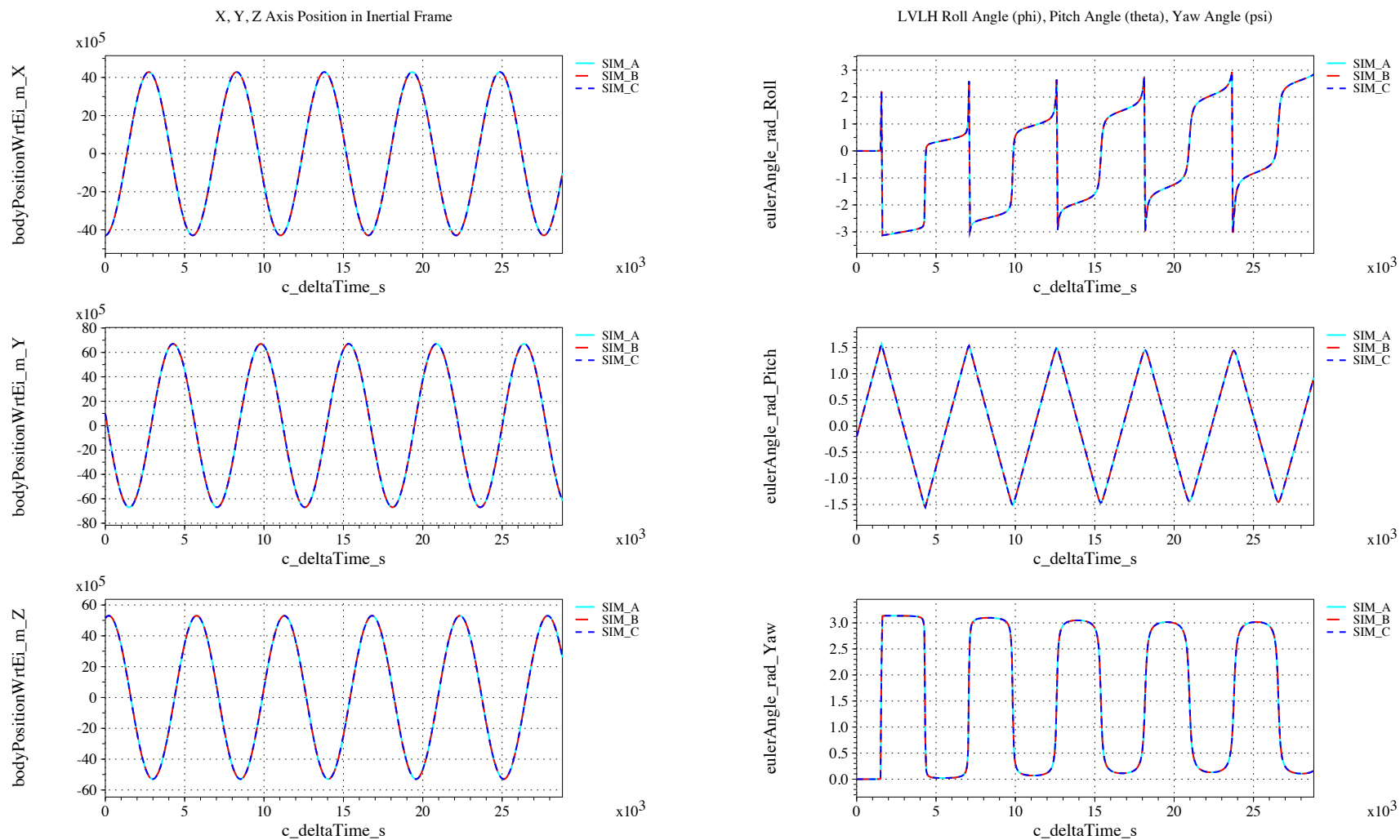
American Institute of Aeronautics and Astronautics

Figure 82. Inertial positions and Euler angles vs. time (check-case 09C: ISS under torque and force with zero initial rates)

IX.B.21.   Check-case 9D – ISS under torque and force with non-zero initial rates

This section shows cross-plots for three of the selected simulation tools in modeling the dynamics of the ISS in responding to external torque and force starting with a non-zero inertial rate.

Figures 83 and 85 compare results between NASA simulation tools in inertial acceleration, atmospheric quantities, rates and velocities and positions and attitudes.

As in other cases, SIM_A shows slightly higher peaks in atmospheric density than SIM_B and SIM_C. There may be a difference in either MET model implementation or interaction (e.g. input values); this difference is being investigated.
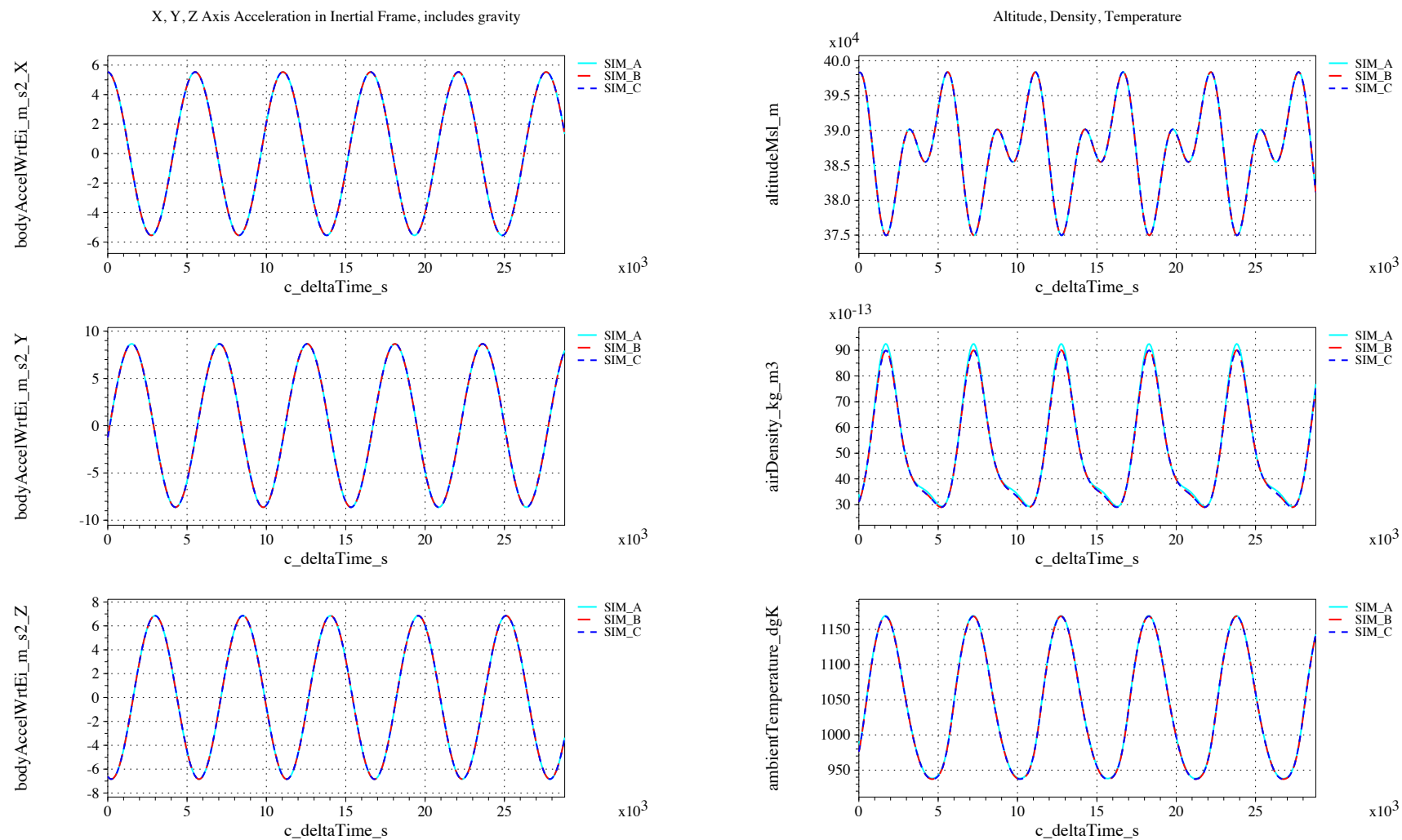
American Institute of Aeronautics and Astronautics

American Institute of Aeronautics and Astronautics

X, Y, Z Axis Acceleration in Inertial Frame, includes gravity

Altitude, Density, Temperature

Figure 83. Accelerations and atmospheric quantities vs. time (check-case 09D: ISS under torque and force with non-zero initial rates)
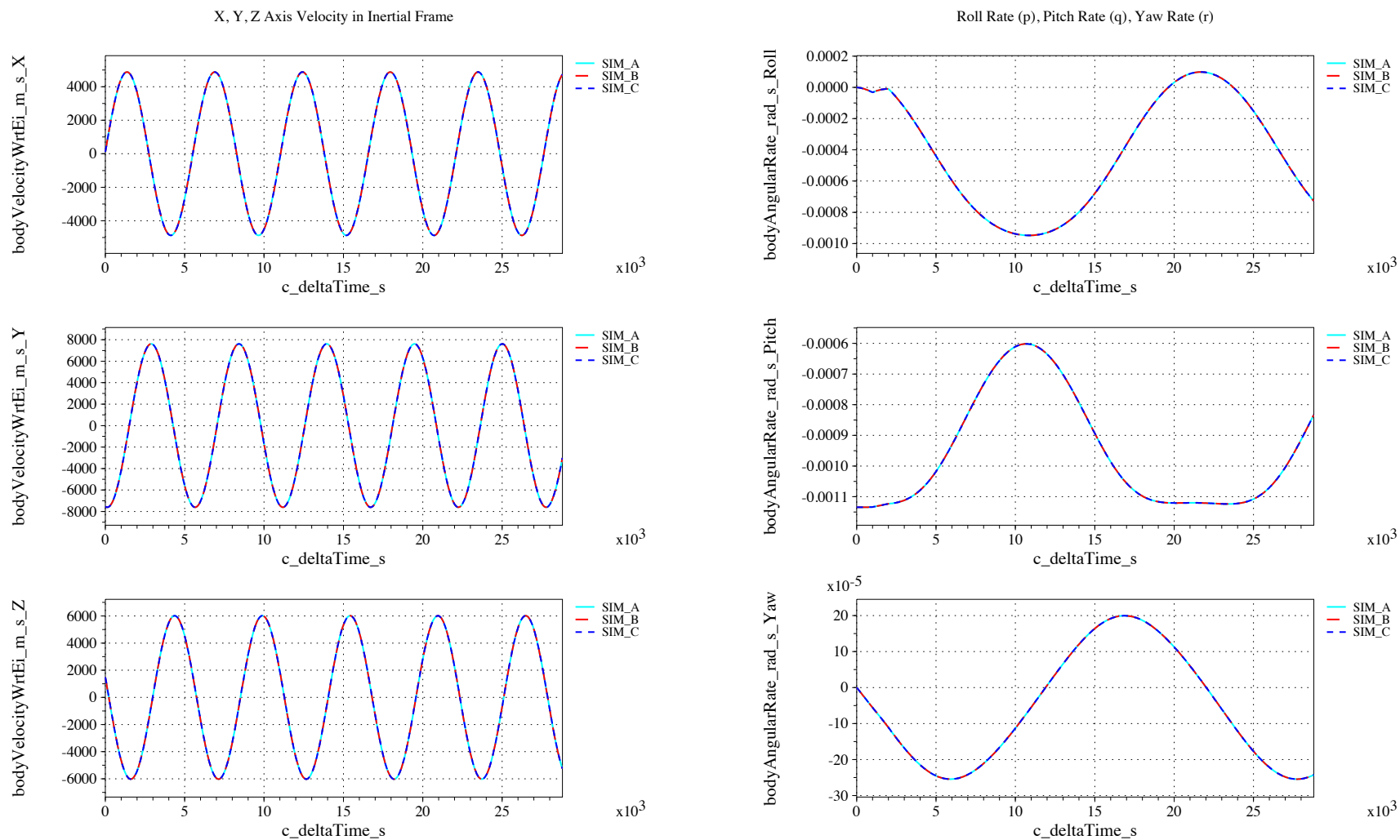
American Institute of Aeronautics and Astronautics

X, Y, Z Axis Velocity in Inertial Frame

Roll Rate (p), Pitch Rate (q), Yaw Rate (r)

Figure 84. Inertial velocity and body angular rates vs. time (check-case 09D: ISS under torque and force with non-zero initial rates)
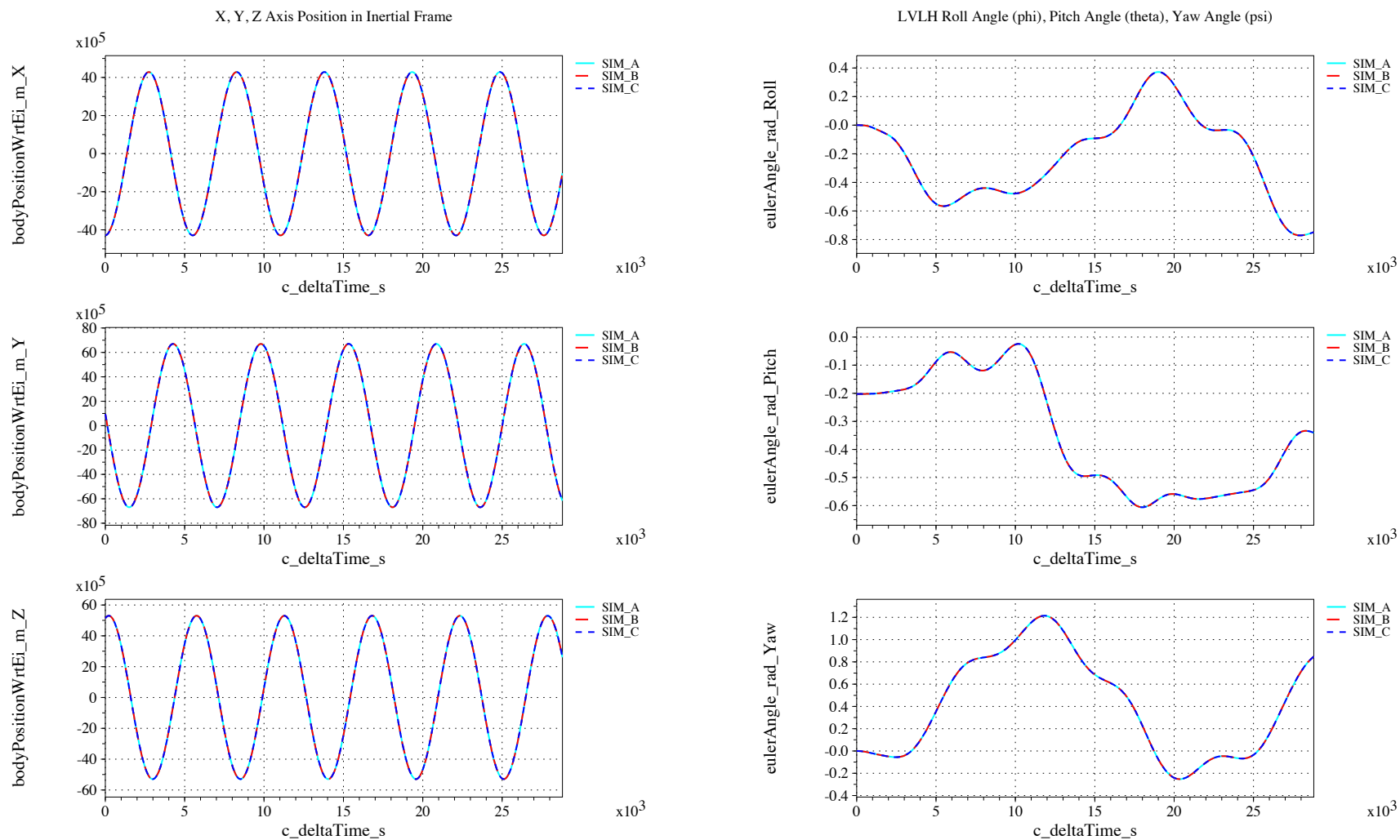
American Institute of Aeronautics and Astronautics

Figure 85. Inertial positions and Euler angles vs. time (check-case 09D: ISS under torque and force with non-zero initial rates)

IX.B.22.   Check-case 10A – cylinder in circular orbit with gravity gradient with zero initial rates

This section shows cross-plots for three of the selected simulation tools in modeling the dynamics of a cylinder in low-Earth orbit responding to the gravity gradient starting with zero inertial rate.

Figures 86 and 88 compare results between NASA simulation tools in inertial acceleration, atmospheric quantities, rates and velocities and positions and attitudes.

Differences in orientation variables for this check case are somewhat curious since matches were achieved on prior check cases.

Matching inertial rotational rates demonstrate that the simulations agree on gravity gradient affects. However, the SIM_C LVLH Euler angles do not match SIM_A and SIM_B in both initial condition and behavior. This is curious since the rotational initial conditions are the same as check-cases 9B and 9D, in which the simulations agree. The inertial orientations (not shown) and the orbits match. Therefore, the probable cause is a mismatch in Euler angle convention; configuring SIM_C for the 3-2-1 rotation sequence convention may have been overlooked.

Difference SIM_A roll rate is exaggerated by scale. It differs by $\approx 1 \times 10^{-9}$ rad/s.

As in other cases, SIM_A shows slightly higher peaks in atmospheric density than SIM_B and SIM_C. There may be a difference in either MET model implementation or interaction (e.g. input values).

All of these differences are under investigation.

American Institute of Aeronautics and Astronautics

American Institute of Aeronautics and Astronautics

X, Y, Z Axis Acceleration in Inertial Frame, includes gravity

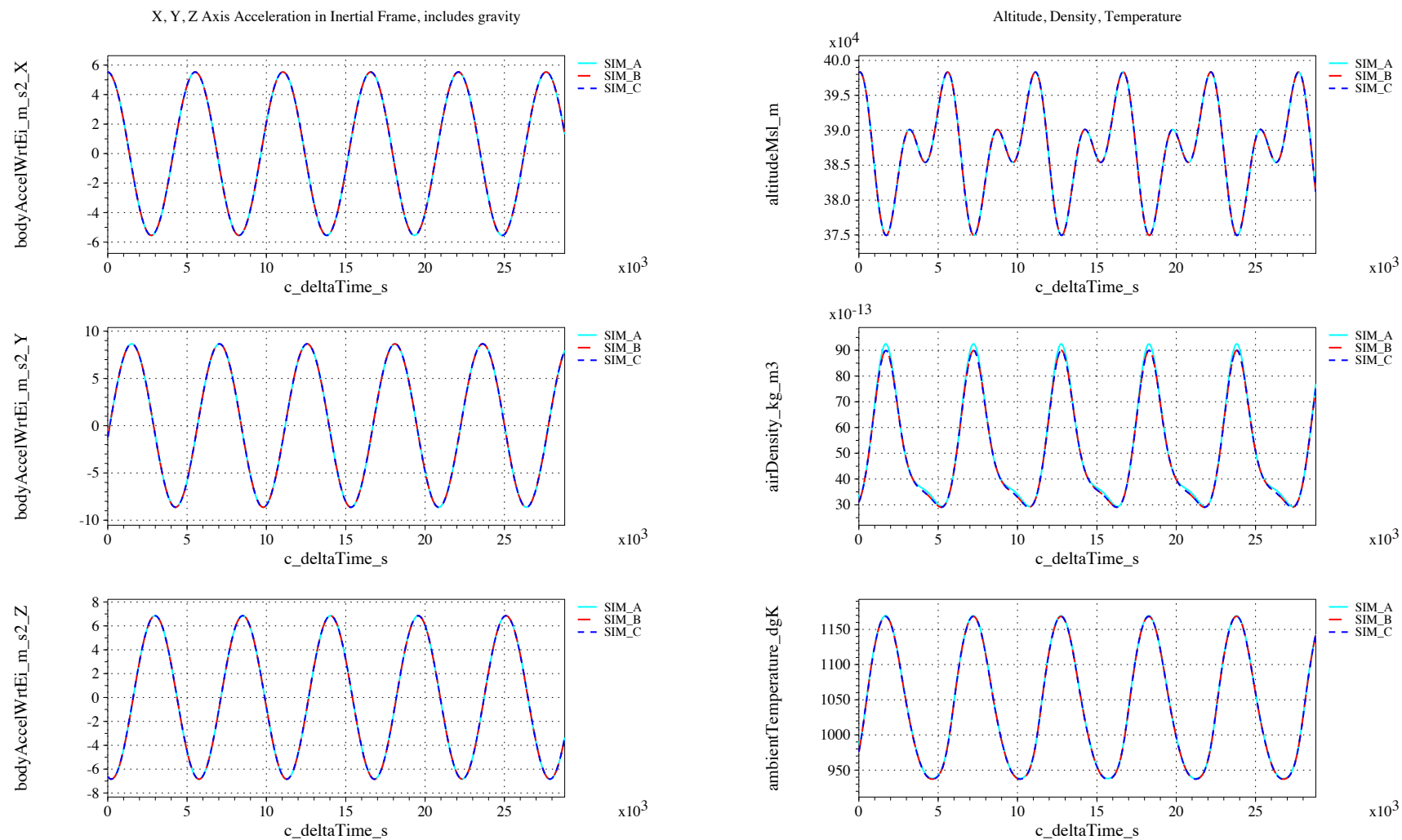Altitude, Density, Temperature

Figure 86.   Accelerations and atmospheric quantities vs. time (check-case 10A: cylinder in circular orbit with gravity gradient with zero initial rates)
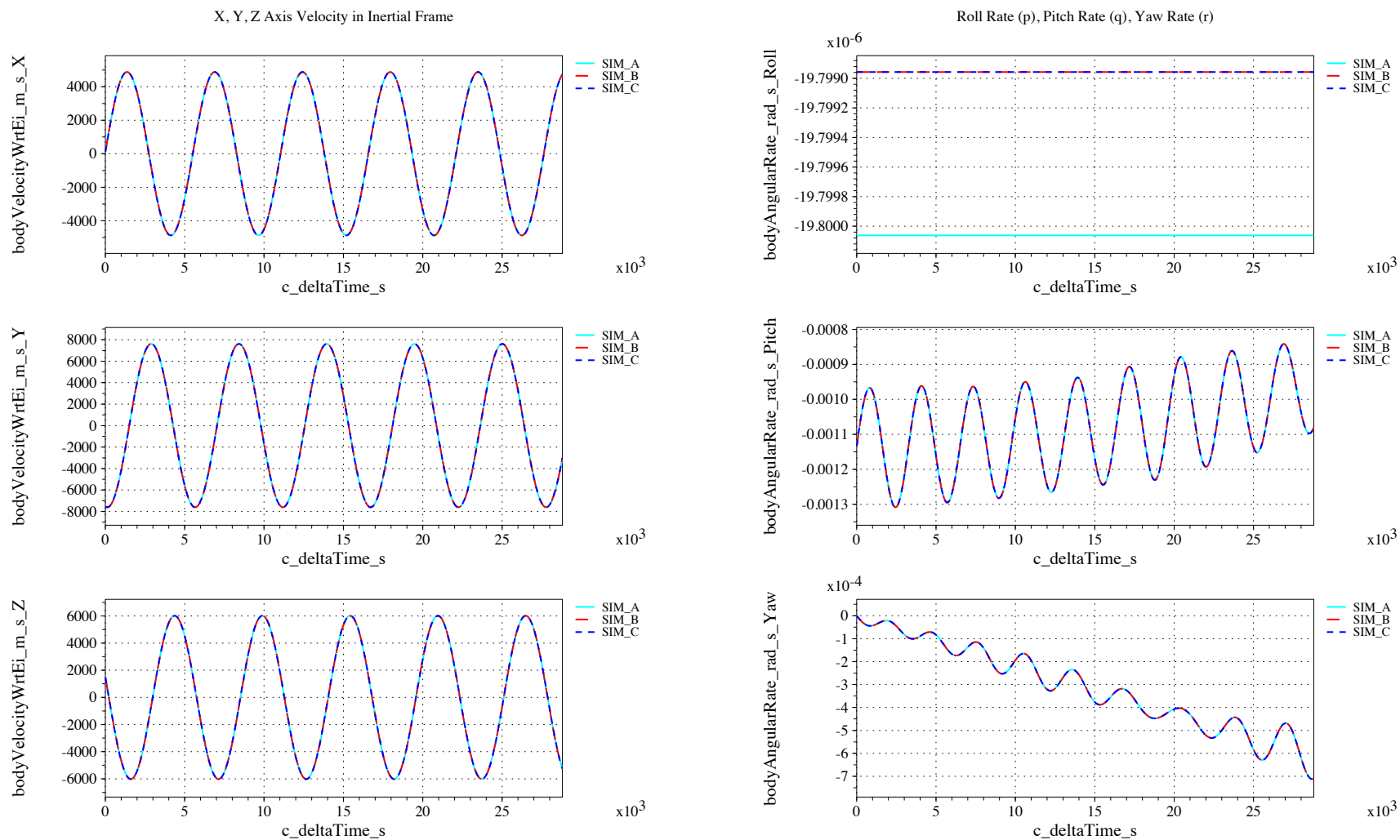
American Institute of Aeronautics and Astronautics

Figure 87. Inertial velocity and body angular rates vs. time (check-case 10A: cylinder in circular orbit with gravity gradient with zero initial rates)
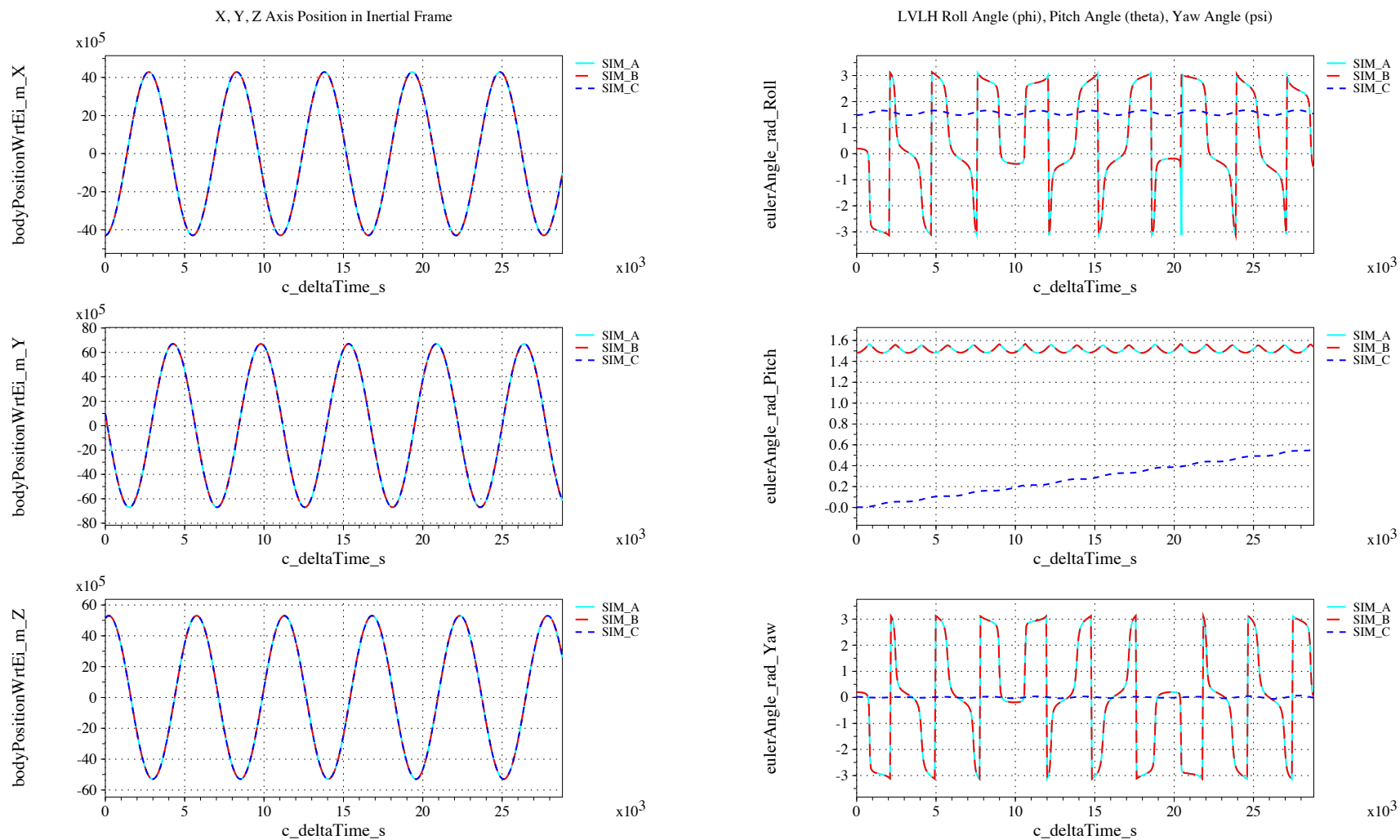
American Institute of Aeronautics and Astronautics

Figure 88. Inertial positions and Euler angles vs. time (check-case 10A: cylinder in circular orbit with gravity gradient with zero initial rates)

IX.B.23. *Check-case 10B – cylinder in circular orbit with gravity gradient with non-zero initial rates*

This section shows cross-plots for three of the selected simulation tools in modeling the dynamics of a cylinder in low-Earth orbit responding to the gravity gradient starting with a non-zero inertial rate.

Figures 89 and 91 compare results between NASA simulation tools in inertial acceleration, atmospheric quantities, rates and velocities and positions and attitudes.

Differences in orientation variables for this check case are somewhat curious since matches were achieved on prior check cases.

Matching inertial rotational rates demonstrate that the simulations agree on gravity gradient affects. However, the SIM_C LVLH Euler angles do not match SIM_A and SIM_B in both initial condition and behavior. This is curious since the rotational initial conditions are the same as check-cases 9B and 9D, in which the simulations agree. The inertial orientations (not shown) and the orbits match. Therefore, the probable cause is a mismatch in Euler angle convention; configuring SIM_C for the 3-2-1 rotation sequence convention may have been overlooked.

Difference SIM_A roll rate is exaggerated by scale. It differs by $\approx 1 \times 10^{-9}$ rad/s.

As in other cases, SIM_A shows slightly higher peaks in atmospheric density than SIM_B and SIM_C. There may be a difference in either MET model implementation or interaction (e.g. input values).

All of these differences are under investigation.

American Institute of Aeronautics and Astronautics

X, Y, Z Axis Acceleration in Inertial Frame, includes gravity
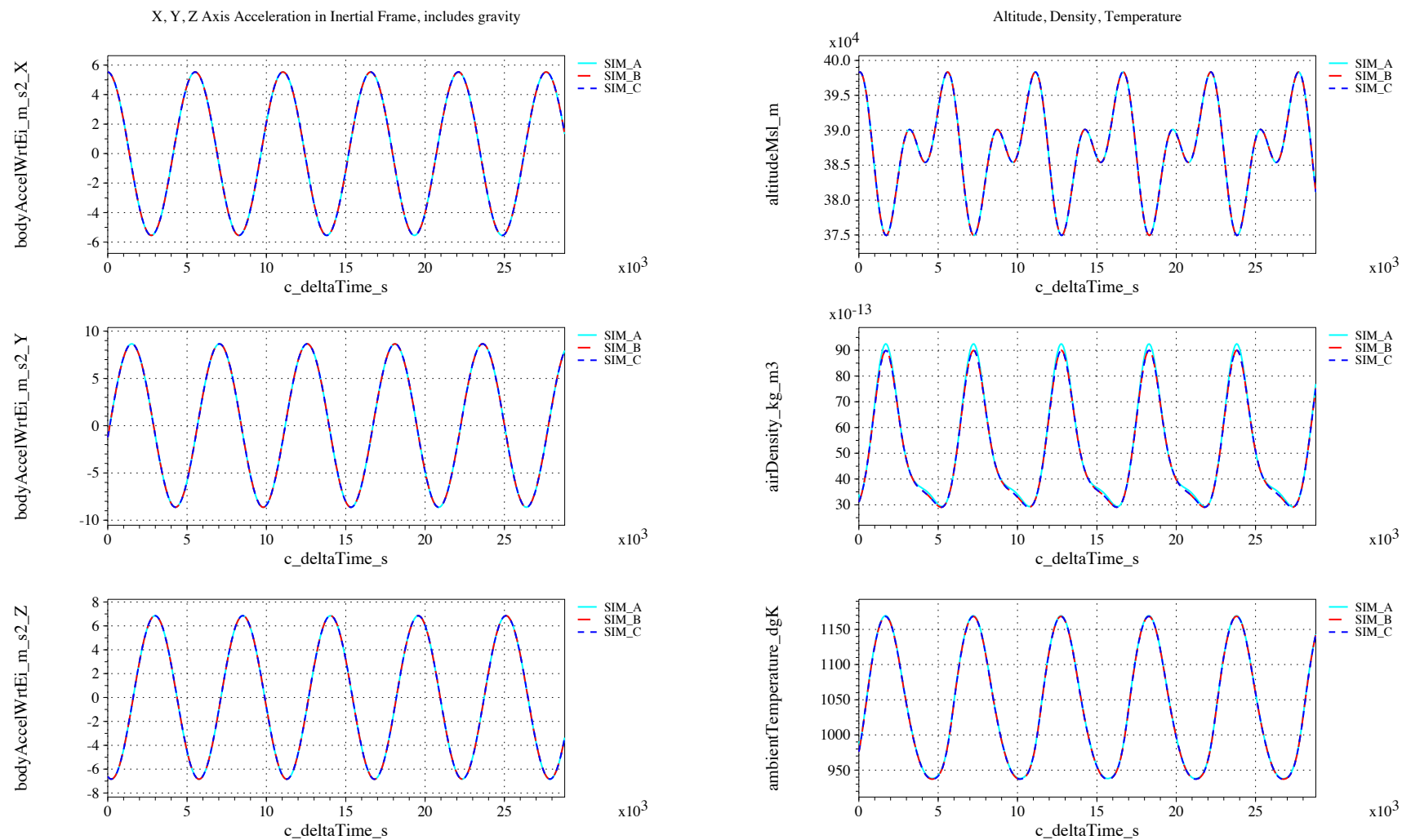
Altitude, Density, Temperature

Figure 89.   Accelerations and atmospheric quantities vs. time (check-case 10B: cylinder in circular orbit with gravity gradient with non-zero initial rates)
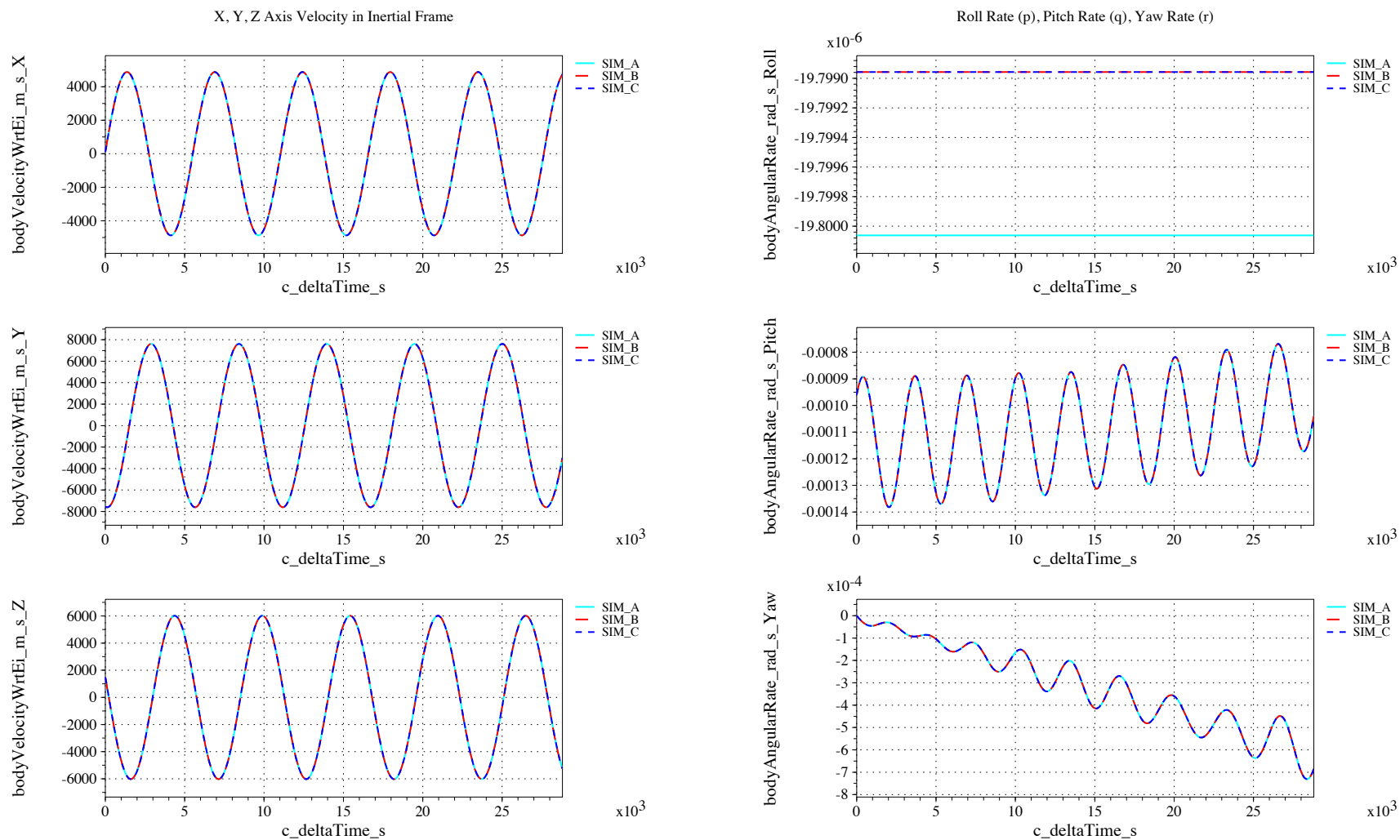
American Institute of Aeronautics and Astronautics

Figure 90. Inertial velocity and body angular rates vs. time (check-case 10B: cylinder in circular orbit with gravity gradient with non-zero initial rates)

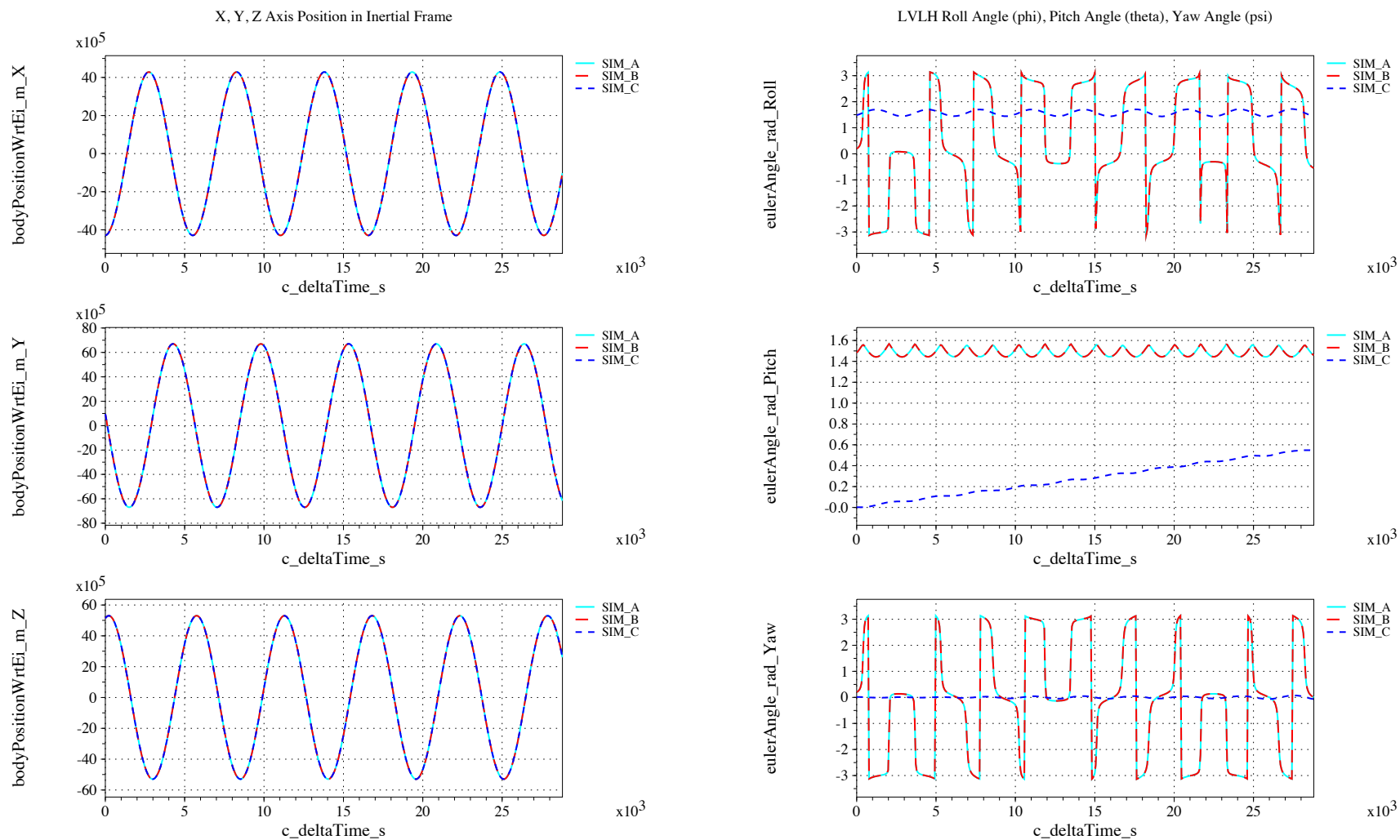American Institute of Aeronautics and Astronautics

143 of 156

Figure 91. Inertial positions and Euler angles vs. time (check-case 10B: cylinder in circular orbit with gravity gradient with non-zero initial rates)

IX.B.24.   Check-case 10C – cylinder in elliptical orbit with gravity gradient with zero initial rates

This section shows cross-plots for three of the selected simulation tools in modeling the dynamics of a cylinder in an elliptical orbit responding to the gravity gradient starting with zero inertial rate.

Figures 92 and 94 compare results between NASA simulation tools in inertial acceleration, atmospheric quantities, rates and velocities and positions and attitudes.

Differences in orientation variables for this check case are somewhat curious since matches were achieved on prior check cases.

Matching inertial rotational rates demonstrate that the simulations agree on gravity gradient affects. However, the SIM_C LVLH Euler angles do not match SIM_A and SIM_B in both initial condition and behavior. This is curious since the rotational initial conditions are the same as check-cases 9B and 9D, in which the simulations agree. The inertial orientations (not shown) and the orbits match. Therefore, the probable cause is a mismatch in Euler angle convention; configuring SIM_C for the 3-2-1 rotation sequence convention may have been overlooked.

As in other cases, SIM_A shows slightly higher peaks in atmospheric density than SIM_B and SIM_C. There may be a difference in either MET model implementation or interaction (e.g. input values).

All of these differences are under investigation.

American Institute of Aeronautics and Astronautics

American Institute of Aeronautics and Astronautics

X, Y, Z Axis Acceleration in Inertial Frame, includes gravity

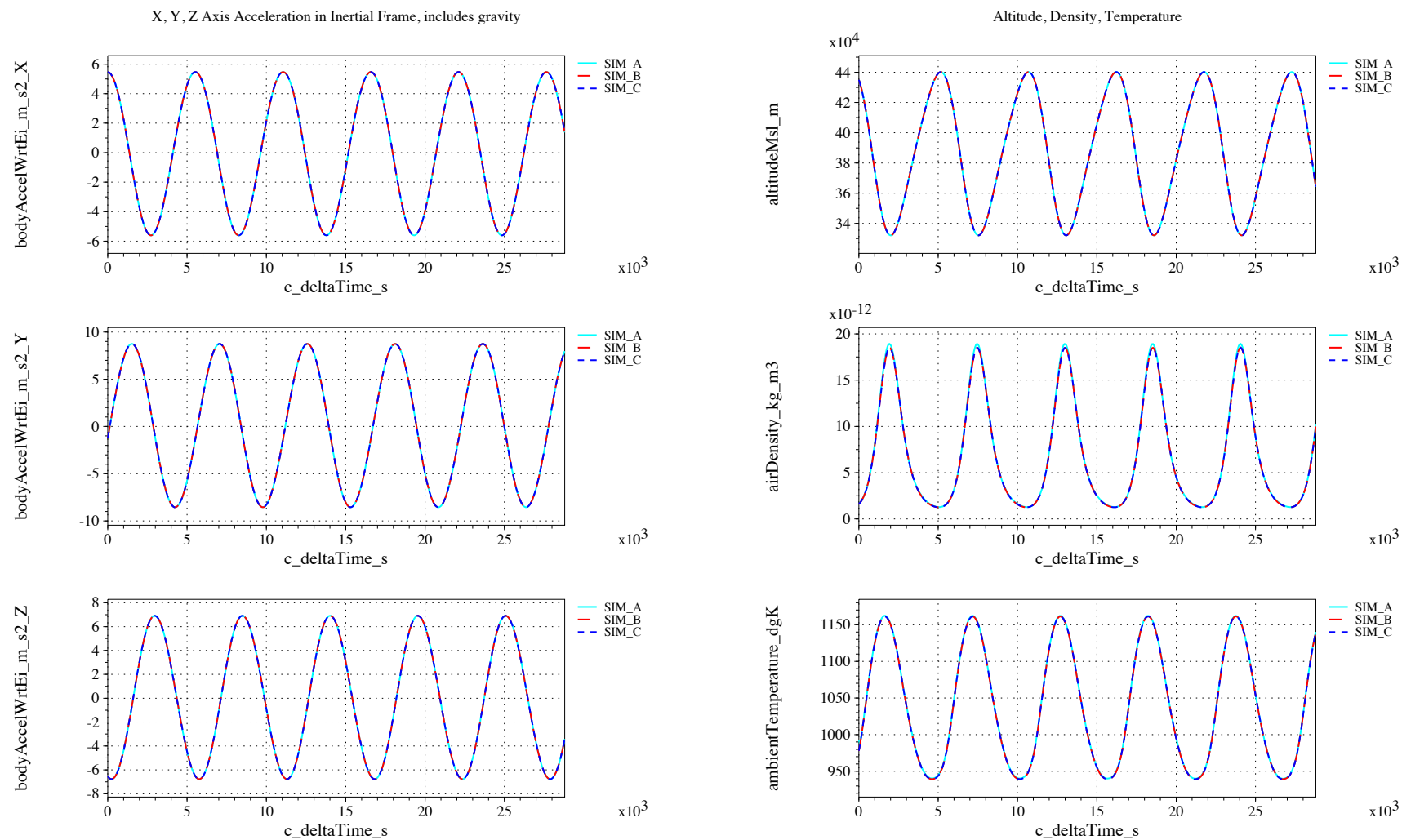Altitude, Density, Temperature

Figure 92. Accelerations and atmospheric quantities vs. time (check-case 10C: cylinder in elliptical orbit with gravity gradient with zero initial rates)

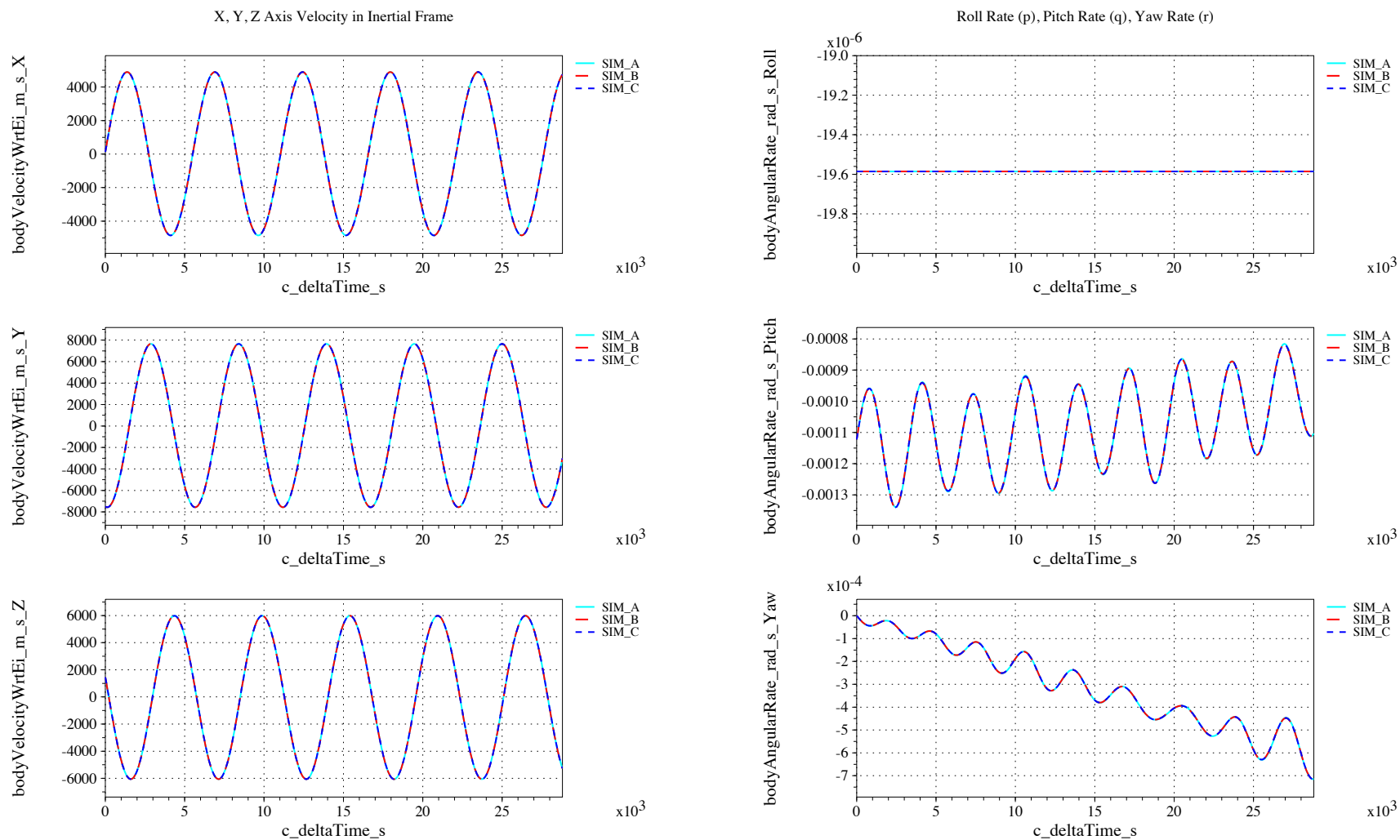American Institute of Aeronautics and Astronautics

Figure 93. Inertial velocity and body angular rates vs. time (check-case 10C: cylinder in elliptical orbit with gravity gradient with zero initial rates)
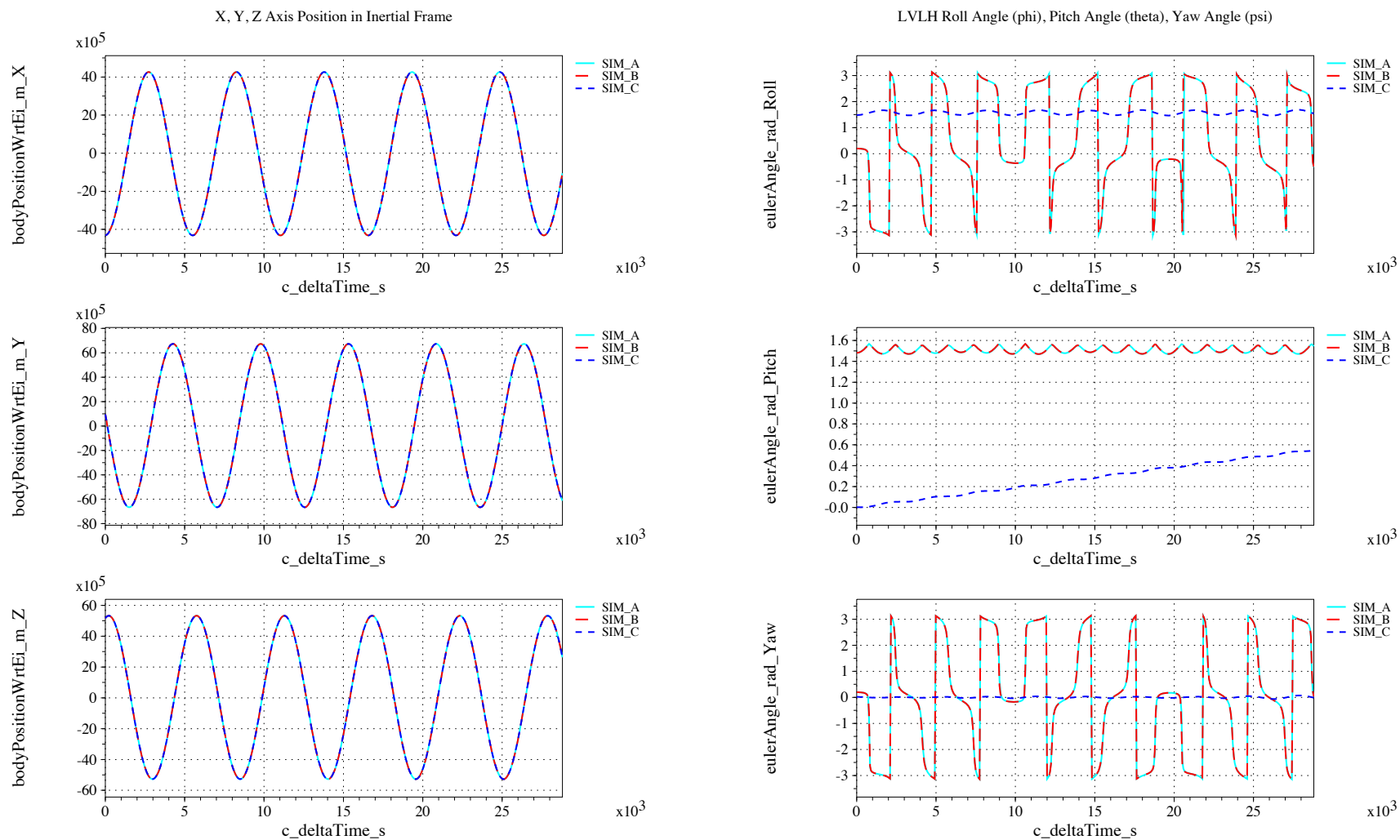
American Institute of Aeronautics and Astronautics

147 of 156

X, Y, Z Axis Position in Inertial Frame

LVLH Roll Angle (phi), Pitch Angle (theta), Yaw Angle (psi)

Figure 94. Inertial positions and Euler angles vs. time (check-case 10C: cylinder in elliptical orbit with gravity gradient with zero initial rates)

IX.B.25.   Check-case 10D – cylinder in elliptical orbit with gravity gradient with non-zero initial rates

This section shows cross-plots for three of the selected simulation tools in modeling the dynamics of a cylinder in an elliptical orbit responding to the gravity gradient starting with a non-zero inertial rate.

Figures 95 and 97 compare results between NASA simulation tools in inertial acceleration, atmospheric quantities, rates and velocities and positions and attitudes.

Differences in orientation variables for this check case are somewhat curious since matches were achieved on prior check cases.

Matching inertial rotational rates demonstrate that the simulations agree on gravity gradient affects. However, the SIM_C LVLH Euler angles do not match SIM_A and SIM_B in both initial condition and behavior. This is curious since the rotational initial conditions are the same as check-cases 9B and 9D, in which the simulations agree. The inertial orientations (not shown) and the orbits match. Therefore, the probable cause is a mismatch in Euler angle convention; configuring SIM_C for the 3-2-1 rotation sequence convention may have been overlooked.

Difference SIM_A roll rate is exaggerated by scale. It differs by $\approx 1 \times 10^{-9}$ rad/s.

As in other cases, SIM_A shows slightly higher peaks in atmospheric density than SIM_B and SIM_C. There may be a difference in either MET model implementation or interaction (e.g. input values).

All of these differences are under investigation.

American Institute of Aeronautics and Astronautics

X, Y, Z Axis Acceleration in Inertial Frame, includes gravity
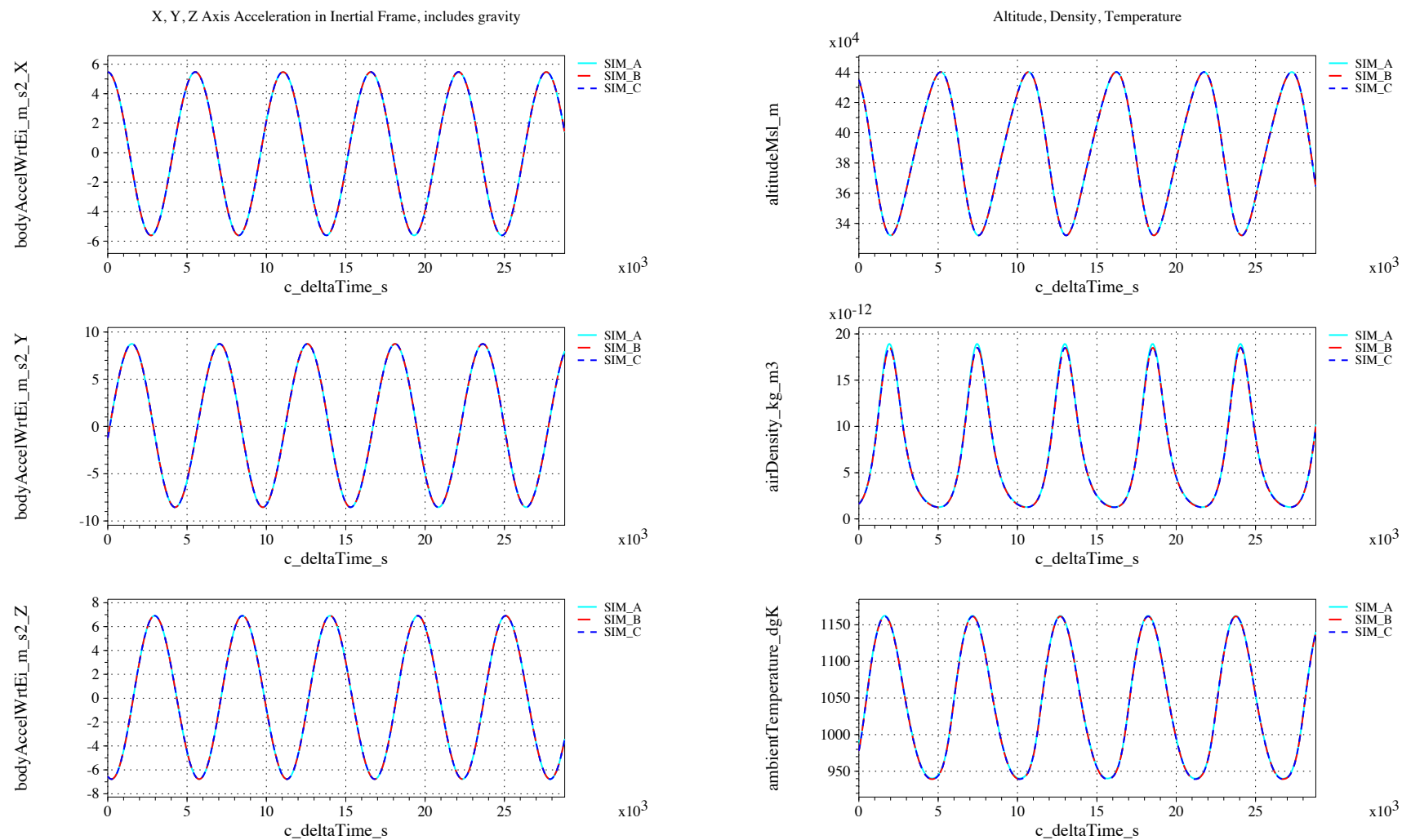
Altitude, Density, Temperature

Figure 95. Accelerations and atmospheric quantities vs. time (check-case 10D: cylinder in elliptical orbit with gravity gradient with non-zero initial rates)

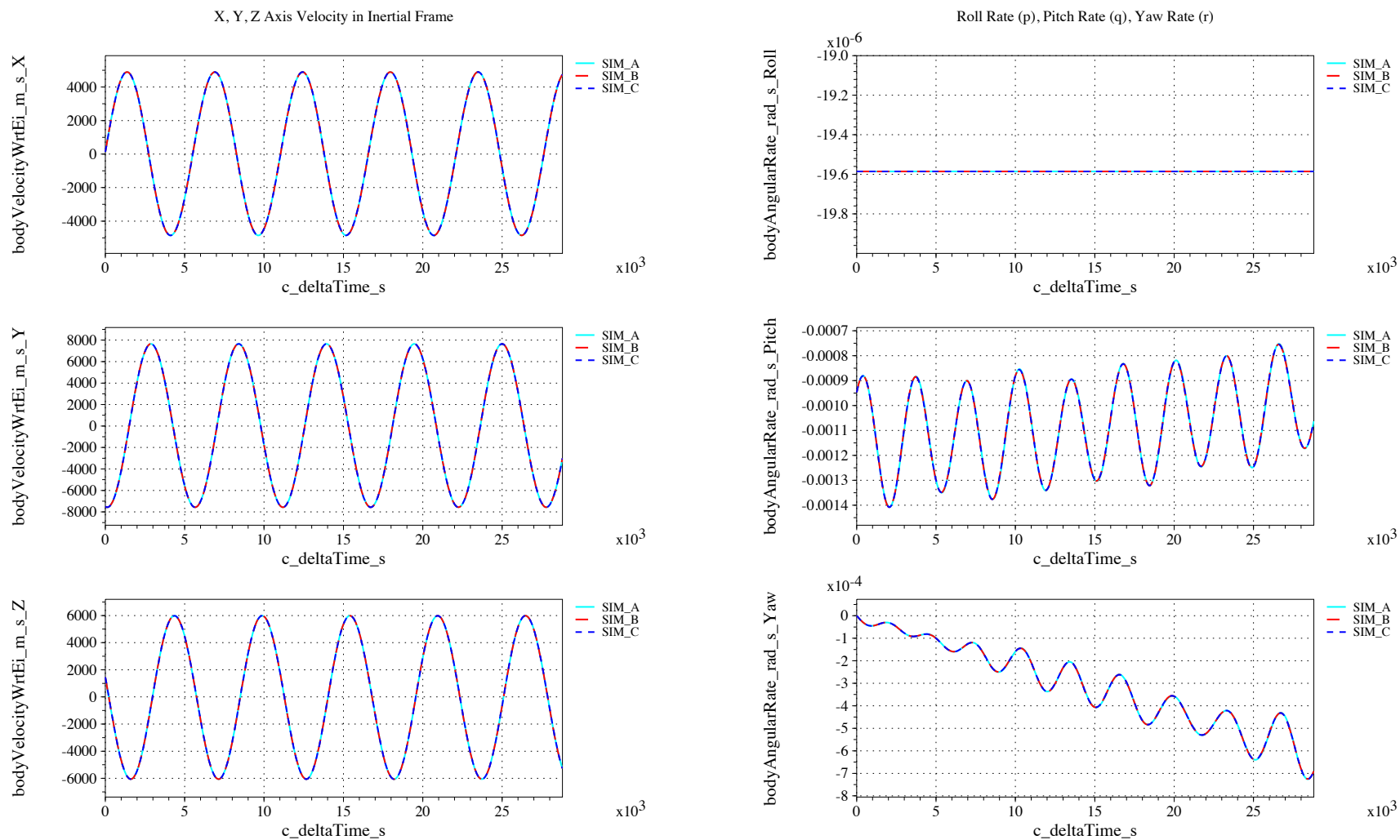American Institute of Aeronautics and Astronautics

Figure 96. Inertial velocity and body angular rates vs. time (check-case 10D: cylinder in elliptical orbit with gravity gradient with non-zero initial rates)
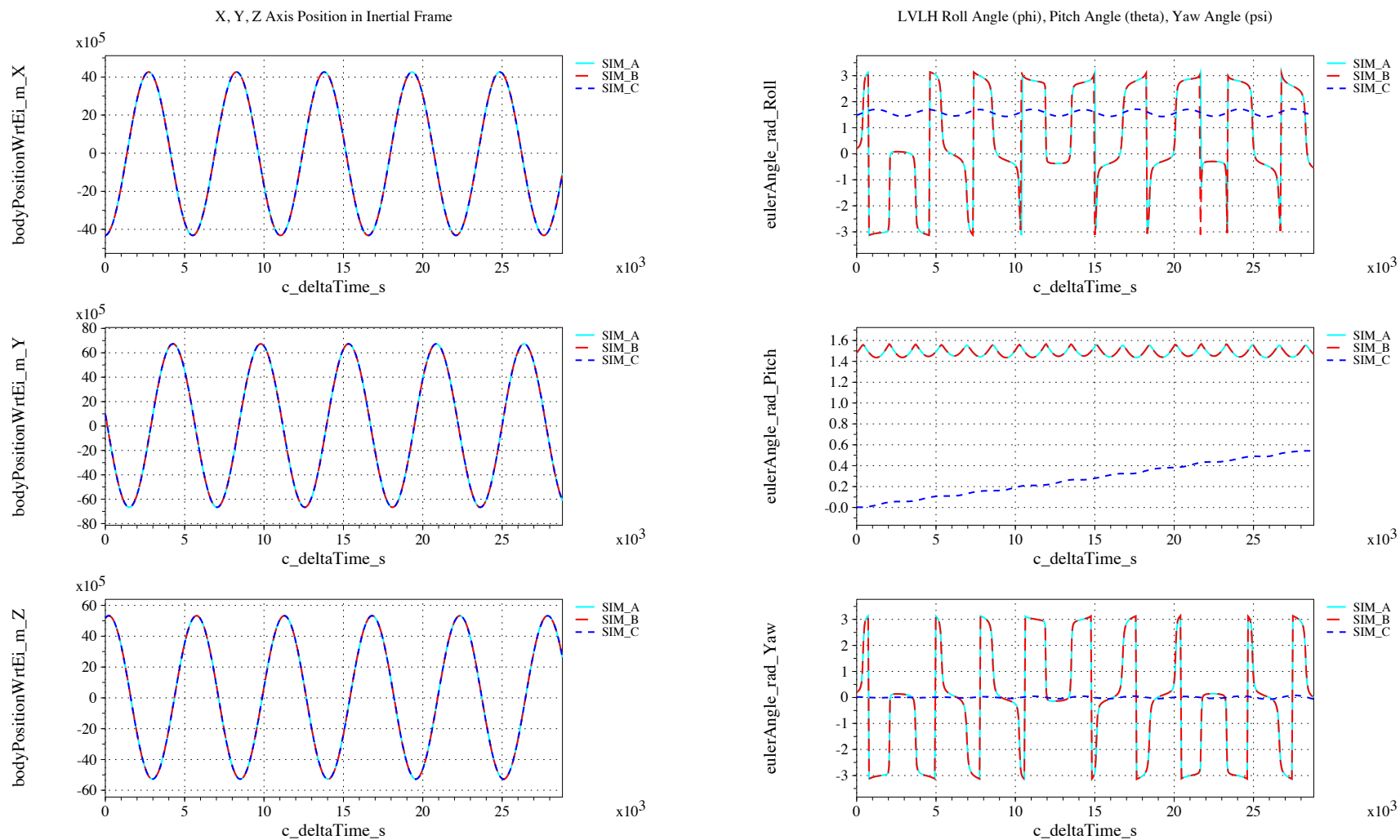
Figure 97. Inertial positions and Euler angles vs. time (check-case 10D: cylinder in elliptical orbit with gravity gradient with non-zero initial rates)

IX.B.26. Check-case Full – ISS responding to all effect

This section shows cross-plots for three of the selected simulation tools in modeling the dynamics of the ISS responding to all effects previously tested.

Figures 98 and 100 compare results between NASA simulation tools in inertial acceleration, atmospheric quantities, rates and velocities and positions and attitudes.

All three simulations diverge on orientation (inertial and LVLH) and body rates. Gravity gradient torque is the only driver of rotational dynamics. Gravity gradient torque is dependent on vehicle position and this test does combine all the environmentally induced forces previously modeled. However, inertial position doesn't differ among the simulations by more than 25 meters by the end of the run. So, the gravity gradient should be a near-perfect match throughout the run. Though the three simulation tools matched inertial orientation with gravity gradient torque in check cases 10A through 10D, one change in this scenario not previously exercised is a non-symmetric body. Therefore, differences may be traceable to the off-diagonal moment-of-inertia terms of the gravity gradient model.

As in other cases, SIM_A shows slightly higher peaks in atmospheric density than SIM_B and SIM_C. There may be a difference in either MET model implementation or interaction (e.g. input values); this difference is being investigated.
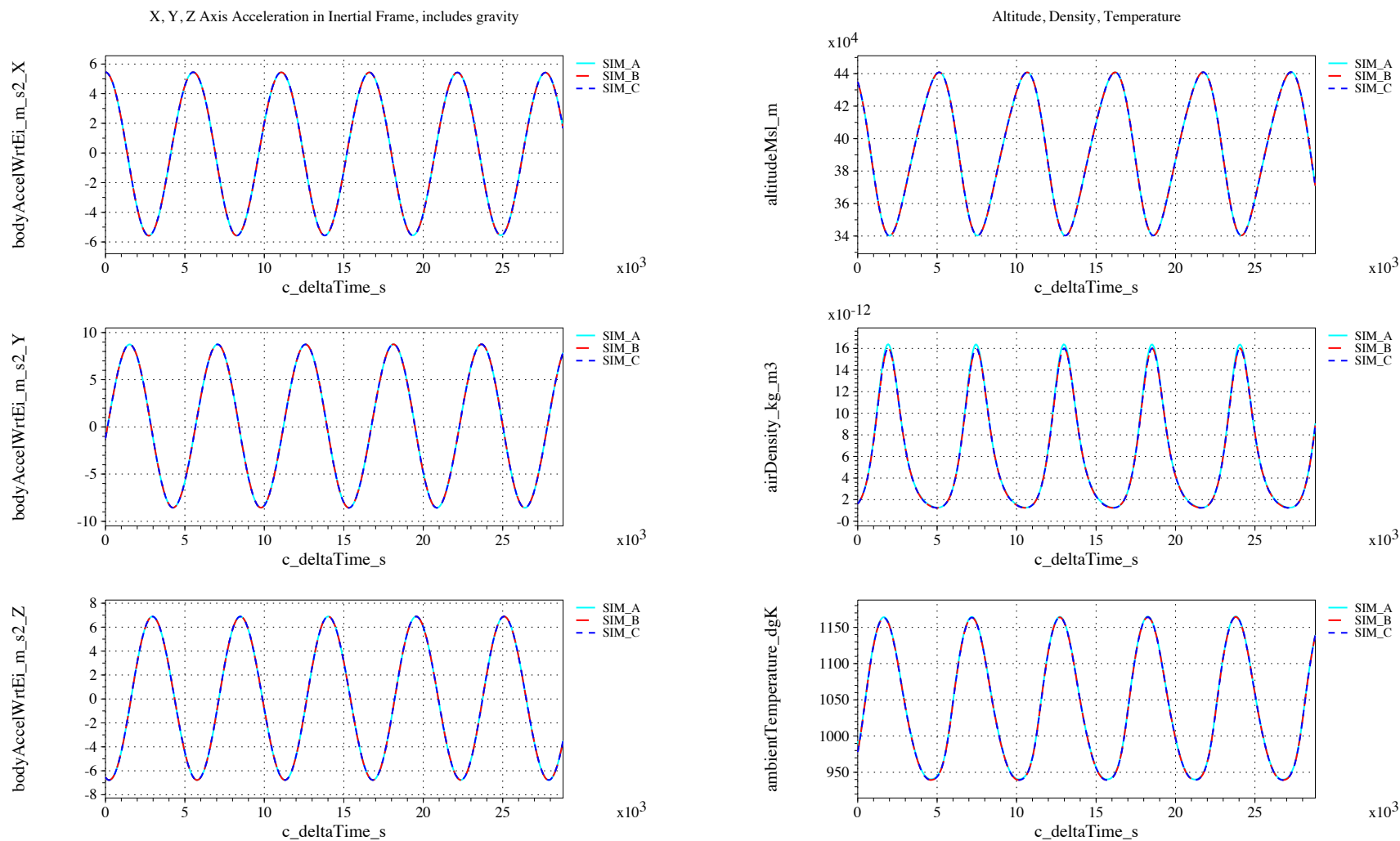
American Institute of Aeronautics and Astronautics

X, Y, Z Axis Acceleration in Inertial Frame, includes gravity

Altitude, Density, Temperature

Figure 98. Accelerations and atmospheric quantities vs. time (check-case Full: ISS responding to all effects)

American Institute of Aeronautics and Astronautics

X, Y, Z Axis Velocity in Inertial Frame

Roll Rate (p), Pitch Rate (q), Yaw Rate (r)

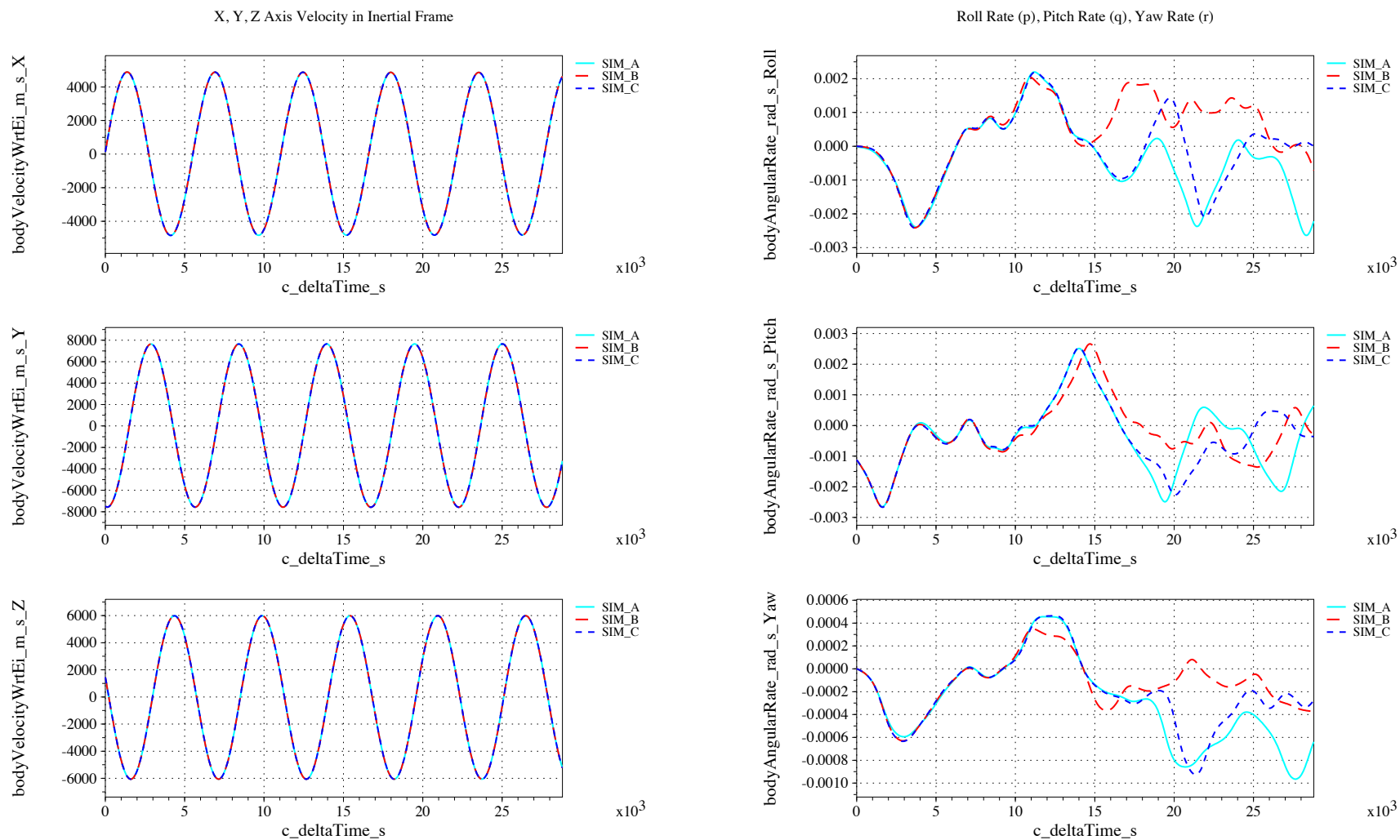Figure 99. Inertial velocity and body angular rates vs. time (check-case Full: ISS responding to all effects)

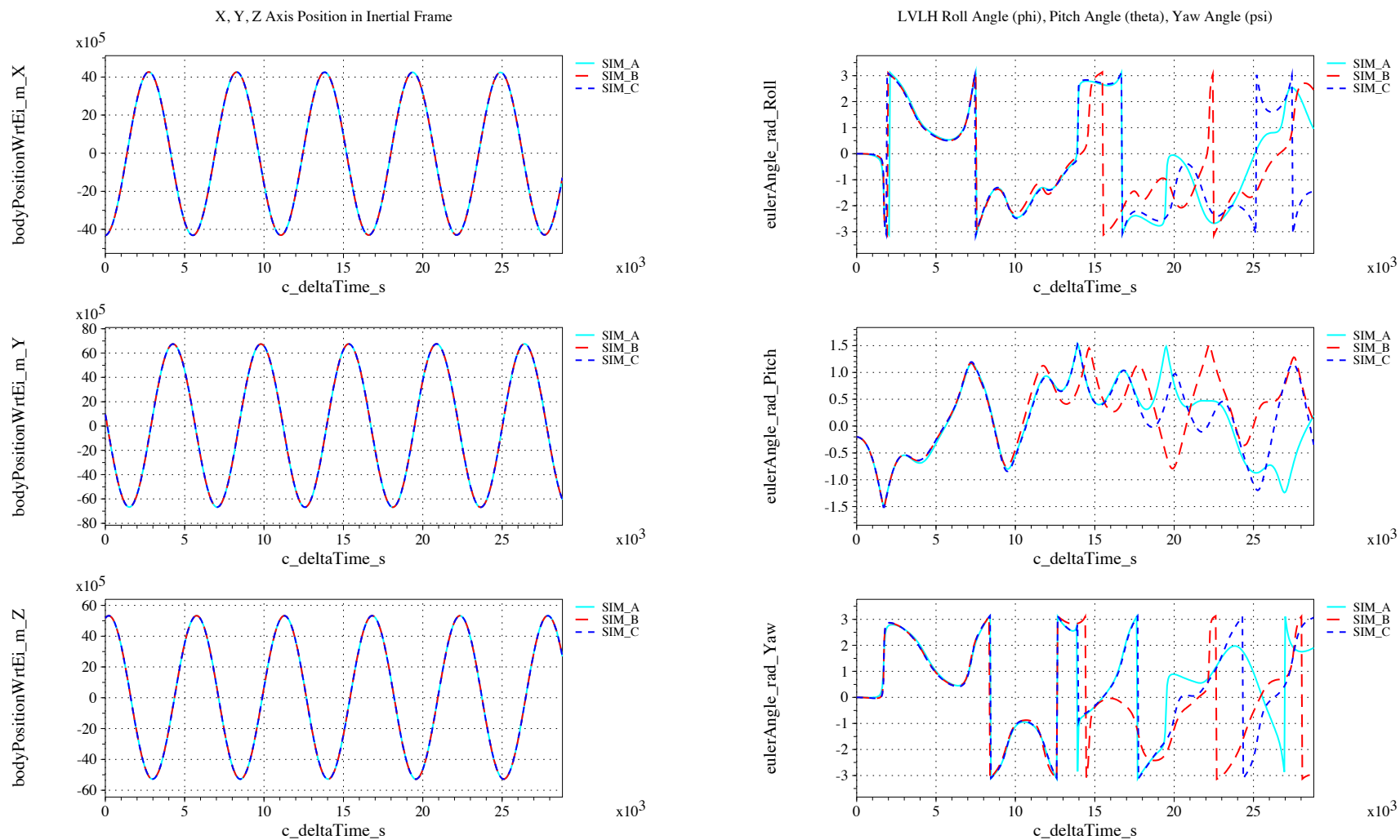American Institute of Aeronautics and Astronautics

Figure 100. Inertial positions and Euler angles vs. time (check-case Full: ISS responding to all effects)

X. Concluding remarks

This report shows some of the results of a NASA cross-agency 6-DOF flight simulation comparison study running a specified set of models and flight maneuvers in well-defined check-cases. It will allow NASA to resolve differences in its own toolsets but it is hoped that a more important contribution will be to provide confidence in other industry-developed simulation tools that they too provide similar results for the same check-cases.

Several differences in the implementation of fairly simple vehicle models are apparent; these arise primarily from differences in interpretation of the scenario and initial conditions. However, initial attempts to model these scenarios led to some fairly significant mis-compares that revealed differences in physical constants and other modeling errors that have been addressed in several tools prior to generating this set of comparisons.

In general, the orbital cases (implemented in three different simulation tools) match fairly well, but minor differences are apparent.

In general, the atmospheric cases match not as well as the orbital cases; atmospheric flight is by its very nature non-linear, thanks to forces and moments due to motion through air being related to the square of the air-relative velocity of the vehicle. A larger number of simulation tools were applied to these initial cases, which also increased the chances of mis-matches.

Ongoing work is to resolve as many differences as possible. Additional atmospheric check-cases involving winged maneuvering flight, two-stage to orbit, and reentry vehicles are planned or have been attempted, but an insufficient number of implementations were completed in time for inclusion in this paper.

The authors would welcome other simulation tool developers who might wish to participate in this comparison.

References

[1] Crues, Edwin Z.; Jackson, A. A. and Morris, J. C., "A Process for Comparing Dynamics of Distributed Space Systems Simulations," *Joint 2009 Simulation Interoperability Workshop*, No. JSC-CN-17561, San Diego, CA, 2009.

[2] Anon., "Department of Defense World Geodetic System 1984," Tech. Rep. NIMA TR8350.2, National Imagery and Mapping Agency, Washington, DC, 2000.

[3] Borkowski, K. M., "Transformation of Geocentric to Geodetic Coordinates Without Approximations," *Bulletin Geodesique 63*, Vol. 139, December 1987, pp. 1–4.

[4] Montenbruck, O. and Gill, E., *Satellite Orbits: Models, Methods, and Applications*, Springer-Verlag, Berlin, 2000.

[5] Vallado, D., *Fundamentals of Astrodynamics and Applications*, Microcosm Press, El Segundo, CA, 2nd ed., 2001.

[6] Kaula, W., *Theory of Geodesy: Applications of Satellites to Geodesy*, Blaisdell Publishing Company, Waltham, Massachusetts, 1966.

[7] Torge, W., *Geodesy*, Walter de Gruyter, Berlin, 3rd ed., 2001.

[8] Anon., "US Standard Atmosphere, 1976," Tech. rep., NOAA, NASA, USAF joint publication, Washington, DC, 1976.

[9] Johnson, D. L. and Smith, R. E., "The MSFC/J70 Orbital Atmosphere Model and the Data Bases for the MSFC Solar Activity Prediction Technique," Tech. Rep. NASA TM-86522, National Aeronautics and Space Administration, Washington, D.C., 1985.

[10] Hickey, M. P., "The NASA Engineering Thermosphere Model," Tech. Rep. NASA CR-179359, National Aeronautics and Space Administration, Washington, D.C., 1988.

[11] Hickey, M. P., "An Improvement in the Integration Procedure Used in the Marshall Engineering Thermosphere Model," Tech. Rep. NASA CR-179389, National Aeronautics and Space Administration, Washington, D.C., 1988.

[12] Anon., "Flight Dynamics Model Exchange Standard," Tech. Rep. ANSI/AIAA S-119-2011, American National Standard, Washington, DC, March 2011.

[13] Jackson, E. B., *Dynamic Aerospace Vehicle Exchange Markup Language*, AIAA Modeling and Simulation Technical Committee, version 2.0.2 ed., July 2011, available from http://daveml.org.

American Institute of Aeronautics and Astronautics